The experimental study of stable and unstable breaches

J.K.H. Choi

April 10, 2018

1519379

Preface

This graduation thesis is the final examination of the study Offshore & Dredging Engineering. Specialisation: Dredging, Trenching and Deepsea Mining at Delft University of Technology. The research is conducted in the Dredging Laboratory of the University of Technology of Delft.
I am grateful for the opportunity to do this experimental study on breaching and gain new experiences in combining theory and simulations. My supervisor for this thesis, Ir. D. Weij helped me out with many things and guided me towards the right direction with the research and thesis.
I would also like to thank the members of the graduation committee such as Dr. ir. Talmon and Prof. dr. ir. van Rhee for their support and special thanks to Ed Stok and Freek Brakel.

Joshua Choi,
Delft.

Abstract

In case of dredging close to underwater sand slopes, steep slopes might form. In dense sand with low permeability this might lead to breaching. The creation of a steep underwater slope marks the beginning of a breaching process.
Pore volumes of densely packed sand tend to increase during shear deformations. This effect is called dilating. Due to the dilation, the sand becomes loosened. Water has to flow in to compensate the enlargement of the pores. This can only occur simultaneously with the development of underpressure in the densely packed sand. This underpressure keeps the sand body, temporarily, stable. When enough water has flowed in and the sand has dilated enough, sand particles release at the front. This leads to a density current consisting of sand mixed with the surrounding water, which runs down the slope. This density current might cause erosion. The steep front of the slope moves with a certain velocity, which is called the headwall velocity.

The thesis focuses on the differences between the stable and unstable states of the breaching process. A breach is stable if the breaching height decreases in time and unstable if the breaching height increases in time. The stability of the breach is dependent on the angle at the toe of the breach. If this angle is steeper relative to the bed angle at the top of the breach, the breach is stable. And it is unstable if the angle at the toe of the breach is milder relative to the top of the breach.
This thesis is mainly based on physical experiments that have been conducted.
The main research question is:

Can an unstable breach be predicted?

The three most important parameters are discussed: sliding wedges, (head)wall velocity and angle at the toe of the breach.

Sliding wedges of sand are an important part of the breaching process. The test data show that the sliding wedges can be predicted, their frequency as well as the percentage of sliding wedges compared to the pure breaching process. Some empirical formulas are obtained to predict the percentage of the sliding wedges at certain breaching heights.
Afterwards, a model (You, 2014) is used to calculate the factor of safety of slopes using the data obtained from the experiments to predict the sliding wedges.

The headwall velocity of a breach is also an important parameter. There are two different wall velocities, the headwall velocity, which does not take the effect of sliding wedges into account. The wall velocity takes the effects of sliding wedges into account.
The headwall velocity can be estimated, but this is not a realistic velocity, as sliding wedges occur during breaching processes. The wall velocity can be estimated using the headwall velocity and the percentage of sliding wedges. This gives a wall velocity close to the wall velocity that was measured in the experiments. A factor is empirically determined to calculate the wall velocity with the headwall velocity.

The angle at the toe of the breach is another important parameter for unstable breaching. When the angle at the toe decreases relative to the angle on top of the breach, it will be an unstable breach. The experiments show that the angle at the toe converges towards the angle that is predicted using the equation and is applicable after some time passes, dependent on the breaching height.

The equation (Van Rhee, 2015) includes the breaching height and the wall velocity. And this critical angle should be compared to the angle at the toe to determine whether the breach is stable or unstable. These three parameters all have their effects on the critical angle equation and thus are all leading to the main research question.

Contents

List of figures

List of tables

Nomenclature

C_v	Coefficient of consolidation $[m^2/s]$
c	Concentration of the sand [-]
D_{50}	50% particle size distribution [m]
f_{wedge}	Frequency sliding wedge [1/s]
g	Gravitational acceleration [m/s^2]
h	Active breaching height [m]
i	Gradient of inward flow [-]
k	Permeability of the soil [m/s]
L	Length of the pressure drop [m]
m_u	Isotropic unloading compressibility [1/Pa]
m_q	Volumetric strain [1/Pa]
n_0	Initial porosity of the soil [-]
n_{loose}	Loose porosity of the soil [-]
p_{wedge}	Sliding wedge percentage [%]
q	Inflow of the water [m/s]
s	Specific sand production [kg/ms]
t	Time [s]
t_{con}	Time to converge to the theoretical angle [s]
u^*	Excess pore pressure [Pa]
v	Wall velocity [m/s]
$v_{headwall}$	Headwall velocity [m/s]
V_{wedge}	Volume of a sliding wedge [m^3]
v_z	Velocity suction tube [m/s]
w	Width of a sliding wedge [m]
x	Length of a sliding wedge [m]
α	Angle toe of the breach [°]
α_{crit}	Critical angle at toe of the breach [°]
α_{eq}	Equilibrium of angle at toe of the breach [°]
β	Breaching angle [°]
Δn	Relative porosity change [-]
Δp	Pressure difference [Pa]
θ	Angle of a sliding wedge [°]
ρ_s	Density particles [kg/m^3]
ρ_w	Density water [kg/m^3]
σ_1	Major principal stress [Pa]
σ_3	Minor principal stress [Pa]
ϕ	Internal friction angle [°]

1. Introduction

1.1 Problem description

Dredging encompasses all activities that are involved with the removal of silt, sand, clay or other sediments from the seabed. There are three main reasons for dredging: capital dredging, land reclamation (figure 1-1) and maintenance. Capital dredging is usually carried out to create new waterways or harbours. The creation of artificial islands or the expansion of land is called land reclamation. The Netherlands has two of the world's largest dredging companies.

Figure 1- 1: Land reclamation

There are many different techniques of dredging, dependent on the sediment, location and application. If sand is involved in the dredging process, underwater slopes may develop. Not everything is known about these underwater slopes, for example how they arise, when they occur and how they influence the dredging process. Important research and modelling have been conducted earlier.

In case of dredging close to underwater sand slopes, steep slopes might form. In dense sand with low permeability this might lead to breaching. In case of breaching, the front of this steep slope is called the headwall. The creation of this steep underwater slope marks the beginning of a breaching process. Pore volumes of densely packed sand tend to increase during shear deformations. This effect is called dilating. Due to the dilation, the sand becomes loosened. Water has to flow in to compensate the enlargement of the pores. This can only occur simultaneously with the development of underpressure in the densely packed sand. This underpressure keeps the sand body, temporarily, stable. When enough water has flowed in and the sand has dilated enough, sand particles release at the front. This leads to a density current consisting of sand mixed with the surrounding water, which runs down the slope. This density current might cause erosion. The headwall will move with a certain horizontal velocity, this is called the headwall velocity (Figure 1-2).

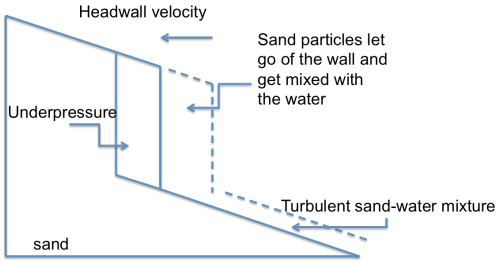

Figure 1- 2: A breaching process

Breaching processes can be stable or unstable. When it is stable, the height of the headwall will decrease in time (Figure 1-4). But in the case of an unstable breach, the height of the headwall will increase in time. This occurs when with a decreasing slope angle at the toe relative to the angle on top of the breach (Figure 1-5). This is the case when the angle at the toe of the breach erodes, caused by the interaction with the turbidity current. The angle at the toe is crucial for the development of a stable or an unstable breach. When this angle is milder during breaching, relative to the angle on top of the breach, an unstable breach might develop. This might be an unwanted effect, because the breach does not stop quickly compared to a stable breach. Unstable breaching might cause a lot of damage to its surrounding. This effect can in some cases threaten the stability of dikes. Furthermore it is difficult to predict when an unstable breaching process will end. Depending on the slope, it could take hours before it finishes.

Beinssen et al. (2014) investigated large land slides at Amity point and Inskip Point. Observations clearly showed that these events are caused by breaching of fine sands that were relatively dense packed. Figure 1-3 is in Inskip point and it is the result of one of these unstable breaches. This shows how dangerous unstable breaching can be, given that 300 campers had to be evacuated. Cars, caravans, tents and camping trailers were swallowed by this event.

Figure 1- 3: Inskip point

During breaching, sometimes large sliding wedges of sand slide off the breaching front (Figure 1-6), this is called a sliding wedge which also has consequences for the breaching process; it increases the wall velocity. Figure 1-7 shows a sliding wedge in practice. The headwall velocity does not take sliding wedges into account. The wall velocity is the headwall velocity with the effects of sliding wedges taken into account.

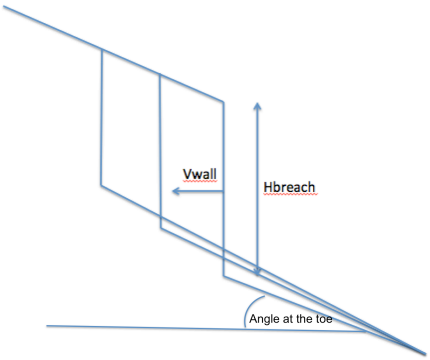

Figure 1- 4: A stable breach

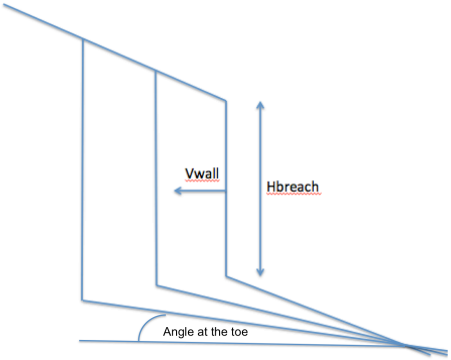

Figure 1- 5: An unstable breach

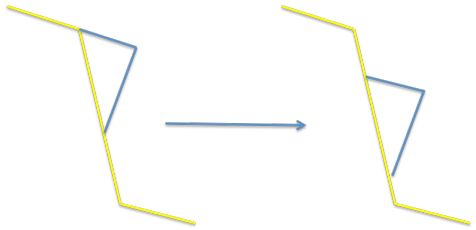

Figure 1- 6: A sliding wedge

Figure 1- 7: A sliding wedge in a laboratory test

1.2 Objectives

The objective of this research is to gain more insight into the physics of breaching processes. Specifically focusing on whether a breaching process is stable or unstable.

Simple indications can be given to indicate whether a slope is vulnerable for unstable breaching. The stability of a breach depends on a couple of variables: the slope angle at the toe of the breach, the critical slope angle, the sand characteristics and the breaching height. It is hypothised that a breach becomes unstable when the slope angle at the toe becomes smaller than the existing slope angle at the top of the breach. This increases the breaching height (Figure 1-5), which results into an unstable breach. Unstable breaching is dangerous and can cause events like in Inskip point (Beinssen, et al., 2014).
To avoid these dangerous situations, the research question to be answered is as follows:

Can an unstable breach be predicted?

To answer the main question, subquestions are defined.
During breaching, sometimes large sliding wedges of sand slide off the slope.
This affects the breaching process and increases the wall velocity. The angle at the toe is dependent on the wall velocity via the size of the turbidity current. So it is important to know how often sliding wedges occur and why they occur. Based on this problem, the first subquestion:

Is the frequency of large sliding wedges during breaching predictable and what are the effects?

Predicting the slope angle is important, because it is hypothisised that the slope angle is a significant parameter that determines the difference between stable and unstable breaching processes. Which leads to the second subquestion:

How can we predict the angle at the toe of the breach?

The wall velocity determines the size of the turbidity current, which in turn influences the angle at the toe of the breach. Using this information the third subquestion is defined:

What are the predictions that can be made for the wall velocity?

1.3 Approach

To answer the researchquestions and subquestions, experiments are conducted.
The experiments are conducted in a setup. This setup is designed, calculated and built. This is done based on a literature review. Next the experiments are conducted and everything is recorded.
From the recorded data, results are obtained and analyzed.

The thesis is divided into the following chapters:

- Chapter 2: A literature review.
- Chapter 3: A description of the whole laboratory setup, individual parts of the setup, followed by the used measuring devices and ending with the testing procedures.
- Chapter 4: Presents the results obtained from the experiments.
- Chapter 5: Contains the analysis of the results and answers the subquestions.
- Chapter 6: Explains the model for sliding wedges used to compare with the data from the experiments.
- Chapter 7: Summarizes the main conclusions from previous chapters followed by recommendations.

2. Literature Review

The literature review is divided in sections focusing on different aspects. Some of the sections touch on multiple aspects.

2.1 Headwall velocities

Breusers (1974) tested the suction of sand by means of small-scale tests. These tests showed that the amount of sand that was dredged depended mainly on the characteristics of the sand, such as grain size, permeability and relative density. The vertical movement of suction tubes in sand created narrow holes with almost vertical walls. The velocity of the walls that moved with a constant velocity was the so-called: 'wall velocity'. The wall velocity is only dependent on sediment sizes and packing. The displacement of the walls is caused by grains or thin layers that become detached from the wall and form a sand-water mixture that flows down as a turbidity current.

Then Breusers (1977) studied the process of suction by means of small-scale tests in a basin of 2 x 7 x 1 m. He found that the wall velocity was only dependent of sediment size and packing. By moving a wide suction mouth towards the wall, the material that detaches forms a sand-water mixture and flows as a turbidity current under an angle (angle at the toe, Figure 2-1), close to the natural angle of repose. He found that when the suction tube moved towards the wall, from Figure 2-2, it follows that:

$$v_z = v_{headwall} * \left(1 - \frac{\tan(\phi)}{\tan(\beta)}\right) \quad (1)$$

Where:
v_z is the velocity that the suction tube moves horizontally [m/s]
$v_{headwall}$ is the velocity of the headwall [m/s]
ϕ is the internal friction angle [°]
β is the breaching angle [°]

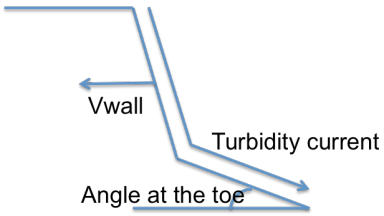

Figure 2- 1:Angle at the toe

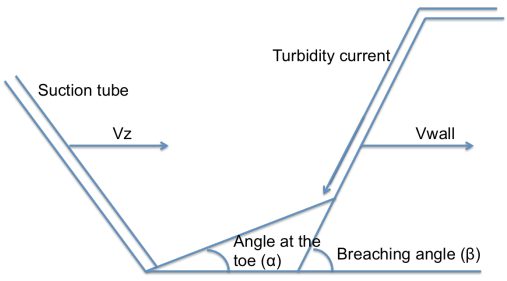

Figure 2- 2: Suction tube

The wall velocity can be derived from the force balance of a block of soil (figure 2-3). This block has a volume of ΔL^3. Assuming that the breaching wall is 90°, the block is in equilibrium before it breaches off. This block is being pulled by the gravity force F_g. Due to the pressure difference over the block, a normal force N acts on the block in horizontal direction. This normal force generates a vertical friction force. The friction force is in equilibrium with the gravity force.

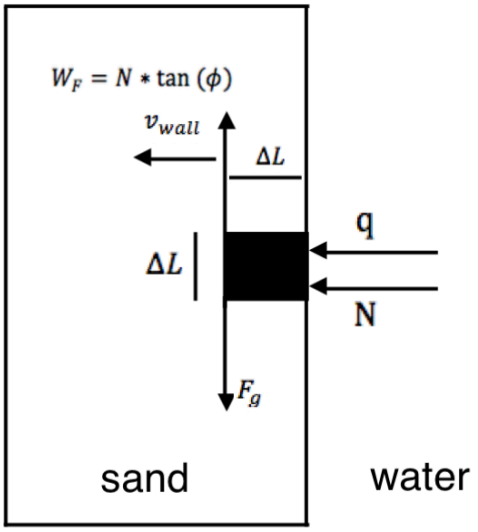

Figure 2- 3: The forces during a breaching process. The block is in equilibrium before it breaches off, assuming that the breaching wall is 90°.

Pore volumes of densely packed sand tend to increase during shear deformations. This effect is called dilating. Due to the dilation, the porosity of the sand increases. A continuous inflow of water fills the increased pore space:

$$q = v_{headwall} * \Delta n \qquad (2)$$

Where:
q is the flux or discharge [m/s]
Δn is the relative porosity increase [-]

$$\Delta n = \frac{n_{loose} - n_0}{1 - n_{loose}} \qquad (3)$$

This can only occur simultaneously with the development of underpressure in the densely packed sand. This underpressure keeps the sand body, temporarily, stable. Darcy's law describes the relation between pressure difference and inflow:

$$q = k * \frac{\Delta p}{\rho_{water} * g * \Delta L} \qquad (4)$$

Where k is the permeability [m/s]
Δp is the pressure difference [Pa]
ρ_w is the density of the water [kg/m^3]
g the gravitational acceleration [m/s^2]
ΔL being the length over which the pressure drop is taking place [m]

When enough water has flowed in and the sand has dilated enough, sand particles release at the front. This leads to a density current consisting of sand mixed with the surrounding water, which runs down the slope. When individual grains or thin layers soil get detached from the wall, they turn into turbidity currents. The headwall velocity is the constant horizontal velocity of the wall.

The formula for the headwall velocity is derived by taking the formula for the amount of water that flows into the wall:

$$q = \Delta n * v_{headwall} = \frac{n_1 - n_0}{1 - n_1} * v_{headwall} \qquad (5)$$

This flow causes a pressure gradient in the sand and its magnitude is:

$$\frac{\Delta p}{\Delta L} = \frac{q * \rho_{water} * g}{k} \qquad (6)$$

Balance is achieved when the gravity force is in balance with the friction force.
Balance is achieved when $W_F = F_g$:

The gravity force and friction force are:

$$F_g = \Delta L^3 * (\rho_{sand} - \rho_{water}) * g * (1 - n_0) \qquad (7)$$

$$W_F = N * \tan(\phi) \qquad (8)$$

The normal force:

$$N = \frac{\Delta p}{dx} * \Delta L * \Delta L^2 \qquad (9)$$

with this we can rewrite N and q is replaced with equation 5:

$$N = \frac{q * \rho_{water} * g}{k} * \Delta L^3 = \frac{\Delta n * v_{headwall} * \rho_{water} * g}{k} * \Delta L^3 \qquad (10)$$

$$W_F = F_g : \frac{q * \rho_{water} * g}{k} * \Delta L^3 * \tan(\phi) = (1 - n_0) * g * (\rho_{sand} - \rho_{water}) * \Delta L^3$$

$$\tan(\phi) * \frac{\Delta n * v_{headwall} * \rho_{water}}{k} = (\rho_{sand} - \rho_{water})(1 - n_0)$$

And the headwall velocity can be rewritten as:

$$v_{headwall} = \frac{\rho_{sand} - \rho_{water}}{\rho_{water}} * k * \frac{1 - n_0}{\Delta n} * \frac{1}{\tan(\phi)} \qquad (11)$$

In this equation, it is assumed that the breaching wall β has an angle of 90°. The breaching wall is not always a perfect vertical wall and must be larger than the internal friction angle. An equation for a wall with angle β was derived (Van der Schrieck, 2012):

$$v_{headwall} = \frac{\rho_{sand} - \rho_{water}}{\rho_{water}} k * \frac{1 - n_0}{\Delta n} * \frac{\sin(\beta - \phi)}{\sin(\phi)} \qquad (12)$$

2.2 Angle at the toe

Mastbergen et al. (1988) conducted large scale testing in a horizontal flume with dimensions 32 x 2.5 x 0.5 m, to investigate the behaviour of the flowing sand-water mixtures, and their sedimentation during the construction of sand water dams. Especially the influence of the flowing sand-water mixture on the development of underwater slopes was investigated. They found that at a small production rate, the flow on the slope was laminar and the slope angles were steep and close to the internal friction angle. However, at higher production rates, the density flow on the slope became turbulent, which would result in a shallower slope angle. Increasing grain size and decreasing production rate give steeper slope angles.

Mastbergen and Winterwerp (1988) investigated the development of underwater slopes during sand fill operations and also the slope angles in such situations. They concluded that the angle at the toe during

the deposit is determined by the specific sandproduction and particle size. The steepest possible slopes were visible at lower sandproductions. From observations they derived the following relation: i ~ $s^{-0.4}$ where i is the average slope angle and s the specific sandproduction.
The equation for the equilibrium slope angle at the toe is given by an empirical relation:

$$i_{eq} = 0.0049 * D_{50}^{0.92} * s^{-0.39} \quad (13)$$

with $i_{eq} = \tan(\alpha_{eq})$,
D_{50} is the median particle size [µm]
s is the sand flux [kg/ms]

Mastbergen and Van den Berg (2003) created a model that was applied to simulate large flushing events in submarine canyon. Predicted velocities were compared with values that were measured during such flushing events.
They found that when there is a certain shear stress or flow velocity, medium to coarse sand will give the maximum erosion rate in the sand bed. With smaller sediment sizes, the erosion rate will be slowed due to shear dilatancy effect which leads to negative pore pressure in the bed, while larger sediment sizes the weight of the grains will reduce its erosion rate.
The model supported the hypothesis that breaching and turbidity currents are the main mechanisms of sand erosion from canyon heads.

2.3 Sliding wedges and pore pressure

Meijer and van Os (1976) made calculations of pore pressures near a moving underwater slope with and without the dilatancy effect.
A deformation problem in saturated sand can be solved mathematically by adopting a moving boundary in the model.
The influence of dilatancy on the generation of negative excess pore pressure could be adequately deduced with Rowe's stress-dilatancy relationship combined with a schematized relation between principal stress ratio and principal strain.
They concluded that dilatancy played a dominating role in the generation of negative excess pore pressure.

You et al. (2012) conducted pore pressure measurements during breaching failure and presented a theoretical model that shows how the pore pressure field in the failing deposit is connected to the erosion rate and the failure surface. The pressure sensors were all lined up horizontally. He did breaching experiments (figure 2-4) with silty sand in a flume filled with water and restrained the sediment with a vertical plate. It allowed water to flow in but holds back the sediments. When the plate was removed, the breaching front retrograded slowly and formed turbidity currents. The pressure was monitored at the same time and a pore pressure drop was noticed immediatly after the plate was removed.
The physical model of (Meijer and van Os, 1976) was used, but some simplifications were made. You assumed in his model that the dilative volumetric strain was only a function of differential stress, where Meijer and van Os also considered the effects of confining stress and effective stress ratio. He also assumed the volumetric strain to be proportional to the minimum pore pressure. The simplifications were made because some dilation analytical solutions were unobtainable. To obtain analytical solutions and to get a better understanding of the interactions between each of the processes connected to breaching the simplification was made.

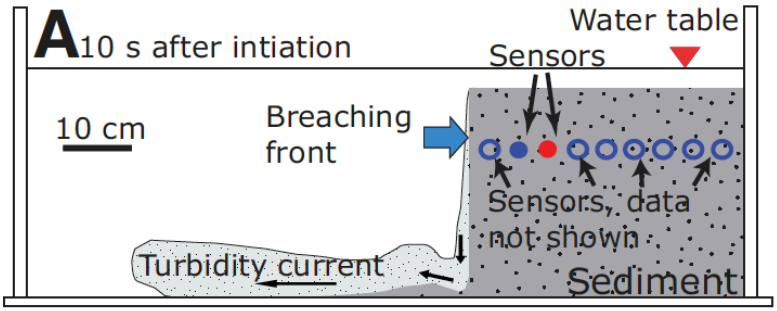

Figure 2- 4: The breaching experiments of You (You et al., 2012)

You (2013) combined lab experiments with mathematical models and concluded that there were two types of dilative failure of a slope. Dual mode slope failure and pure breaching. Pure breaching is characterized by a slow process of releasing sediments from its surface grain by grain, while the dual mode slope failure consists of breaching with at the same time large wedges that slide of the slope. If the pore pressure is not large enough to keep the deposit stable, periodic sliding will occur. A sliding wedge drops the pore pressure more than pure breaching and generates a transient negative excess pore pressure, which stabilizes the deposit temporarily in order to let the slope failure return to breaching again. The transient pore pressure dissipates during breaching and sliding occurs again whenever the transient pore pressure isn't able to keep the deposit stable.

You (2014) investigated this dual mode dilative failure with a geomechanical model. This showed that slope failures occur by periodic switching between sliding and breaching and that the switching between breaching and sliding is caused by the cyclic evolution of excess pore pressure. The negative excess pore pressure dissipates during breaching and this make the deposit more unstable, which results in sliding.
When the sliding door opens (figure 2-5), the sand package tends to become unstable. The underpressure in the sand will increase which keeps the deposit stable. This is the start of a breaching process. The underpressure will decrease when the water flows into the sand. The sand particles will slowly release from the surface of the breach. When the underpressure drops, the sand package will lose its stability and shear starts to play a role. During shearing, dilatancy arises and expands the sand. Due to this, the underpressure will increase, which makes the package stable after sliding wedges. The pore pressure rises until the breachfront passes the pore pressure sensor. Then the pore pressure will be the hydrostatic pressure. Furthermore, when a sliding wedge occurs, the pressure drops a bit. The larger the wedge, the bigger the decrease is.

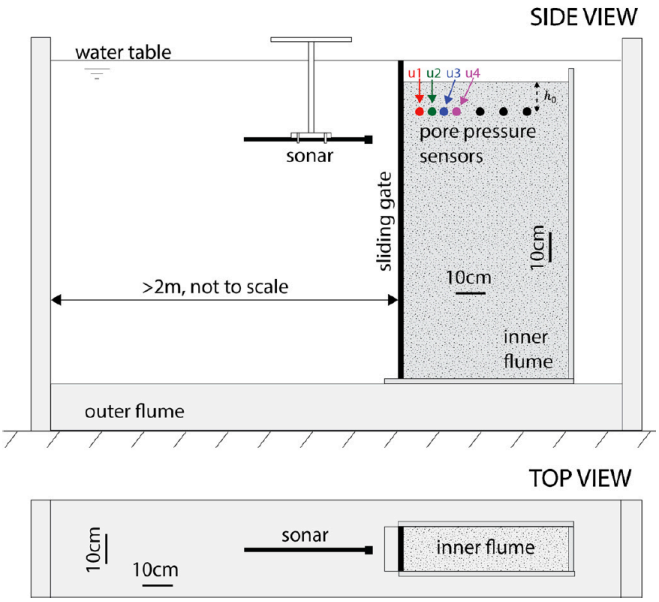

Figure 2- 5: Side and top view of You's experiment (You et al., 2014)

Weij et al. (2016) researched on the subject of unstable breaching. A numerical model was made and was designed to investigate unstable breaching. With the model, it is possible to reproduce stability of a sand body at its internal friction angle. However, the pore pressure feedback has not been implemented into the model yet.

2.4 Type of failures

Hampton (1996) investigated inclined areas of the seafloor and saw that landslides are very common. He concluded that subaqueous landslides can be very enormous and can start on low slopes, where the basic elements of a initiation of a landslide and postfailure behaviour are understood, the timing and the recurrence interval is not so well-known.

Van den Berg (2002) described the difference between two types of failure: liquefaction slope failure and breaching. A sudden liquefaction of a thick layer of sand can initiate large bank failures in clean and fine sands. Breaching however, occurs in compacted sand, where the pore volume increases when there is shear deformation. But in case of liquefaction there is a reduction of pore volumes. For the two types of failure, the post-event morphology is the same, but the sand transportation mechanism and timescales are different.

Hance (2003) gathered all information and data of seafloor slope failures available and analysed them. He found two different groups of mechanisms that triggered the slope failures. The first group is a trigger that reduces the shear strength of the soil (and decreases the resisting force in the slope). The second group increases the driving force in the slope. Both groups of mechanism can happen simultaneously at the same slope failure.

Beinssen et al. (2014) researched the geomorphological processes which are driving the so-called retrogressive breach failures (RBF). RBF are natural events which are the results of unstable breaching. Three pre-conditions for RBF are:

1. Dilatant fine sand, that is densely packed.
2. It's on a subaqueous slope.
3. A mechanism that triggers the start of the breach.

The observations made clear that RBF was mainly caused by the breaching of fine sand, that was relatively densely packed. It was observed that the trigger happens offshore and retrogress towards the shoreline. Sometimes RBF cause significant erosion and damage to shoreline erosion defences.

Van Rhee (2015) came to the conclusion that unstable breaching could result in failure of densely packed slopes, but this was only simulated in a 2DV numerical mixture model using a boundary condition combined with the pickup formula for sand. By adjusting the pickup formula at the sand water interface, the effects of pore pressure feedback are taken into account.
The difference with (Weij, 2016) is that Weij's model is no longer limited to the physical location of a slide in experiments.

Van Rhee and Bezuijen (1998) investigated the breaching of sands in large scale model tests (32m x 1m x 2.5m for the length, width and height, respectively). Afterwards they analysed some physical principles which are important in the breaching process. From field experience it follows that the maximum headwall velocity and production of sand did not only depend on the sand characteristics, but that it also depends on the height and the effects of the density currents. High breaches could lead to gentler slope angles. And over a large distance, this could lead to unstable breaching. This was proved by Van Rhee and Bezuijen with experiments and theory.
They combined equation 13 with the following equation:

$$s = \rho_s * (1 - n_0) * H * v_{headwall} \qquad (14)$$

An equation for the critical slope angle is obtained by combining equation 13 and equation 14:

$$i_{crit} = 0.0049 * [\rho_s * (1 - n_0) * H * v_{headwall}]^{-0.39} * D_{50}^{0.92} \qquad (15)$$

with $i_{crit} = \tan(\alpha_{crit})$. This is the expected angle with a flux based on the headwall velocity at that moment.
This stability criterion, can give an indication whether a slope is sensitive to become an unstable breach (figure 2-6). The resulting angle should be compared to the angle at the top of the breach. When the critical angle is steeper than the angle at the top of the breach, the active breaching height will decrease. This means that the breach is stable. An unstable breach is when the active breaching height increases, thus when the critical angle is shallower than the angle at the top of the breach.

The stability criterion is thus mostly dependent on the breaching height and the headwall velocity (see equation 15) and determines the angle at the toe of the breach.
Validation for the 2DV numerical mixture model (Van Rhee, 2015) is still needed.

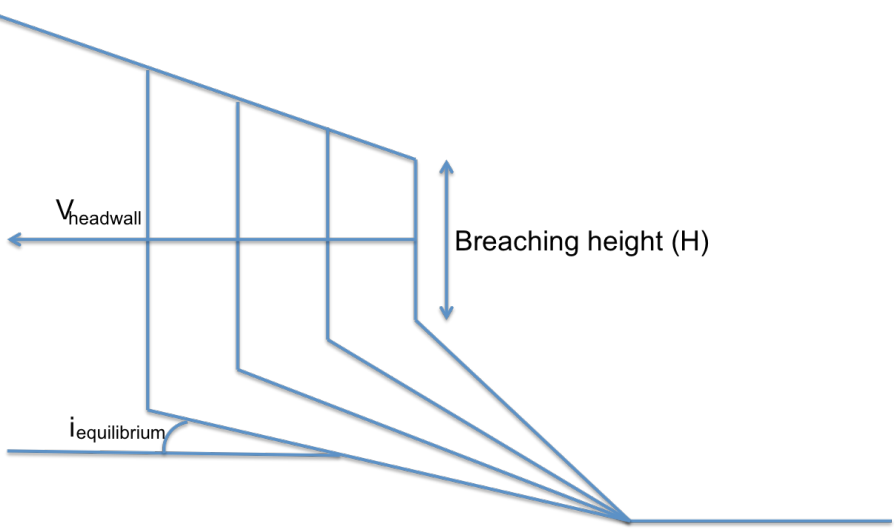

Figure 2- 6: An unstable breach with its important parameters

2.5 Discussion

Van Rhee and Bezuijen (1998) proposed an equation to predict the angle at the toe of a breach, based on two equations for the angle at the toe (equation 13) and the equation for sandflux using the wall velocity (equation 14). Van Rhee (2015) believed this angle can be used to predict the stability of a breach.
Whether this can be combined, has not been proved yet and therefore still needs validation.

They assumed that when this critical angle at the toe is steeper than the angle at the top of the breach, the active breaching height will decrease, thus the breach is stable. And that the breach is unstable if the angle at the top is steeper than the critical angle. This assumption should be validated.

Furthermore, the equation for the angle at the toe (equation 13) has only been tested by Mastbergen and Winterwerp (1988) with sandtypes with a D_{50} of 135μm and 225μm, during the construction of sand fill dams. It is not known whether this equation is also valid for other (coarser) sandtypes and whether it is valid for breaching processes.

It is also not known until what height equation 14 is valid. It is hypothesised that at greater heights, the sliding wedges become more important for determining the wall velocity. However, little is known about the frequency, size and speed of these sliding wedges, and how they influence the wall velocity.

You et al. (2014) attempted to predict the frequency of these sliding wedges, using a numerical model to predict underpressures. This model is interesting, but has only been applied to the experiments of You (2014) until now. The model is evaluated in chapter 6

Based on this, we propose the following to improve our ability to predict unstable breaches:

- Check whether the difference between the critical angle and the slope on top of the breach can be used to predict the stability of breaches.
- Check whether the equation of Mastbergen can be applied to breaches.
- Investigate the frequency of sliding wedges.
- Investigate the relation between sliding wedges and wall velocity.

Earlier experiments all have their limitations. No experiments have been conducted with a slope on top of the breach, so no theoretically unstable breach experiments have been conducted. Furthermore, experiments conducted with pressure sensors were all lined up horizontally, thus no data on the vertical distribution of pore pressure is available. This is important for the validation of pore pressure models. Earlier experiments all had limited breaching heights and did not measure the sliding wedges, its frequency and volume.

In order to attempt validation of equation 15, we propose to do experiments with:
- different breaching heights and heights large enough to observe sliding wedges.
- different slopes on top of the breach

During these experiments we will measure:
- the frequency of the sliding wedges
- the volume of the sliding wedges

3. Laboratory experiments

To answer the research questions various experiments are carried out, with varying initial breaching heights, a slope on top of the breach and differential pressure meters on different locations.
To create a breaching process, a special test setup is designed. It is the intention to record the breaching processes by a video camera. That is why this setup needs glass panels, where the breaching process can be seen, and a door, to hold back the sand-water mixture. To prevent reflection of the turbidity current, a false bottom is placed inside the tank. To prevent the reflection of the turbidity current at the end of the tank a pump is placed to pump away the density mixture to a sedimentation tank. At the end of this sedimentation tank, there is another pump. This can pump back clean water into the tank in order to keep the water level constant in the tank.

3.1 Test setup

Figure 3-1 shows the total test setup with the different subsections. This does not only show how the test setup was placed, but also the directions of the waterflow in the test setup. The following paragraphs will give information about the different parts of the test setup separately.

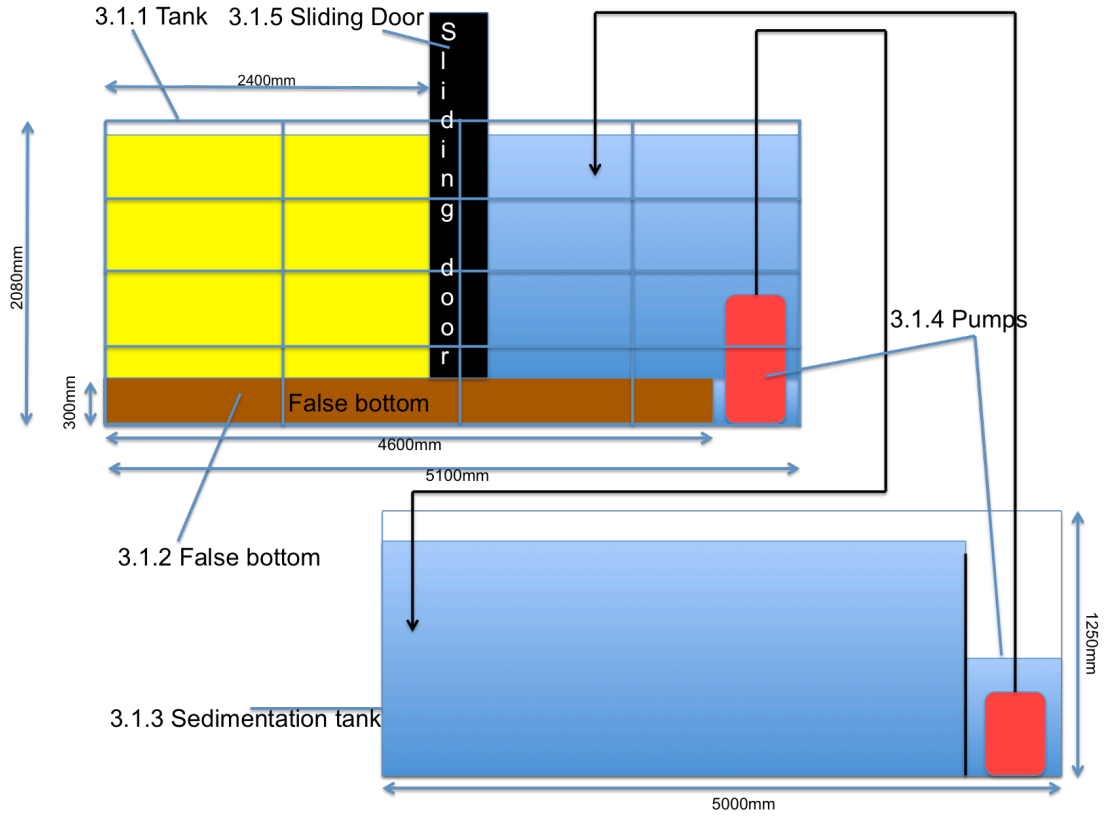

Figure 3- 1: The test setup

3.1.1 Tank

The breaching process takes place in the tank. Before this research, parts are already available to create this tank. There are glass panels and steel panels available. The tank is limited to certain sizes, due to the limited amount and size of the panels and available space. To record the whole breaching process with a camera, it is decided to use the glass panels on one side and the steel panels for the other side. The length of this tank needs to be long enough for the sand to become a density mixture and long enough to let it flow and enough space to form a slope. Also it needs to be high enough to create a breaching process where the relevant processes are present. And to see what the influences are of the height on the wall velocities. Finally it is determined that the optimal size (with the available parts) for the tank is: 5100mm x 500mm x 2080mm for the length, width and height (Figure 3-2)

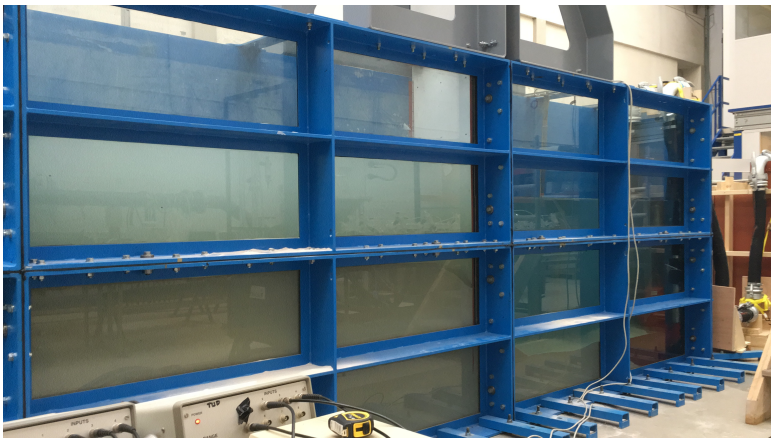

Figure 3- 2: The tank

3.1.2 False bottom

A false bottom (Figure 3-3) is designed to fit into the tank and it has to be long enough for the sand to reach the end of the tank. This false bottom is designed to create a pump sump. The pump can pump all the density mixture away to the sedimentation tank, to prevent the turbidity current from reflecting against the end wall. The false bottom is made with a size of 4600mm x 500mm x 300mm. The pump, with a diameter of 0.4m, fits in the created pump sump.

Figure 3- 3: The false bottom

3.1.3 Sedimentation tank

A sedimentation tank is needed to let the sand-water mixture settle, so that clean water can be reused and pumped back into the tank. Concrete plywood is chosen as construction material for the sedimentation tank (figure 3-4).

The reason for choosing concrete plywood is its watertightness, thanks to its epoxy layer and its high strength to weight ratio. Concrete plywood has a standard dimension of 2500mm x 1250mm. As a result of these standard measurements and the calculations of the particle settling velocity (Choi, 2017), the sedimentation tank dimensions are 5000mm x 1250mm x 1250mm for the length, width and height respectively. The sedimentation tank has to be divided in two parts by a barrier (also concrete plywood). The first part is where the sand-water mixture enters and settles. The second part is where the water can overflow, so that only 'clean' water will be pumped back into the tank. The outside of the sedimentation tank is strengthened with wooden beams.

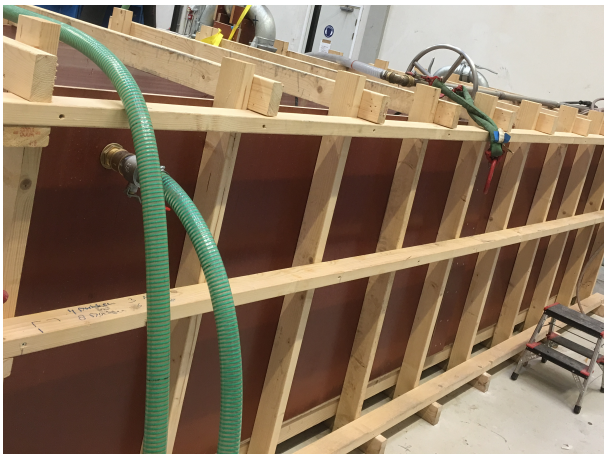

Figure 3- 4: The sedimentation tank

3.1.4 Pumps

A sand-water mixture pump (Grindex Bravo 200) pumps the sand-water mixture from the experimentation tank to the sedimentation tank. Simultaneously a sludge pump (Flygt 2640.180) pumps clean water back into the experimentation tank. See appendix J for the pump details.

3.1.5 Sliding door

In the middle of the tank, a sliding door is required to hold back the sand. The door has to be able to slide up. However, all this sand requires a strong door that is able to hold the sand package. Based on structural calculations, a sliding door is made that is able to slide up and down, without bending. To create a seal with the side of the tank, rubber flaps are fixed to the sides of the door. It takes approximately 5 seconds on average to fully lift the sliding door.

Figure 3- 5: The sliding door

3.2 Measuring devices

To record the data from all the experiments, various sensors are needed. Differential pressure meters and conductivity meters were used. The following sections provide information on instrumentation.

3.2.1 Differential pressure meter

Differential pressure (DP) meters were used during the experiments. A DP meter can measure the difference in pressure between two points, in this case a pressure point and a reference point with a known pressure. The reference point is placed inside the water of the experimentation tank and thus measures the hydrostatic pressure. The pressure points are at the side of the experimentation tank with the steel panels. Holes are made in the steel panels to connect the pressure taps (see appendix I). This way, the DP meters can measure the pressure difference between the hydrostatic pressure and the pore pressure inside the sand.
DP meters measure the pressure via the deflection of a membrane, this deflection is translated into voltage by the meter. Before the experiments the meters were calibrated, which resulted in formulae to convert voltage to pressure difference (Appendix K).
The experiments have different reference points, some of the experiments have a reference point outside of the water of the breaching tank, in a watercup above the tank. This means that when the waterlevel drops, this will affect the outcome of the DP meters. In these experiments, it is not clear from the data when the DP meters are out of the sandpackage and thus only measuring hydrostatic pressure (figure 3-6). In these experiments (experiment 3, 4 and 5), the use of the video data is required to see exactly when breaching front passes the DP meters.

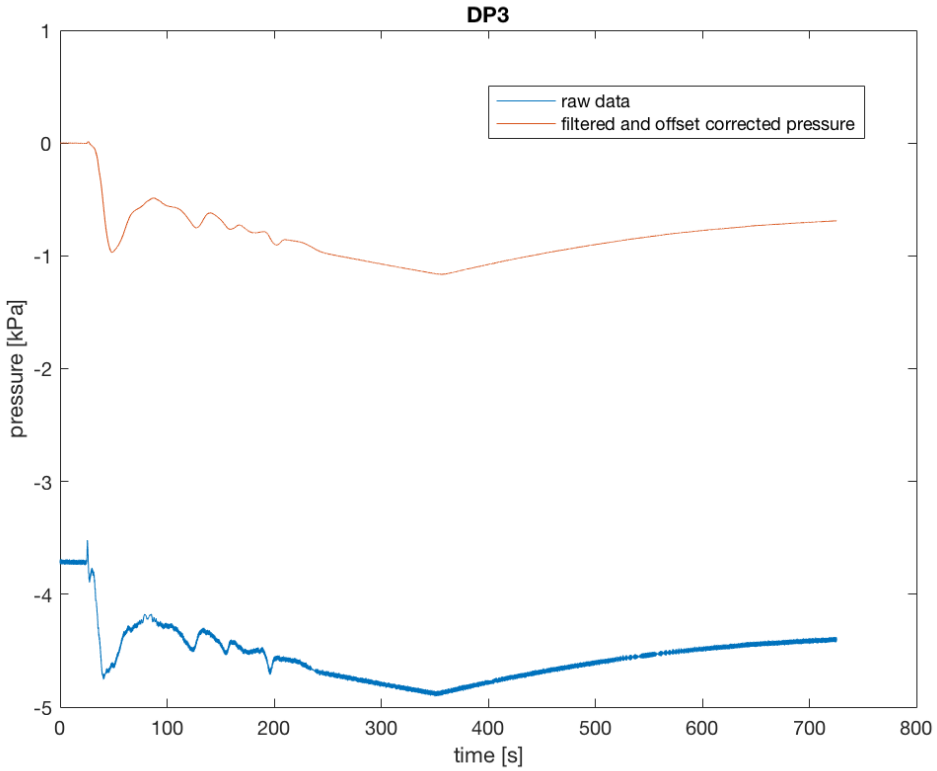

Figure 3- 6: Pressure registration with reference outside the breaching tank.

The biggest problem is that we want to know the underpressure relative to the hydrostatic pressure, but not in all of our experiments, the reference point was inside the water in the tank.
In the other experiments, the reference point was inside the water of the breaching tank. This way it measures the difference between the hydrostatic pressure with a fixed pressure and therefore the waterlevel does not affect the outcome of the DP meters.

Some of the pressure meters give unexpected data, see figure 3-7. This is probably due to some sand in the polyflex hoses. These are connected with a pressure tap in the water first. Then it is closed off and sand is added to the water side. Those pressure results (like figure 3-7) are not included in the results and analysis.

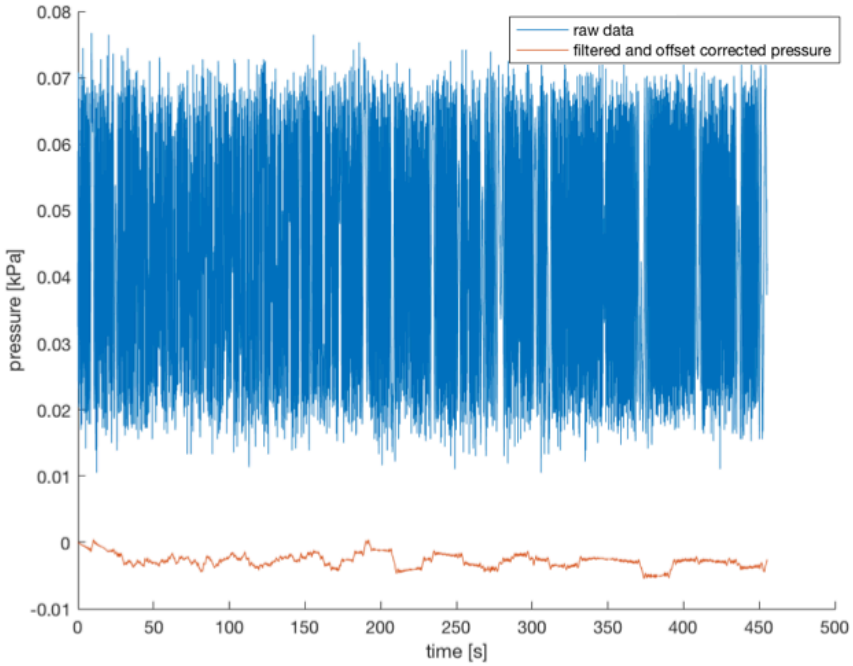

Figure 3- 7: Wrong pressure registration

3.2.2 Conductivity meter

Two conductivity meters (Figure 3-8) were used in the tank. Each conductivity meter consists of ten sensors. The spacing between these sensors is 4 cm. The two meters were both placed (Figure 3-9) after the sliding door to measure the density and height of the density current.
A conductivity sensor consists of two points and the conductivity is measured between those two point. This gives a voltage, which is converted into the concentration. Calibration of the conductivity meters by Noordermeer (2017) led to formulas to convert the voltage into concentration. The higher the conductivity, the lower the concentration of the sand in the water. Because the conductivity of water is much higher than the conductivity of sand, an increase in sand concentration leads to a reduction in conductivity.

Figure 3- 8: Conductivity meter

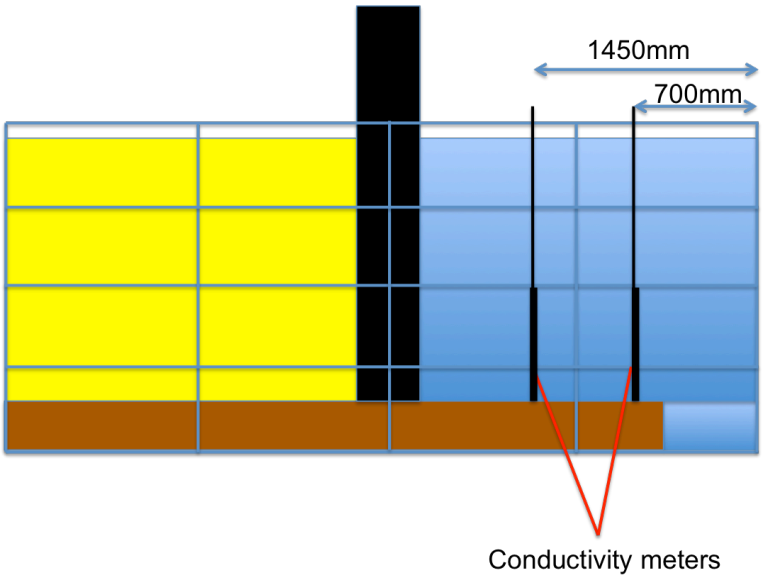

Figure 3- 9: Placement of conductivity meters

3.2.3 High definition video camera

A Go Pro Hero 3 camera is used to record every experiment. The used settings during recording are: 16x9w with 25 frames per second. The camera is placed two meters from the middle of the tank at a height of 1 meter. The Go Pro camera has a fisheye lens. This is removed in the videos on the computer using Go Pro Studios.

3.3 Test procedure

The whole tank is first filled with water. After that the DP meters are vented, because when there is air inside, it affects the outcome of the DP meters. This has to be done before the tank is filled with sand. Afterwards the left side of the tank is filled with several layers of sand. To densify the sand and to make sure there will not be any air inside the sand package, a vibrating needle (with a diameter of 45mm and length of 1 meter, see Appendix M) is used at 1/4, 1/2, 3/4 and at full height. To avoid damaging the glass, the vibrating needle was not used too close to the glass panels, which might affect the final density of the sand here.
Before an experiment starts, it is necessary to make sure no sand would flow along the door. This happens when the rubber flaps, folds to the wrong side, which causes sand to flow along the sliding door. Also the conductivity meters start and are put inside the water, on both sides of the door, to see if it works correctly, for an extra calibration and for a zero measurement.
The camera, the pumps and the measurement tools are started before the sliding door is lifted and the breaching process starts.

3.4 Test parameters

Several parameters are varied to help answering the research question: the breaching height, the slope above the breach and the sand type. The breaching height and sandtypes are varied, because those affect the critical angle (equation 11). Breaching processes that are done with sandtypes with larger particle size distributions will, according to equation 11, result in a larger critical angle.
The experiments are done with two different types of sand, the GEBA Weiss with D_{50} of 103µm and Dorsilit 9 with D_{50} of 330µm (see Appendix L).
There are different starting heights of the breach. Three different heights are used, based on the limitations of the test setup.
The last variable is the slope above the breach (figure 3-10) varying between 0, 20 and 30 degrees. These values are chosen to create an unstable breach by letting the breaching height increase during the breaching process. An angle larger than 30 degrees was not feasible due to the internal friction angle being around 35-40 degrees. A slope above the breach means that the breachfront would increase, which is an important characteristic for unstable breaches. In the end, sixteen experiments are conducted in total. Table 1 shows the experiments that are conducted and what the starting conditions

are in those experiments. Table 2 shows the different placements of the DP sensors per experiment. The DP sensors are placed on different locations per experiment.

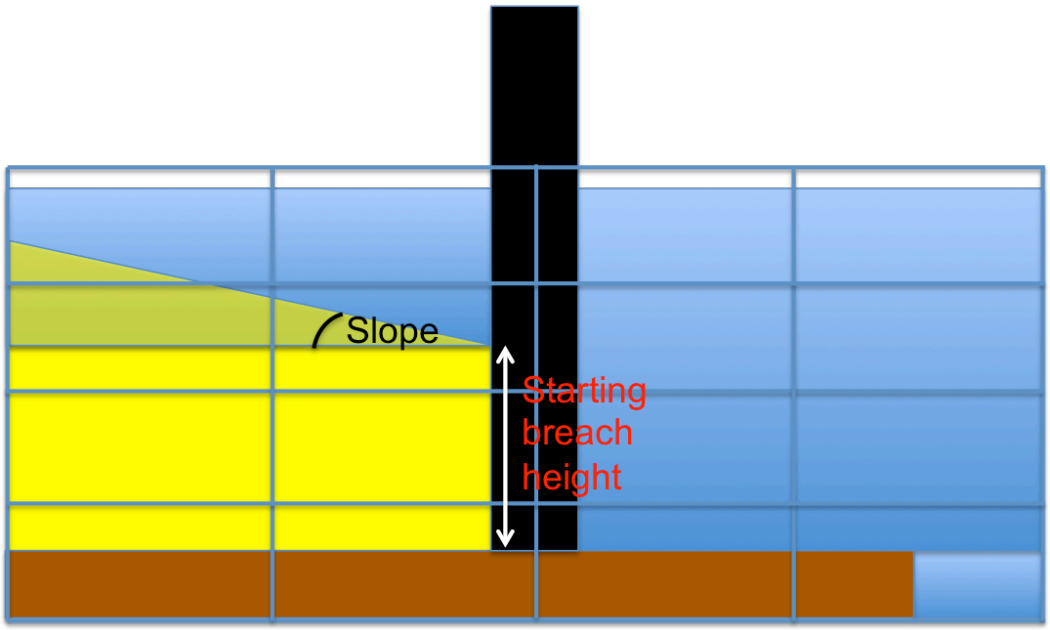

Figure 3- 10: Slope and starting breach height

Experiment	Sand type	Starting breach height [m]	Slope [deg]
1	GEBA Weiss	0.655	0
2	GEBA Weiss	0.655	0
3	GEBA Weiss	0.655	0
4	GEBA Weiss	1.17	0
5	GEBA Weiss	1.17	0
6	GEBA Weiss	1.17	0
7	GEBA Weiss	1.17	20
8	GEBA Weiss	1.47	0
9	GEBA Weiss	1.17	30
10	GEBA Weiss	1.47	0
11	GEBA Weiss	1.17	30
12	GEBA Weiss	1.17	20
13	Dorsilit 9	0.655	0
14	Dorsilit 9	1.17	0
15	Dorsilit 9	1.17	30
16	Dorsilit 9	1.47	0

Table 1: The experiments

The location of the pressure taps of the DP meters is different in every experiment. Figure 3-11 shows all the different locations of the pressure taps of the DP sensors.

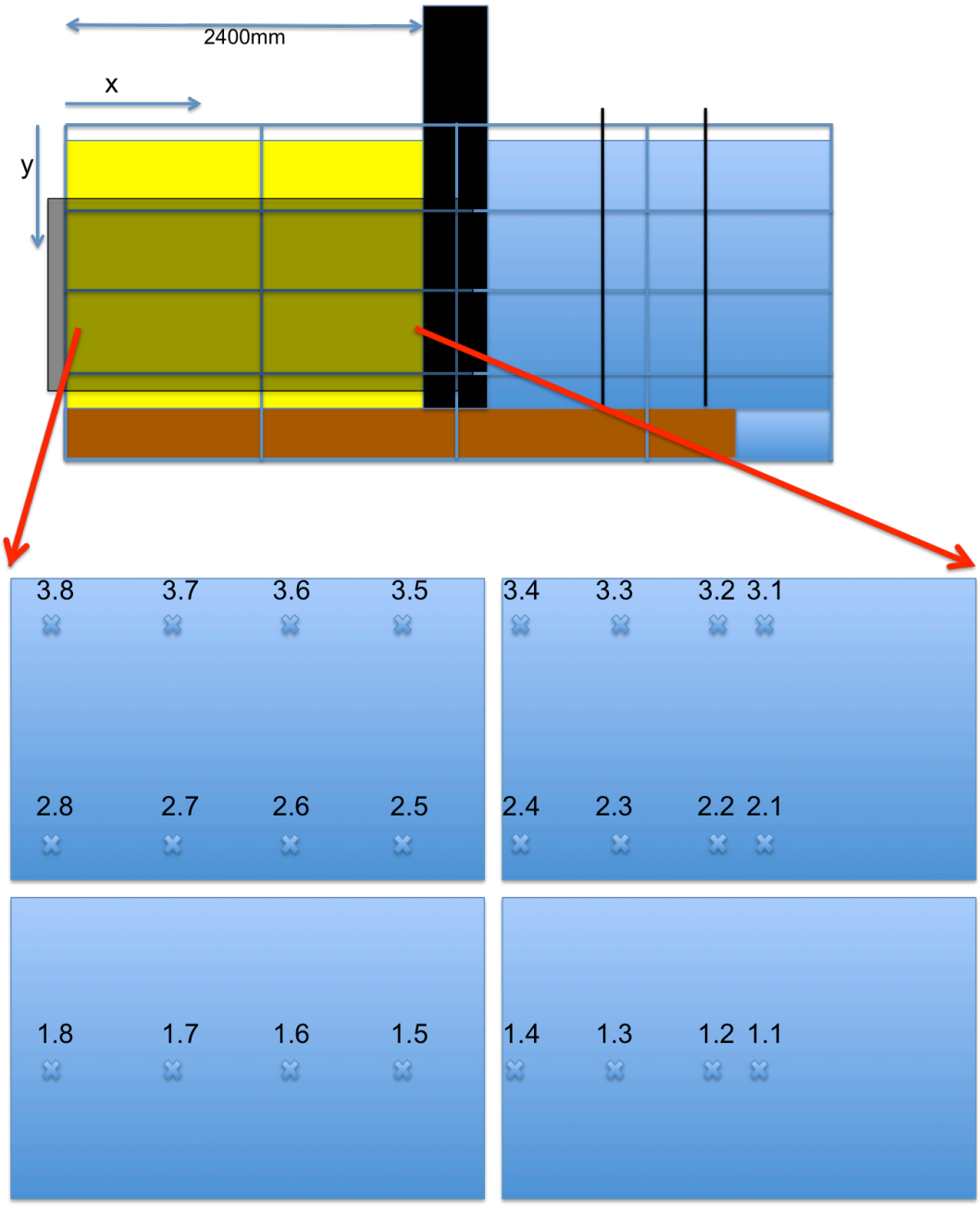

Figure 3- 11: Locations of the pressure taps

The pressure taps are numbered and in Table 2 the coordinates are given in millimeters, where x and y start at the left upper corner of the tank.

x-coordinates y-coordinates	200	500	800	1100	1400	1600	1800	1900
635	3.8	3.7	3.6	3.5	3.4	3.3	3.2	3.1
935	2.8	2.7	2.6	2.5	2.4	2.3	2.2	2.1
1385	1.8	1.7	1.6	1,5	1.4	1.3	1.2	1.1

Table 2: Coordinates of pressure taps for the DP sensors [mm]

Experiment	DP1	DP2	DP3	DP4	DP5	DP6	DP7	DP8	DP9
1	1.1	1.2	1.3	1.4	1.5	1.6	-	-	-
2	1.1	1.2	1.3	1.4	1.5	1.6	-	-	-
3	1.1	1.2	1.3	1.4	1.5	1.6	-	-	-
4	1.1	1.2	2.1	2.2	2.3	3.1	3.2	-	-
5	1.1	1.2	2.1	2.2	2.3	3.1	3.2	-	-
6	1.1	1.2	2.1	2.2	2.3	3.1	3.2	-	-
7	1.1	1.2	1.3	2.1	2.2	2.3	2.4	-	-
8	1.1	1.2	1.3	2.1	2.2	2.3	3.1	-	-
9	1.1	1.2	1.3	2.1	2.2	2.3	3.3	-	-
10	2.3	2.4	3.1	3.2	3.3	3.4	3.5	-	-
11	1.1	1.2	1.3	2.1	2.2	2.3	2.4	3.4	3.5
12	1.1	1.2	1.3	2.2	2.3	2.4	2.5	3.6	3.7
13	1.1	1.2	1.3	1.4	1.5	1.6	1.7	1.8	ref
14	1.1	1.2	1.3	1.4	1.5	2.1	2.2	2.3	2.4
15	1.1	1.2	1.3	2.1	2.2	2.3	3.3	3.4	3.5
16	1.1	1.2	1.3	2.1	2.2	2.3	3.1	3.2	3.3

Table 3: Connection of the DP sensors to the pressure taps per experiment

3.5 Video analysis

Video data is recorded using a high definition camera. The video data is used to take screenshots which are used to determine the wall velocities, headwall velocities, sliding wedges, breaching angles and the angles at the toe of the breach. For every experiment, eight time instances are selected. Screenshots are taken and processed in Matlab. This leads to eight profiles (figure 3-12). Between these time instances an average wall velocity, an average headwall velocity, the angle at the toe, breaching angle and the active breaching height are calculated. For the average headwall velocity, screenshots are also needed after a sliding wedge and before the next sliding wedge. The breaching fronts of these eight time instances are saved and these can be used for future references. Figure 3-12 shows the breaching fronts of a stable breach and figure 3-13 shows the breaching fronts of an unstable breach. The rest of the breaching fronts can be found in Appendix E.

For the calculation of wall velocities two screenshots are captured with the time known between the screenshots. Then the difference over the whole length is taken and divided by the height, this results in an average wall velocity between the time of the two screenshots. With these screenshots, a corresponding breaching angle and angle at the toe can be obtained in Matlab.

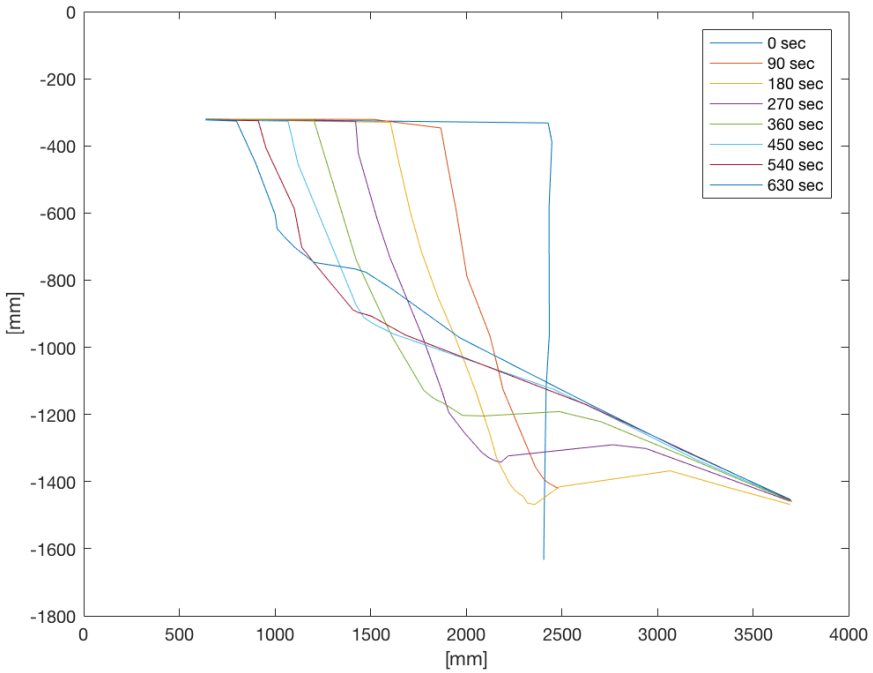

Figure 3- 12: Profiles of the stable breaching fronts at eight different instances

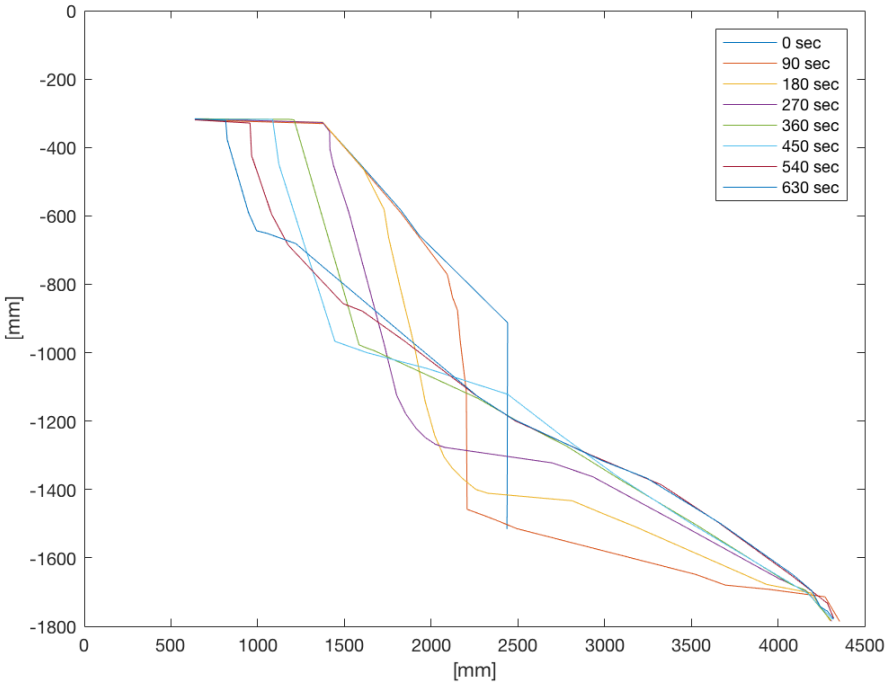

Figure 3- 13: Profiles of the unstable breaching fronts at eight different instances

4. Results

The results of the experiments are presented in this chapter. It is divided into the following sections: sliding wedges, wall velocities, headwall velocities, underpressure, breaching angle, angle at the toe and the breaching height. As mentioned before in chapter 2, these affect the critical angle and the critical angle determines whether a breach is stable or unstable.
In chapter 4 only the test results will be discussed, chapter 5 contains further analysis.

Experiment	Sand type	Starting breach height [m]	Slope [deg]	Duration [sec]	n0
1	GEBA Weiss	0.655	0	180	0.415
2	GEBA Weiss	0.655	0	240	0.415
3	GEBA Weiss	0.655	0	270	0.415
4	GEBA Weiss	1.17	0	465	0.415
5	GEBA Weiss	1.17	0	600	0.415
6	GEBA Weiss	1.17	0	480	0.415
7	GEBA Weiss	1.17	20	600	0.415
8	GEBA Weiss	1.47	0	720	0.415
9	GEBA Weiss	1.17	30	780	0.415
10	GEBA Weiss	1.47	0	830	0.415
11	GEBA Weiss	0.655	30	600	0.415
12	GEBA Weiss	1.17	20	510	0.415
13	Dorsilit 9	0.655	0	55	0.43
14	Dorsilit 9	1.17	0	120	0.43
15	Dorsilit 9	1.17	30	120	0.43
16	Dorsilit 9	1.47	0	135	0.43

Table 4: The results of the experiments with the duration and the n0

The experiments are started by lifting the door. It starts with a vertical wall of 90° and an angle at the toe of 0°. The underpressures are measured during the whole experiment.

An example of the results of one experiment are given here. For example, experiment 8 (the starting conditions of all experiments can be found in table 4). The angle at the toe of the breach starts at 0°, while the breaching angle starts at 90°. The angle at the toe will slowly increase, while the breaching angle decreases (table 5). Figure 4-1 shows the headwall velocities, wall velocities and the sliding wedges of experiment 8. It starts of with a wall velocity of approximately 3.5mm/s and it slowly decreases. The headwall velocity and wall velocity become the same, the moment when the sliding wedges stop occurring.

Experiment 8	Breaching angle [deg]	Angle at the toe [deg]
0	90	0
90 sec	69.8501	12.85
180 sec	67.2189	7.76
270 sec	57.9513	13.26
360 sec	63.6867	16.2
450 sec	61.4557	17.03
540 sec	61.9036	17.12
630 sec	66.7171	17.21

Table 5: The breaching angle and angle at the toe of experiment 8.

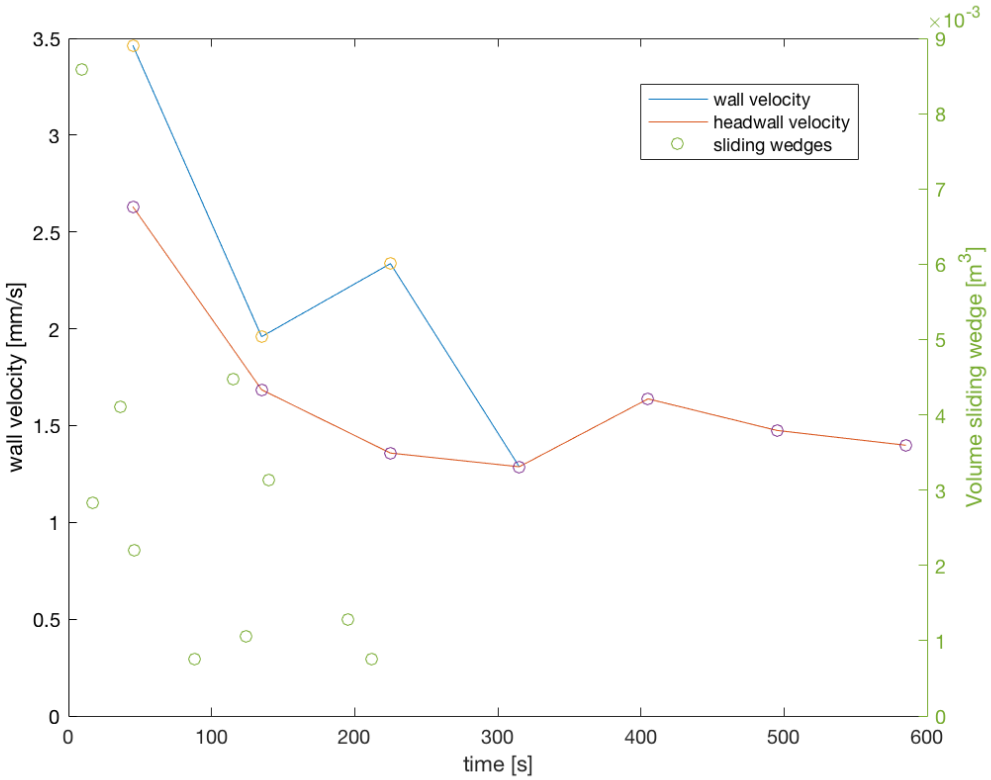

Figure 4- 1: Headwall velocity, wall velocity and sliding wedges of experiment 8. Plotted velocities are averaged over 90 second intervals.

4.1 Sliding wedges

The sliding wedges are observed in the videos and the screenshots before and after are processed in Matlab to determine the volume of the wedges. Two different sand types are used and they will be treated separately in this chapter.

4.1.1 Geba Weiss, no slopes

The wedges are observed in the videos, the time instances are noted and the volumes of the wedges are calculated in Matlab. Screenshot are taken, one for every second of the videos of the experiments. The results of the sliding wedges are divided between sand type and initial breaching height. The results from experiments with lowest initial height (0.655m) are plotted in Figure 4-2. A descending trend is visible.

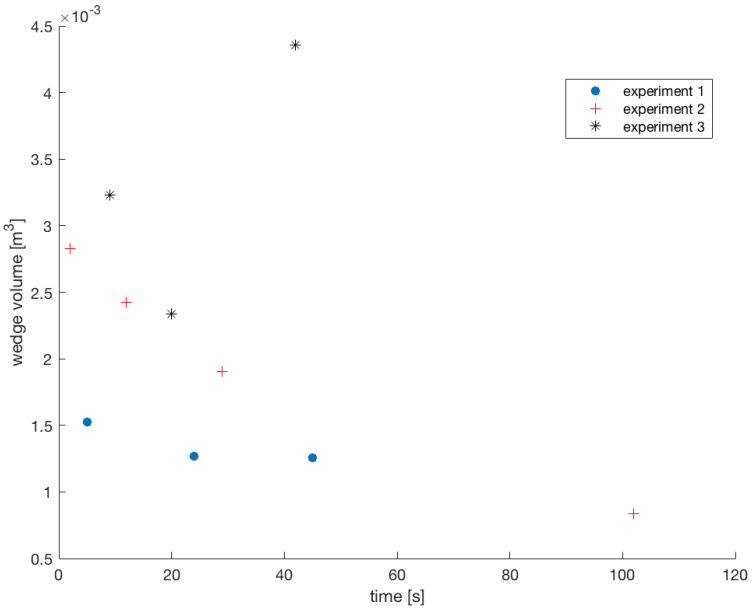

Figure 4- 2: Wedge volume versus time (experiments with initial height of 0.655m, Geba Weiss)

The experiments with an initial height of 1.17m are plotted in Figure 4-3. Another descending trend is visible in this plot. However the experiments take longer and contain more sliding wedges. The experiments almost take three times longer and also almost triples the amount of sliding wedges compared to the experiments with an initial height of 0.65m

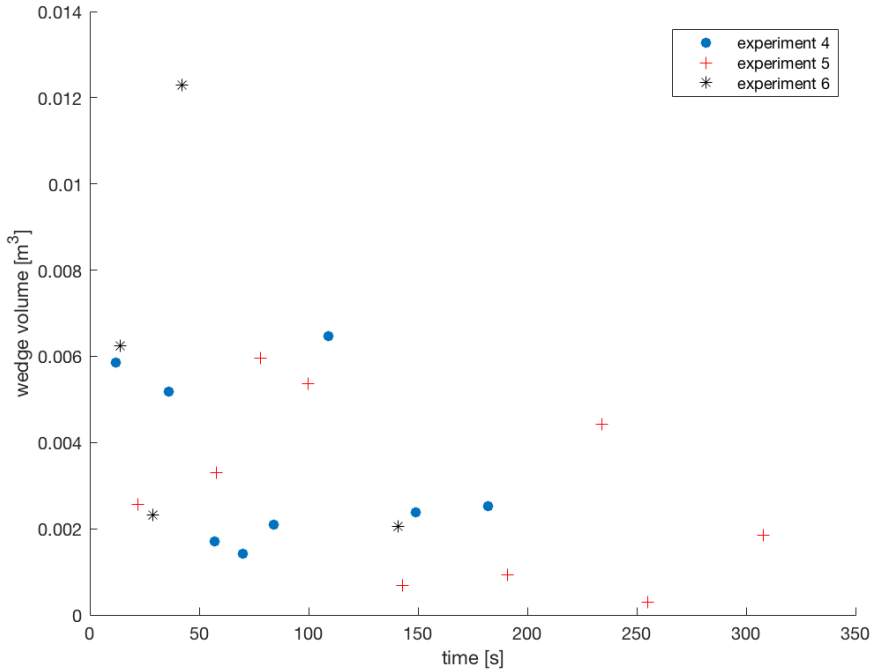

Figure 4- 3: Wedge volume versus time (experiments with initial height of 1.17m, Geba Weiss)

The wedges of experiments with 1.47m initial breaching heights are larger (almost twice the size) on average than the experiments with a lower initial height. A descending trend in time can be seen (Figure 4-4).

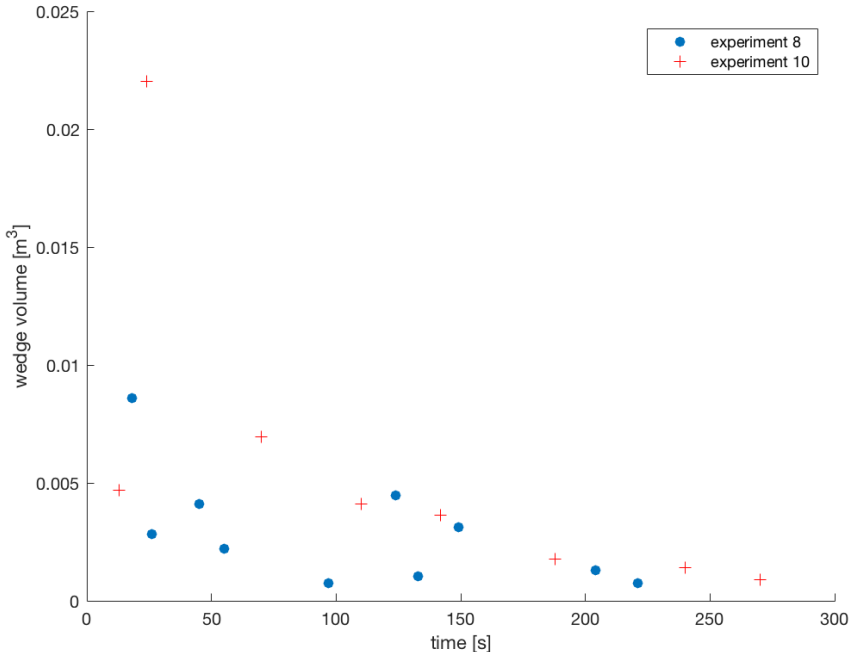

Figure 4- 4: Wedge volume versus time (experiments with initial height of 1.47m, Geba Weiss)

4.1.2 Geba Weiss, with slopes

A same descending trend in time can be noticed for the Geba Weiss experiments with a slope of 20 degrees on top (figure 4-5). The sliding wedges are smaller than the experiments without slopes at the same initial breaching heights (1.17m).

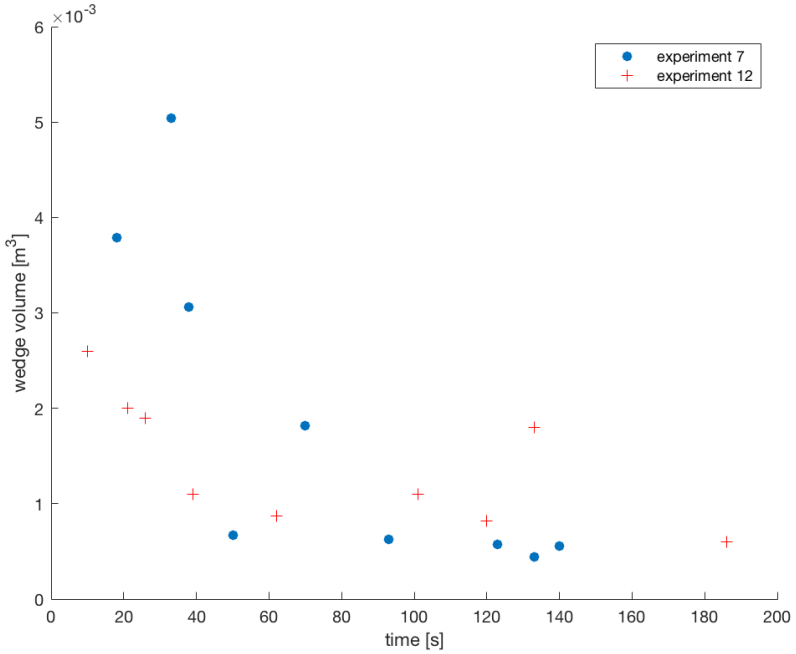

Figure 4- 5: Wedge volume versus time (20deg, Geba Weiss)

The total volumes of the wedges are slightly larger with the experiments with a slope of 30 degrees ($0.039m^3$) than the experiments with a slope of 20 degrees ($0.029m^3$) (figure 4-6). Again, a descending trend is noticeable in time.

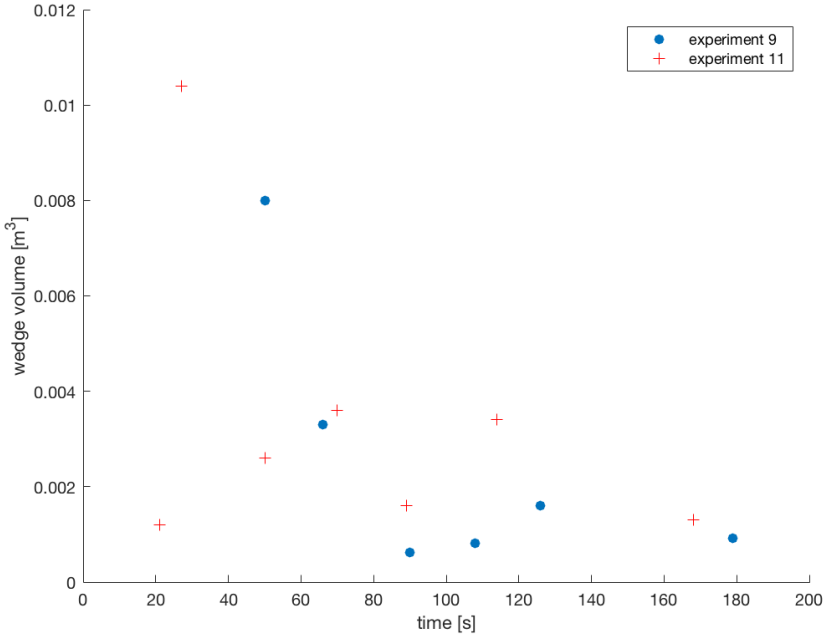

Figure 4- 6: Wedge volume versus time (30deg, Geba Weiss)

4.1.3 Dorsilit 9

Four different experiments are conducted with Dorsilit 9. These are shown together in figure 4-7 These experiments are faster than the Geba Weiss experiments. An experiment of Dorsilit 9 takes 2 minutes approximately, while Geba Weiss experiments have an average duration of 7 minutes. There were only sliding wedges in the first 24 seconds of Dorsilit 9 experiments.

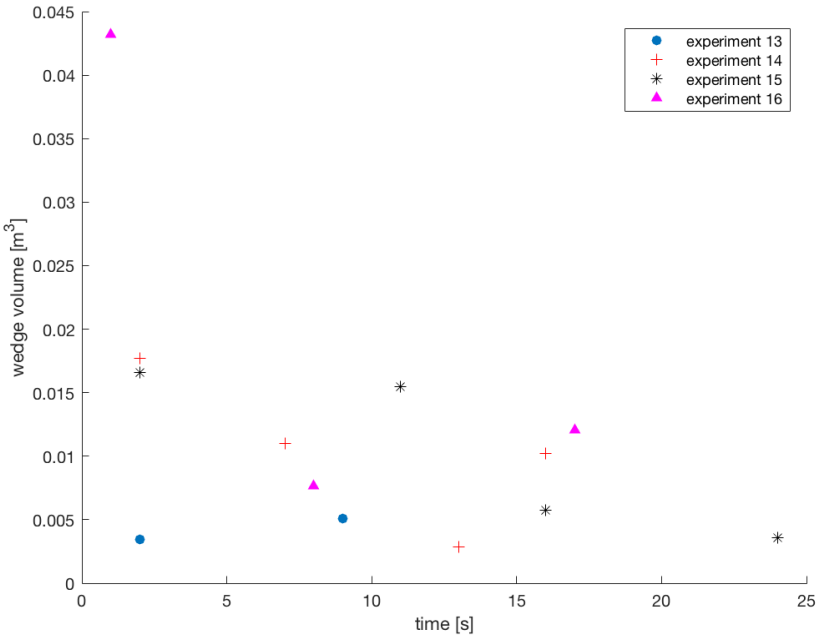

Figure 4- 7: Wedge volume versus time (Dorsilit 9)

4.2 Wall velocities

The average wall velocity during an interval is determined with Matlab. The results are divided between sand types and initial breaching heights.
The wall velocities of the first three experiments are shown in figure 4- 8. The wall velocity usually starts with the highest velocity and slowly decreases, however this is not the case in experiment 3. This has to do with a big sliding wedge that occurs, which causes the velocity to increase after 30 seconds before the velocity slowly decreases again. The velocity plots do not look smooth, because the points indicate the average wall velocity over time intervals of 30, 60 or 90 seconds, depending on the experiment.

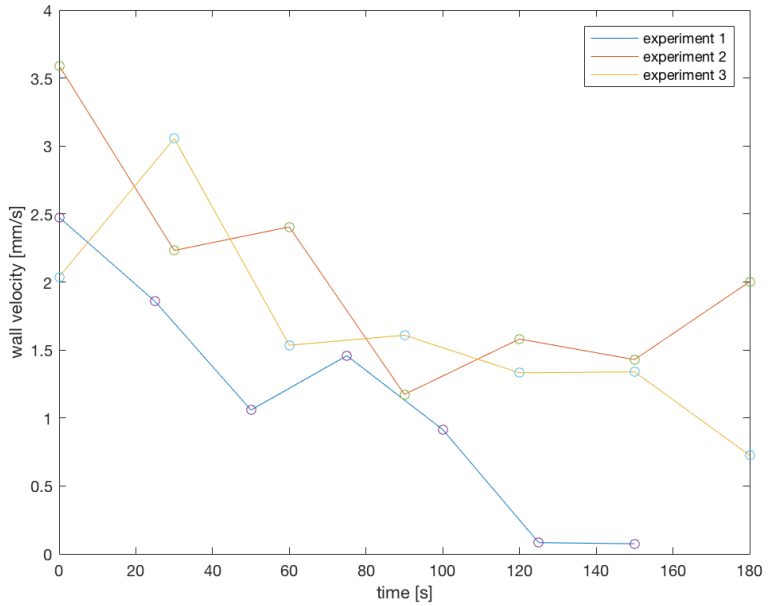

Figure 4- 8: Wall velocities (initial height = 0.655m). The dots are the calculated value from the experiments.

In figure 4- 9 the experiments with an initial height of 1.17m are shown. Like in the experiments with an initial height of 0.65m, they start with a high wall velocity and slowly decrease as time passes. However, the wall velocities here are higher than those of the experiments with an initial height of 0.655m.

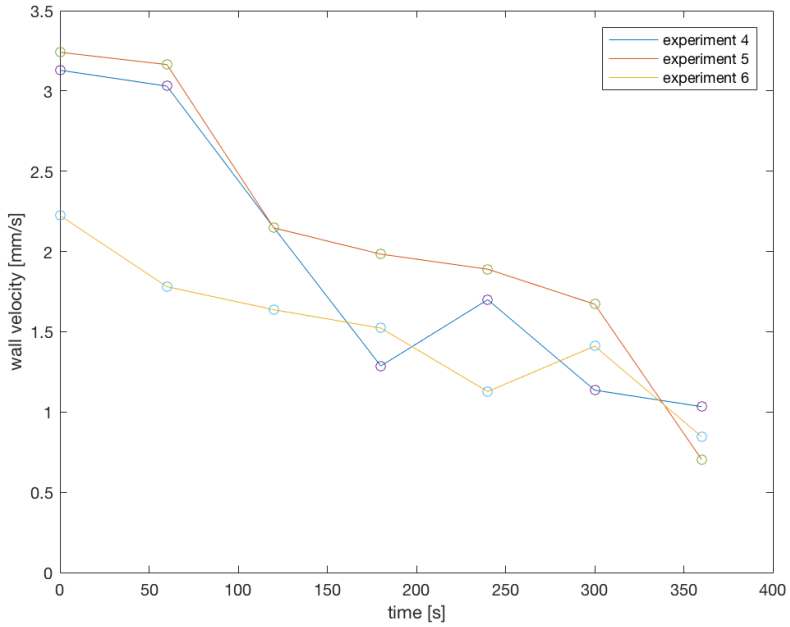

Figure 4- 9: Wall velocities (initial height = 1.17m)

The experiments with initial height 1.47m are shown in figure 4-10. These experiments take longer than the experiments discussed above. The durations of these experiments are almost three times longer than those of the experiments with initial heights of 0.655m. Furthermore, the wall velocities are higher than in both experiments with initial breaching height 0.655m and 1.17m.

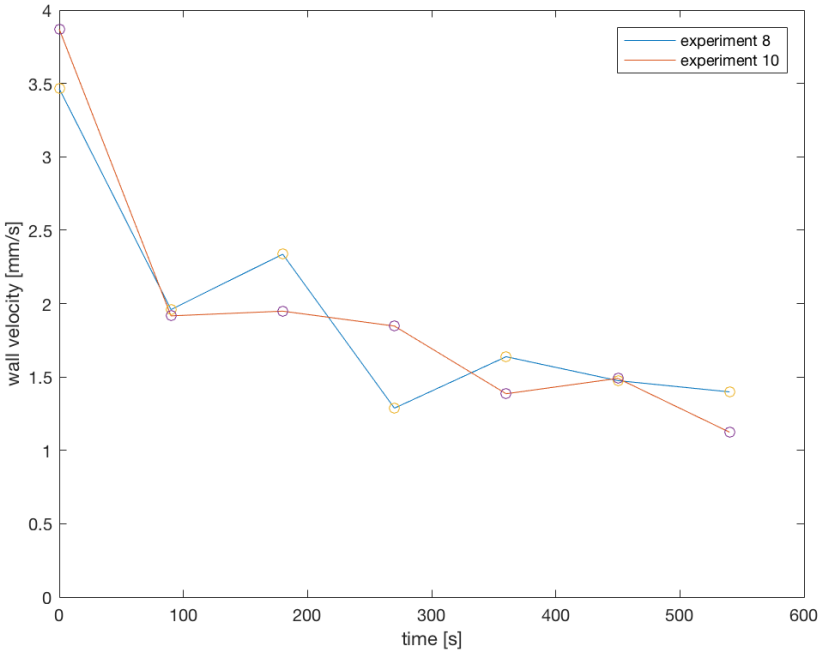

Figure 4- 10: Wall velocities (initial height = 1.47m)

4.3 Headwall velocities

The difference between wall velocities and headwall velocities are the sliding wedges. Headwall velocities is used for pure breaching, while the wall velocity is used to describe pure breaching combined with sliding wedges.
Sliding wedges increase the headwall velocity and this difference results in the wall velocity. The equation for the headwall velocity does not take the effect of sliding wedges into account. The wall velocity is the velocity where the effect of sliding wedges is taken into account.
Headwall velocities are lower than the wall velocities, especially during the beginning of an experiment, when bigger volumes of sliding wedges are occurring.
The difference between the headwall velocity and wall velocity can be seen in Table 6. The rest of the results can be found in Appendix A.

Experiment 1			
Time [s]	Headwall velocity [mm/s]	Wall velocity [mm/s]	Total volume wedge [m^3]
0-25 sec	2.104	2.476	0.00283
25-50 sec	1.694	1.857	0.00125
50-75 sec	1.059	1.059	-
75-100 sec	1.458	1.458	-
100-125 sec	0.914	0.914	-
125-150 sec	0.0833	0.0833	-
150-175 sec	0.075	0.075	-

Table 6: Headwall velocity vs wall velocity (experiment 1)

4.4 Breaching angle & angle at the toe of the breach

The breaching angle is always 90° at the start, because of the sliding door. And the angle at the toe of the breach starts at 0° (figure 4-11).
A trend is visible in both the breaching angles and angle at the toe. The breaching angle decreases in time, while the angle at the toe increases in time. A result of experiment 4 is shown in table 7. It can be seen that the breaching angle drops rapidly at the beginning, after that it slowly drops over time. The angle at the toe rises slowly. The end of the experiment can not be seen in this table, because after the last time step, some parts of the breach are not visible, due to the steel frame.
The results of the other experiments can be found in Appendix D.

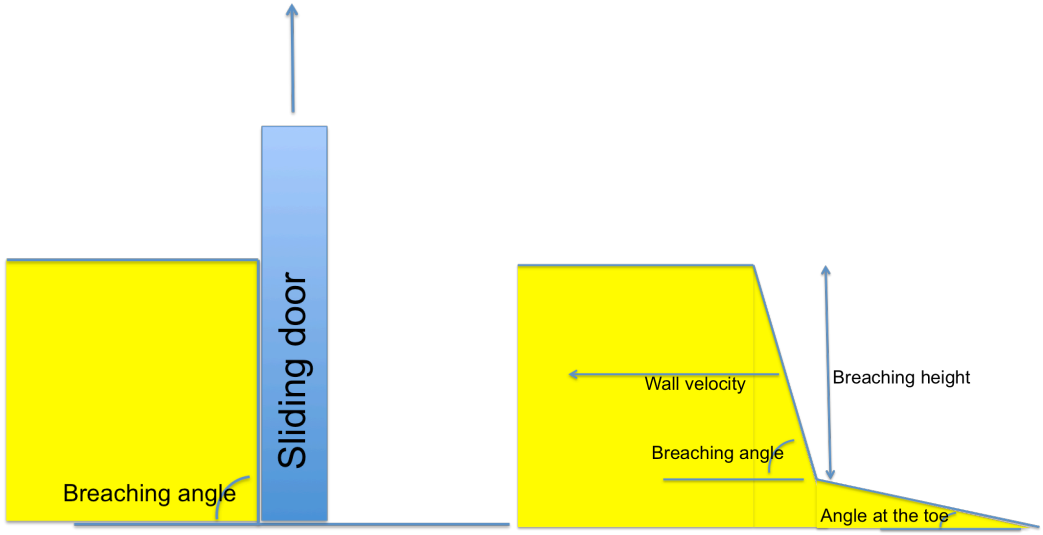

Figure 4- 11: The start of the breach and the breaching process

Experiment 4	Breaching angle [deg]	Angle at the toe [deg]
0 sec	90	0
60 sec	75.86	8.66
120 sec	57.84	5.05
180 sec	55.58	8.59
240 sec	52.01	12.69
300 sec	52.73	12.98
360 sec	49.19	21.85
420 sec	44.53	26.57

Table 7: Breaching angle and angle at the toe versus the time (experiment 4)

4.5 Underpressures in the breach

The underpressure is measured between two points: a pressure point and a reference point. The reference point is placed inside the water of the experiment. The DP meters can measure the pressure difference between the water and the sand-water mixture.

Labview starts recording before the door is opened to include reference conditions. The data before the moment of opening the door is not discarded. This data is used to correct for the offset of the pressure meters. However, the real breaching process starts when the sliding door is opened.
The data is recorded with a sample rate of 10 Hz. This results in a large number of raw data (Figure 4-12). Knowing that the underpressure starts approximately at 0 kPa, the data is corrected for its offset by averaging the first 50 seconds. The raw data minus the average value of the first 50 seconds results into the data starting at approximately 0 kPa. Afterwards, the data is filtered using a moving average of 10 seconds.

The sliding door opens at approximately 80-90 seconds. This corresponds to a big drop in underpressure in the measurements.

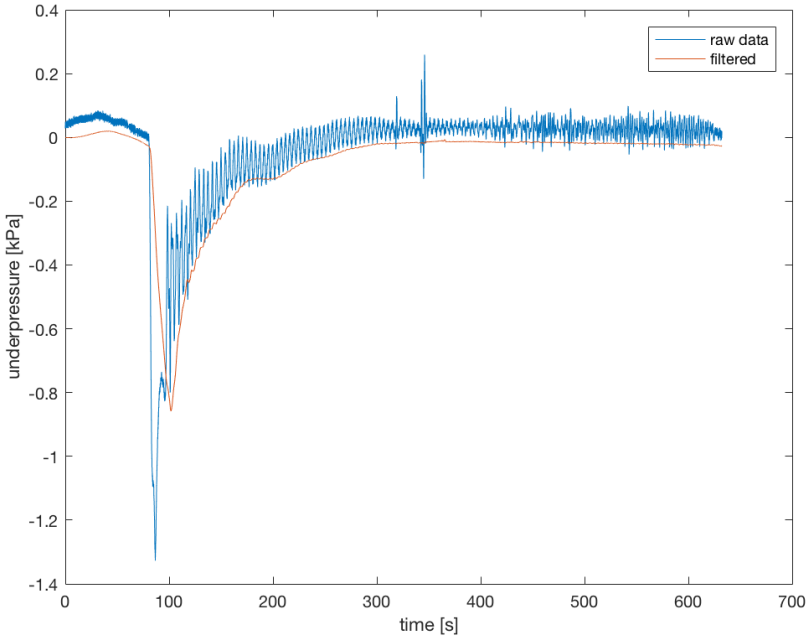

Figure 4- 12: Filtered and offset corrected pressure versus unfiltered pressure

The underpressure in the experiments behaves like expected: after the door opens, the underpressure rises. After that it slowly decreases until the pressure sensor reaches the waterlevel, this means that the sand has breached away. Then the underpressure converges to the hydrostatic pressure level.
According to literature (You, et al., 2014) a sliding wedge results in drop of the underpressure, but in our experiments the wedges that occurred, are not always visible in the underpressure plots.

4.6 Breaching height

The breaching height is an important parameter in the determination of a stable or unstable breach. If the breach is unstable, the breaching height increases during the breaching process.
The breaching height plotted against the time is shown in figure 4-13
Figure 4-14 shows an unstable breach. Between 30 and 45 seconds, the breaching height increases, which is a characteristic for an unstable breach.

Appendix N shows the breaching height for all the other experiments.

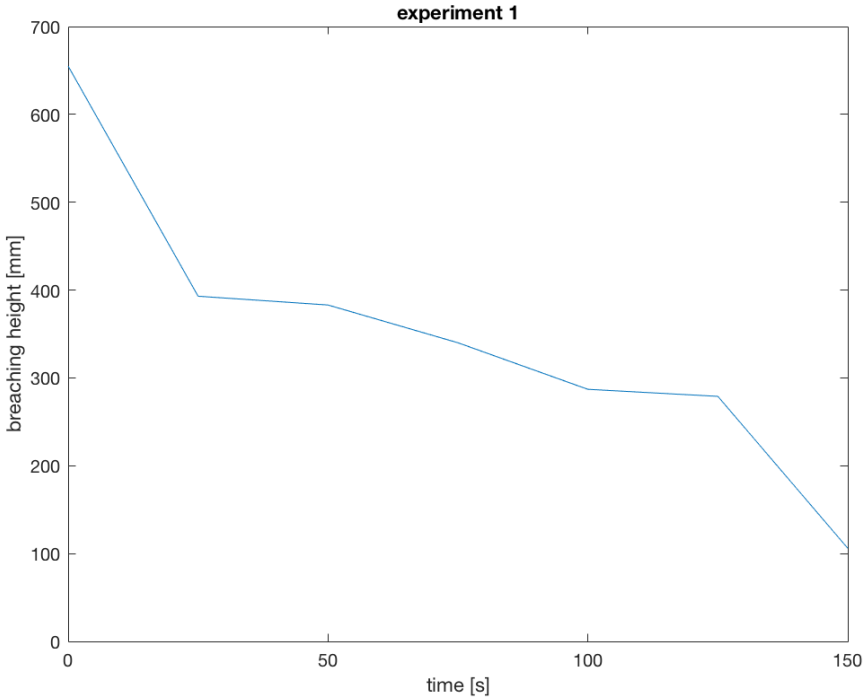

Figure 4- 13: Breaching height of a stable breach versus the time (exp. 1)

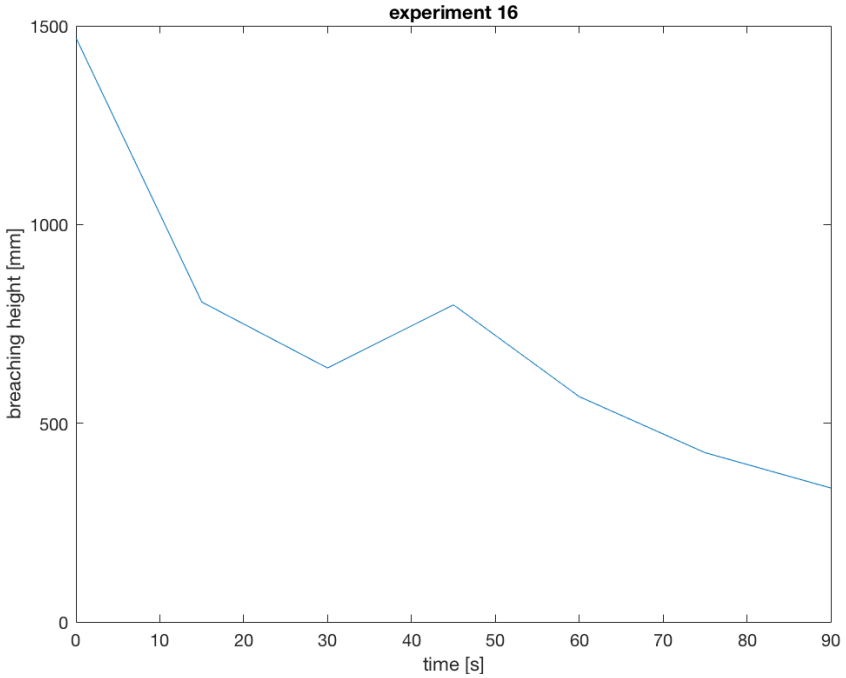

Figure 4- 14 Breaching height of an unstable breach versus the time (exp. 16)

5. Analysis

5.1 Analysis sliding wedges

The sliding wedges are an important parameter for the wall velocity. The equation for the headwall velocity does not take sliding wedges into account. Because sliding wedges are an important part for answering the research question, the first subquestion is:

Is the frequency of large sliding wedges during breaching predictable and what are the effects?

To predict the sliding wedges, the experiments will be analysed seperately first, followed by an analysis of all experiments together, but divided in the active breaching heights. The active breaching height is the length from the top of the breach until the toe of the breach.

5.1.1 Wedges per experiment

Figure 5-1 shows the sliding wedges that occur at the active breaching heights with different starting breaching heights. This shows a slightly ascending trend with increasing initial heights.

The percentages in figure 5-2 are the percentages of the volume of sliding wedges relative to the volume of pure breaching (the volume of the sand that has breached off of the breach). So for example, experiment 1 has a wedge percentage volume of approximately 10%, this means that approximately 90% of the volume of that experiment is pure breaching.

Looking at the volume of the sliding wedges or the frequencies of the sliding wedges (figure 5-2) compared to the whole breaching process, they do not increase with higher initial breaching heights.

In figure 5-3 there are no noticeable differences between the different heights for the frequencies of sliding wedges. The only condition that noticeably affects the volume and frequencies of the sliding wedges are probably due to different permeability of the sand types.

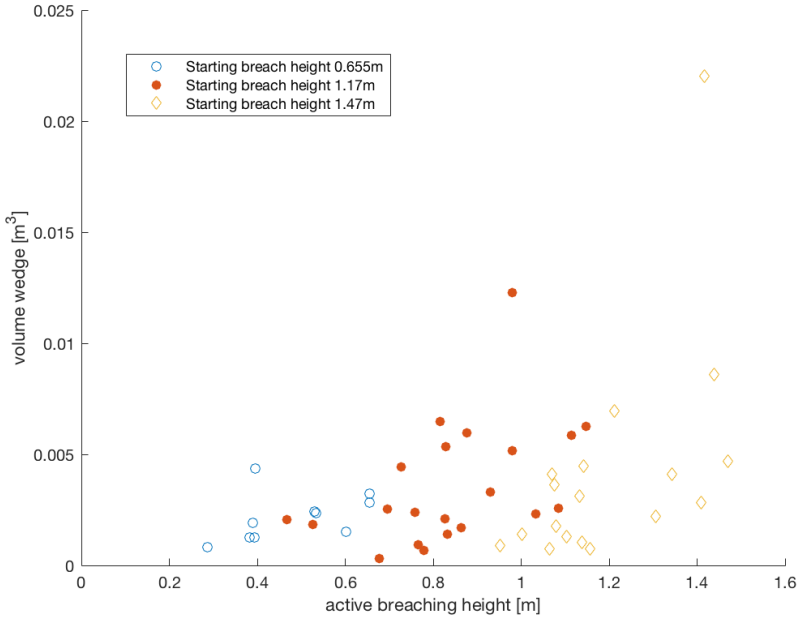

Figure 5- 1: Volume wedges Geba Weiss, no slopes

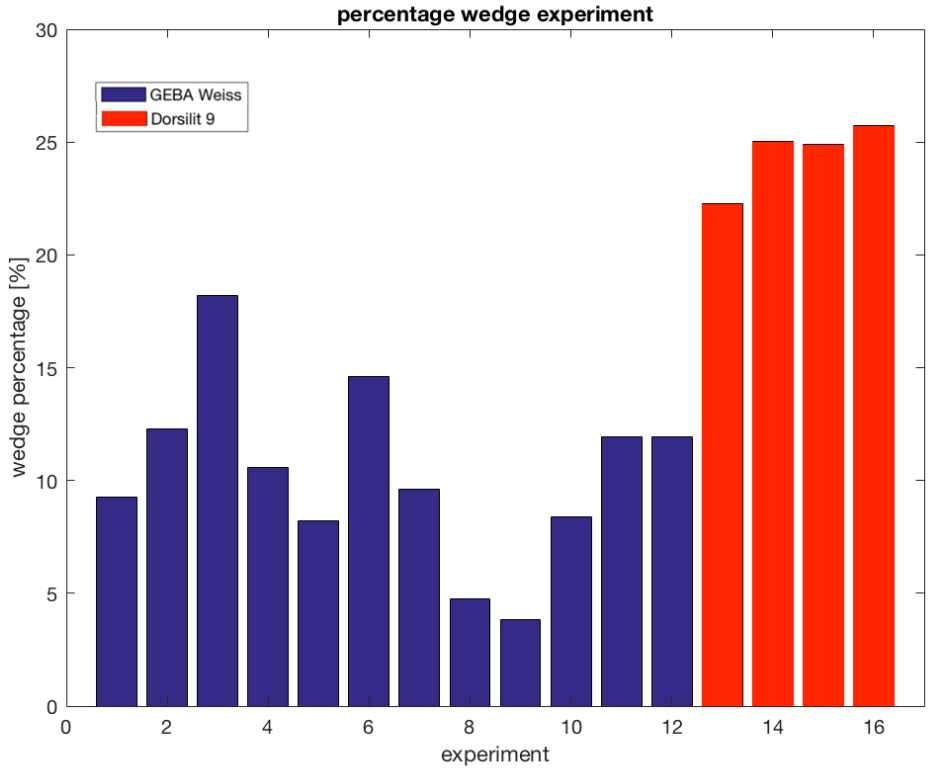

Figure 5- 2: Percentage wedge per experiment. The purple bars are the Geba Weiss experiments, the red bars Dorsilit 9.

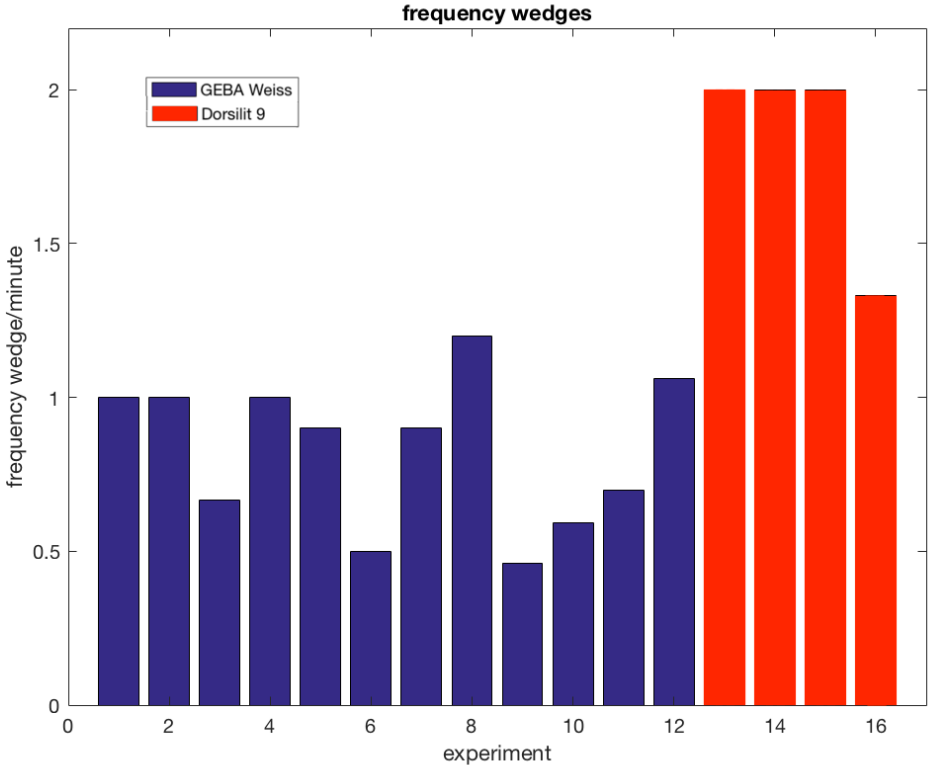

Figure 5- 3: Frequency wedges per experiment. The purple bars are the Geba Weiss experiments, the red bars Dorsilit 9.

5.1.2 Wedges per active height range

If the experiments are not observed separately, but all data of experiments with similar starting conditions are taken together (see table 8) and only separated by different active height, we see clear trends (figure 5-4 and figure 5-5). The active height is the breaching height before a sliding wedge occurs. This is seperated into ranges of 0.2m, for example 1.1m until 1.3m.

Group	Experiments
Geba Weiss no slopes	1,2,3,4,5,6,8,10
Geba Weiss with slopes	7,9,11,12
Dorsilit 9	13,14,15,16

Table 8: The analysis of wedges are divided into three different groups

5.1.2.1 Geba Weiss without slopes

First the experiments with Geba Weiss, without slopes on top of the breach, will be discussed.
The number of slides will be measured per height range. With the active height ranges and the number of slides, the frequencies of slides in a range and the percentage of sliding wedges in a range can be calculated. This gives a trend.
The lowest height range (0-0.5m) has a bigger range (a range of 0.5m) than the other height ranges (0.2m). Table 9 shows the height ranges, how many times a sliding wedge occurs in that height range and the time of the experiments in that range. At larger height ranges, the frequencies of the sliding wedges are higher (figure 5-4). Furthermore, the wedge percentage compared to the whole breaching process also increases with an increasing active height range (figure 5-5).

Height ranges	Time inside range [s]	Number of sliding wedges
0-0.5	1971	6
0.5-0.7	750	8
0.7-0.9	423	10
0.9-1.1	328	11
1.1-1.3	226	8
1.3-1.5	86	6

Table 9: Height ranges, wedges and time inside a height range (Geba Weiss, no slopes)

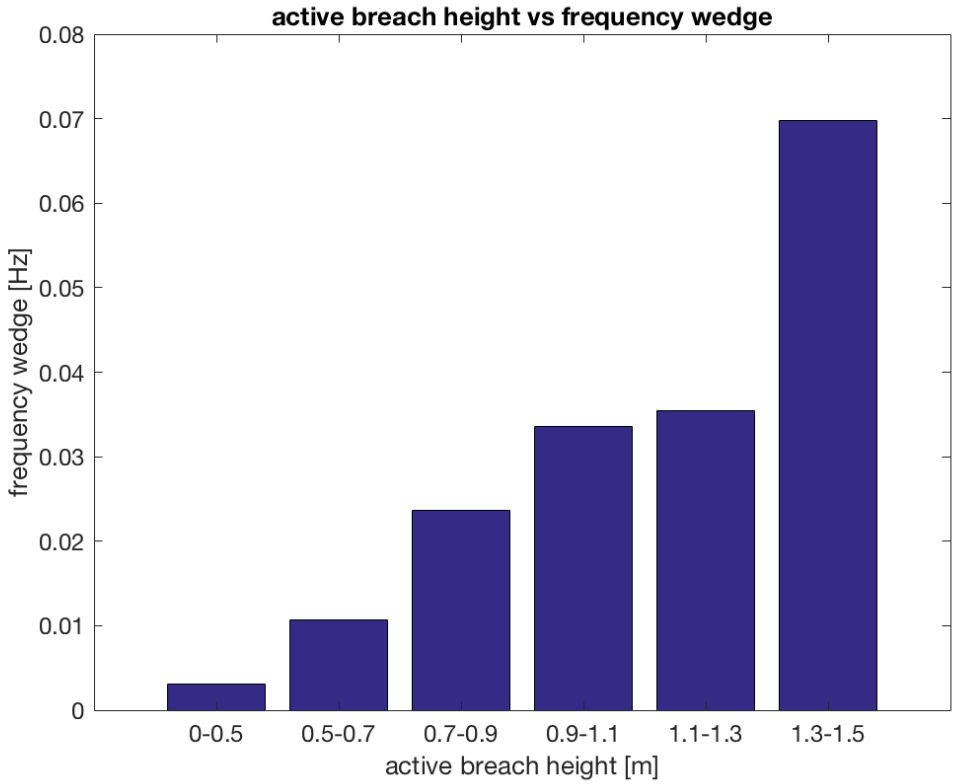

Figure 5- 4: Frequency wedges per height range (Geba Weiss, no slopes)

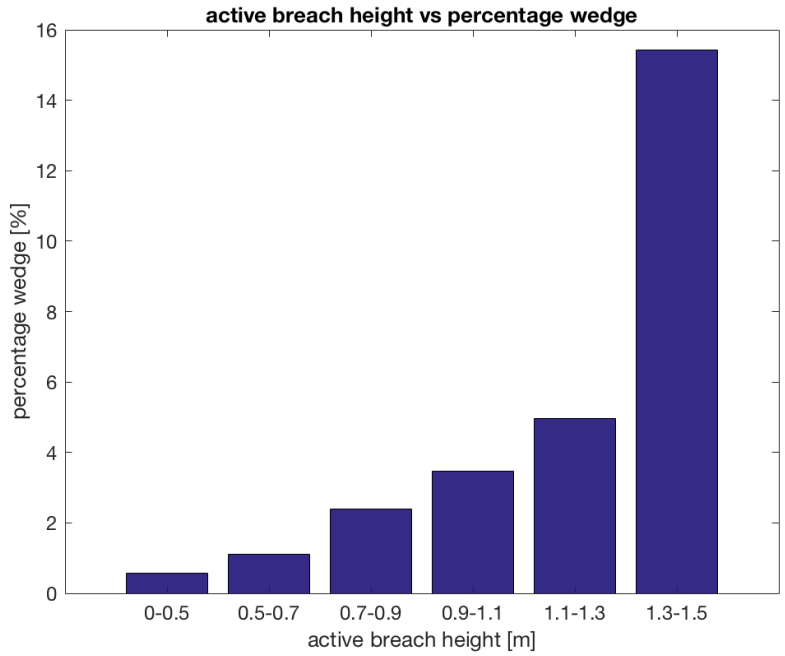

Figure 5- 5: Percentage wedge per height range (Geba Weiss, no slopes)

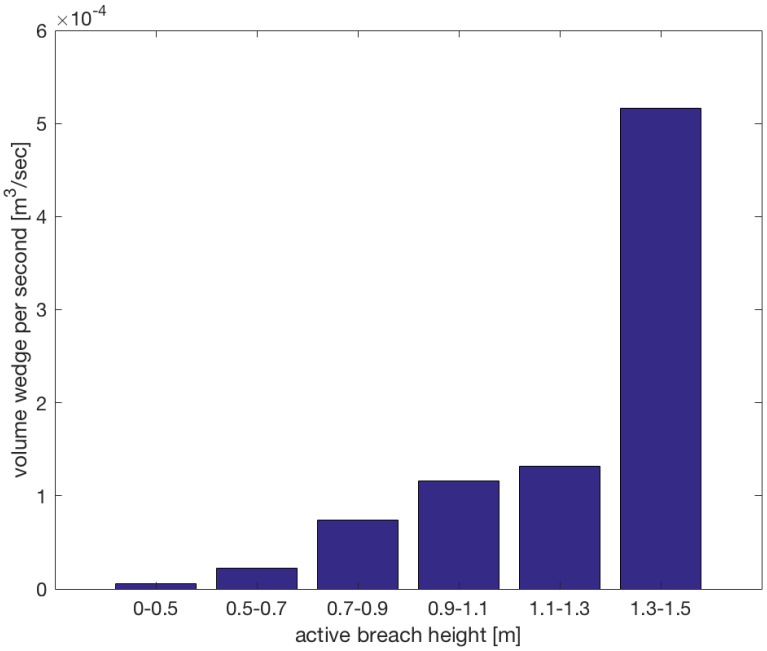

Figure 5- 6: Volume of the wedges per second for every height range (Geba Weiss, no slopes)

One might say that the wedges are divided like in figure 5- 4, figure 5- 5 and figure 5- 6 for the highest height range because the sliding wedges occur more frequently at the start of an experiment, due to the opening of the door. However, figure 5-7 shows that this is not the case. It shows that the volume of the sliding wedges are the highest in the timerange of 20 to 30 seconds, since opening the sliding door, followed by the timerange of 40-50 seconds. Figure 5-8 shows that the breaching angle is also important to the occurrence of sliding wedges, as steeper breaching angles have more percentage of wedges.

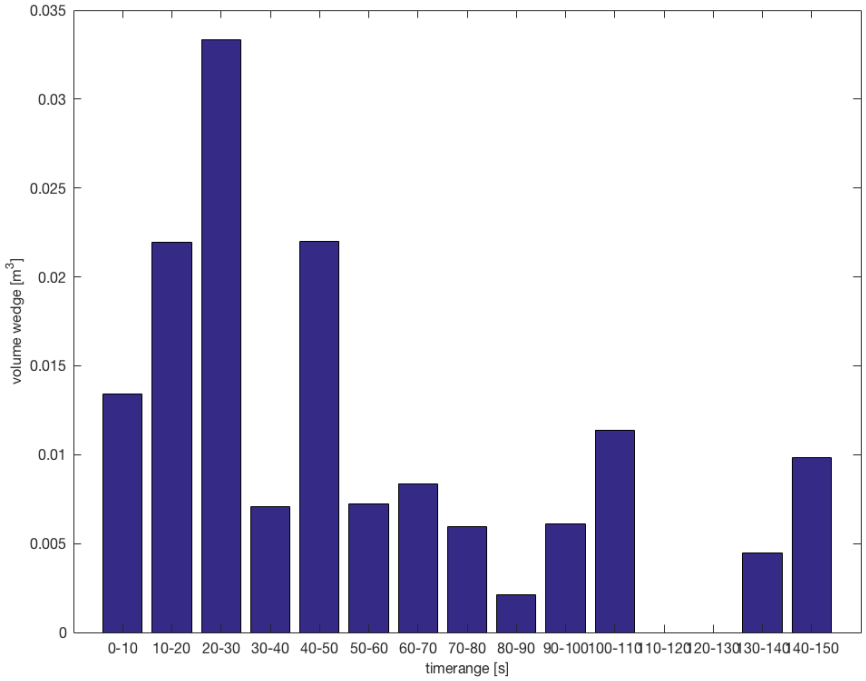

Figure 5- 7: Volume of wedges divided into timeranges (Geba Weiss , no slopes)

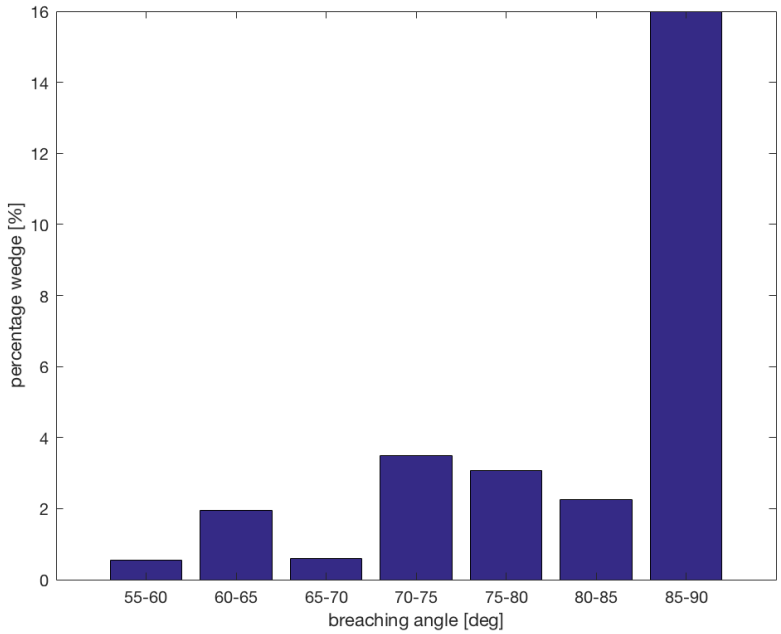

Figure 5- 8: percentage wedge vs breaching angle (Geba Weiss, no slope)

The data of the wedge percentage was plotted versus the active height ranges and a trendline was found for the data, in order to estimate the percentages of sliding wedges (figure 5- 9). The average height range is chosen, for example if the height range is between 0 and 0.5 meters, 0.25m is chosen instead. If we take this into consideration, the wedge percentage of Geba Weiss experiments without slopes can be estimated with the following empirical equation:

$$p_{wedge} = 2.482 * h^{5.34} \qquad (16)$$

p_{wedge} is the percentage of sliding wedges [%]
h is the active height of the breach [m]

This equation is only valid for active breaching heights of 1.4m or lower, because the sliding wedge percentages above these heights are unknown.
However, when the highest data from the experiments is not taken into consideration, the trendline would be a linear line instead.

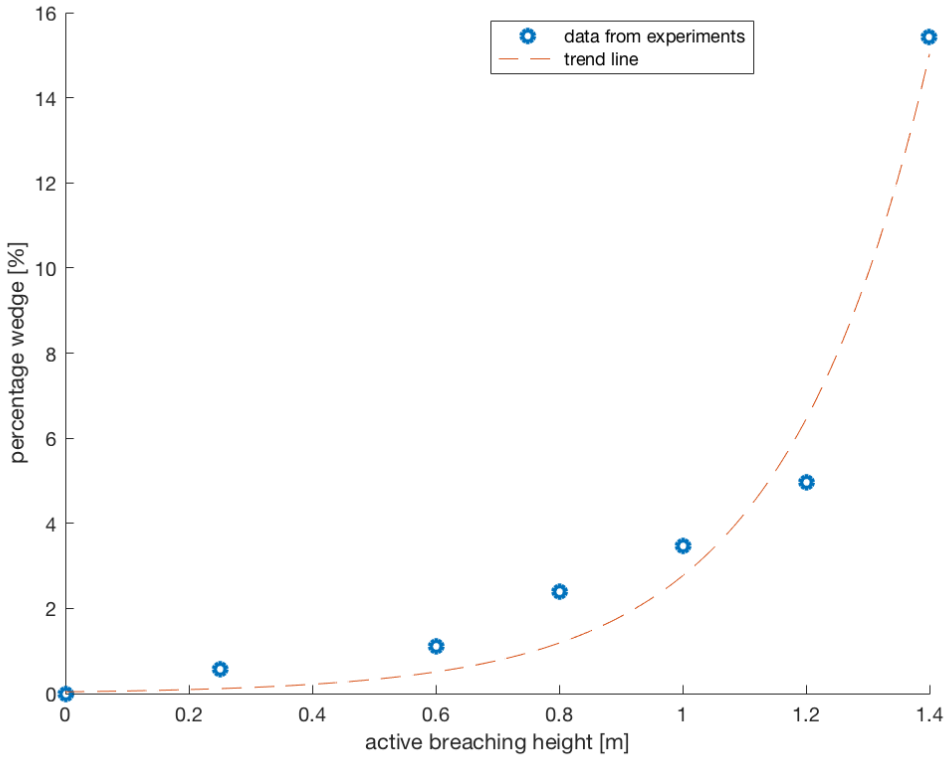

Figure 5- 9: Trendline for percentage of sliding wedges versus active breaching height (Geba Weiss, no slopes)

5.1.2.2 GEBA Weiss experiments with slopes

The experiments with slopes have all been analysed together. The frequency at which the sliding wedges occur (Figure 5-10) are of the same order as the experiments without slopes. There is no initial breaching height of heights larger than 1.17m for experiments with slopes. That is why the highest active height range (1.3m-1.5m) does not contain any data (Table 10). It is not clear whether the slopes in the experiments have a big influence on wedges, because if the data is compared to the data of the experiments without slopes, the biggest height range in these experiments (1.1-1.3m) are comparable to the biggest height range (1.3-1.5m) in the experiments without slopes. So it might be that experiments with slopes on top have a bigger volume and more sliding wedges occurring compared to experiments without a slope on top.

But the same conclusion can be drawn as from the experiments with GEBA Weiss without slopes, that the lower the active breaching height, the less frequent sliding wedges occur. Also the percentage of the wedges are lower with lower active breaching heights.

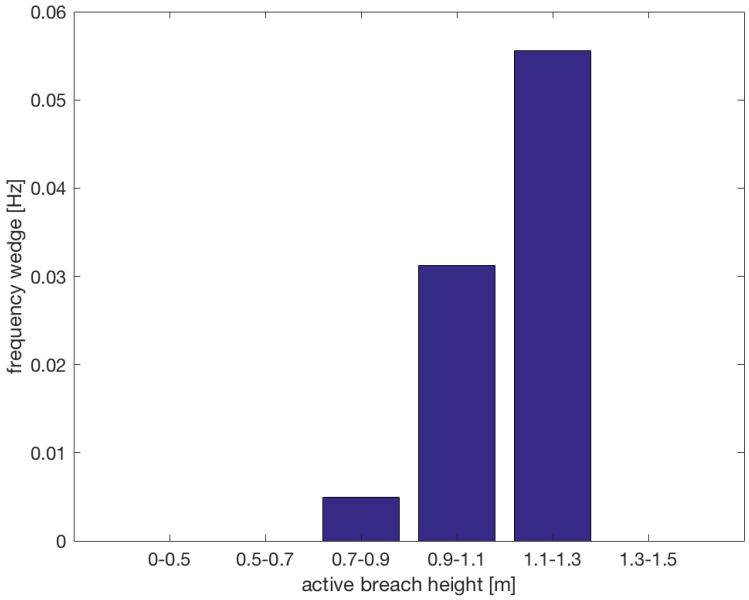

Figure 5- 10: Frequency wedges (Geba Weiss, with slopes)

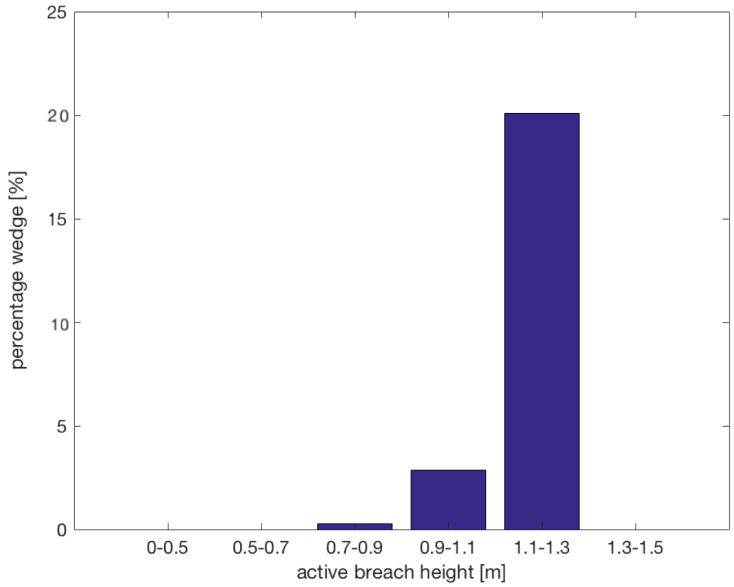

Figure 5- 11: Percentage wedge (Geba Weiss, with slopes)

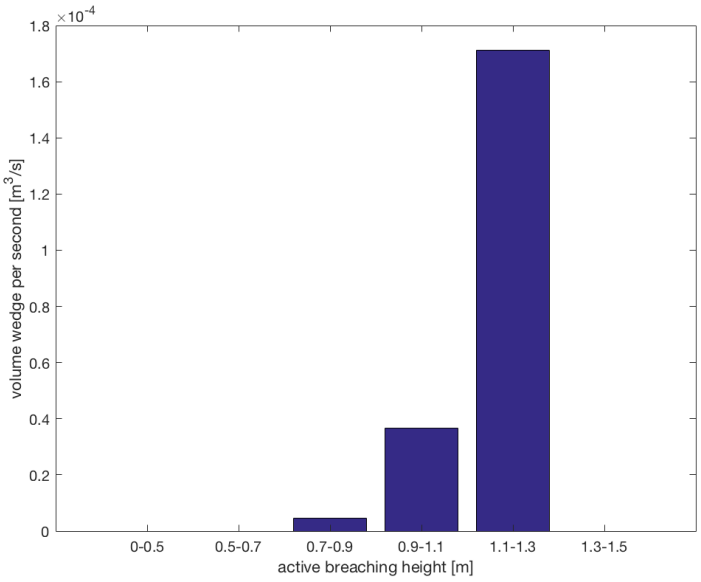

Figure 5- 12: Volume of the wedges per second for every height range (Geba Weiss, with slopes)

Height ranges	Time inside range [s]	Times wedges occur
0-0.5	692	0
0.5-0.7	537	0
0.7-0.9	405	2
0.9-1.1	389	12
1.1-1.3	307	17
1.3-1.5		

Table 10: Height ranges, wedges and time inside a height range (Geba Weiss, with slopes)

Looking at figure 5-13 shows that the biggest volumes of sliding wedges again do not occur at the very start of the experiments, but in the timerange of 20-30 seconds. This is again a counterargument against the argument that sliding wedges occur more frequently when the sliding door opens.
Figure 5-14 shows that the sliding wedges are related to the breaching angle, as steeper breaching angles give a higher percentage of sliding wedges. It is not clear why the breaching angle between 60 and 65 degrees has a higher percentage of sliding wedges than 65 to 70 degrees, but a trend is visible: steeper breaching angles have higher percentages of sliding wedges.

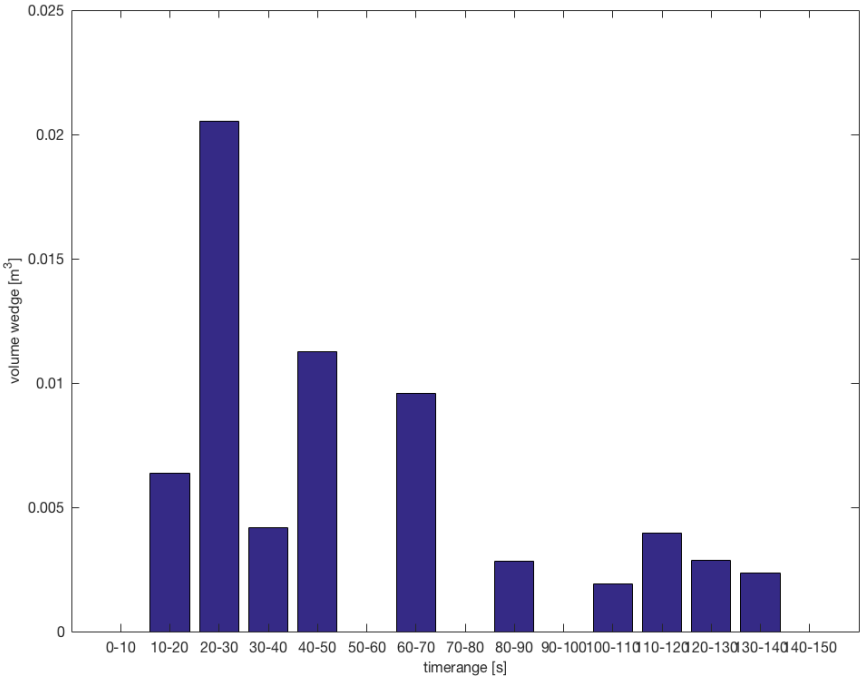

Figure 5- 13: Volume of wedges divided into timeranges (Geba Weiss with slopes)

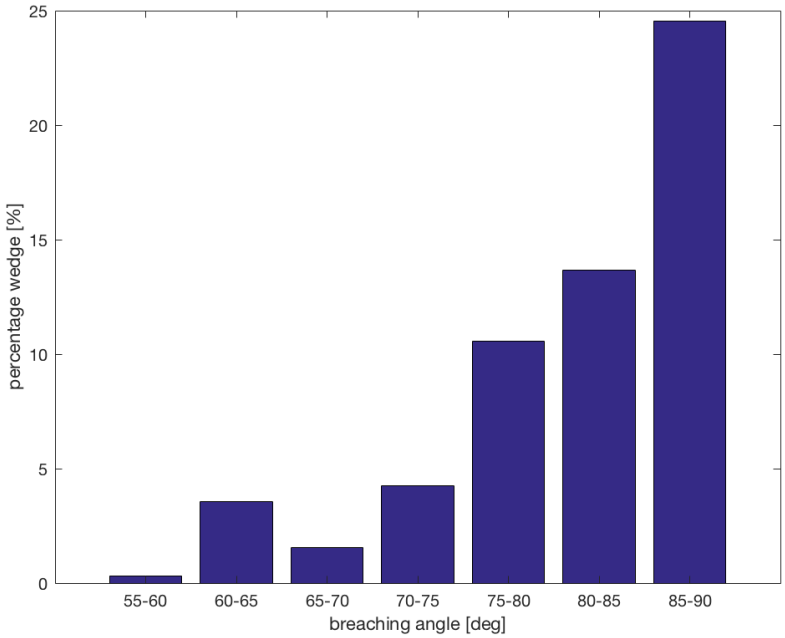

Figure 5- 14: percentage wedge vs range breaching angle (Geba Weiss, with slopes)

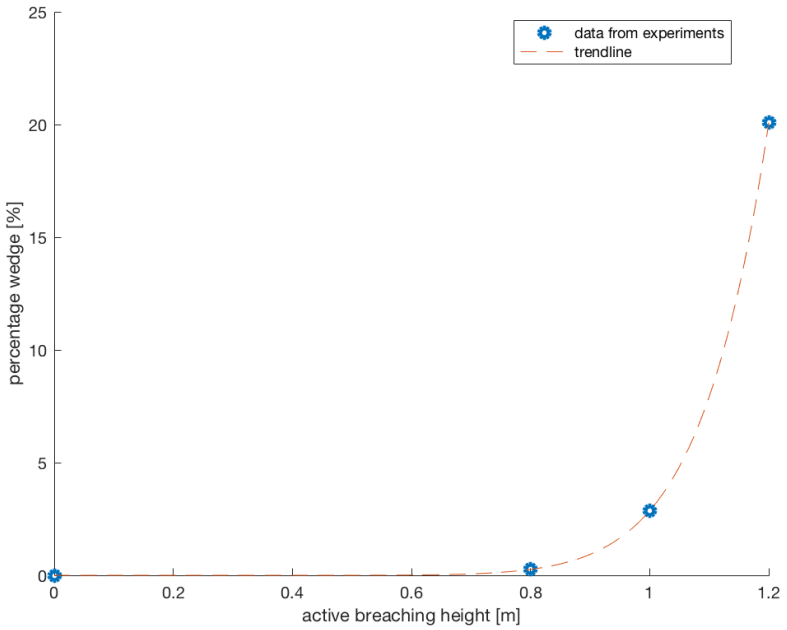

Figure 5- 15: Trendline for percentage of sliding wedges versus active breaching height (Geba Weiss, with slopes)

The data of the sliding wedge percentages is plotted in figure 5- 15 with a trend line. The same height ranges are chosen as data points as the Geba Weiss without slopes. The percentage of the sliding wedges of Geba Weiss experiments with slopes can be estimated with the following emperical equation:

$$p_{wedge} = 2.865 * h^{10.68} \quad (17)$$

This equation is only valid until a active breaching height of 1.2m, as larger heights with slopes were not conducted.

5.1.2.3 Dorsilit 9

Figure 5-16 shows the frequency of the wedges per height range for the experiments that were conducted with Dorsilit 9. The frequency of the wedges in height range 1.1m-1.3m are lower than the frequency in height range 0.9m-1.1m, which is not as expected. However, looking at the percentages (figure 5-17) and volume per second (figure 5-18) of the sliding wedges inside that certain range, it is the same descending trend found when using Geba Weiss.

At the 1.3-1.5m range (figure 5-17), almost the whole displacement of breaching front in this range is due to sliding wedges (almost 96%).

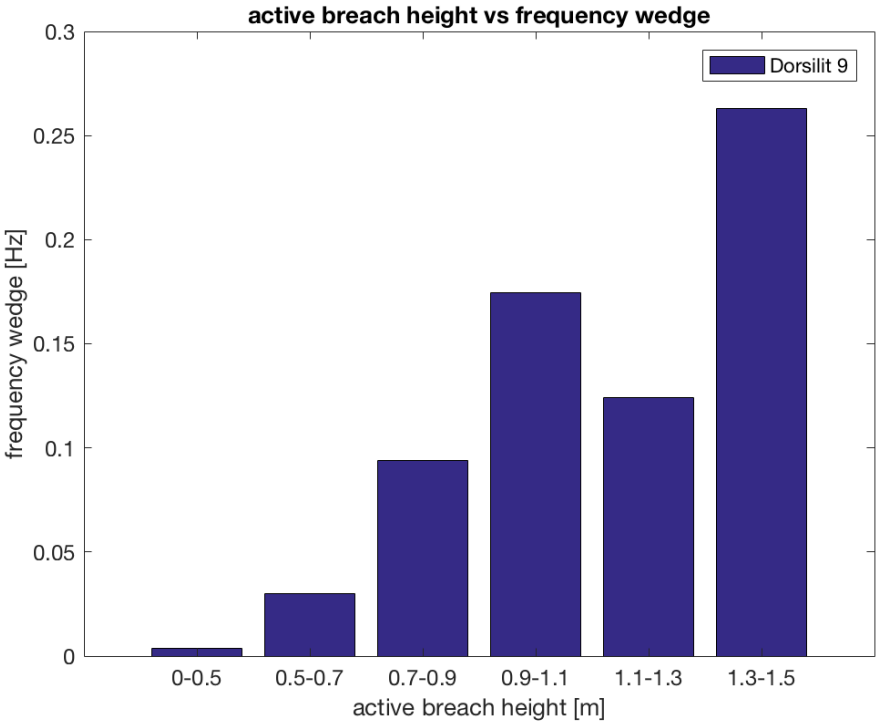

Figure 5- 16: Frequency wedge Dorsilit 9

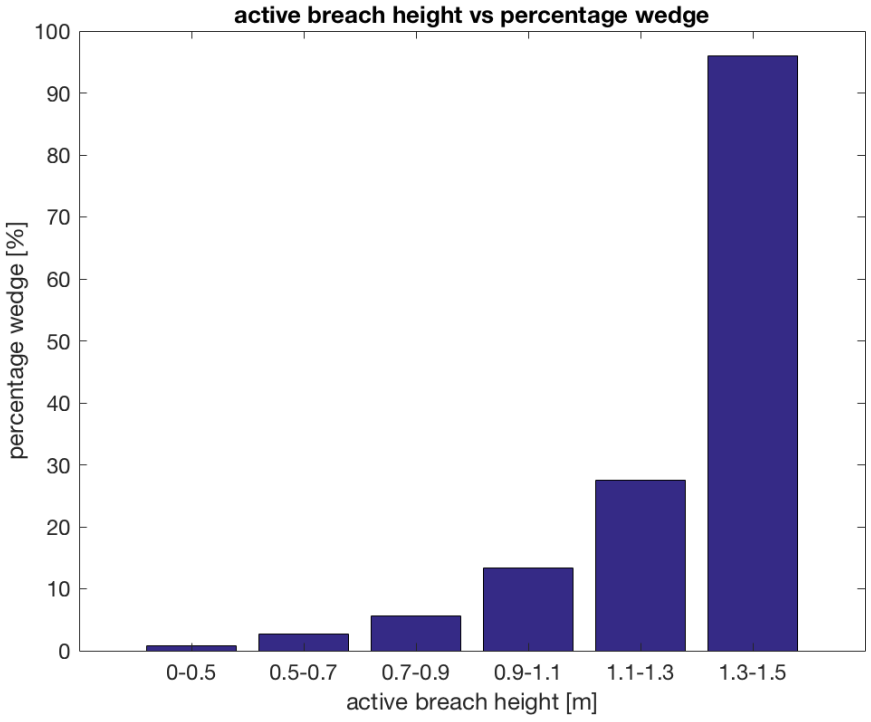

Figure 5- 17: Percentage wedge Dorsilit 9

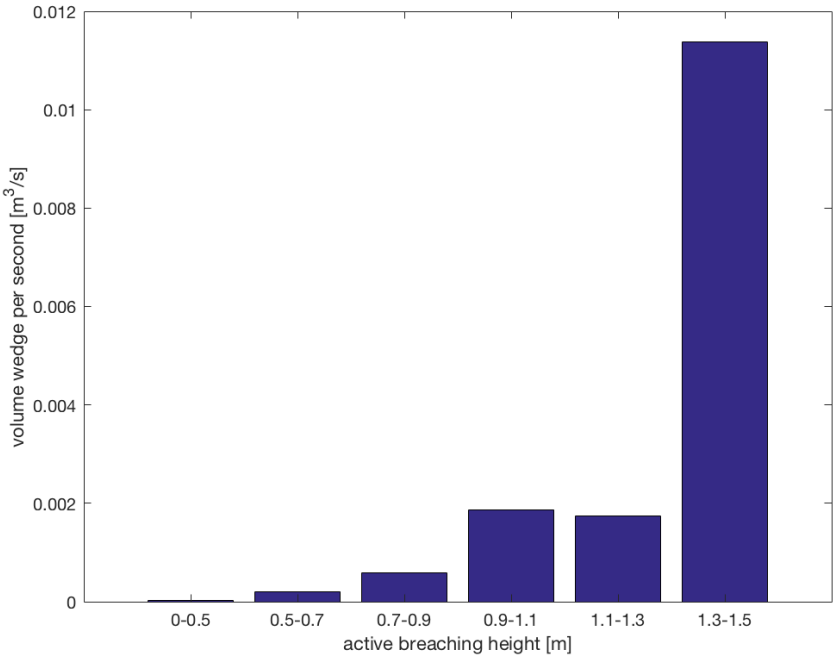

Figure 5- 18: Total volume wedges Dorsilit 9

Height ranges	Time inside range [s]	Times wedges occur
0-0.5	285	1
0.5-0.7	66	2
0.7-0.9	32	3
0.9-1.1	17	3
1.1-1.3	24	3
1.3-1.5	4	1

Table 11: Height ranges, wedges and time inside a height range (Dorsilit 9)

In the case of Dorsilit 9, it can not be concluded whether the sliding wedges occur because it is the beginning of the experiment or because of a certain active breaching height. The experiments are much faster than the Geba Weiss experiments, which gives the following time ranges (figure 5- 19). Here it is not clear whether the sliding wedges occur due to the opening of the sliding door or due to the active breaching height. After 30 seconds all of the Dorsilit 9 experiments displacements of breaching fronts are due to pure breaching. Figure 5- 20 shows the same as in the Geba Weiss experiments, that the breaching angle has an influence on the sliding wedges.

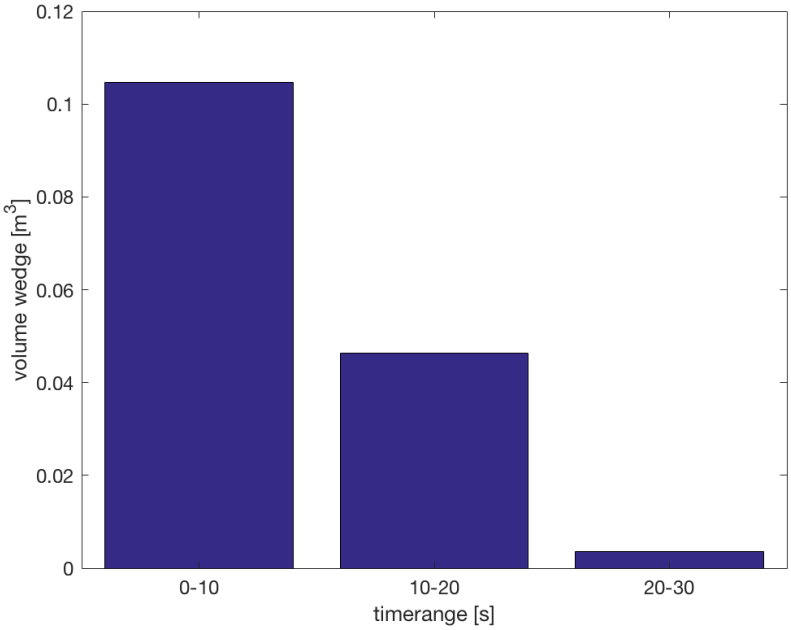

Figure 5- 19: Volume of wedges divided into timeranges (Dorsilit 9)

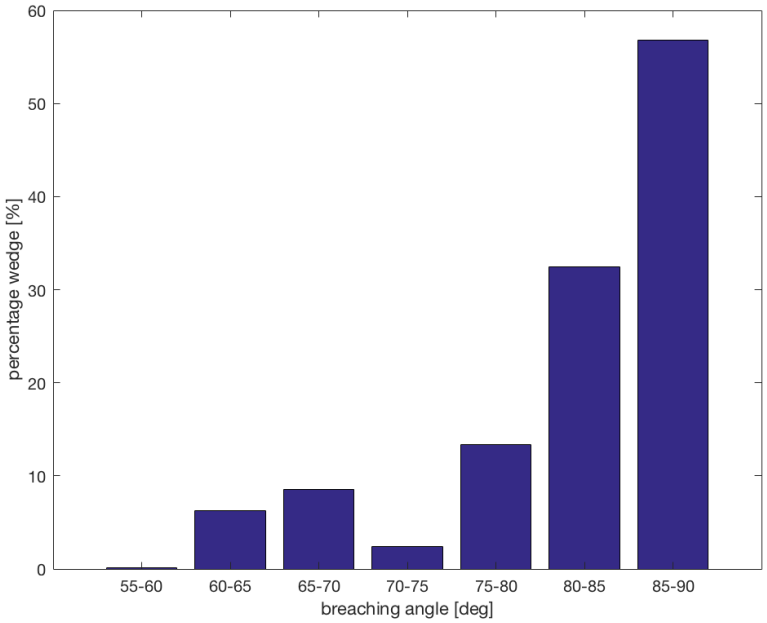

Figure 5- 20: percentage wedge vs range breaching angle (Dorsilit 9)

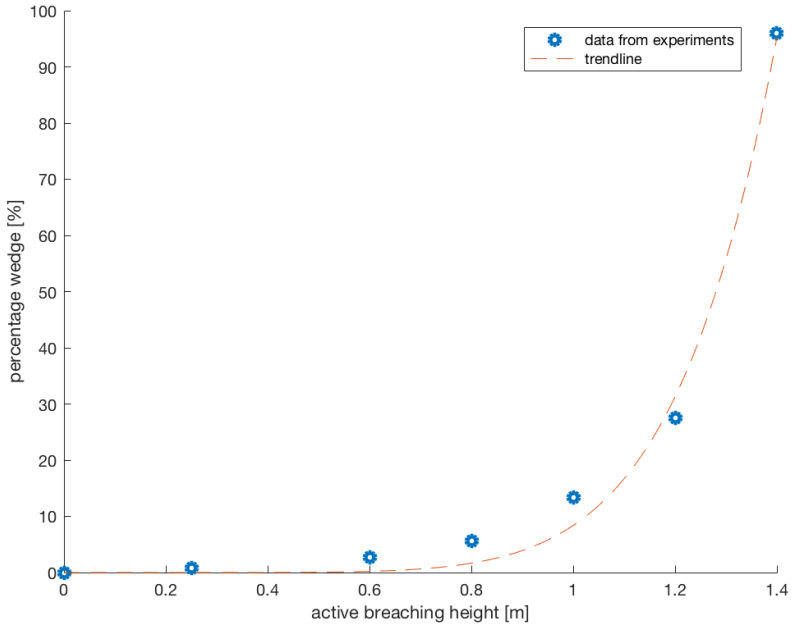

Figure 5- 21: Trendline for percentage of sliding wedges versus active breaching height (Dorsilit 9)

The data of the sliding wedge percentages is plotted in figure 5- 21 along with a fitting curve. The same height ranges were chosen as data points as the Geba Weiss experiments without slope. The percentage of the sliding wedges of Dorsilit 9 experiments can be estimated with the following emperical equation:

$$p_{wedge} = 8.387 * h^{7.223} \quad (18)$$

This equation is only validated until an active breaching height of 1.4m, as larger heights were not in the conducted experiments.

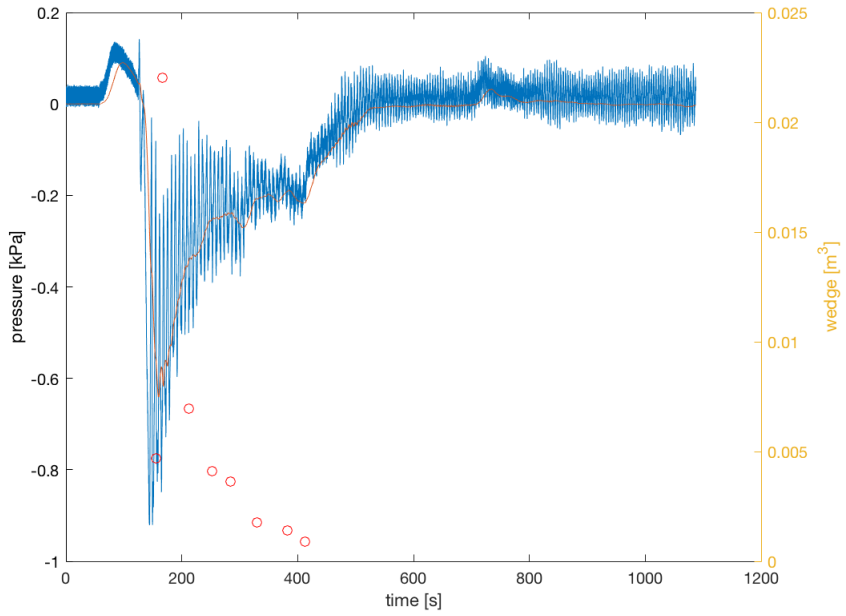

Figure 5- 22: Underpressure with sliding wedges (experiment 10)

Literature study (You et al, 2014) shows that when a breach starts (in our case, when the sliding door opens in the experiments), the underpressure increases, followed by a slow decrease of underpressure. The underpressure increases again during a wedge followed by a decrease. Looking at the underpressures (and filtered underpressures) and wedges does not give information about the wedges (Figure 5-22). This is not consistent in the data of the underpressures.

5.1.3 Conclusion sliding wedges

When the research data of the sliding wedges per experiment and sliding wedges per height range are combined, it can be concluded that the initial breaching height is not the most important parameter in sliding wedges, but the active breaching height. Not only for its frequency, but also its total percentage of volume wedge compared to pure breaching and volume of the sliding wedges per second. There are big differences between GEBA Weiss and Dorsilit 9. Dorsilit 9 has a much higher frequency of wedges. Also the wedge percentage are not of the same order. The Dorsilit 9 has a percentage almost 5 times higher than GEBA Weiss in the same height range.

The start of the breaching experiments probably do not have a big impact on the sliding wedges, as the sliding wedges do not occur immediately at the start of an experiment. What does have a big impact on sliding wedges is the breaching angle. A combination of a large active breaching height and a steep breaching angle might also be the reason for more frequent sliding wedges and more volume of sliding wedges per second.

The percentage, frequency and volume of wedges should not be predicted or estimated based on sand types (or permeability) and starting breaching height. Instead, it should be based on the currently active breaching height and sand types (permeability). It is not clear whether the slopes on top of the breach have an effect on the sliding wedges.

The percentages of sliding wedges can be estimated using the following empirical equations:

$$p_{wedge} = 2.482 * h^{5.34} \quad (16)$$

for Geba Weiss breaches without slopes on top of the breach until a breaching height of 1.4m.

$$p_{wedge} = 2.865 * h^{10.68} \quad (17)$$

for Geba Weiss breaches with slope on top of the breach until a breaching height of 1.2m.

$$p_{wedge} = 8.387 * h^{7.223} \quad (18)$$

for Dorsilit 9 breaches until a breaching height of 1.4m.

These empirical equations are based on the conducted experiments and therefore are limited by a breaching height of 1.4m.

5.2 Angle at the toe

This section contains an analysis of the angle at the toe of a breach. With this we will attempt to answer the following subquestion:
How can we predict the angle at the toe of the breach?

Mastbergen et al. (1988) investigated the behaviour of flowing sand-water mixture by means of sand fill processes. Especially the influence of the flowing sand-water mixture on the development of underwater slopes was investigated. This leads to the following empirical equation for the equilibrium angle:

$$\tan(\alpha_{eq}) = 0.0049 * s^{-0.39} * D_{50}^{0.92} \quad (13)$$

where in our case the sandflux is: $s = \rho_s * (1 - n_0) * H * v_{headwall}$
The flume tests of (Mastbergen et al., 1988) showed different kinds of flow, like flow slides. The processes in these large scale tests were similar to slope development at the toe of breaching, that is why this equation might be applicable for breaching.
The erosion capacity determines the angle at the toe. Lower initial breaching heights have less sand production compared to higher initial breaching heights, this results in steeper angles at the toe of the breach.

5.2.1 Geba Weiss

When the experiments start, the angle at the toe isn't near what is expected from the formula. However, when it reaches the end of the experiment, the angle at the toe becomes approximately (sometimes even exceeds) the theoretical angle.
If this taken into account, we can conclude that the angle at the toe can be predicted. At the start of an experiment, the angle at the toe seems to deviate a lot from the angle at the toe formula. But eventually it exceeds the calculated angle. It looks like in reality the angle at the toe has a steeper curve than the theoretical angle for GEBA Weiss at lower breaching heights. While at the highest starting breaching height and experiments with slopes at the top of the breach, it looks like the real angle at the toe and the theoretical angle are approximately the same.
In figure 5-23 the colors are time indications, blue is the start of the breach, the lighter the colors, the more time has passed. The yellow color is near the end of the experiment. Every experiment has seven different colorpoints. In every initial height range the time between those points have different time instances. The colorbar gives the percentage of the time of an experiment. So for example if an experiment takes 100 seconds, 30 percent in the colorbar is when the experiment is at 30 seconds.

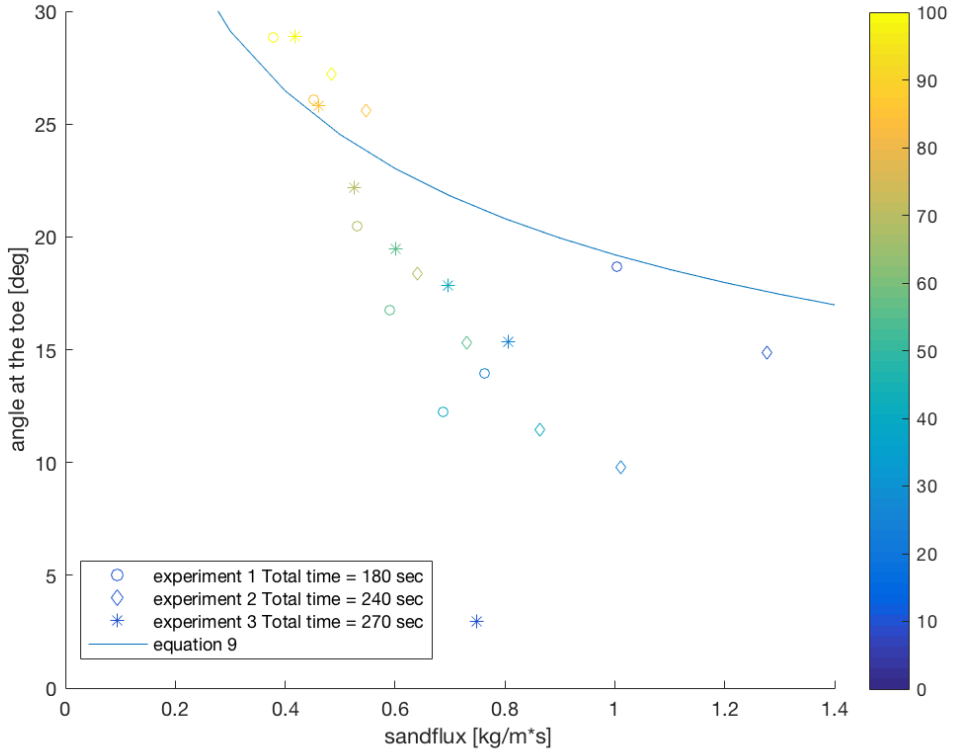

Figure 5- 23: Sandflux versus angle at the toe (Geba Weiss, initial height 0.655m). The colors indicate the time that has passed in percentages. The total time of an experiment is in the legend of the plots.

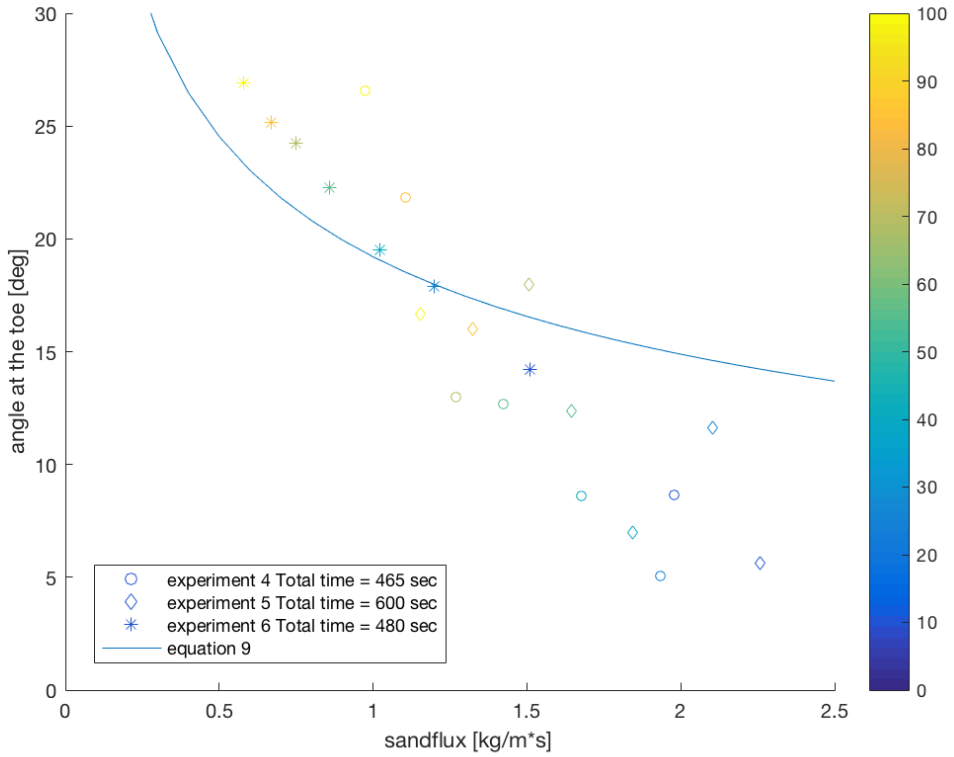

Figure 5- 24: Sandflux versus angle at the toe (Geba Weiss, initial height 1.17). The colors indicate the time that has passed in percentages. The total time of an experiment is in the legend of the plots.

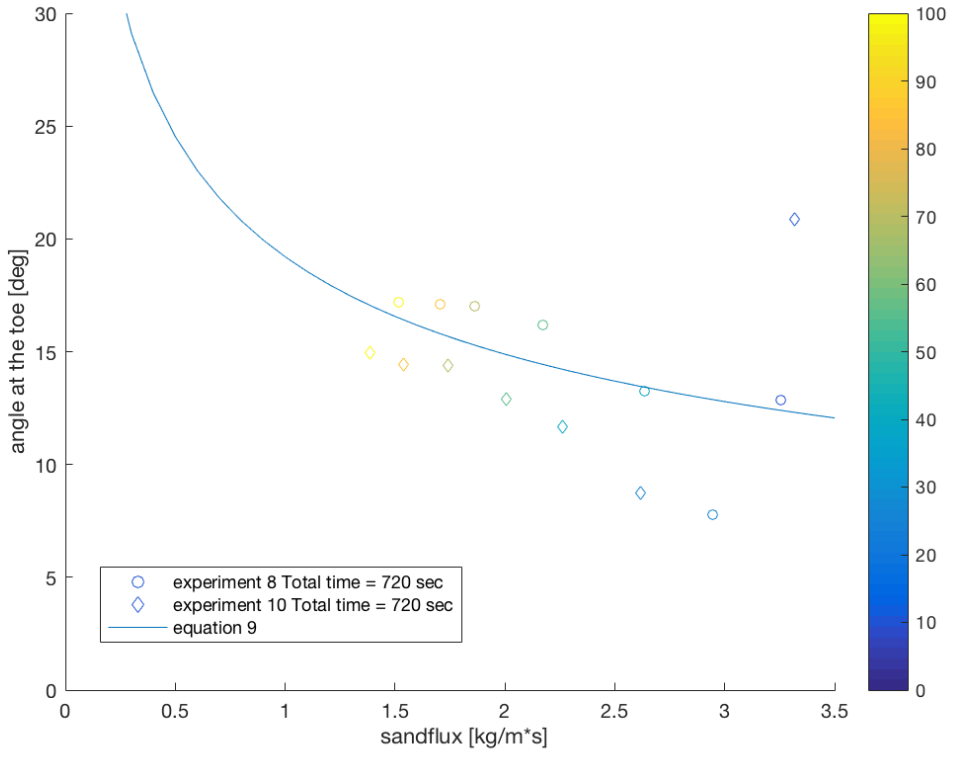

Figure 5- 25: Sandflux versus angle at the toe (Geba Weiss, initial height 1.47m). The colors indicate the time that has passed in percentages. The total time of an experiment is in the legend of the plots.

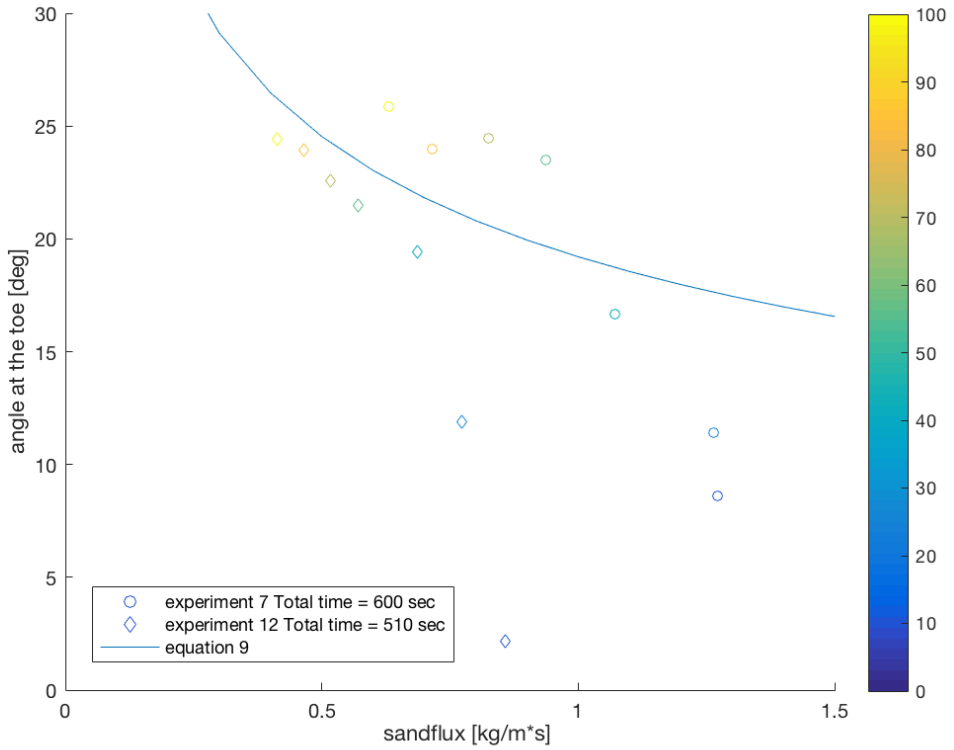

Figure 5- 26: Sandflux versus angle at the toe (Geba Weiss, 20 degrees). The colors indicate the time that has passed in percentages. The total time of an experiment is in the legend of the plots.

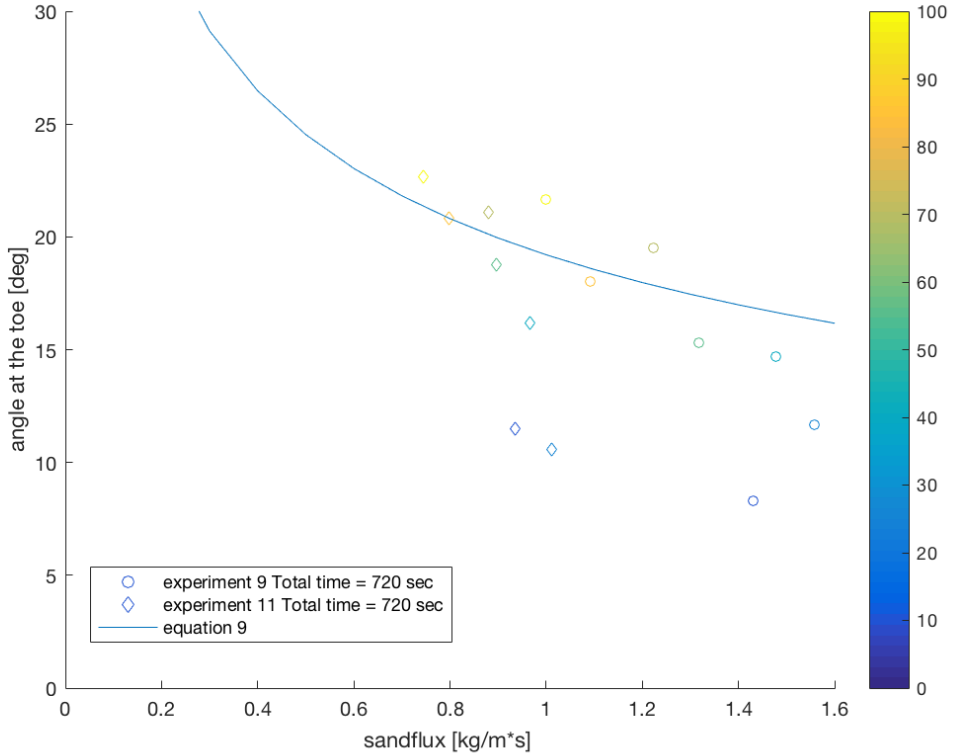

Figure 5- 27: Sandflux versus angle at the toe (Geba Weiss, 30 degrees). The colors indicate the time that has passed in percentages. The total time of an experiment is in the legend of the plots.

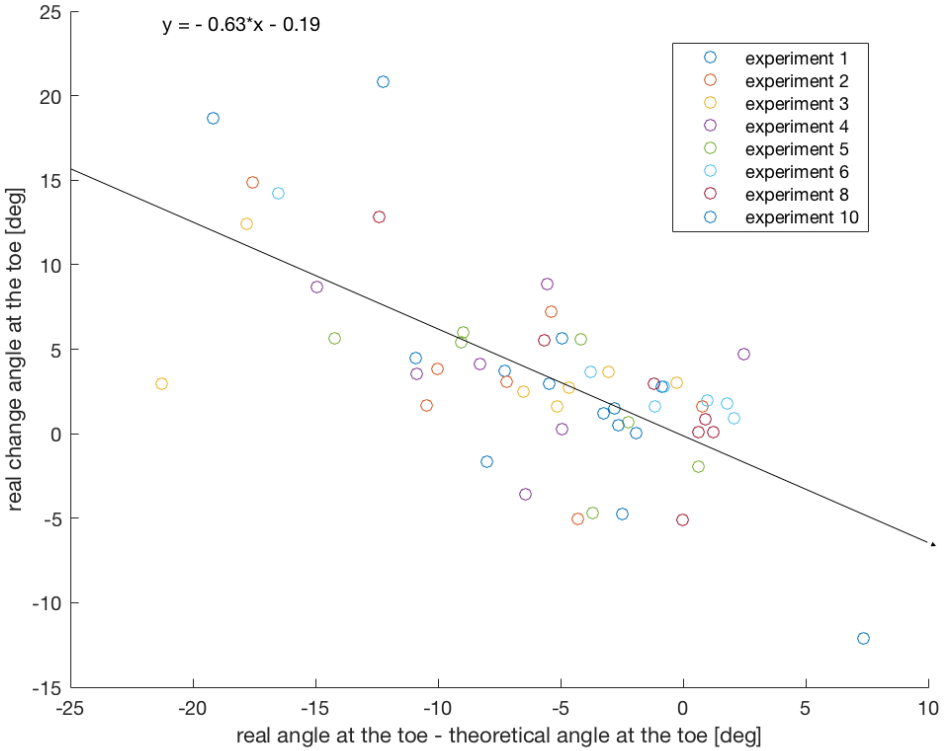

Figure 5- 28: real angle at the toe minus the theoretical angle at the toe versus real change of the angle at the toe.

Figure 5-28 shows the real angle at the toe minus the theoretical angle at the toe plotted against the real change of angle at the toe. The expectation is that if the difference between the real and theoretical angle at the toe is negative, the angle change is positive. The higher the negative value, the bigger the positive angle change is. And when the difference between real and theoretical angle at the toe is positive, the angle change will be negative. A clear trend can be seen in figure 5-28, where it matches the expectation. An equation follows from this figure, which is just a trend line of all the scatter points:

$$\Delta\alpha_{real} = -0.63 * (\alpha_{real} - \alpha_{theory}) - 0.19 \quad (19)$$

5.2.2 Dorsilit 9

With Dorsilit 9 experiments, the angle at the toe of the breach is approximately 20-30% lower than the theoretical angle. From experiment 16, the experiment with the highest starting breaching height, the angle at the toe has a small deviation from the theoretical angle. This might have to do with the large sliding wedges that occur at the start of the experiment. This causes the angle at the toe to be steep from the start (figure 5-29) and it takes less time to converge to the equation angle. It was expected that the higher starting breaching height would give shallower angle at the toes. Especially in experiment 16 (1.47m Dorsilit 9 experiment), the angle at the toe is steep already and eventually converges to the angle at the toe from the formula. For the other experiments, the angle at the toe is lower and it never converges to the formula. This might have to do with the fact that the formula was designed for finer sands (135μm and 225μm) and not for coarse sands like Dorsilit 9 (330 μm). Equation 9 depends on the particle size distribution. When the D_{50} becomes much larger, the angle at the toe will also become steeper according to the formula. This does not necessarily have to be true for sand types that are much coarser like Dorsilit 9. Another possibility is that the formula does not apply for higher sand flux.

Figure 5- 29: A large sliding wedge, which result into a steep angle at the toe.

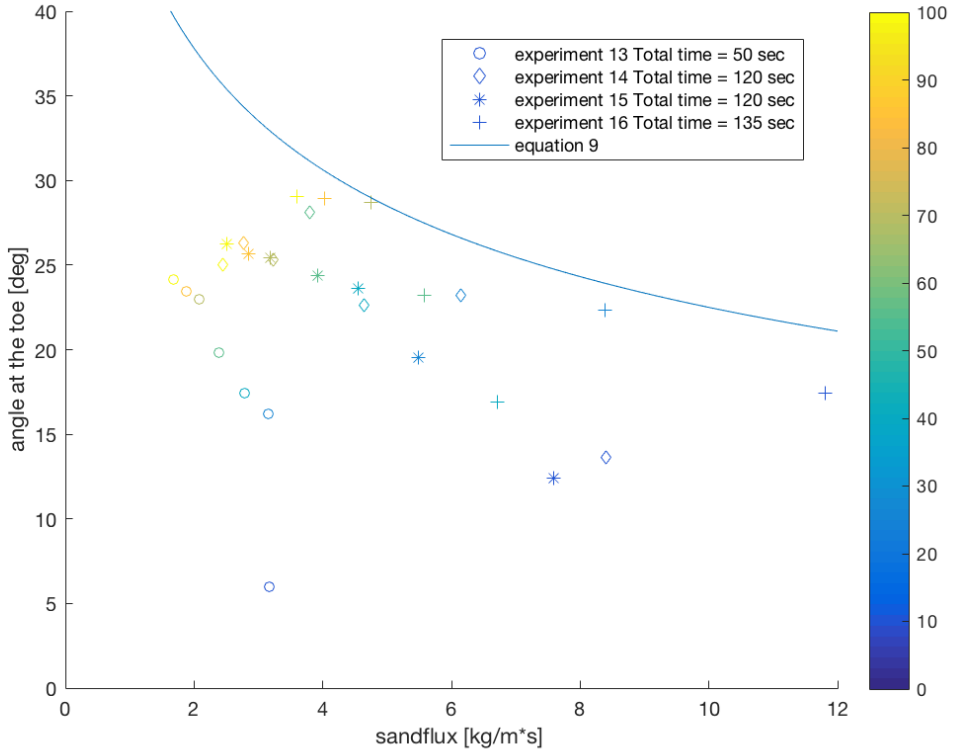

Figure 5- 30: Sandflux vs angle at the toe (Dorsilit 9)

5.2.3 Conclusion angle at the toe

It was observed that experiments with Geba Weiss, the angle at the toe is much smaller than expected from the formula (9) at the start of the experiments. The bigger the difference between the real angle at the toe and the theoretical angle at the toe, the bigger the angle change is.
Equation 15 follows from a trendline:

$$\Delta\alpha_{real} = -0.63 * (\alpha_{real} - \alpha_{theory}) - 0.19 \quad (19)$$

The experiments with 0.655m initial breaching heights start with an angle that is much smaller than the angle obtained from the formula and ends with an angle that converges to the angle of equation 9. At lower starting breaching heights, angles at the toe are steeper than the angles at the higher starting breaching heights. This was already expected from equation 9, because lower heights leads to lower sand fluxes and lower sand fluxes result in steeper angles.

With Dorsilit 9 the opposite seems to be true, higher initial heights result in steeper angles. This might have to do with the sliding wedges that occur with Dorsilit 9. Due to the higher permeability of Dorsilit 9, water flows faster through Dorsilit 9 than through Geba Weiss. The result is that sliding wedges occur more frequently and bigger volumes of sliding wedges occur during the experiments with Dorsilit 9.
Looking at experiment 16 (Dorsilit 9, 1.47m starting breaching height), it might be that the angle at the toe is steep from the start because of the first large sliding wedge. This is the reason that the higher starting breaching height with Dorsilit 9 have steeper angles at the toe than the lower heights despite lower sand fluxes, while the opposite is expected. The angle at the toe never converges or exceeds the formula in the Dorsilit 9 experiments. This might have to do with the fact that the formula was designed for finer sands and not for coarse sand types.

5.3 Analysis headwall velocity

For the analysis of the headwall velocity, the 16 conducted experiments are used. The wall velocities and headwall velocities are calculated from these experiments and compared to the theories (for example equation 8). In the following paragraphs the subquestion about the headwall velocity is answered:
What are the predictions that can be made for the wall velocity?

5.3.1 Wall velocity

5.3.1.1 Geba Weiss

The first twelve experiments were all conducted with GEBA Weiss sand ($D_{50} = 103\mu m$). With three different starting heights. And there were experiments where the breach began with a slope (20 or 30 degrees) on top of the breach. This was to mimic an unstable breach where the active breaching height increases.
The equation of the headwall velocity (equation 8) does not take sliding wedges into account. An example of the results of wall velocities of an experiment (experiment 1) can be seen in table 12 (the other experiments in Appendix A).

Experiment 1	Wall velocity [mm/s]
0-25 sec	2.476
25-50 sec	1.857
50-75 sec	1.059
75-100 sec	1.458
100-125 sec	0.914
125-150 sec	0.0833
150-175 sec	0.075

Table 12: Wall velocity of experiment 1

5.3.1.2 Dorsilit 9

For the last four experiments, Dorsilit 9 ($D_{50} = 330\mu m$) was used. Breaching experiments with this sand type have a much higher wall velocity than GEBA Weiss. This has to do with the permeability of the sand. This causes the water to flow faster into the sand, which will give higher wall velocities. Furthermore, as it was was shown in 5.1, Dorsilit 9 also has more sliding wedges, which causes the wall velocity to be much higher than GEBA Weiss.
Because there were not many experiments with the Dorsilit 9, all results of the experiments with Dorsilit 9 were combined and plotted together in the results and analysis.
The wall velocities of the experiments can be seen in Appendix A.

5.3.2 Headwall velocity

5.3.2.1 Geba Weiss

The headwall velocities are calculated from the experiments by excluding the sliding wedges. This is done by taking a screenshot of a breaching front after a sliding wedge and before the following sliding wedge. For the GEBA Weiss experiments, the headwall velocity is plotted versus the theoretical headwall velocity from equation 5. There is one unknown term, the n_{loose}, which can not be calculated or determined from the experiments. The least square method is used to calculate this value. The least square method is a calculation method where the best fitting value is determined, this is done by using many curves, where the best fitting value is used.

$$v_{headwall} = k * \frac{1 - n_0}{\Delta n} * \frac{\rho_s - \rho_w}{\rho_w} * \frac{\sin(\beta_{breach} - \phi)}{\sin(\phi)} \qquad (12)$$

with $n_0 = 0.415$
and

$$\Delta n = \frac{n_{loose} - n_0}{1 - n_{loose}} \qquad (3)$$

n_0 has been measured from the experiments from Geba Weiss by taking a sediment sample out of the sand package with a known volume, subsequently dry it and weight the mass of the sand.

In figure 5-31 the grey lines are indicating the root mean square. A value for n_{loose} is found for Geba Weiss: $n_{loose} = 0.455$. This is comparable with the results found from literature study (between 0.44-0.48).

Initial breaching height [m]	Root Mean Square [mm/s]
0.655	0.555
1.17	0.48
1.47	0.308

Table 13: Root mean square

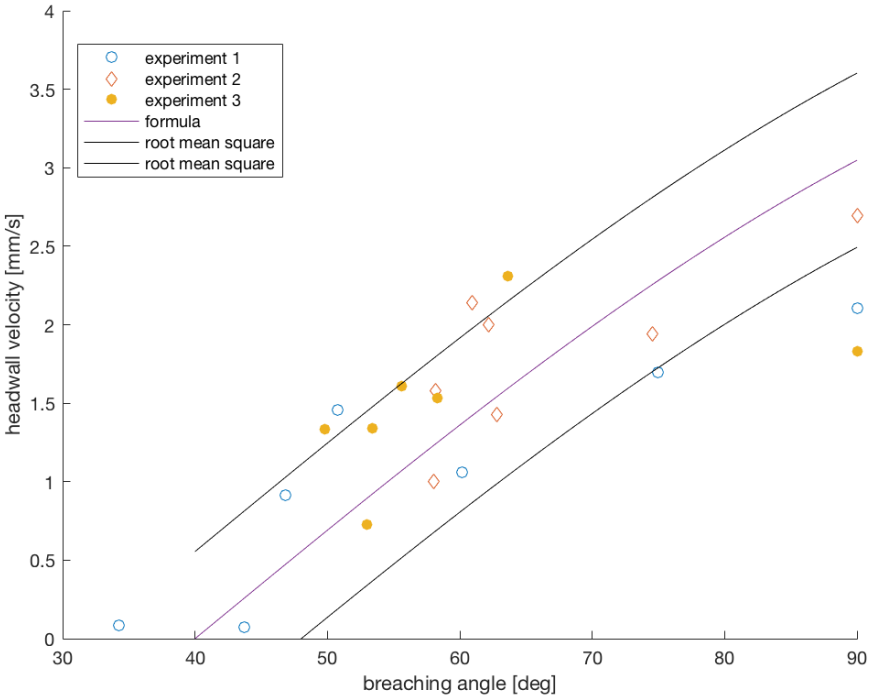

Figure 5- 31: Headwall velocities (Geba Weiss, initial height = 0.655m)

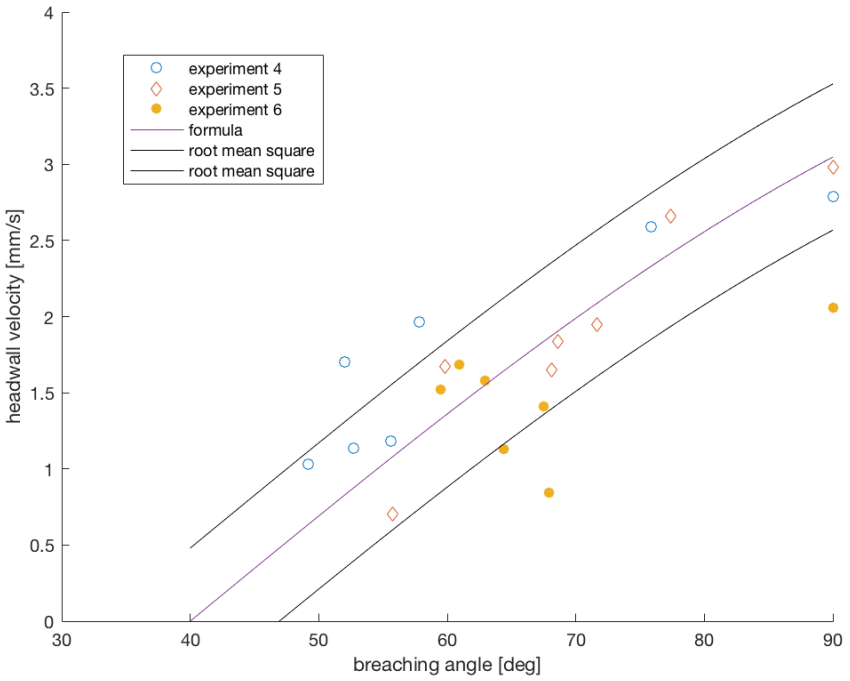

Figure 5- 32: Headwall velocities (Geba Weiss, initial height = 1.17m)

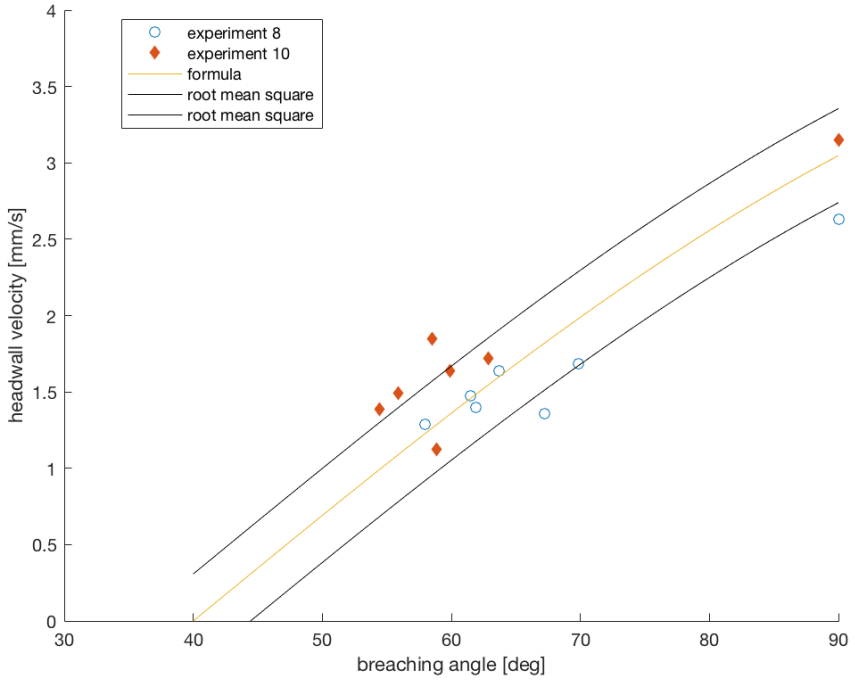

Figure 5- 33: Headwall velocities (Geba Weiss, initial height = 1.47m)

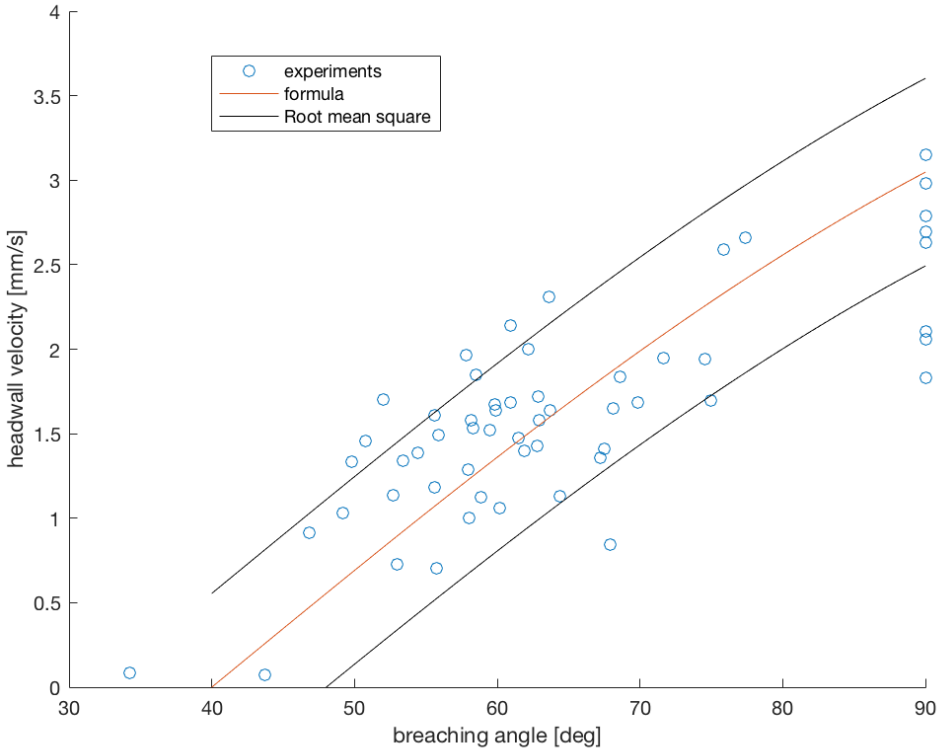

Figure 5- 34: Headwall velocity with nloose = 0.455 (all Geba Weiss experiments)

If the Geba Weiss experiments are all plotted together, a RMS value of 0.525 mm/s is calculated.

When the headwall velocities were compared with the wall velocities, a ratio was found by dividing the wall velocity by the headwall velocity. This ratio was plotted against the wedge percentage during the time of the wall velocity. Using these data points, for Geba Weiss, a linear line was plotted (see figure 5- 35) with the following equation:

$$M_{headwall} = 1.7 * p_{wedge} + 1.1 \qquad (20)$$

where $M_{headwall}$ is the ratio between the wall velocity and the headwall velocity [-]
The formula is only valid for $p_{wedge} > 0$. This means that when p_{wedge} is zero, $M_{headwall}$ is also zero. However, the values are not really close to the line and the deviation of the values is large.

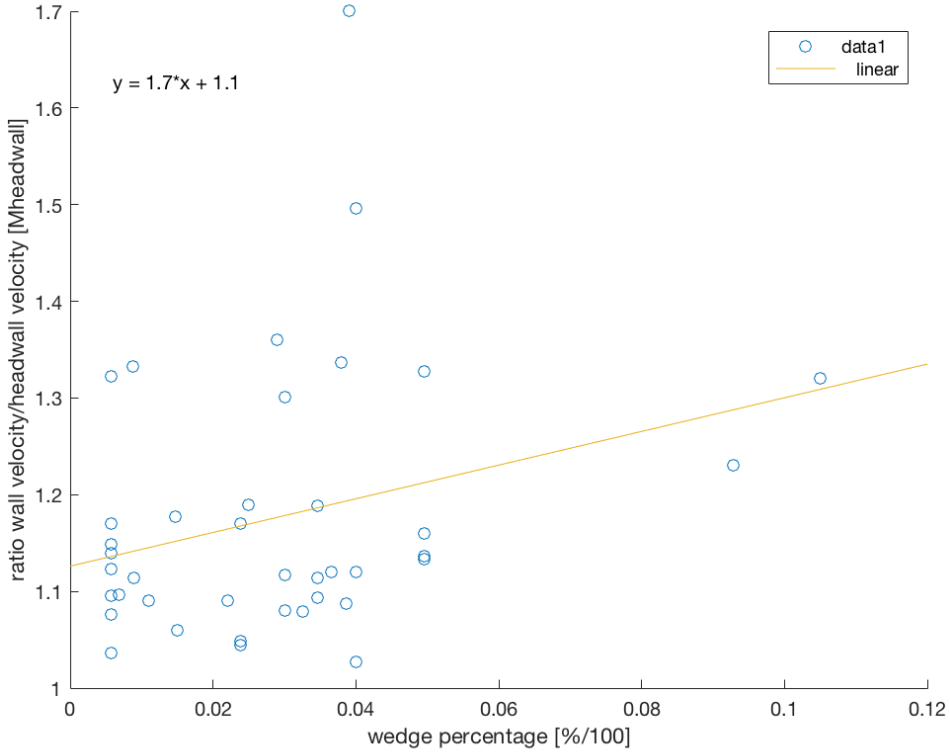

Figure 5- 35: Wedge percentage plotted against ratio wall velocity/headwall velocity (Geba Weiss)

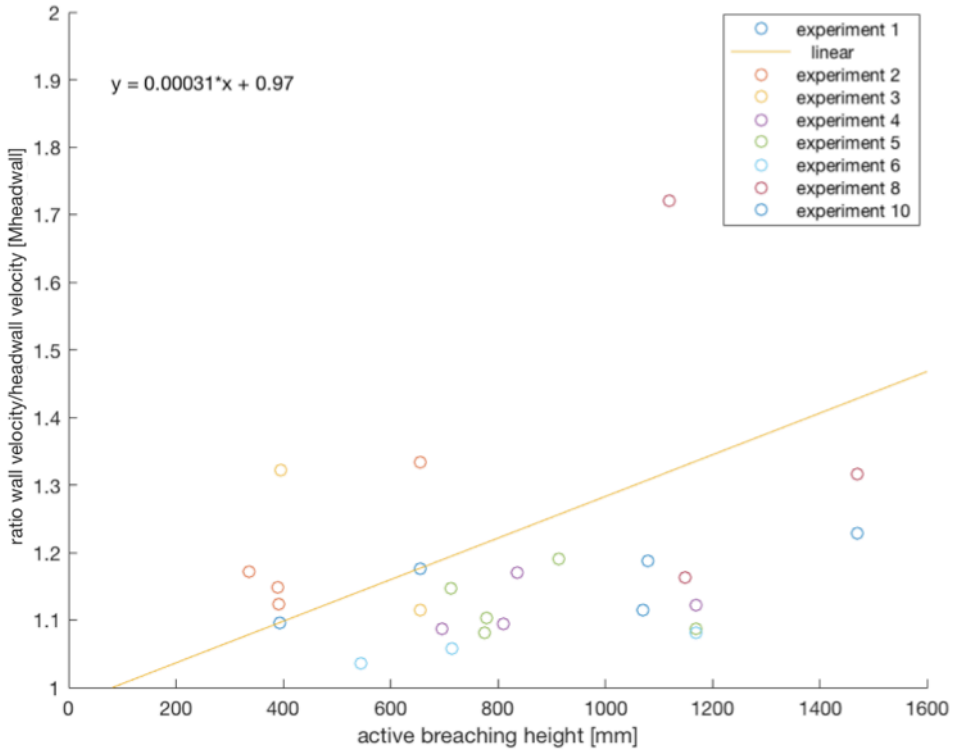

Figure 5- 36: Active breaching height plotted against ratio wall velocity/headwall velocity (Geba Weiss)

If we plot the ratio of wall velocity/headwall velocity against the active breaching height (figure 5-36), the deviation is a lot smaller and the following equation can be used:

$$M_{headwall} = 0.00031 * h + 0.97 \qquad (21)$$

However, looking at the scatter points of figure 5-36, it can be seen that it does not really increase with higher active breaching heights. There is no strong correlation between the ratio of wall and headwall velocity and active breaching height if the outlier is ignored. Based on this, the ratio of the wall velocity and headwall velocity should not be based on the active breaching height.

The ratio between headwall and wall velocity is used to estimate the wall velocity from the headwall velocity:

$$v = v_{headwall} * M_{headwall} \qquad (22)$$

This can be used to calculate the wall velocity from the headwall velocity and expected wedge percentages, which are discussed in 5.1, at the currently active breaching height. An example is given in figure 5- 37.

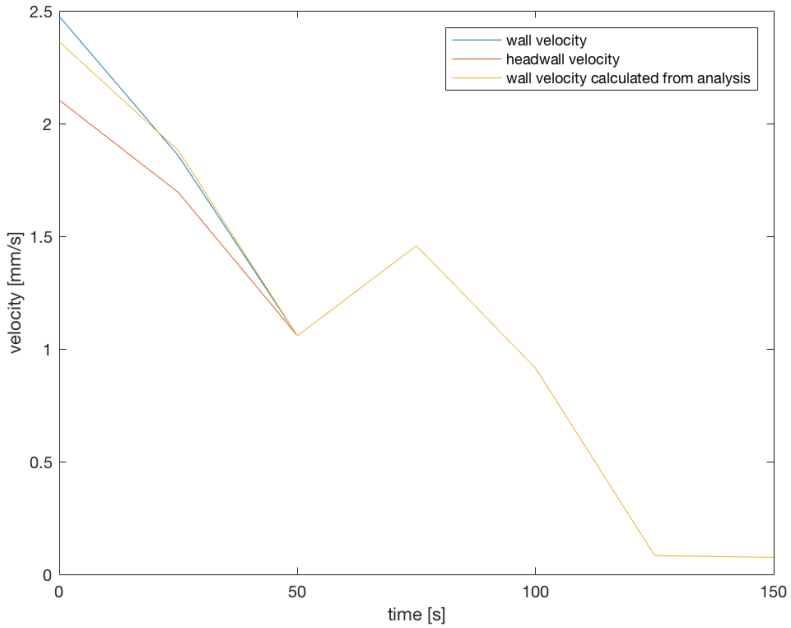

Figure 5- 37: The headwall velocity, wall velocity and calculated wall velocity (experiment 1)

In figure 5- 37 the wall velocity, headwall velocity and the calculated wall velocity are shown. After 50 seconds, the three lines become one because there are no more sliding wedges, which results in the same headwall and wall velocity. Therefore the wall velocity does not have to be calculated there. The results of the other experiments are plotted in Appendix H. The calculated wall velocity is in many cases close to the wall velocity, except in the experiments with a slope on top of the breach. The wall velocities in those experiments are being overestimated, while in the lower initial breaching heights, the wall velocities are being underestimated.

5.3.2.2 Dorsilit 9

The headwall velocity of Dorsilit 9 is not as predictable as Geba Weiss. Due to the higher wall velocity, the RMS value for Dorsilit 9 (RMS = 3.22 mm/s) is also higher compared to Geba Weiss. From the experiments, $n_0 = 0.43$.

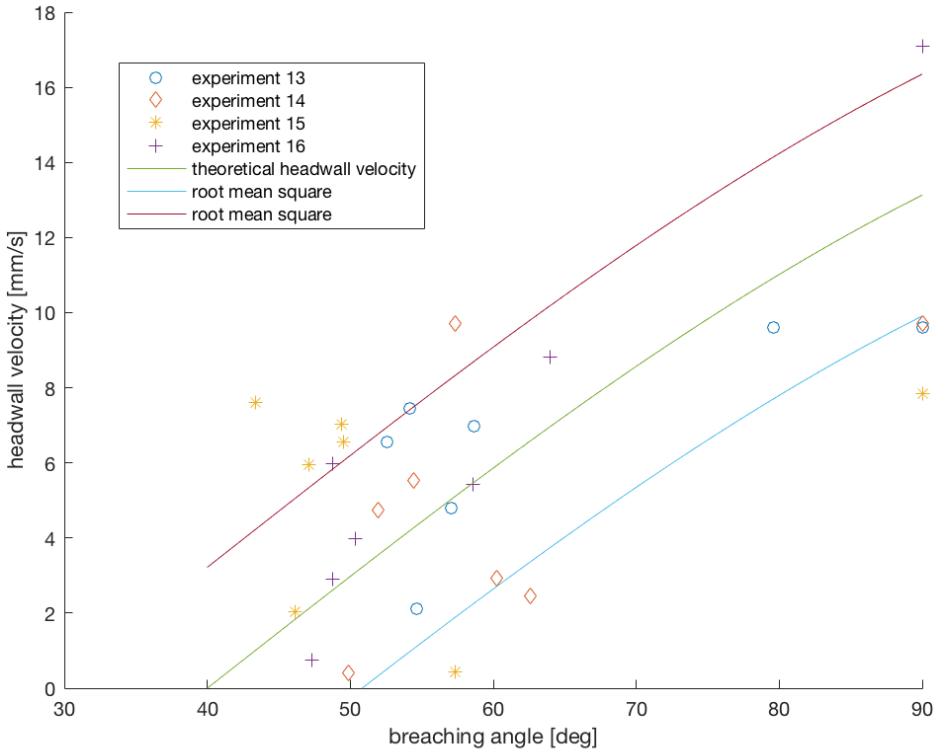

Figure 5- 38: Headwall velocities with nloose = 0.441 (Dorsilit 9)

The analysis with the percentage of sliding wedges was also done with the Dorsilit 9 experiments. The datapoints of the wedge percentage are plotted against the ratio between headwall velocity and wall velocity (see figure 5-38).

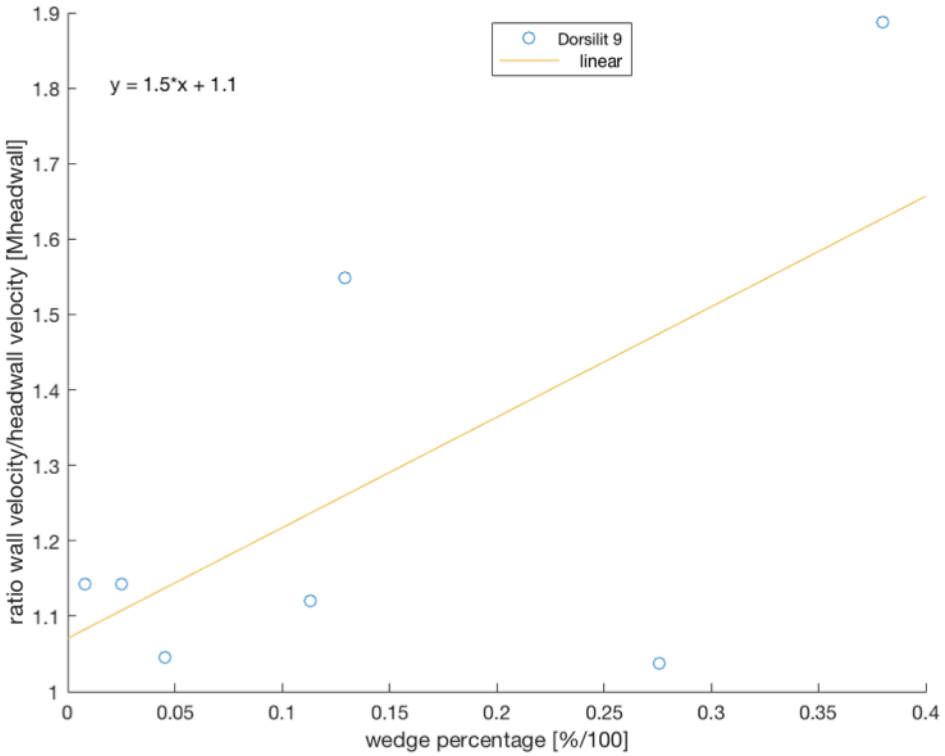

Figure 5- 39: Wedge percentage plotted against ratio wall velocity/headwall velocity (Dorsilit 9)

The following ratio was found for Dorsilit 9:

$$M_{headwall} = 1.5 * p_{wedge} + 1.1 \qquad (23)$$

A result can be seen in figure 5-40. The calculated wall velocity is close to the wall velocity and it does approximately predict the wall velocity, while the headwall velocity is almost twice as low at the start of the experiment.

However, the prediction is not always correct (figure 5- 41). This figure shows that the calculated wall velocity overestimates the wall velocity almost 50% at the start of experiment 15.

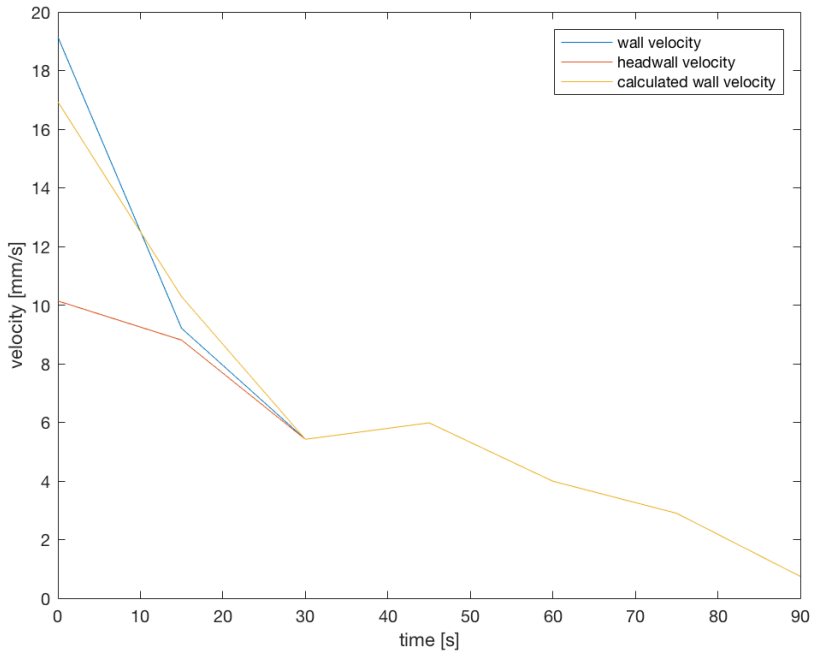

Figure 5- 40: The headwall velocity, wall velocity and calculated wall velocity (experiment 16)

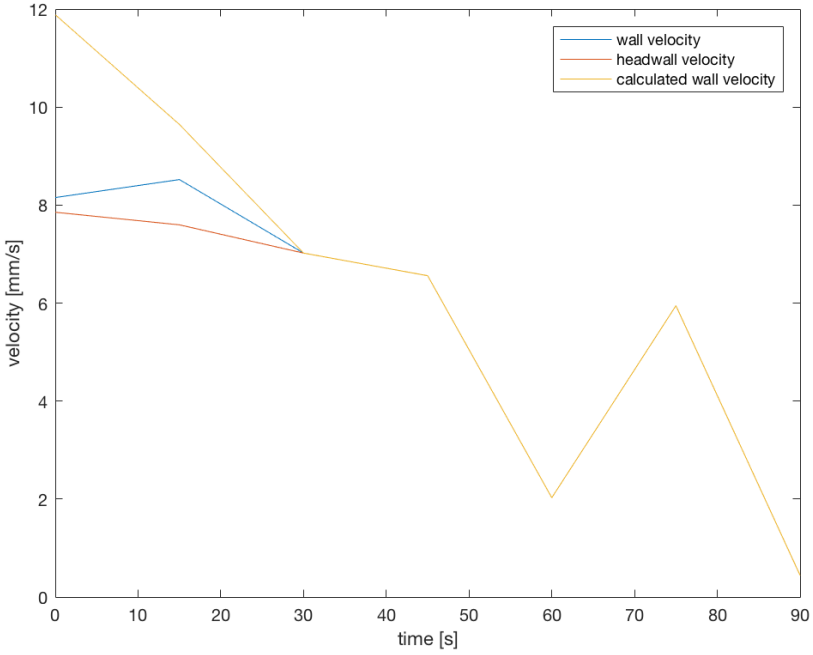

Figure 5- 41: The headwall velocity, wall velocity and calculated wall velocity (experiment 15)

5.3.3 Conclusion wall velocity

The wall velocity is an important parameter in the determination for a stable or unstable breach. The wall velocity can sometimes be calculated from a combination of the headwall velocity and sliding wedge analysis. Due to inaccurate results, it should be used as an indication of what the wall velocity might be.

Sliding wedges increase the headwall velocities and the sliding wedge percentages from section 5.1 can be used to estimate the wall velocity. Using the headwall velocity, active breaching height and the percentage of sliding wedges, the wall velocity is obtained.
The following formula can be used to estimate the wall velocity from the headwall velocity.

$$v = v_{headwall} * M_{headwall} \quad (22)$$

The percentages of sliding wedges can be estimated using the following empirical formulas:

$$p_{wedge} = 2.482 * h^{5.34} \quad (16)$$

for Geba Weiss breaches without slopes on top of the breach until a breaching height of 1.4m.

$$p_{wedge} = 2.865 * h^{10.68} \quad (17)$$

for Geba Weiss breaches with slope on top of the breach until a breaching height of 1.2m.

$$p_{wedge} = 8.387 * h^{7.223} \quad (18)$$

for Dorsilit 9 breaches until a breaching height of 1.4m.

The $M_{headwall}$, the ratio between the headwall velocity and the wall velocity, can be estimated with the following formulas:

$$M_{headwall} = 1.7 * p_{wedge} + 1.1 \quad (20)$$

for Geba Weiss.

$$M_{headwall} = 1.5 * p_{wedge} + 1.1 \quad (23)$$

for Dorsilit 9.

5.4 Stable and unstable breaches

This section contains an analysis of the breaches, whether they are stable or unstable. The research question to be answered is: Can an unstable breach be predicted?

5.4.1 Geba Weiss

Van Rhee (2015) proposed the following equation to predict the stability of a breach:

$$i_{crit} = 0.0049 * D_{50}^{0.92} * s^{-0.39} \quad (15)$$

This is the critical angle at the toe of a breach and this equation should be compared with the angle at the top of the breach. When the critical angle is steeper than the angle on top of the breach, the active breaching height will decrease, which means that the breach is stable. An unstable breach develops when the active breaching height increases, thus when the critical angle is shallower than the angle on top of the breach.

When equation 9 is applied for our conducted experiments, some of the experiments are expected to be unstable (experiments 7, 9, 11 and 12).

One of the results (experiment 9) can be seen in figure 5-42 and table 14. It can be seen that the first step to the second is unstable, as the active breaching height increases.

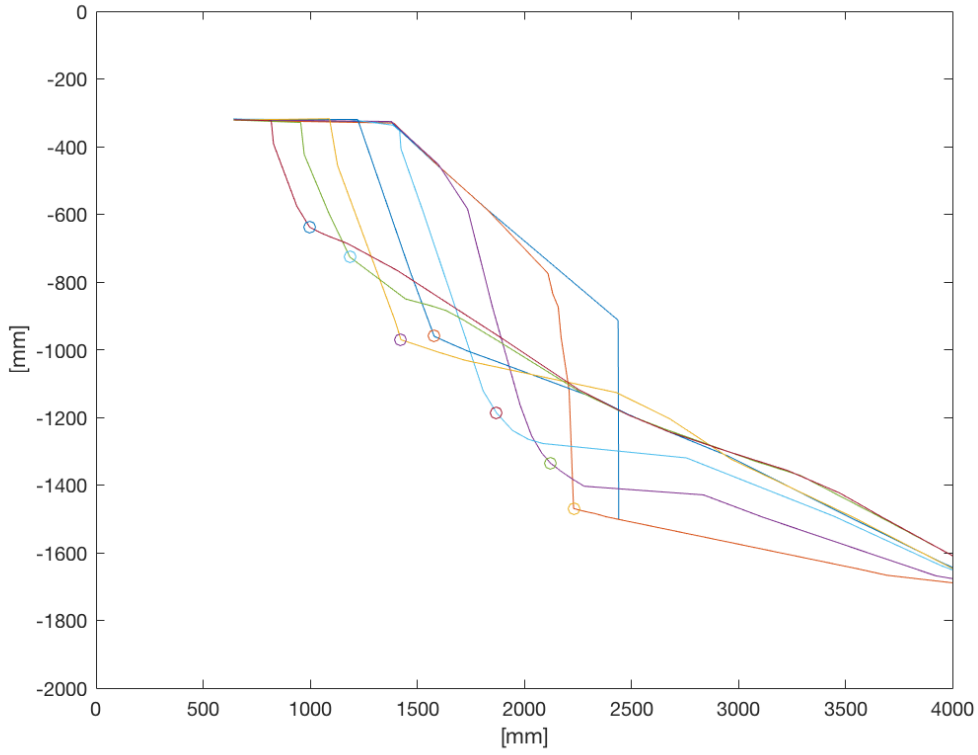

Figure 5- 42: Unstable breach (Geba Weiss)

Experiment 9	Active breaching height [mm]
0 sec	890
90 sec	1140
180 sec	988
270 sec	863
360 sec	661
450 sec	649
540 sec	366
630 sec	327

Table 14: Unstable breach

Equation 15 is used to calculate the critical angle of at the toe of the breach. The sandflux (s) is determined by comparing the profile of the timestep to the initial profile.

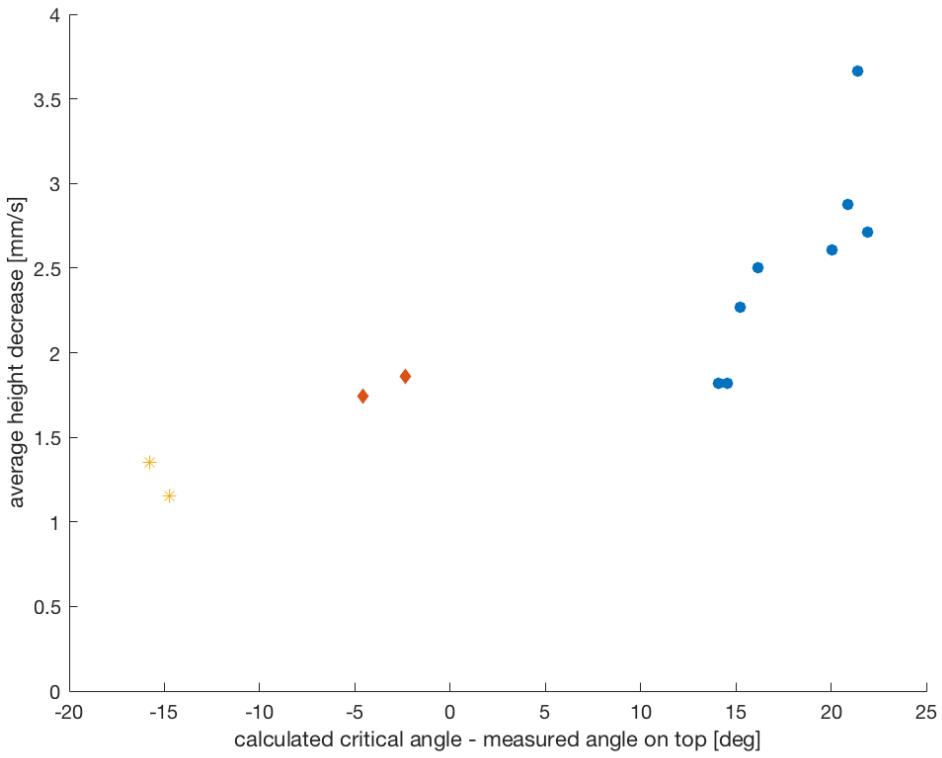

Figure 5- 43: critical angle minus the slope on top of the angle versus the decrease of the active breaching height

The more stable the breach is, the faster the active breaching height should decrease. In figure 5-43, the critical slope angle minus the slope on top of the breach is plotted against the average decrease of the active breaching height in mm/s. The right side of the graph is stable, according to equation 9 and the more to the left, the more unstable the breach should be.
The average decrease of every experiment is plotted, to see whether the more unstable breaching processes (when the critical angle minus the angle on top is negative) have differences with the stable breaching processes. Figure 5-43 shows that the more stable a breach is, the faster the height decreases.

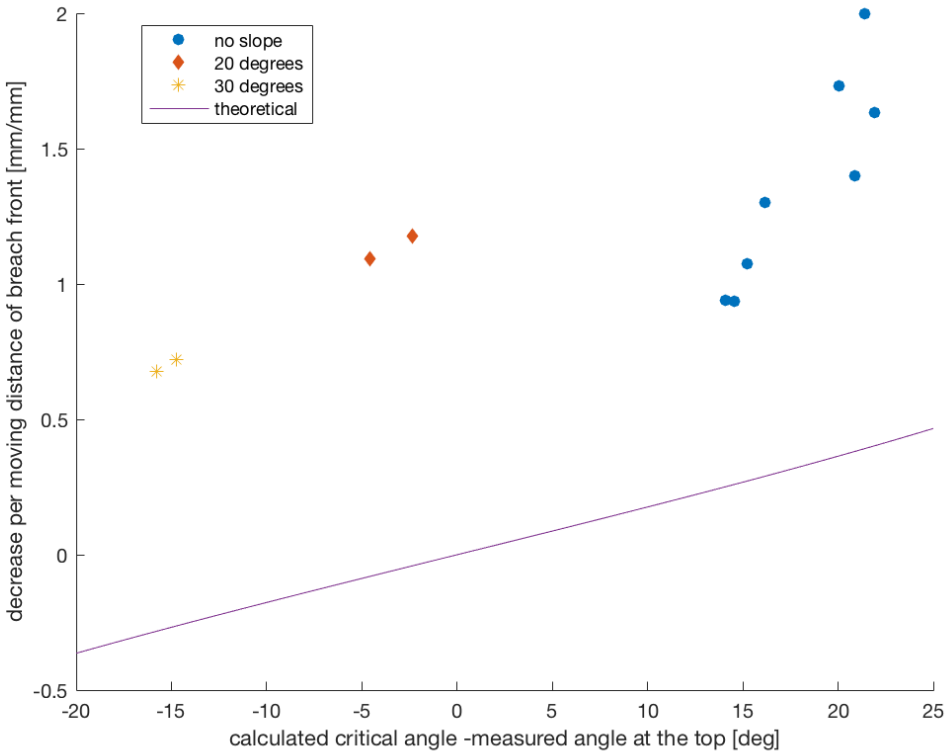

Figure 5- 44: the decrease per moving distance of the breach plotted with the theoretical decrease

Figure 5-44 shows the decrease of the active breaching height and the theoretical decrease of the active breaching height per traveled distance of the breaching front. However, the decrease and the theoretical decrease are very different. Where the theoretical line is much lower than the observed decrease. Equation 15 (Van Rhee, 2015) assumes that if the critical angle at the toe of the breach is smaller than the angle on top of the breach, the breach is unstable, which does not always seem to be the case.

Figure 5-44 also shows that the more stable a breaching process is, the bigger the decrease of active breaching height is per distance. And the most unstable breaching processes, in theory, (experiments with a slope of 30 degrees) have the smallest decrease in active breaching height.

5.4.2 Dorsilit 9

With the experiments in Dorsilit 9, only one experiment had an initial slope on top of the breach. This experiment was only unstable from the first to second timestep, as the active breaching height increases only there. After that, a sliding wedge occurred making it become stable.

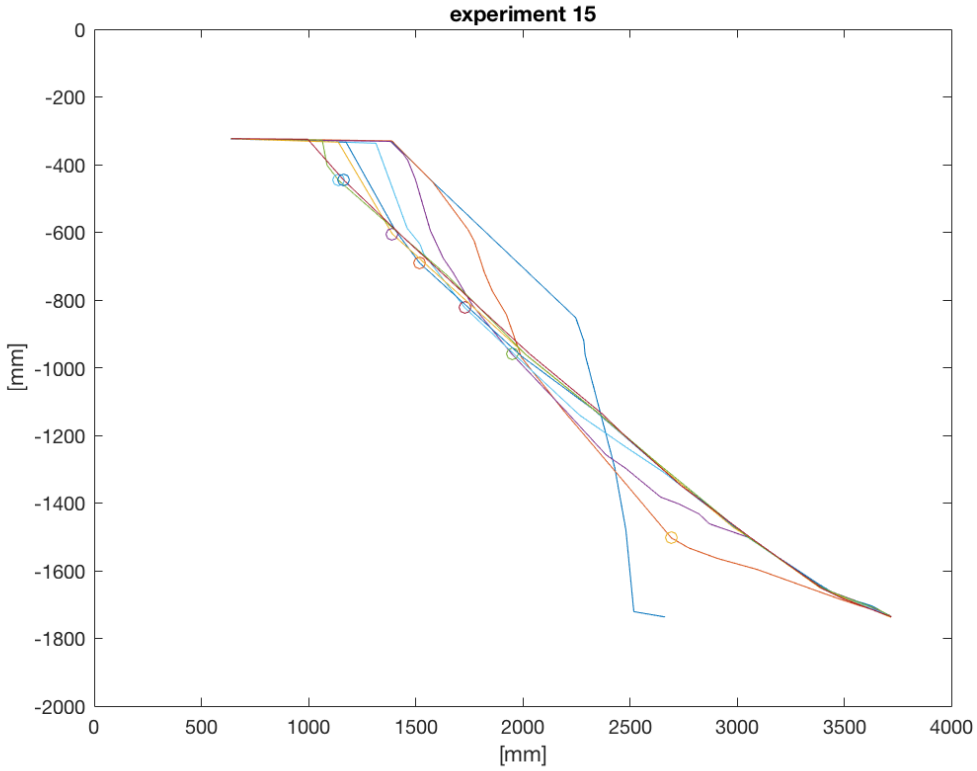

Figure 5- 45: Unstable breach (Dorsilit 9)

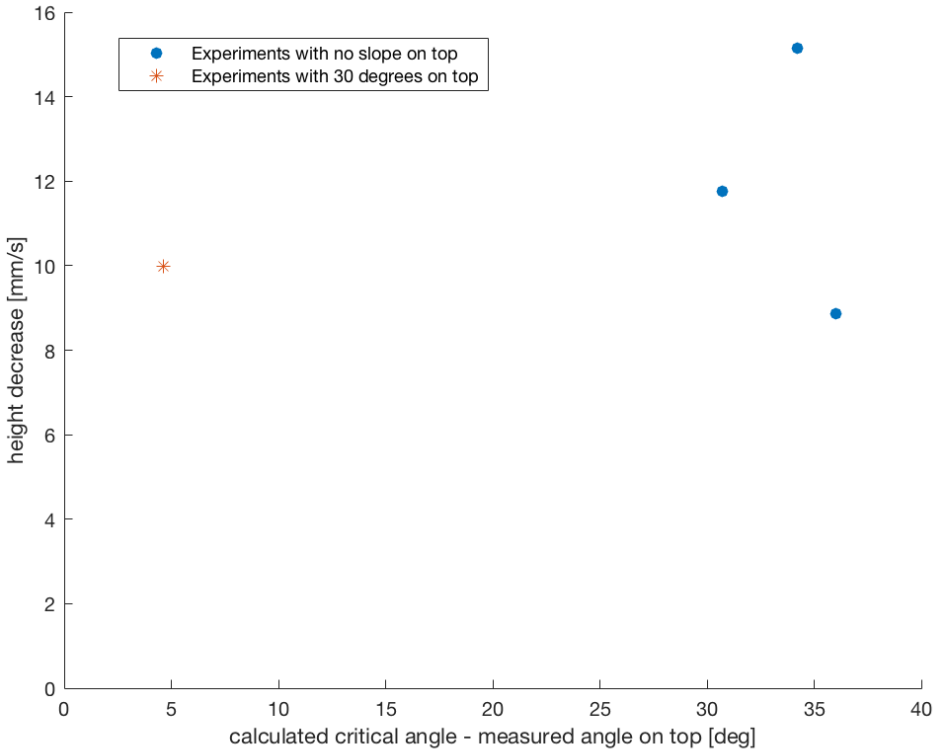

Figure 5- 46: critical angle minus the slope on top of the angle versus the decrease of the active breaching height

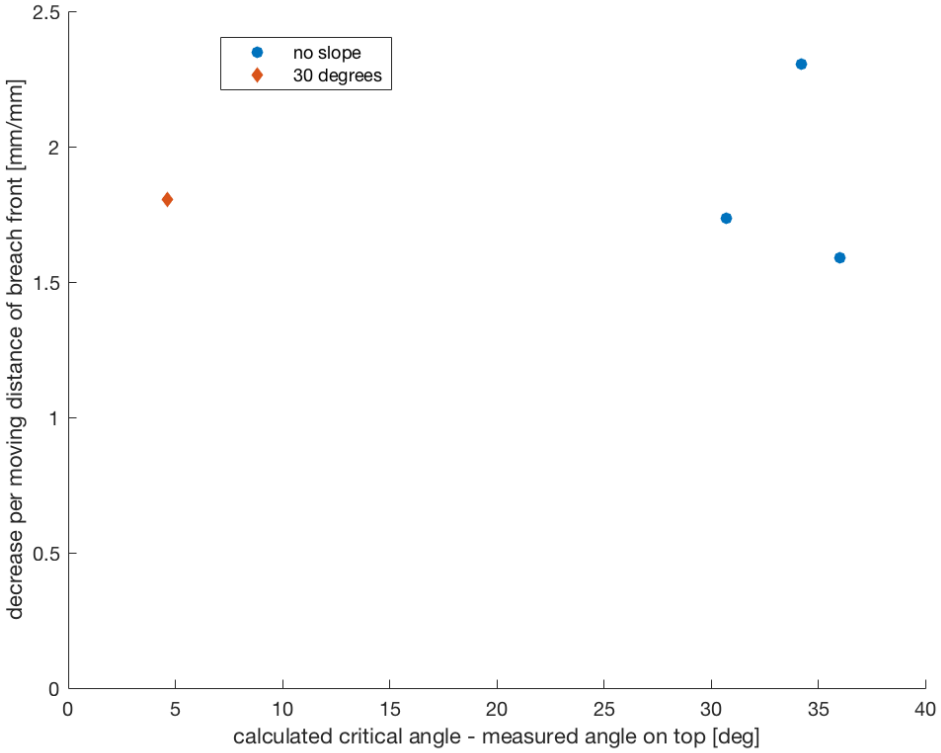

Figure 5- 47: the decrease per moving distance of the breaching front

Figure 5-45 shows that the height decrease for Dorsilit 9 is faster than Geba Weiss. This has to do with the bigger particle size distribution of Dorsilit 9 compared to Geba Weiss. The bigger particle size distribution is causing the sand to move faster, have bigger sliding wedges, which results into a faster decrease in height.
Also the decrease is bigger per moving distance of the breaching front for Dorsilit 9.

5.4.3 Conclusion stable/unstable breach

It might be true that sliding wedges make a breach more stable, however this can not be concluded from this research yet, where this is only observed in the experiments.
The decrease of the breaching height per moved distance shows that experiments that do meet the requirements of equation 15 are more unstable, as the decrease of breaching height is slower per moved distance.

Further research is required, and should contain the critical angle versus active breaching height decrease, when only looked at the pure breaching aspect. So the sliding wedges should be excluded when analyzing this.

Equation 15 does not guarantee an unstable breach. It should only be used for indications, because it seems like the critical angle is not the only decisive factor for unstable breaches.

6. Modelling

This chapter contains a validation of the model (You et al., 2012 and You et al., 2014) with our experimental data. The model gives an indication of the underpressures during breaching. To validate the model, the outcome of the model has been compared to the results of the experiments. After fitting the model with the available test data, sliding wedges can be used as an indication to predict sliding wedges.

6.1 Two dimensional transient pore pressure model

You et al. (2012) derived an equation to predict the evolution of excess pore pressure u^*. It is assumed that there is only pure breaching (so no occurance of sliding wedges). The model of You is almost the same as the model of Meijer and van Os (1976), the difference will be discussed later in this section.

In this model of You it is assumed that the fluid is incompressible, and that flow inside the sand follows Darcy's law:

$$q = -\frac{k}{\rho_w * g} \nabla u^* \quad (24)$$

Where q is the flux or the discharge per area, ρ_w is the density of water, k is the permeability and g the gravitational force.
From mass balance follows:

$$\nabla \cdot q_f = -\frac{\partial e}{\partial t} \quad (25)$$

Where e is the volumetric strain. Combining Darcy's law and the mass balance equation results into:

$$\nabla \cdot \left(\frac{k}{\rho_w * g} * \nabla \cdot u^*\right) = \frac{\partial e}{\partial t} \quad (26)$$

The coordinate system used in this model moves along with the moving breaching front. It is assumed that it moves with a constant velocity v_{wall}. In this new frame of reference, the time derivative becomes:

$$\frac{\partial}{\partial t} = \frac{\partial}{\partial t} - v_{wall} * \frac{\partial}{\partial x} \quad (27)$$

Combining equation 26 and equation 27 results in:

$$\frac{k}{\rho_w * g} * \nabla^2 u^* = \frac{\partial e}{\partial t} - v_{wall} * \frac{\partial e}{\partial x} \quad (28)$$

As mentioned the x-coordinate in this case is the x-coordinate in the moving frame of reference. Until equation 28 the model from You et al. (2012) and Meijer and van Os (1976) follows the same approach. The difference between the two models is the way the volumetric strain e is calculated. The volumetric strain e is composed of two terms. It is the sum of the elastic component e_{el} and dilatancy component e_{dil}.
You et al. (2012) and Meijer and van Os (1976) both calculated the elastic volumetric strain in the same manner. The relation of elastic stress strain was assumed for the soil skeleton and can be deduced as:

$$e_{el} = -\Delta p' * m_u = \Delta\left(\frac{\sigma_1 + \sigma_3}{2} - u^*\right) * \frac{1}{m_u} \quad (29)$$

Where σ_1 is the major principal stress and σ_3 is the minor principal stress, and m_u is the isotropic unloading compressibility:

$$m_u = \frac{G}{1 - 2v} \quad (30)$$

With G the shear modulus and ν is the Poisson ratio.

$$e_{dil} = \Delta q' * m_q = \Delta \left(\frac{\sigma_1 - \sigma_3}{2}\right) * m_q \quad (31)$$

The dilatancy component of the volumetric strain (e_{dil}) is where the models of You et al and Meijer and van Os differ. To create a more stable outcome of the model, You et al. (2012) chose for a constant m_q in order to be able to give an analytical solution. However in his latest model (You et al., 2014), his m_q (the volumetric strain per unit differential stress) was dependent on σ_1/σ_3, just like in Meijer and van Os. In this research, the simpler version with the constant m_q is used.

Combining equation 28, 29 and 31 result in:

$$\begin{aligned}\frac{k}{\rho_w * g} * \nabla^2 u^* = \frac{m_u}{2} * \left(\frac{\partial \sigma_1}{\partial t} + \frac{\partial \sigma_3}{\partial t}\right) - m_u * \frac{\partial u^*}{\partial t} + \frac{m_q}{2} - \frac{\partial \sigma_3}{\partial t} \\ + v_{wall} * m_u * \left(0.5 * \frac{\partial \sigma_1}{\partial x} + 0.5 * \frac{\partial \sigma_3}{\partial x} - \frac{\partial u^*}{\partial x}\right) \\ - v_{wall} * m_q * \left(0.5 * \frac{\partial \sigma_1}{\partial x} - 0.5 * \frac{\partial \sigma_3}{\partial x}\right) \quad (32)\end{aligned}$$

σ_1 is assumed to be constant in the x-direction and in time. And σ_3 is assumed to be constant in time, but not in x direction. This results into the following equation:

$$\frac{\partial u^*}{\partial t} + \frac{k}{\rho_w * m_u * g} \nabla^2 u^* = v_{wall} * \frac{\partial u^*}{\partial x} + v_{wall} \left(0.5 + \frac{m_q}{2 * m_u}\right) * \frac{\partial \sigma_3}{\partial x} \quad (33)$$

The evolution of excess pore pressure u^* can then be rewritten (You et al., 2014) as follow:

$$\frac{\partial \mathrm{u}^*}{\partial \mathrm{t}} = C_{vx} \left(\frac{\partial^2 u^*}{\partial \mathrm{x}^2}\right) + C_{vy} \left(\frac{\partial^2 u^*}{\partial \mathrm{y}^2}\right) + \mathrm{v_{wall}} \left(\frac{\partial \mathrm{u}^*}{\partial \mathrm{x}}\right) - \mathrm{v_{wall}} * \beta \left(\frac{\partial \sigma_\mathrm{h}}{\partial \mathrm{x}}\right) \quad (34)$$

With C_{vx} and C_{vy} the coefficients of consolidation for the deposit in horizontal and vertical directions $[m^2/s]$:

$$C_v = \frac{k}{m_u * \rho_w * g} \quad (35)$$

And β is defined as the relative dilation strength, based on triaxial experiments on the sand:

$$\beta = \frac{1}{2} + \frac{m_q}{2 * m_u} \quad (36)$$

The first two terms on the right hand side describe the pore pressure dissipation by Darcy flow with a moving boundary.
The fourth term on the right hand side is a pore pressure sink caused by continuous dilation, which is a function of the change in least principal stress.
The pore pressure dissipation caused by the pore water flow is defined by $C_{vx} \left(\frac{\partial^2 u^*}{\partial \mathrm{x}^2}\right) + C_{vy} \left(\frac{\partial^2 u^*}{\partial \mathrm{y}^2}\right)$
The term $\mathrm{v_{wall}} \left(\frac{\partial \mathrm{u}^*}{\partial \mathrm{x}}\right)$ represents the pore pressure changes from the retreating failure front.
$\mathrm{v}\beta \left(\frac{\partial \sigma_\mathrm{h}}{\partial \mathrm{x}}\right)$ is the source for pore pressure drop, in this case $\left(\frac{\partial \sigma_\mathrm{h}}{\partial \mathrm{x}}\right)$ is the change in horizontal effective stress. The spatial change in horizontal stress σ_h is modelled as an exponential function of the distance from the failure front:

$$\frac{\partial \sigma_\mathrm{h}}{\partial \mathrm{x}} = k_0 * \rho_s * g * \eta * y * e^{-\eta x} \quad (37)$$

Equation 34 will be used in the numerical implementation in Matlab for the modelling of underpressures.

6.2 Numerical implementation

The grid that is used is a rectangular grid with a length and width of 2m x 1.1m, with square gridcells. The used boundary conditions are as follows:

- the left and bottom side are modelled as no flow, this is done in Matlab by making the last cell the same value as the second-last cell.
- Another boundary condition is that the underpressure is assumed to be zero at the right and upper boundary. The excess pore pressure is assumed to be zero at the breaching front and at the end of the breach.

In the model, using the pore pressure of the current timesteps at the following locations in the grid: $u^n_{i,j}, u^n_{i-1,j}$ and $u^n_{i+1,j}$, the pore pressure of the next timestep $u^{n+1}_{i,j}$ can be calculated.

To obtain the solution at the next timestep, this can be discretized with the following steps:

$$\frac{\partial u^*}{\partial t} = \frac{{u_{i,j}}^{n+1} - {u_{i,j}}^{n}}{\Delta t} \quad (38)$$

$$\frac{\partial^2 u^*}{\partial x^2} = \frac{{u^n}_{i-1,j} - 2 * {u^n}_{i,j} + {u^n}_{i+1,j}}{\Delta x^2} \quad (39)$$

$$\frac{\partial^2 u^*}{\partial y^2} = \frac{{u^n}_{i,j-1} - 2 * {u^n}_{i,j} + {u^n}_{i,j+1}}{\Delta y^2} \quad (40)$$

$$\frac{\partial u^*}{\partial x} = \frac{u^n_{i,j} - u^n_{i-1,j}}{\Delta x} \quad (41)$$

An explicit method is used to create this model in Matlab, this means that the data from the current timestep is used to calculate the next timestep. This method is less stable than the implicit method, but the implicit ones are more complicated and more time consuming (in calculation time).
When the partial derivitive with respect to time of equation 34 is zero, the model will reach its steady state. In Matlab this is implemented by running the simulations until the underpressure drop is less than 0.01 Pa per timestep.

6.3 Stability analysis

A stability analysis (Figure 6-1) can be done with Coulomb's method.

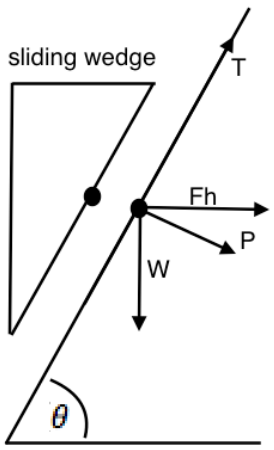

Figure 6- 1: Stability analysis

If the lowest point of the sliding wedge is assumed to be the lowest point of the breach, the resistant force T can be calculated by:

$$T = (W * \cos(\theta) + F_h * \sin(\theta) - P) * \tan(\phi) \quad (42)$$

Where W is the buoyant gravitational force on the wedge.

$$W = \frac{(\rho_s - \rho_w) * g * H^2}{2 * \tan(\theta)} \quad (43)$$

The horizontal intergranular force F_h, generated from lateral earth pressure and the force P from the excess pore pressure that is acting on the slope, are calculated by integrating the horizontal stress σ_h and excess pore pressure u^* along the slope θ:

$$F_h = \frac{1}{\tan(\theta)} \int_0^H \sigma_h \left(\frac{h - y}{\tan(\theta)}, y \right) dy \quad (44)$$

$$P = \frac{1}{\sin(\theta)} \int_0^H u^* \left(\frac{h - y}{\tan(\theta)}, y \right) dy \quad (45)$$

$$\sigma_h = k_0 * (\rho_s - \rho_w) * c * g * y * (1 - e^{-\eta x}) \quad (46)$$

The integrals are determined, by using small intervals of Δy, equal to the height of gridcells. Over this interval a constant value of u^*, determined by the cell centre closest to the point halfway the interval, is used (figure 6-2).

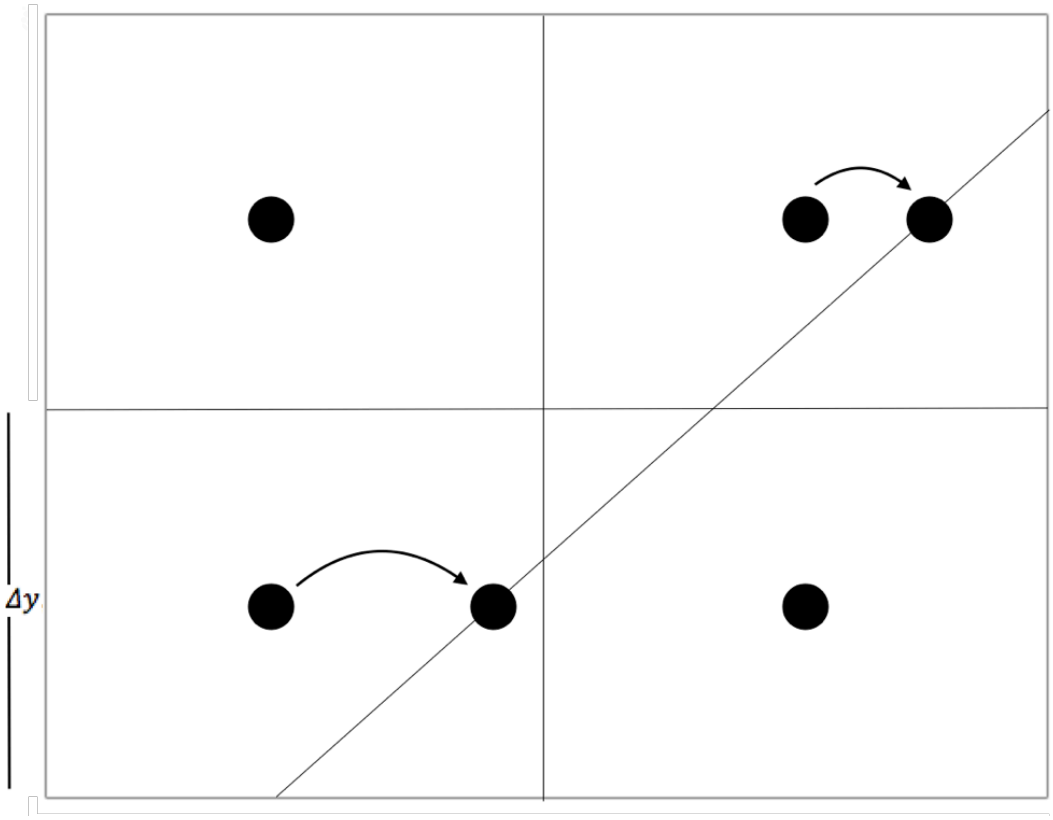

Figure 6- 2: the cell centre closest to the point halfway of the interval is used

To predict when sliding wedges occur in our breach, a stability analysis is needed. The so-called Factor of Safety (FoS) can be used to analyse this. The FoS is the ratio of the shear resistance and gravitational driving force along the slope. If the driving force is larger than the resistance force on the slope, it will start to slide off (sliding wedge). This happens when FoS < 1. The stability condition shows that when the excess pore pressure drops, the FoS increases (FoS ≥ 1), which means that the deposit is more stable (thus the deposit will not slide off).
The Factor of Safety can be calculated with (You et al., 2014):

$$FoS = \frac{\tan(\phi)\,(W * \cos(\theta) + F_h * \sin(\theta) - P) + F_h * \cos(\theta)}{W * \sin(\theta)} \quad (47)$$

Symbol		Unit
c	0.585	[-]
k	$7.22*10^{-5}$	[m^{-2}]
v	$3.5*10^{-3}$	[m/s]
H	1.07	[m]
g	9.81	[m/s^2]
L	2	[m]
ρ_s	2650	[kg/m^3]
ρ_w	1000	[kg/m^3]
m_u	$5*10^{-6}$	[Pa^{-1}]
β	3.1	[-]

Table 15: The used parameters in the model of You (2014).

6.4 Underpressures: model versus experiment data

The values for m_u and β are fitted in a manner that the data from the model fits the data from the experiment. The rest of the used parameters are shown in table 15. Only certain heights of the steady state solution of the model will be analyzed. In this case it is not unclear whether the results of the experiment are also steady state.

Figure 6-3 shows a steady state plot of the underpressure calculated by the model and the underpressures from an experiment. It can be seen that the shape and size of the underpressure of the model is similar to the underpressure of the experiment (experiment 10). Both the model and experiment used a breaching height of 1.07m high and a pressure measurement at 0.8m. Afterwards a FoS calculation is done using this data (figure 6-4).

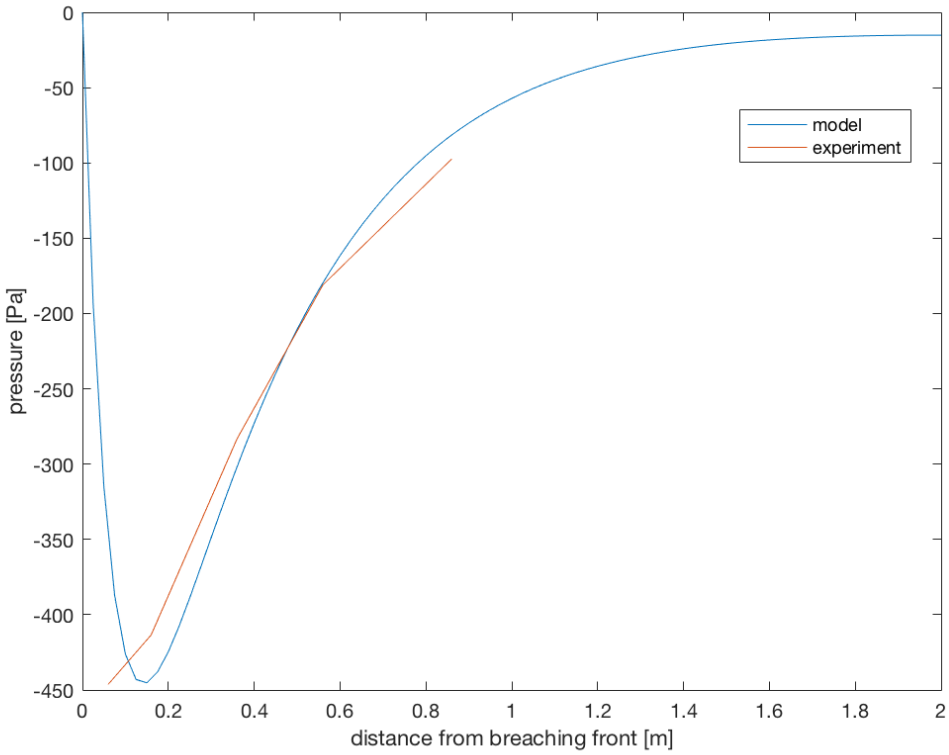

Figure 6- 3: The underpressure from the model compared to the measured underpressure from the experiment (experiment 10, after 90 seconds) at a height of 1.07m. Both profiles are at a height of 0.3m from the top.

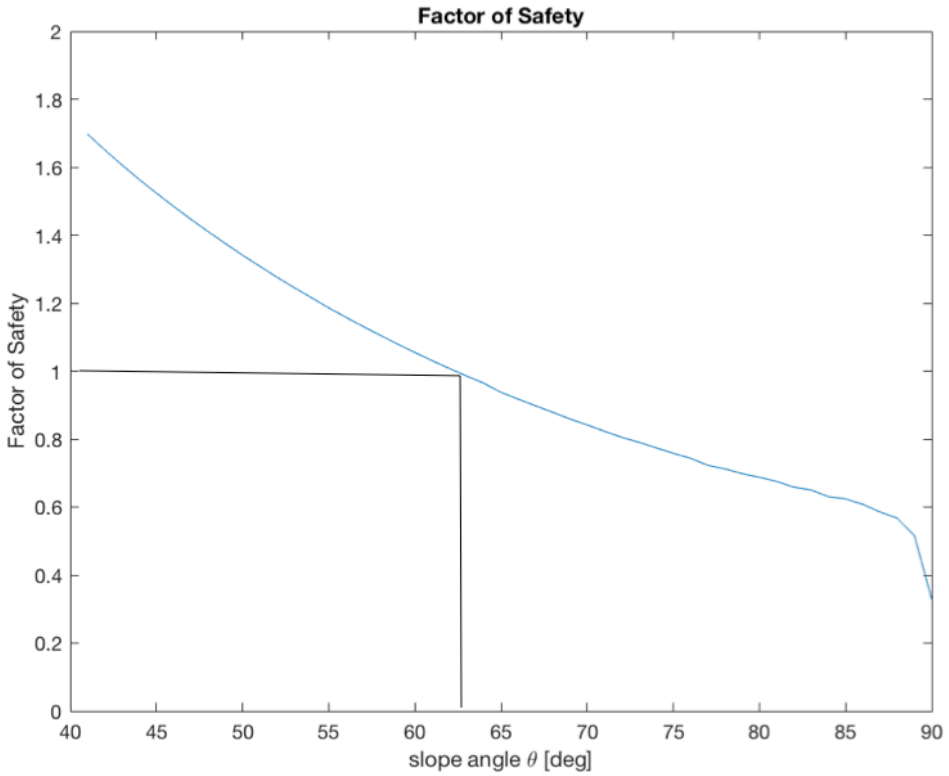

Figure 6- 4: Factor of Safety at a height of 1.07m.

What can be seen in figure 6-4 is that the breach is susceptible for sliding wedges at slope angles above approximately 63°.
However, in the model it is assumed that the breach is 90° and sliding wedges did occur in the experiment around the time of the calculated pore pressures.

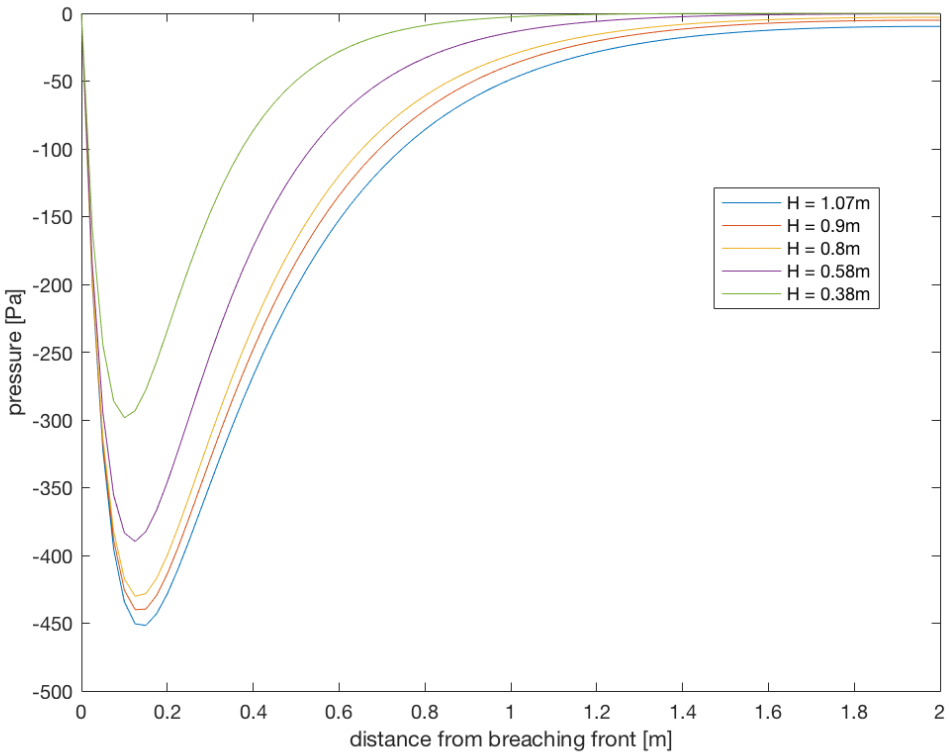

Figure 6- 5: The steady state solution of the underpressure of the model at different breaching heights. All underpressures are measured at 0.3m from the top.

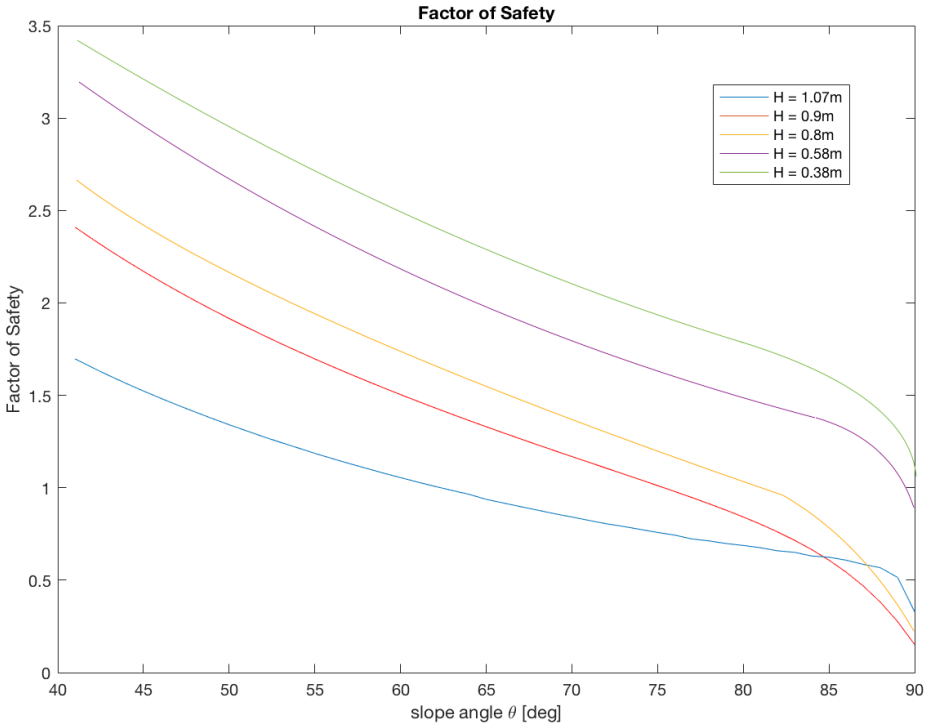

Figure 6- 6: The Factor of Safety calculation of different breaching heights.

Figure 6-5 and figure 6-6 show the steady state solution of other breaching heights and the corresponding FoS calculations, respectively. It can be seen that it predicts that the breach with a height of 0.58m, sliding wedges will still occur, which is not the case in the experiment (experiment 10). So this shows that the model is not accurate enough yet to exactly predict when breaches are susceptible to sliding wedges. However, this can also be due to the fact that the data in the experiment was not steady state.

An important remark to be made is that You et al. had data that did not fit the model, so they lowered the permeability with a factor 5 to ensure the outcome of the model fitted his measured data. Furthermore, the underpressure is dependent of the dilatancy potential, which makes it dilate even if the sandpackage does not shear. It is expected that at a certain breaching height the maximum underpressure is not dependent of the material, because the underpressure that is needed to keep the sand stable is the same for all materials (if the same density is assumed). However, in the model of You, the maximum underpressure is dependent on the dilatancy potential, which is material dependent. Another shortcoming of the model is the lack of concentration as a variable. The current concentration should have a strong effect on the dilation (Rondon et al., 2011).

Further research is needed to take a look at non steady state solutions and compare the data with this research to see whether that gives a better prediction of the sliding wedges at certain heights. Furthermore, in future research the concentration should be implemented as a variable in the model instead of a constant value, in order to have a more accurate model.

6.5 Conclusion

From the steady state solution of the underpressure model (You et al., 2014), it can not be exactly predicted when the breach will produce sliding wedges or not. However, it does show that the height of a breach affects its susceptibility to sliding wedges, with more sliding wedges expected for higher breaches. Therefore it can and should only be used as an indication. The underpressure of the model was fitted to the data from the experiments in order to get the same kind of results in underpressure. Also, in this model only the steady state solution of the model was used. This resulted in a Factor of Safety calculation, which gives an indication whether the breach is susceptible to sliding wedges (FoS > 1) or not (FoS < 1).
You et al. (2014) also had data that did not fit their model, so they lowered the permeability with a factor 5 in order to fit the data. The model also does not have the concentration as a variable, which might have an effect on the dilation.

7. Conclusions and recommendations

This chapter contains a summary of all the conclusions and recommendations from the previous chapters. Finally conclusions regarding the main research question are addressed.

7.1 Wall velocities, sliding wedges

The sliding wedges can be predicted using the active height range and sand type. The experiments show that a sand type with a higher permeability (Dorsilit 9, compared to Geba Weiss) produces larger volumes of sliding wedges and also more frequent sliding wedges.
The active breaching height affects the frequency and volumes of the sliding wedges. Higher active breaching heights give higher frequencies as well as larger volumes of sliding wedges. Until a height of 1.4m, this is an exponential growth. However, without a height of 1.4m, the trendline is a linear line. Further research should include higher breaching heights, to see whether the exponential growth is valid.

A sliding wedge affects the angle at the toe. After a large sliding wedge, the angle at the toe of the breach becomes steeper, compared to the angle at the toe before a sliding wedge or after a small sliding wedge. Another effect of the sliding wedge is that it affects the breaching angle. After every sliding wedge, the breaching angle decreases. This keeps the sand body more stable as a shallower breaching angle means a more stable sand body.

Measured headwall velocities were compared to the analytical theory for the headwall velocities. This theory does not take the effects of sliding wedges into account.
However, the wall velocities including the sliding wedges can be estimated using the sliding wedge analysis and headwall velocity. This does not work for every initial breaching height. This only works for experiments with higher initial breaching heights.

Future research concerning the sliding wedges and wall velocities are useful.
The prediction of sliding wedges needs more attention, as higher active breaching heights have not been tested. The empirical formula to predict the percentages of sliding wedges is an exponential formula, which has not been tested for heights above 1.4 meters.
This means that more experiments should be conducted, with higher and more different initial heights.

Also more research is needed to be able to predict the wall velocity more accurately. The calculation of wall velocity can now be used as an indication. Future research for sliding wedges can also be linked to the future research of wall velocity, because the sliding wedges affect the wall velocity.

7.2 Angle at the toe

The experiments show that the angle at the toe can be calculated using the sandflux analysis. At the beginning of an experiment, the angle at the toe can not exactly be calculated, as the theoretical angle at the toe is not similar to the real angle at the toe. The angle converges towards the angle predicted by the equation. This might have to do with the higher sand fluxes at the start of the experiments.

From the experiments, for Geba Weiss, the angle at the toe converges to the angle predicted by the formula. This is dependent on the initial breaching height and is a linear function.

For Dorsilit 9, the angle at the toe did not converge to the formula angle, this might have to do with the fact that the formula was designed for finer sands and not for coarse sand types like Dorsilit 9. More experiments should be done with Dorsilit 9, before one is able to predict the angle at the toe with Dorsilit 9. The experiments that were conducted, contained too few experiments with Dorsilit 9 to make any conclusions.

Because the angle at the toe is not accurate with higher sand fluxes, further research is needed in order to have a more precise formula for the angle at the toe, especially at greater heights, due to the higher sandflux compared to smaller heights.

7.3 Modelling

The steady state solution of the model of (You et al, 2014) can not exactly predict when the breach is susceptible to sliding wedges. However, it does show that the height affects whether a breach is susceptible to sliding wedges or not, where more sliding wedges are expected at higher breaching heights. Therefore it can be used as an indication to check whether a breach will have sliding wedges or not. This was realized after fitting the data from the model to the data from the experiments.
You et al (2014) also had to fit their data to their model's data, by lowering the permeability with a factor 5, in order to get results from the model that were similar to the data from his experiment. Besides, the model also does not have concentration as a variable. The current concentration should have a strong effect on dilation.
In our model, only the steady state solution was used, however in the experiments it is not clear if the situation was at steady state.

Further research should contain the model with non steady state solutions, to see whether it has better predictions than in this research. Eventually the model should have concentration as a variable instead of a constant value.

7.4 Stable and unstable breach

The three subquestions were answered to check whether the stable/unstable equation is right or has to be adjusted. The equation to determine its stable or unstable is:

$$i_{crit} = 0.0049 * [\rho_s * (1 - n_0) * H * v_{headwall}]^{-0.39} * D_{50}^{0.92}$$

The $v_{headwall}$ does not take sliding wedges into account, which results into a steeper angle, as the wall velocity will be greater than expected. If $v_{headwall}$ is replaced by v_{wall}, the equation will be more accurate.

When using the critical angle at the toe to estimate the change of breaching height, this change is underestimated. This leads to a faster decreasing breaching height than expected, which means the stability of the breach is higher than the critical angle suggests.

The decrease of breaching height might be affected by the sliding wedges.
Therefore further research is required and should contain the critical angle versus the active breaching height decrease, for pure breaching (or the headwall velocity). This means that it should not contain the sliding wedges.
The experiments from this thesis can also be used for this by measuring the decrease of the breaching height between two sliding wedges.

Bibliography

Beinssen, K., Neil, D.T., Mastbergen, D.R. (2014). Field observations of retrogressive breach failures at two tidal inlets in Queensland, Australia. *Australian Geomechanics (Engineers Australia)*.

Bezuijen, A., Mastbergen, D.R. (1988). On the constructions of sand fill dams - Part 2: Soil mechanical aspects. *Int. Symp. on Modelling Soil-Water-Structure Int., Delft*.

Breusers, H.N.C. (1974). Suction of sand. *Engineering geology* no.10, 65-66.

Breusers, H.N.C. (1977). Hydraulic excavation of sand. *Delft Hydraulics Laboratory*.

Choi, J.K.H. (2017). OE54000 Internship report: The setup and calculations for a breaching process. *Delft University of Technology*.

Hampton, M.A., Lee, H.J. (1996). Submarine landslides. *Department of Geology and Geological Engineering Laval University, Quebec City, Canada*.

Hance, J.J. (2003). Submarine slope stability. *The University of Texas at Austin*.

Mastbergen, D.R., Van den Berg, J.H. (2003). Breaching in fine sands and the generation of sustained turbidity currents in submarine canyons. *Sedimentology,* 50, 625-637.

Mastbergen, D.R., Winterwerp, J.C., Bezuijen, A. (1988). On the constructions of sand fill dams - Part 1: Hydraulic aspects. *Int. Symp. on Modelling Soil-Water-Structure Int., Delft*.

Meijer, K.L., Van Os, A.G. (1976). Pore pressure near moving underwater slope. *Journal of the geotechnical engineering division*. 361-372.

Noordermeer, B.M. (2017). OE4611-13 Calibration of the measurement devices for the vertical breaching process . *Delft University of Technology*.

Rondon, L., Pouliquen, O., Aussillous, P., (2011). Granular collapse in a fluid: Role of the initial volume fraction. *Physics of Fluids*.

Van der Schrieck, G.L.M. (2012). CIE5300 Lecture notes dredging technology. *Delft University of Technology*.

Weij, D., Keetels, G.H., Goeree, J., van Rhee, C. (2016). An approach to research of the breaching process. *Wodcon XXI Proceedings*.

Weij, D., Keetels, G.H., Goeree, J., van Rhee, C. (2016). An extension of the drift-flux model for submarine granular flows. *International Journal of Computational Methods and Experimental Measurements,* Vol 4. No. 4.

Van den Berg, J.H., Van Gelder, A., Mastbergen, D.R. (2002). The importance of breaching as a mechanism of subaqueos slope failure in fine sand. *Sedimentology*, 49(1), 81-95.

Van Rhee, C. (2015). Slope failure by unstable breaching. *Maritime Engineering*. Vol. 168. 84-92.

Van Rhee, C., Bezuijen, A. (1998). The breaching of sand investigated in large-scale model tests. *Proceedings 26th. Coastal Engineering Conference, (ASCE)*, 2509-2519.

You, Y., Flemings, P., Mohrig, D. (2012). Dynamics of dilative slope failure. *Geology,* 40(7), 663-666.

You, Y., Flemings, P., Mohrig, D. (2014). Mechanics of dual-mode dilative failure in subaqueous sediment deposits. *Earth and Planetary Science Letters 397,* 10-18.

Appendix A Test Results Wall Velocity

All results of the wall velocities can be seen. The wall velocities are the average wall velocities between the times. For example, experiment 1, 0-25sec had an average wall velocity of 2.476 mm/s.

Experiment 1	Wall velocity [mm/s]
0-25 sec	2.476
25-50 sec	1.857
50-75 sec	1.059
75-100 sec	1.458
100-125 sec	0.914
125-150 sec	0.0833
150-175 sec	0.075

Experiment 2	Wall velocity [mm/s]
0-30 sec	3.591
30-60 sec	2.232
60-90 sec	2.405
90-120 sec	1.173
120-150 sec	1.581
150-180 sec	1.429
180-210 sec	2.003

Experiment 3	Wall velocity [mm/s]
0-30 sec	2.038
30-60 sec	3.054
60-90 sec	1.535
90-120 sec	1.609
120-150 sec	1.332
150-180 sec	1.339
180-210 sec	0.725

Experiment 4	Wall velocity [mm/s]
0-60 sec	3.129
60-120 sec	3.03
120-180sec	2.149
180-240sec	1.286
240-360sec	1.70
360-420 sec	1.136
420-480 sec	1.033

Experiment 5	Wall velocity [mm/s]
0-60 sec	3.241
60-120 sec	3.164
120-180sec	2.147
180-240sec	1.983
240-360sec	1.89
360-420 sec	1.672
420-480 sec	0.705

Experiment 6	Wall velocity [mm/s]
0-60 sec	2.224
60-120 sec	1.781
120-180sec	1.637
180-240sec	1.523
240-360sec	1.128
360-420 sec	1.410
420-480 sec	0.846

Experiment 7	Wall velocity [mm/s]
0-60 sec	1.332
60-120 sec	1.481
120-180sec	1.240
180-240sec	0.764
240-360sec	0.738
360-420 sec	0.407
420-480 sec	0.0919

Experiment 8	Wall velocity [mm/s]
0-90 sec	3.463
90-180 sec	1.959
180-270 sec	2.336
270-360 sec	1.287
360-450 sec	1.638
450-540 sec	1.475
540-630 sec	1.398

Experiment 9	Wall velocity [mm/s]
0-90 sec	1.833
90-180 sec	2.137
180-270 sec	1.991
270-360 sec	1.876
360-450 sec	1.857
450-540 sec	1.724
540-630 sec	1.418

Experiment 10	Wall velocity [mm/s]
0-90 sec	3.869
90-180 sec	1.916
180-270 sec	1.948
270-360 sec	1.847
360-450 sec	1.386
450-540 sec	1.490
540-630 sec	1.124

Experiment 11	Wall velocity [mm/s]
0-60 sec	1.169
60-120 sec	1.61
120-180sec	1.323
180-240sec	1.093
240-360sec	1.699
360-420 sec	1.195
420-480 sec	1.131

Experiment 12	Wall velocity [mm/s]
0-60 sec	0.879
60-120 sec	0.998
120-180sec	0.865
180-240sec	0.468
240-360sec	0.427
360-420 sec	0.513
420-480 sec	0.559

Experiment 13	Wall velocity [mm/s]
0-5 sec	7.147
5-10 sec	10.98
10-15 sec	6.972
15-20 sec	4.785
20-25 sec	2.128
25-30 sec	7.453
30-35 sec	6.562

Experiment 14	Wall velocity [mm/s]
0-15 sec	15.03
15-30 sec	7.91
30-45 sec	5.532
45-60 sec	4.75
60-75 sec	2.937
75-90 sec	2.446
90-105 sec	0.418

Experiment 15	Wall velocity [mm/s]
0-15 sec	8.153
15-30 sec	8.520
30-45 sec	7.020
45-60 sec	6.558
60-75 sec	2.027
75-90 sec	5.946
90-105 sec	0.444

Experiment 16	Wall velocity [mm/s]
0-15 sec	19.15
15-30 sec	9.206
30-45 sec	5.422
45-60 sec	5.983
60-75 sec	3.992
75-90 sec	2.899
90-105 sec	0.7447

Appendix B Test Results Headwall velocity

The headwall velocities can be seen. Note that after some time, the headwall velocities are the same as the wall velocities, as there are no sliding wedges occurring.

Experiment 1	Pure wall velocity [mm/s]
0-25 sec	2.104
25-50 sec	1.694
50-75 sec	1.059
75-100 sec	1.458
100-125 sec	0.914
125-150 sec	0.0833
150-175 sec	0.075

Experiment 2	Pure wall velocity [mm/s]
0-30 sec	2.694
30-60 sec	1.943
60-90 sec	2.141
90-120 sec	1.001
120-150 sec	1.581
150-180 sec	1.429
180-210 sec	2.003

Experiment 3	Pure wall velocity [mm/s]
0-30 sec	1.829
30-60 sec	2.31
60-90 sec	1.535
90-120 sec	1.609
120-150 sec	1.332
150-180 sec	1.339
180-210 sec	0.725

Experiment 4	Pure wall velocity [mm/s]
0-60 sec	2.789
60-120 sec	2.589
120-180sec	1.963
180-240sec	1.184
240-360sec	1.70
360-420 sec	1.136
420-480 sec	1.033

Experiment 5	Pure wall velocity [mm/s]
0-60 sec	2.983
60-120 sec	2.657
120-180sec	1.945
180-240sec	1.836
240-360sec	1.648
360-420 sec	1.672
420-480 sec	0.705

Experiment 6	Pure wall velocity [mm/s]
0-60 sec	2.058
60-120 sec	1.684
120-180sec	1.580
180-240sec	1.523
240-360sec	1.128
360-420 sec	1.410
420-480 sec	0.846

Experiment 7	Pure wall velocity [mm/s]
0-60 sec	1.173
60-120 sec	1.108
120-180sec	0.911
180-240sec	0.764
240-360sec	0.738
360-420 sec	0.407
420-480 sec	0.0917

Experiment 8	Pure wall velocity [mm/s]
0-90 sec	2.630
90-180 sec	1.685
180-270 sec	1.358
270-360 sec	1.287
360-450 sec	1.638
450-540 sec	1.475
540-630 sec	1.398

Experiment 9	Pure wall velocity [mm/s]
0-90 sec	1.378
90-180 sec	1.432
180-270 sec	1.529
270-360 sec	1.876
360-450 sec	1.857
450-540 sec	1.724
540-630 sec	1.418

Experiment 10	Pure wall velocity [mm/s]
0-90 sec	3.15
90-180 sec	1.72
180-270 sec	1.64
270-360 sec	1.847
360-450 sec	1.386
450-540 sec	1.490
540-630 sec	1.124

Experiment 11	Pure wall velocity [mm/s]
0-60 sec	1.029
60-120 sec	1.437
120-180sec	1.185
180-240sec	1.047
240-360sec	1.699
360-420 sec	1.195
420-480 sec	1.131

Experiment 12	Pure wall velocity [mm/s]
0-60 sec	0.857
60-120 sec	0.913
120-180sec	0.801
180-240sec	0.446
240-360sec	0.427
360-420 sec	0.513
420-480 sec	0.559

Experiment 13	Pure wall velocity [mm/s]
0-5 sec	9.6
5-10 sec	9.6
10-15 sec	6.972
15-20 sec	4.785
20-25 sec	2.128
25-30 sec	7.453
30-35 sec	6.562

Experiment 14	Pure wall velocity [mm/s]
0-15 sec	9.7
15-30 sec	9.7
30-45 sec	4.84
45-60 sec	4.75
60-75 sec	2.937
75-90 sec	2.446
90-105 sec	0.418

Experiment 15	Pure wall velocity [mm/s]
0-15 sec	7.853
15-30 sec	7.597
30-45 sec	7.020
45-60 sec	6.558
60-75 sec	2.027
75-90 sec	5.946
90-105 sec	0.444

Experiment 16	Pure wall velocity [mm/s]
0-15 sec	10.14
15-30 sec	8.806
30-45 sec	5.422
45-60 sec	5.983
60-75 sec	3.992
75-90 sec	2.899
90-105 sec	0.745

Appendix C Test Results Sliding Wedges

All sliding wedges of all experiments are in the tables. These are the sliding wedges that were observed from the videos, with the active breaching height at the moment of the sliding wedge.
Followed by the volume of the sliding wedges plotted against the time.

Experiment 1	Height [m]	Volume wedge [m^3]
5 sec	0.603	0.00152
24 sec	0.393	0.00127
45 sec	0.383	0.00125
Experiment 2	**Height [m]**	**Volume wedge [m^3]**
2 sec	0.655	0.00283
14 sec	0.530	0.00242
31 sec	0.389	0.00190
104 sec	0.287	0.000836
Experiment 3	**Height [m]**	**Volume wedge [m^3]**
10 sec	0.655	0.00323
21 sec	0.533	0.00234
43 sec	0.395	0.00435
Experiment 4	**Height [m]**	**Volume wedge [m^3]**
10 sec	1.114	0.00585
34 sec	0.98	0.00517
55 sec	0.863	0.00171
68 sec	0.832	0.00142
82 sec	0.827	0.00210
107 sec	0.816	0.00646
147 sec	0.759	0.00239
180 sec	0.695	0.00252
Experiment 5	**Height [m]**	**Volume wedge [m^3]**
22 sec	1.084	0.00257
58 sec	0.93	0.00330
78 sec	0.877	0.00596
100 sec	0.828	0.00536
143 sec	0.778	0.000687
191 sec	0.767	0.000923
234 sec	0.728	0.00443
255 sec	0.677	0.000305
308 sec	0.527	0.00185
Experiment 6	**Height [m]**	**Volume wedge [m^3]**
14 sec	1.147	0.00625
29 sec	1.034	0.00233
42 sec	0.980	0.0123
141 sec	0.467	0.00206
Experiment 7	**Height [m]**	**Volume wedge [m^3]**
13 sec	1.165	0.00379
28 sec	1.16	0.00504
33 sec	1.159	0.00306
45 sec	1.155	0.000672
65 sec	1.132	0.00182
88 sec	1.053	0.000625
118 sec	0.95	0.000576
128 sec	0.923	0.000445
135 sec	0.906	0.000556

Experiment 8	Height [m]	Volume wedge [m^3]
18 sec	1.438	0.00859
26 sec	1.409	0.00284
45 sec	1.342	0.00411
55 sec	1.306	0.00220
97 sec	1.157	0.000753
134 sec	1.142	0.00447
143 sec	1.139	0.00106
159 sec	1.133	0.00313
214 sec	1.104	0.00128
231 sec	1.064	0.00076
Experiment 9	**Height [m]**	**Volume wedge [m^3]**
50 sec	1.153	0.008
66 sec	1.147	0.0033
90 sec	1.137	0.000614
108 sec	1.103	0.000812
126 sec	1.076	0.0016
179 sec	0.988	0.000921
Experiment 10	**Height [m]**	**Volume wedge [m^3]**
13 sec	1.47	0.00468
24 sec	1.417	0.0220
70 sec	1.212	0.00696
110 sec	1.07	0.00409
142 sec	1.075	0.00362
188 sec	1.08	0.00176
240 sec	1.002	0.0014
270 sec	0.953	0.00088
Experiment 11	**Height [m]**	**Volume wedge [m^3]**
21 sec	1.156	0.0012
27 sec	1.152	0.0104
50 sec	1.137	0.0026
70 sec	1.111	0.0036
89 sec	1.077	0.0016
114 sec	1.031	0.0034
168 sec	0.889	0.0013
Experiment 12	**Height [m]**	**Volume wedge [m^3]**
11 sec	1.152	0.0026
22 sec	1.15	0.002
27 sec	1.125	0.0019
40 sec	1.103	0.0011
63 sec	1.067	0.000875
102 sec	1.028	0.0011
121 sec	1.006	0.000821
134 sec	0.96	0.0018
187 sec	0.8	0.000604

Experiment 13	Height [m]	Volume wedge [m^3]
2 sec	0.598	0.00342
9 sec	0.362	0.00507
Experiment 14	**Height [m]**	**Volume wedge [m^3]**
2 sec	1.113	0.0177
7 sec	0.972	0.011
13 sec	0.803	0.00285
16 sec	0.524	0.0102
Experiment 15	**Height [m]**	**Volume wedge [m^3]**
2 sec	1.17	0.0166
11 sec	1.027	0.0155
16 sec	0.939	0.00577
24 sec	0.797	0.0036
Experiment 16	**Height [m]**	**Volume wedge [m^3]**
1 sec	1.426	0.0432
8 sec	1.115	0.00762
17 sec	0.783	0.0121

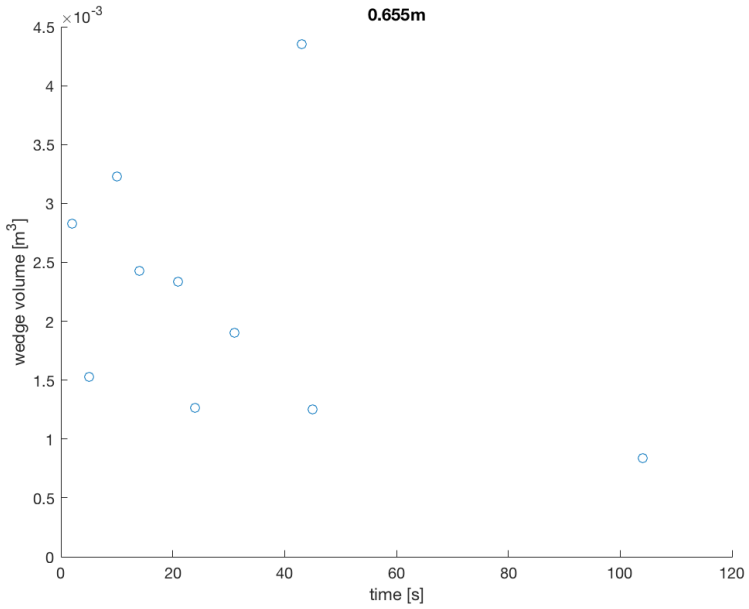
0.655m
×10^-3
wedge volume [m^3]
time [s]
0
0.5
1
1.5
2
2.5
3
3.5
4
4.5
0
20
40
60
80
100
120

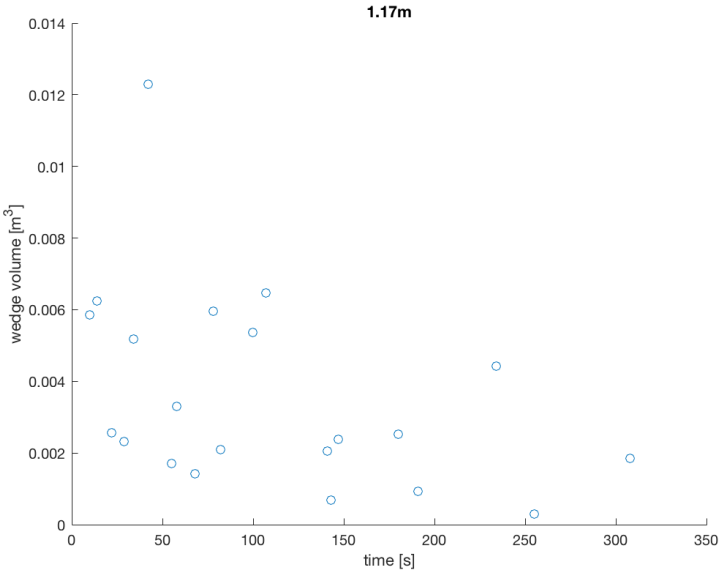
1.17m
wedge volume [m^3]
time [s]
0
0.002
0.004
0.006
0.008
0.01
0.012
0.014
0
50
100
150
200
250
300
350

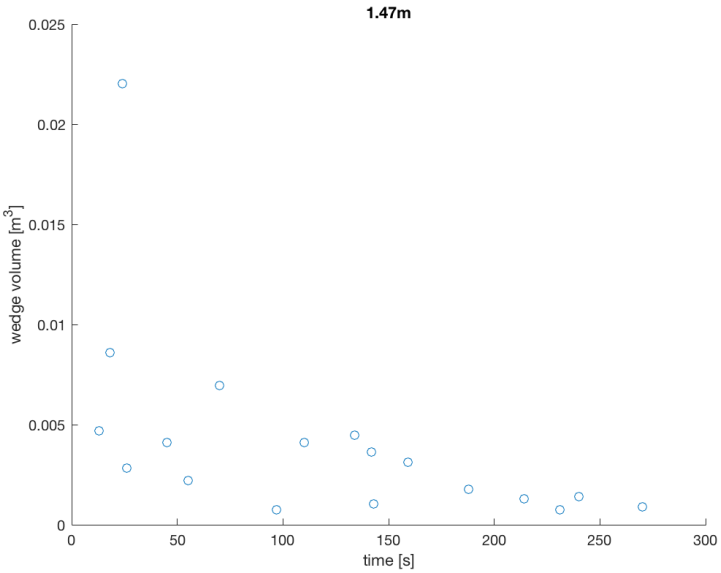
1.47m
wedge volume [m3]
time [s]
0.025
0.02
0.015
0.01
0.005
0
0
50
100
150
200
250
300

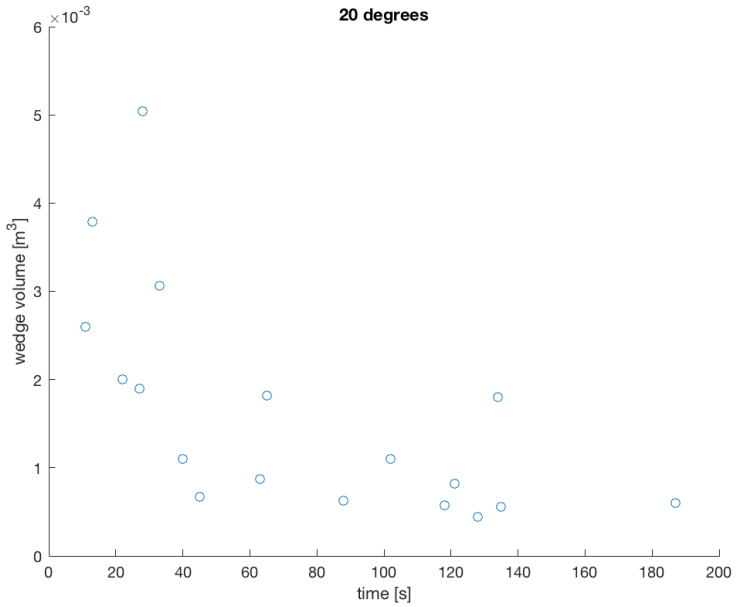
20 degrees
×10-3
wedge volume [m3]
time [s]
6
5
4
3
2
1
0
0
20
40
60
80
100
120
140
160
180
200

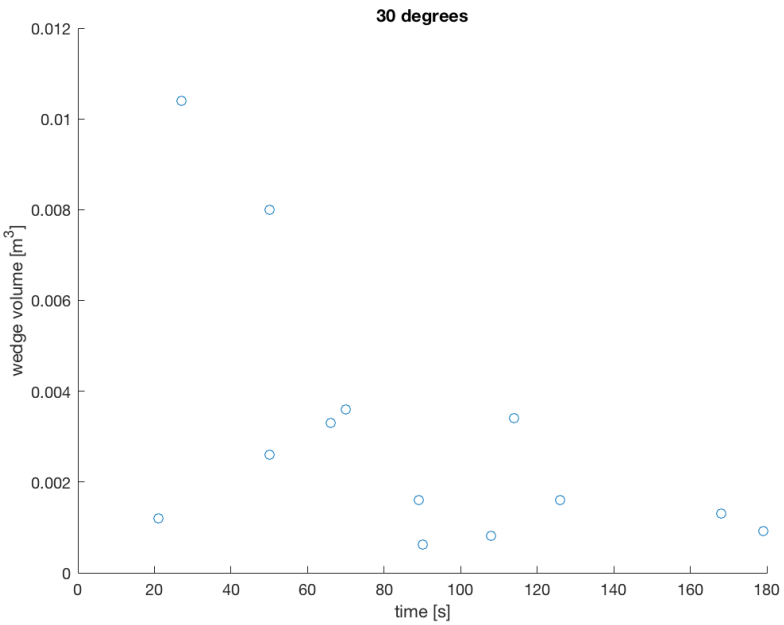
30 degrees
wedge volume [m3]
time [s]
0.012
0.01
0.008
0.006
0.004
0.002
0
0
20
40
60
80
100
120
140
160
180

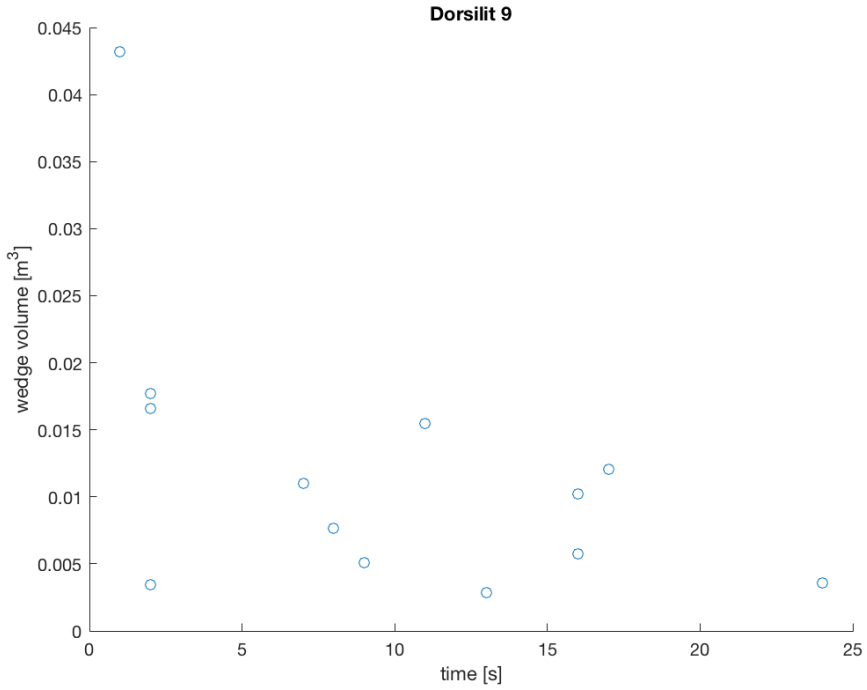
Dorsilit 9
wedge volume [m3]
time [s]
0.045
0.04
0.035
0.03
0.025
0.02
0.015
0.01
0.005
0
0
5
10
15
20
25

Appendix D Test Results Angle At The Toe & Breach Angle

The results of the angle at the toe and breaching angle can be seen in the tables. The breaching angle and angle at the toe is taken at the end of a time, so for example for experiment 1, after 25 seconds, the breaching angle is 74.93 degrees and the angle at the toe is 18.67 degrees. All experiments start with a breaching angle of 90 degrees and 0 degrees for the angle at the toe.

Experiment 1	Breaching angle [deg]	Angle at the toe [deg]
0-25 sec	74.93	18.67
25-50 sec	60.15	13.93
50-75 sec	50.77	12.26
75-100 sec	46.82	16.74
100-125 sec	34.28	20.46
125-150 sec	43.72	26.1
150-175 sec	67.61	28.86

Experiment 2	Breaching angle [deg]	Angle at the toe [deg]
0-30 sec	74.57	14.86
30-60 sec	60.90	9.8
60-90 sec	58.02	11.47
90-120 sec	58.18	15.32
120-150 sec	62.77	18.38
150-180 sec	62.16	25.61
180-210 sec	51.89	27.21

Experiment 3	Breaching angle [deg]	Angle at the toe [deg]
0-30 sec	63.65	2.95
30-60 sec	58.30	15.34
60-90 sec	55.61	17.85
90-120 sec	49.82	19.45
120-150 sec	53.41	22.18
150-180 sec	53.00	25.83
180-210 sec	54.27	28.87

Experiment 4	Breaching angle [deg]	Angle at the toe [deg]
0-60 sec	75.86	8.66
60-120 sec	57.84	5.05
120-180 sec	55.58	8.59
180-240 sec	52.01	12.69
240-300 sec	52.73	12.98
300-360 sec	49.19	21.85
360-420 sec	44.53	26.57

Experiment 5	Breaching angle [deg]	Angle at the toe [deg]
0-60 sec	77.40	5.63
60-120 sec	71.65	11.64
120-180 sec	68.60	6.97
180-240 sec	68.13	12.37
240-300 sec	59.86	17.97
300-360 sec	55.72	16.01
360-420 sec	50.99	16.66

Experiment 6	Breaching angle [deg]	Angle at the toe [deg]
0-60 sec	60.92	14.23
60-120 sec	62.92	17.9
120-180 sec	59.51	19.49
180-240 sec	64.42	22.26
240-300 sec	67.50	24.25
300-360 sec	67.94	25.14
360-420 sec	66.35	26.9

Experiment 7	Breaching angle [deg]	Angle at the toe [deg]
0-60 sec	71.3172	8.62
60-120 sec	60.4461	11.41
120-180 sec	51.5803	16.66
180-240 sec	47.9988	23.48
240-300 sec	54.7059	24.46
300-360 sec	58.2962	23.96
360-420 sec	36.2834	25.88

Experiment 8	Breaching angle [deg]	Angle at the toe [deg]
0-90 sec	69.8501	12.85
90-180 sec	67.2189	7.76
180-270 sec	57.9513	13.26
270-360 sec	63.6867	16.2
360-450 sec	61.4557	17.03
450-540 sec	61.9036	17.12
540-630 sec	66.7171	17.21

Experiment 9	Breaching angle [deg]	Angle at the toe [deg]
0-90 sec	80.5801	8.32
90-180 sec	64.4429	11.68
180-270 sec	61.9947	14.69
270-360 sec	60.3602	15.3
360-450 sec	61.0507	19.49
450-540 sec	58.3737	18
540-630 sec	61.1076	21.66

Experiment 10	Breaching angle [deg]	Angle at the toe [deg]
0-90 sec	62.8406	20.85
90-180 sec	59.91	8.75
180-270 sec	58.5216	11.69
270-360 sec	54.4628	12.88
360-450 sec	55.855	14.4
450-540 sec	58.8934	14.45
540-630 sec	56.4526	14.97

Experiment 11	Breaching angle [deg]	Angle at the toe [deg]
0-60 sec	67.5808	11.48
60-120 sec	54.2763	10.59
120-180 sec	50.3105	16.17
180-240 sec	48.0975	18.75
240-300 sec	44.4934	21.08
300-360 sec	44.0231	20.82
360-420 sec	43.4304	22.66

Experiment 12	Breaching angle [deg]	Angle at the toe [deg]
0-60 sec	64.7493	2.15
60-120 sec	54.2748	11.89
120-180 sec	54.5457	19.42
180-240 sec	46.8135	21.49
240-300 sec	68.3539	22.59
300-360 sec	69.7652	23.95
360-420 sec	69.4182	24.43

Experiment 13	Breaching angle [deg]	Angle at the toe [deg]
0-5 sec	79.592	5.99
5-10 sec	58.6354	16.18
10-15sec	57.0901	17.45
15-20 sec	54.6558	19.82
20-25 sec	54.1581	22.99
25-30 sec	52.5433	23.45
30-35 sec	49.0868	24.13

Experiment 14	Breaching angle [deg]	Angle at the toe [deg]
0-15 sec	57.3044	13.63
15-30 sec	54.4575	23.24
30-45sec	51.9593	22.61
45-60 sec	60.258	28.1
60-75 sec	62.6219	25.29
75-90 sec	49.8614	26.31
90-105 sec	41.6016	25.04

Experiment 15	Breaching angle [deg]	Angle at the toe [deg]
0-15 sec	43.3602	12.43
15-30 sec	49.3624	19.53
30-45sec	49.5536	23.61
45-60 sec	46.1169	24.36
60-75 sec	47.1013	25.45
75-90 sec	57.3562	25.67
90-105 sec	35.7279	26.25

Experiment 16	Breaching angle [deg]	Angle at the toe [deg]
0-15 sec	63.9838	17.43
15-30 sec	58.598	22.31
30-45sec	48.7917	16.89
45-60 sec	50.3361	23.2
60-75 sec	48.7726	28.69
75-90 sec	47.3172	28.91
90-105 sec	40.6073	29.03

Angle at the toe: real angle versus calculated angle

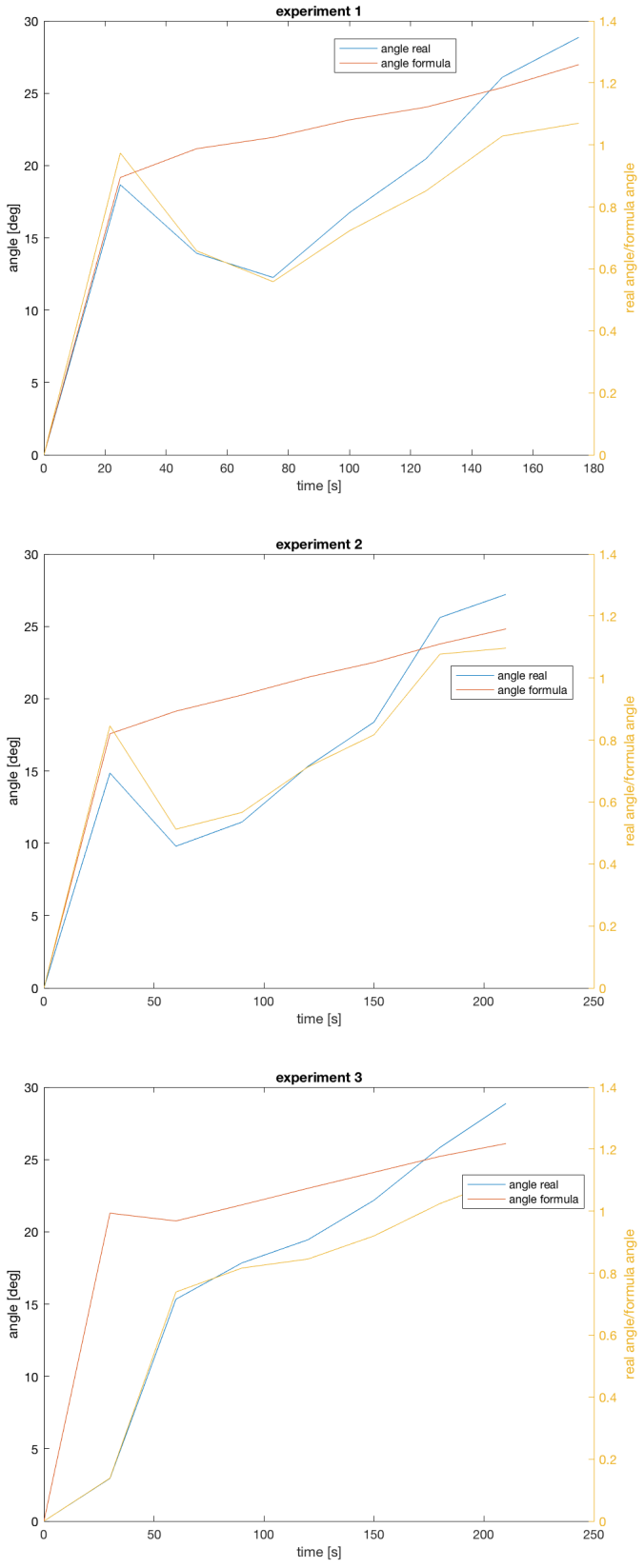

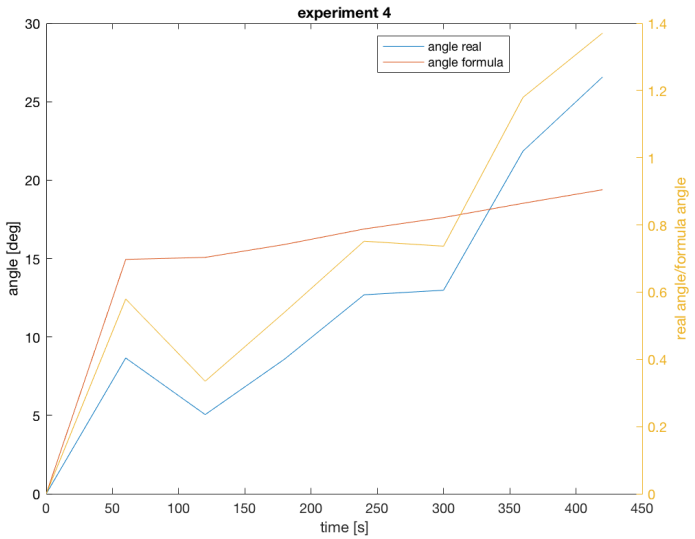
experiment 4
angle real
angle formula
angle [deg]
real angle/formula angle
time [s]

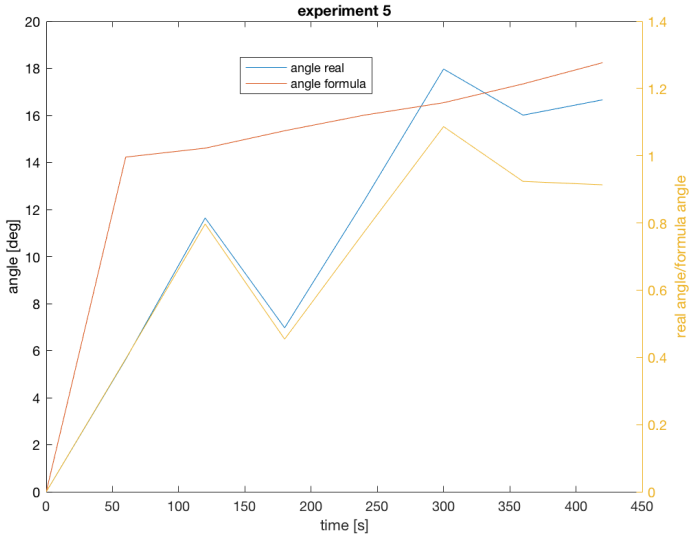
experiment 5
angle real
angle formula
angle [deg]
real angle/formula angle
time [s]

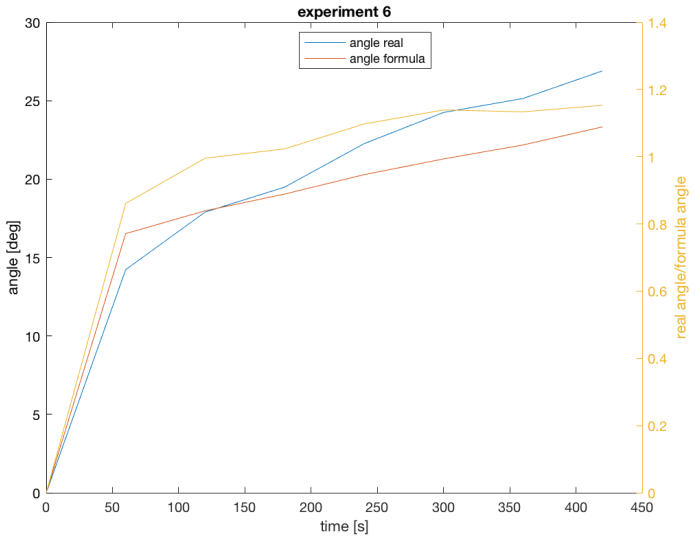
experiment 6
angle real
angle formula
angle [deg]
real angle/formula angle
time [s]

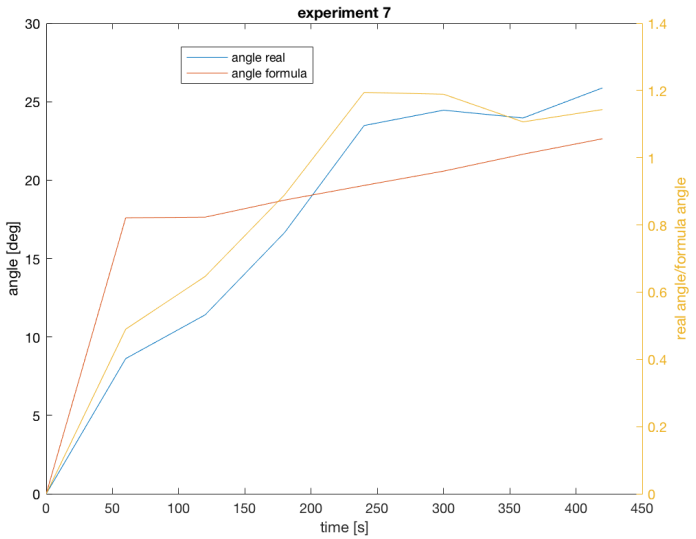
experiment 7
angle real
angle formula
angle [deg]
real angle/formula angle
time [s]

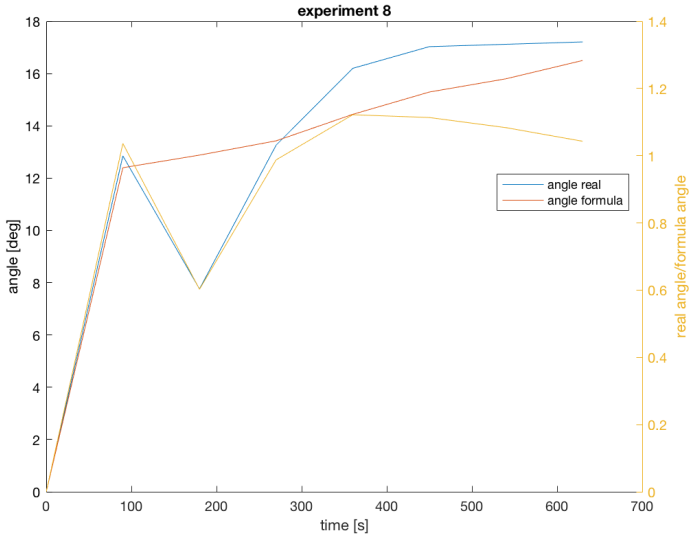
experiment 8
angle real
angle formula
angle [deg]
real angle/formula angle
time [s]

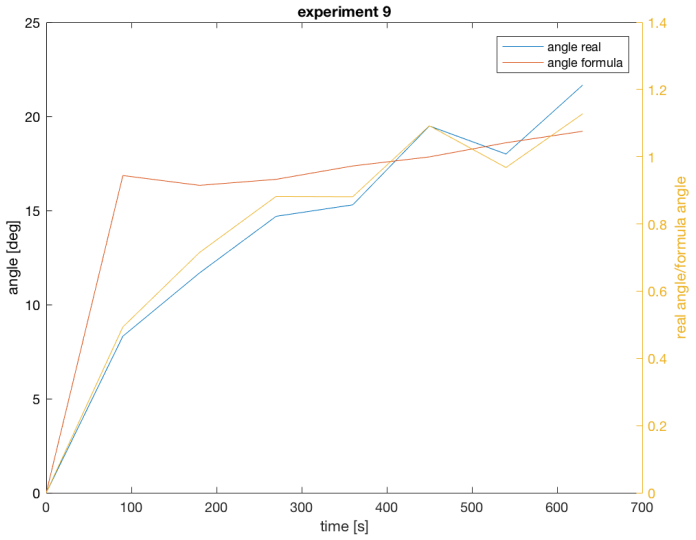
experiment 9
angle real
angle formula
angle [deg]
real angle/formula angle
time [s]

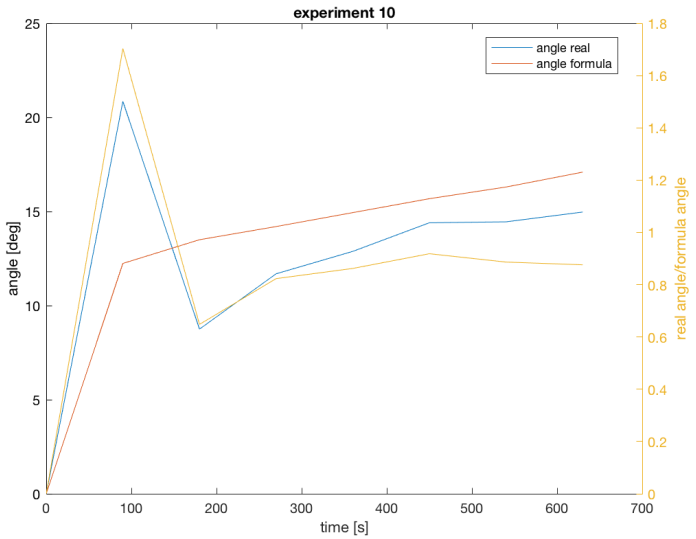
experiment 10
angle real
angle formula
angle [deg]
real angle/formula angle
time [s]
0
5
10
15
20
25
0
0.2
0.4
0.6
0.8
1
1.2
1.4
1.6
1.8
0
100
200
300
400
500
600
700

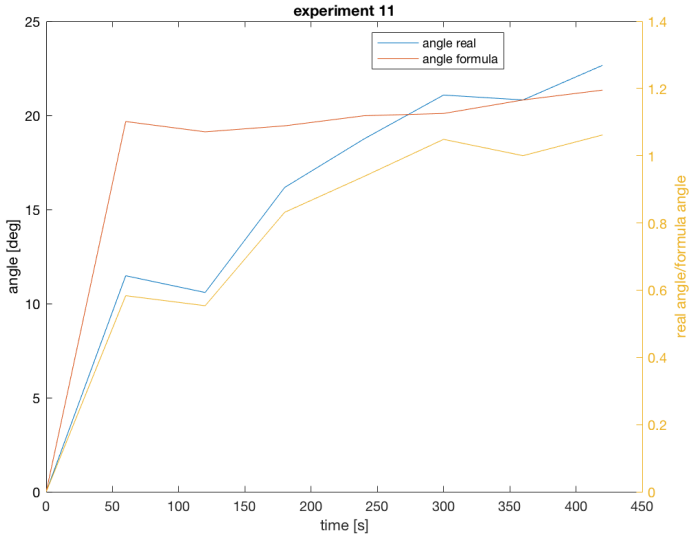
experiment 11
angle real
angle formula
angle [deg]
real angle/formula angle
time [s]
0
5
10
15
20
25
0
0.2
0.4
0.6
0.8
1
1.2
1.4
0
50
100
150
200
250
300
350
400
450

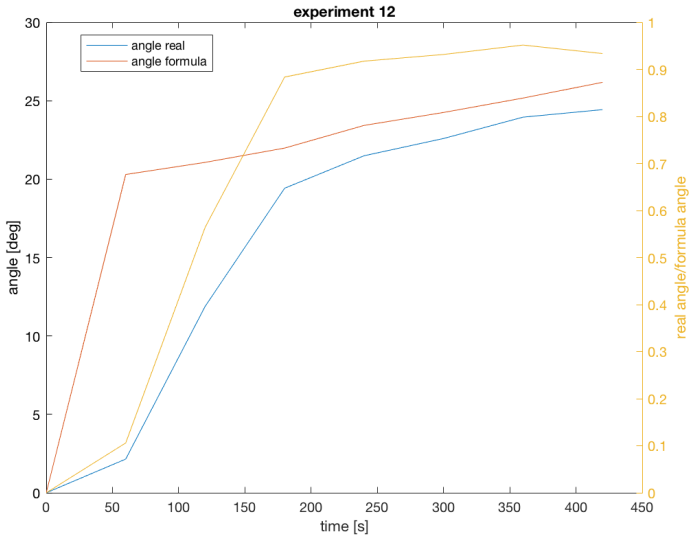
experiment 12
angle real
angle formula
angle [deg]
real angle/formula angle
time [s]
0
5
10
15
20
25
30
0
0.1
0.2
0.3
0.4
0.5
0.6
0.7
0.8
0.9
1
0
50
100
150
200
250
300
350
400
450

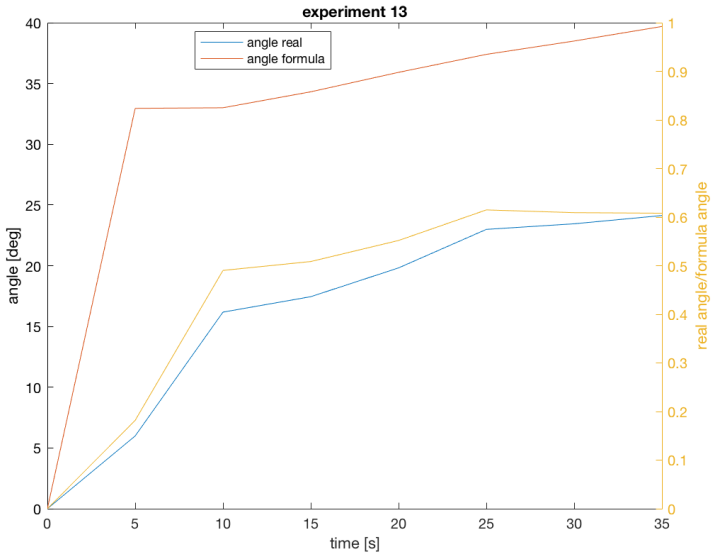
experiment 13
angle real
angle formula
angle [deg]
real angle/formula angle
time [s]

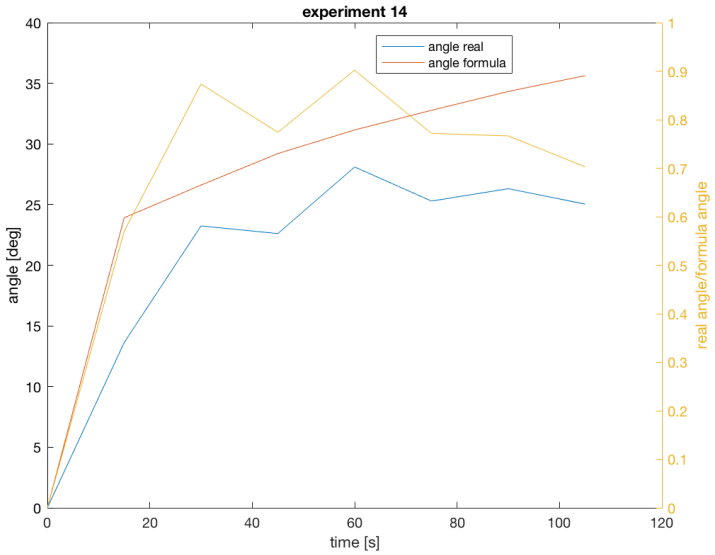
experiment 14
angle real
angle formula
angle [deg]
real angle/formula angle
time [s]

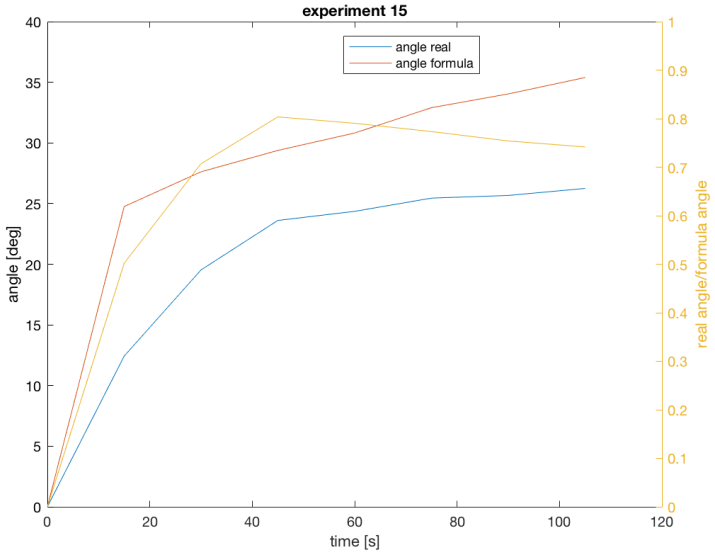
experiment 15
angle real
angle formula
angle [deg]
real angle/formula angle
time [s]

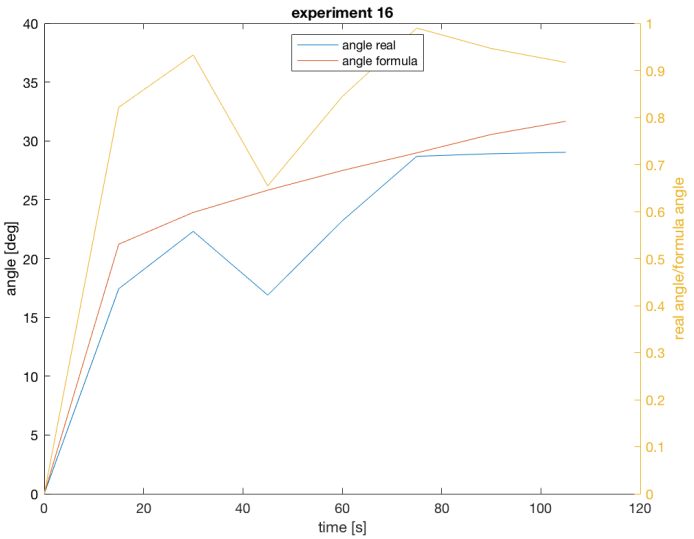
experiment 16
angle real
angle formula
angle [deg]
time [s]
real angle/formula angle
0
5
10
15
20
25
30
35
40
0
20
40
60
80
100
120
0
0.1
0.2
0.3
0.4
0.5
0.6
0.7
0.8
0.9
1

Appendix E Profile Front

The profile fronts of all experiments are plotted.

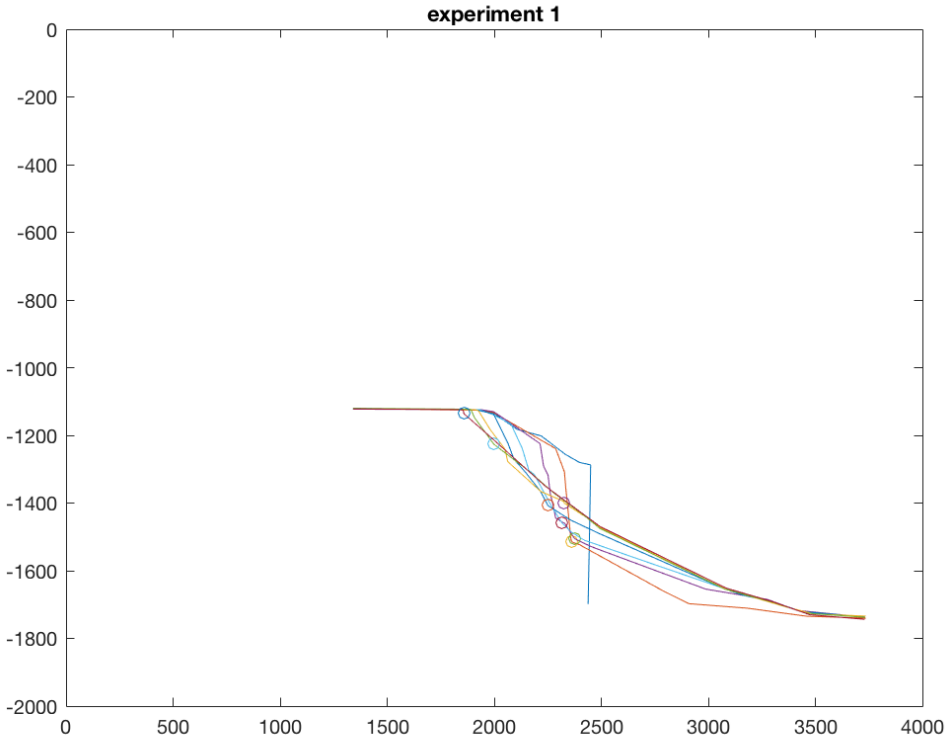

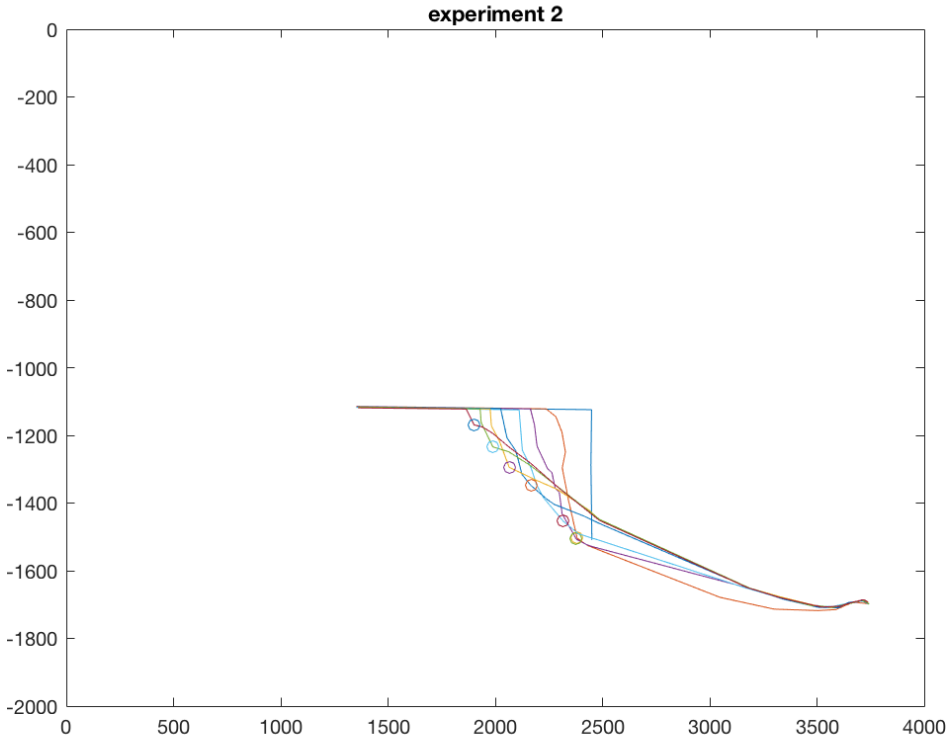

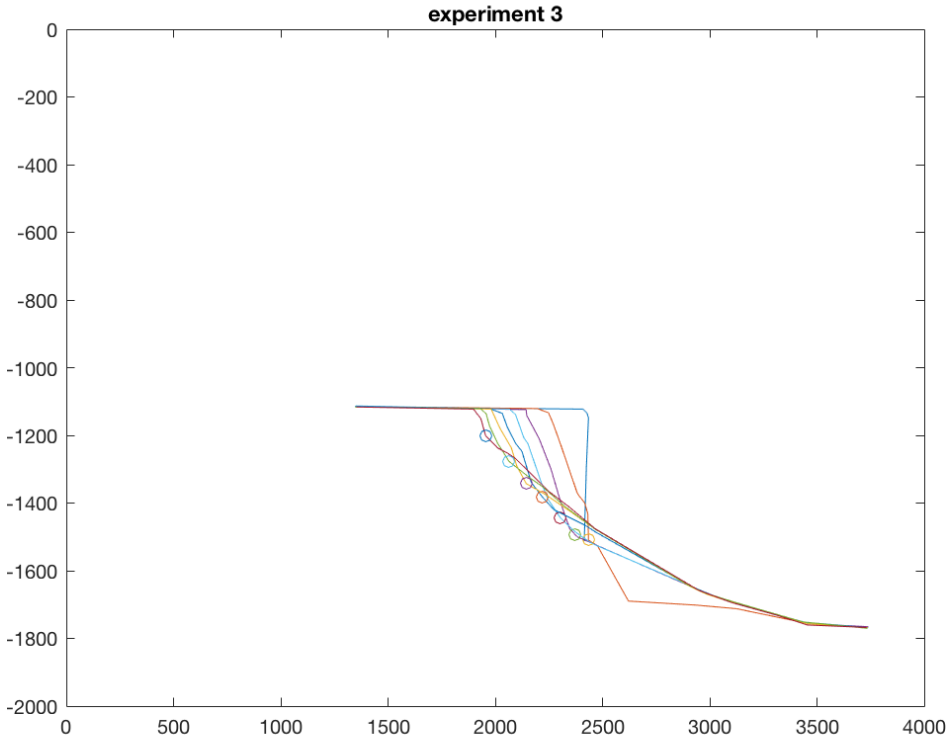
experiment 3
0
-200
-400
-600
-800
-1000
-1200
-1400
-1600
-1800
-2000
0
500
1000
1500
2000
2500
3000
3500
4000

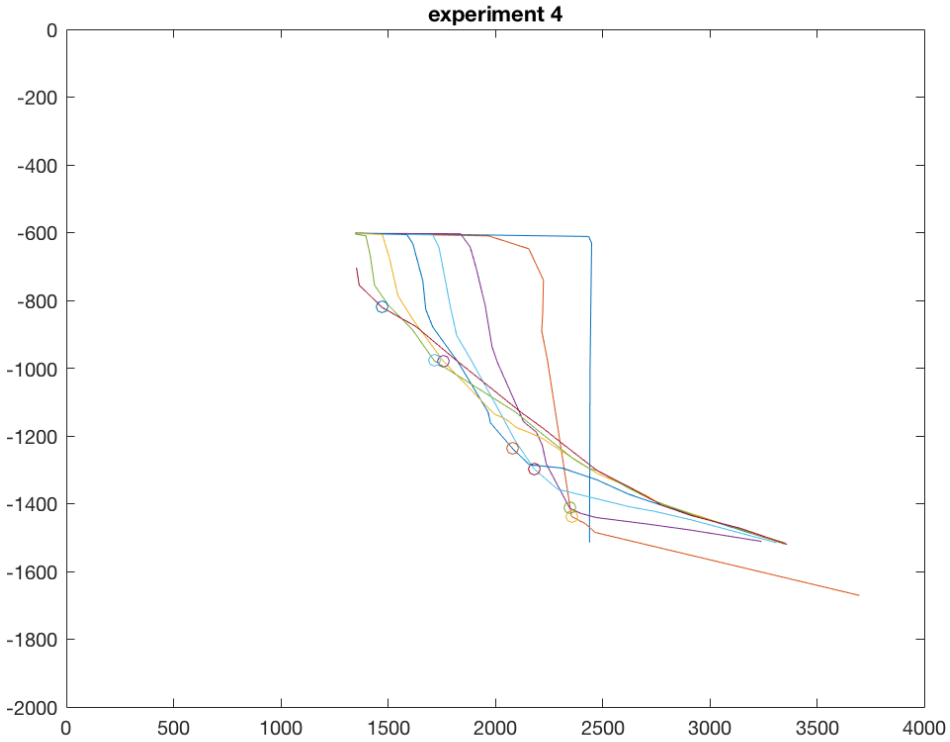
experiment 4
0
-200
-400
-600
-800
-1000
-1200
-1400
-1600
-1800
-2000
0
500
1000
1500
2000
2500
3000
3500
4000

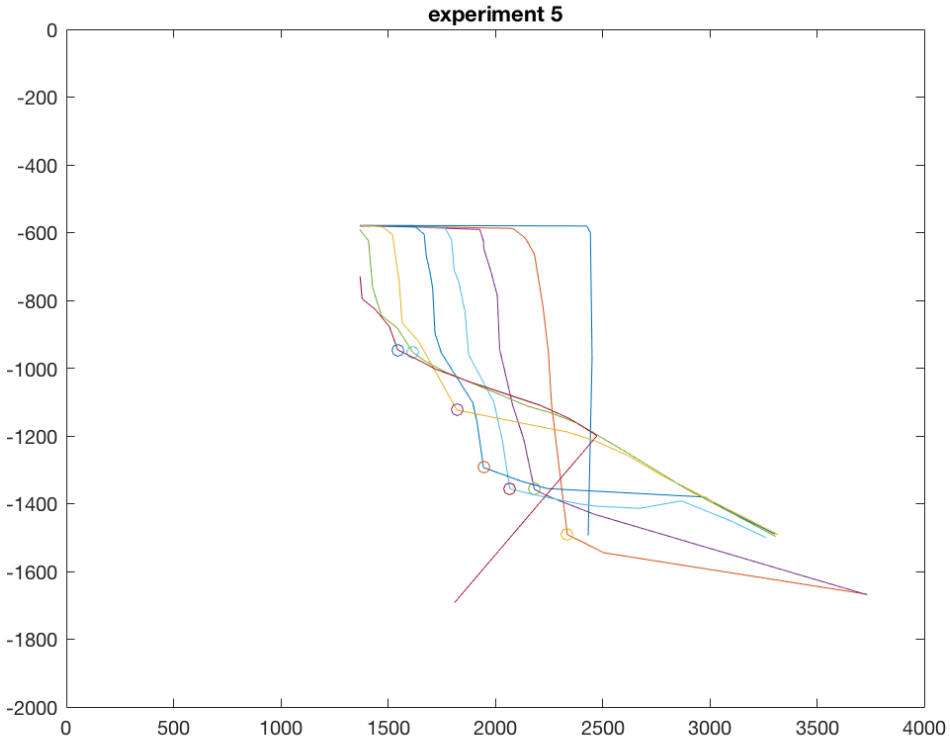
experiment 5
0
-200
-400
-600
-800
-1000
-1200
-1400
-1600
-1800
-2000
0
500
1000
1500
2000
2500
3000
3500
4000

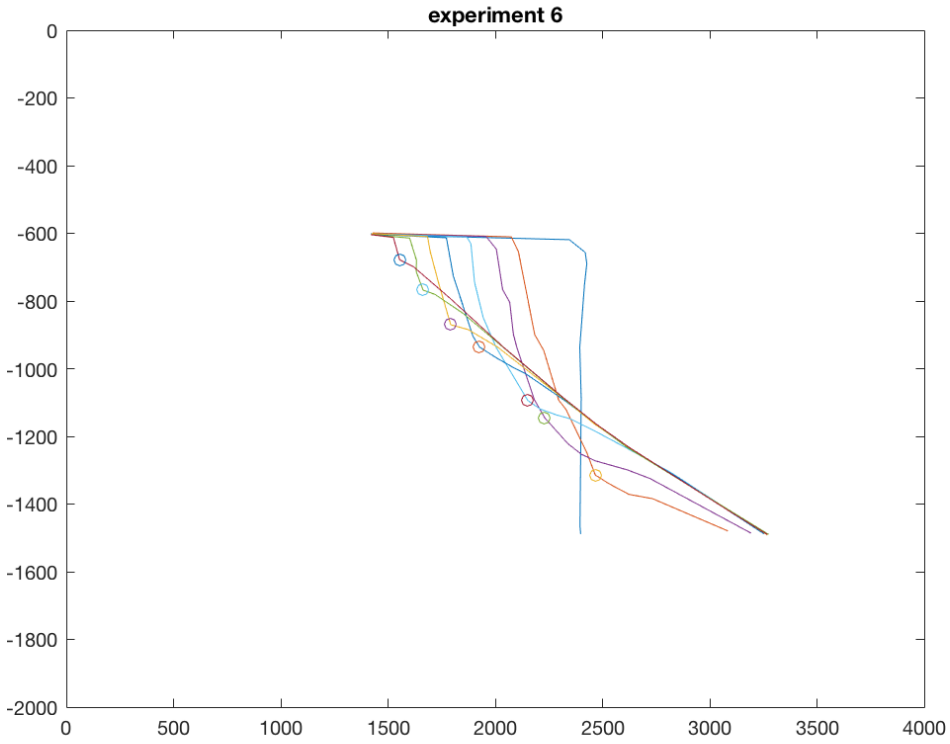
experiment 6
0
-200
-400
-600
-800
-1000
-1200
-1400
-1600
-1800
-2000
0
500
1000
1500
2000
2500
3000
3500
4000

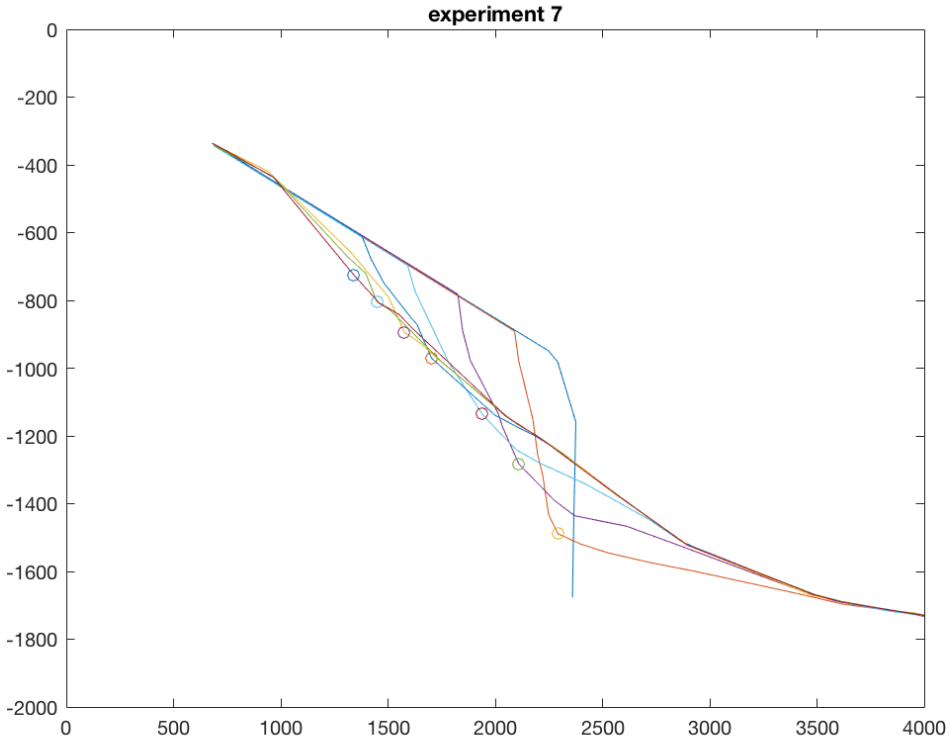
experiment 7
0
-200
-400
-600
-800
-1000
-1200
-1400
-1600
-1800
-2000
0
500
1000
1500
2000
2500
3000
3500
4000

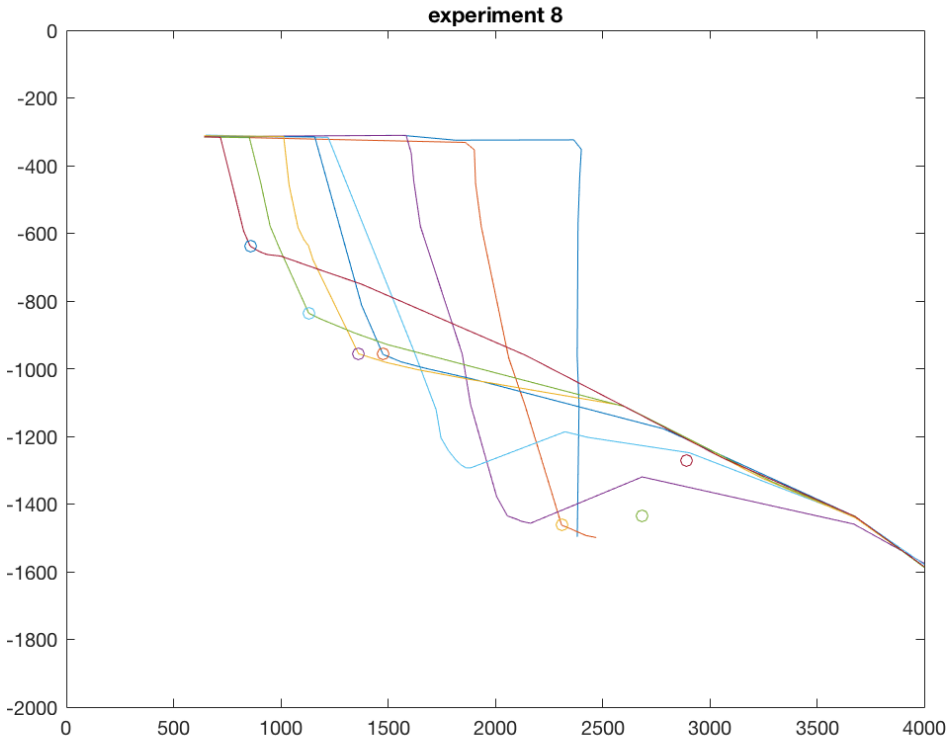
experiment 8
0
-200
-400
-600
-800
-1000
-1200
-1400
-1600
-1800
-2000
0
500
1000
1500
2000
2500
3000
3500
4000

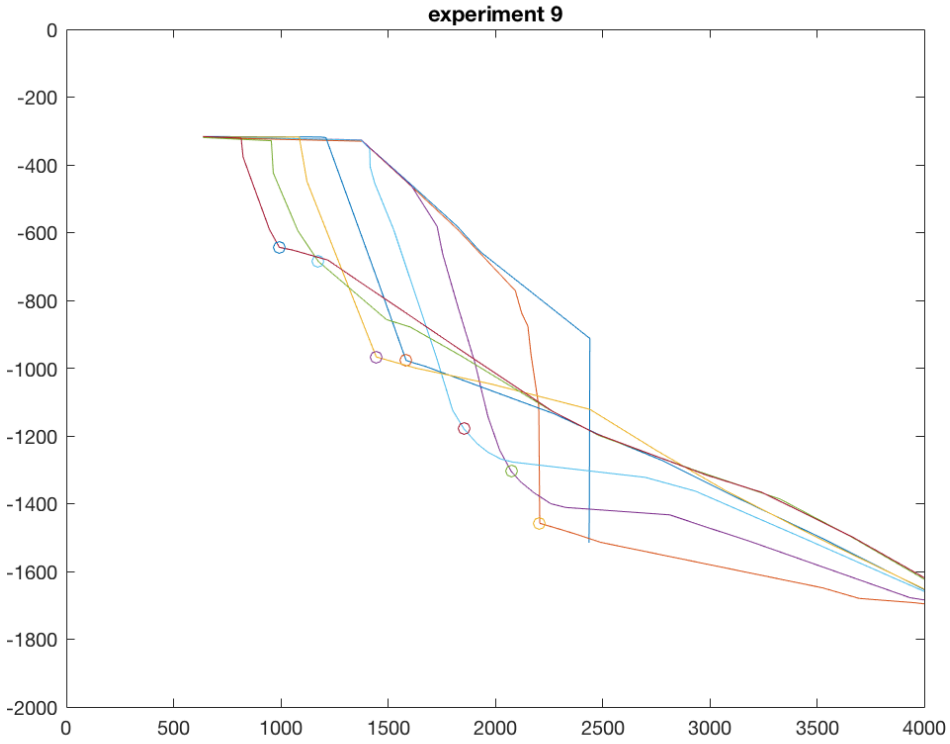
experiment 9
0
-200
-400
-600
-800
-1000
-1200
-1400
-1600
-1800
-2000
0
500
1000
1500
2000
2500
3000
3500
4000

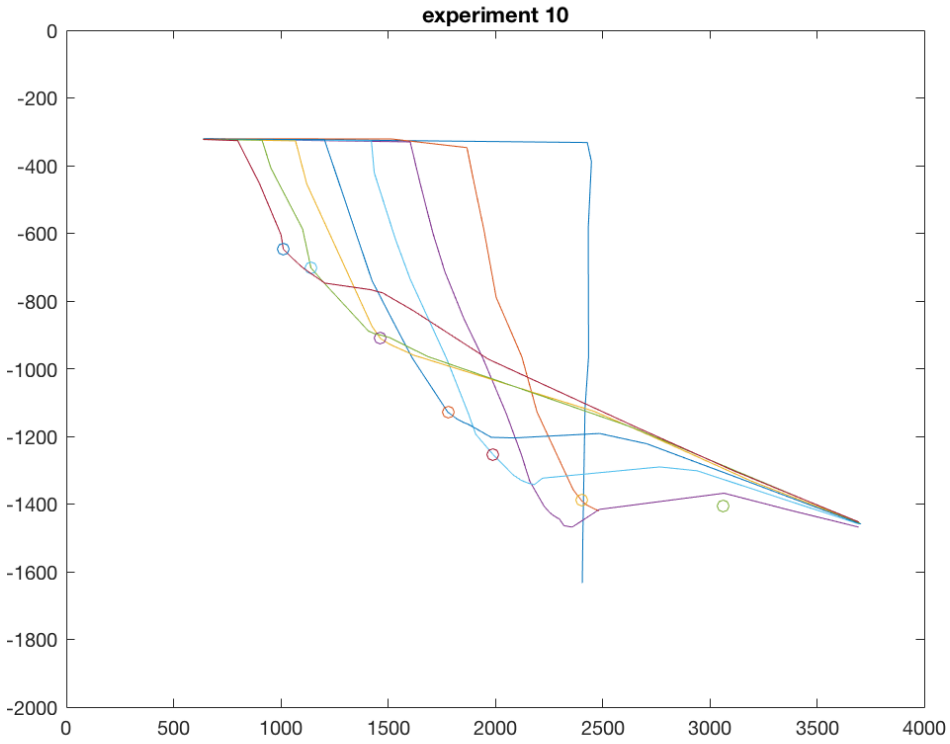
experiment 10
0
-200
-400
-600
-800
-1000
-1200
-1400
-1600
-1800
-2000
0
500
1000
1500
2000
2500
3000
3500
4000

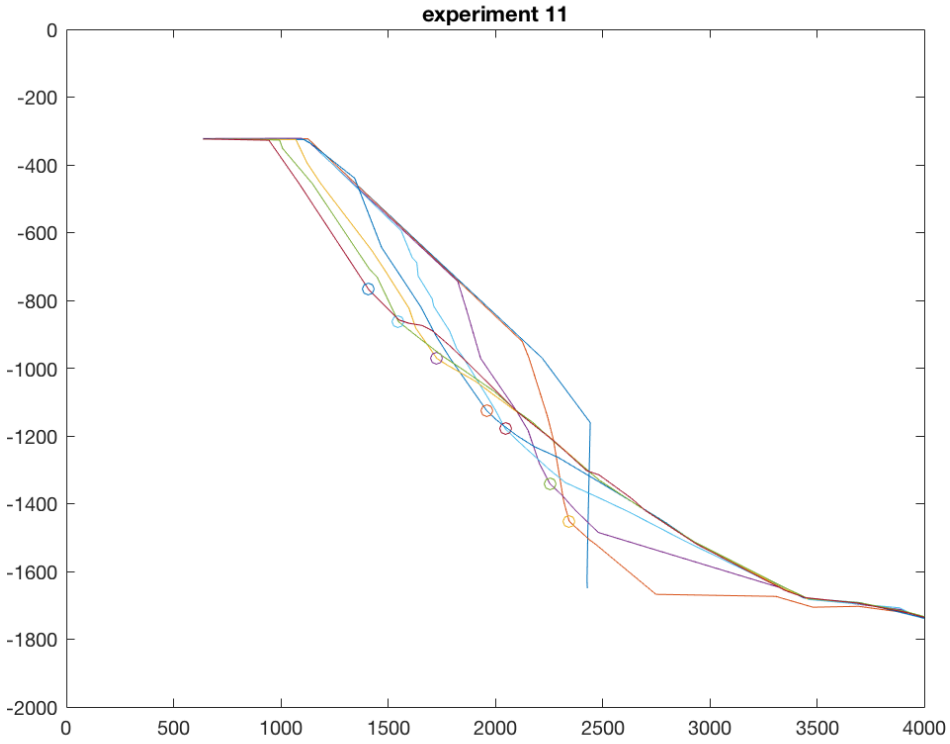
experiment 11
0
-200
-400
-600
-800
-1000
-1200
-1400
-1600
-1800
-2000
0
500
1000
1500
2000
2500
3000
3500
4000

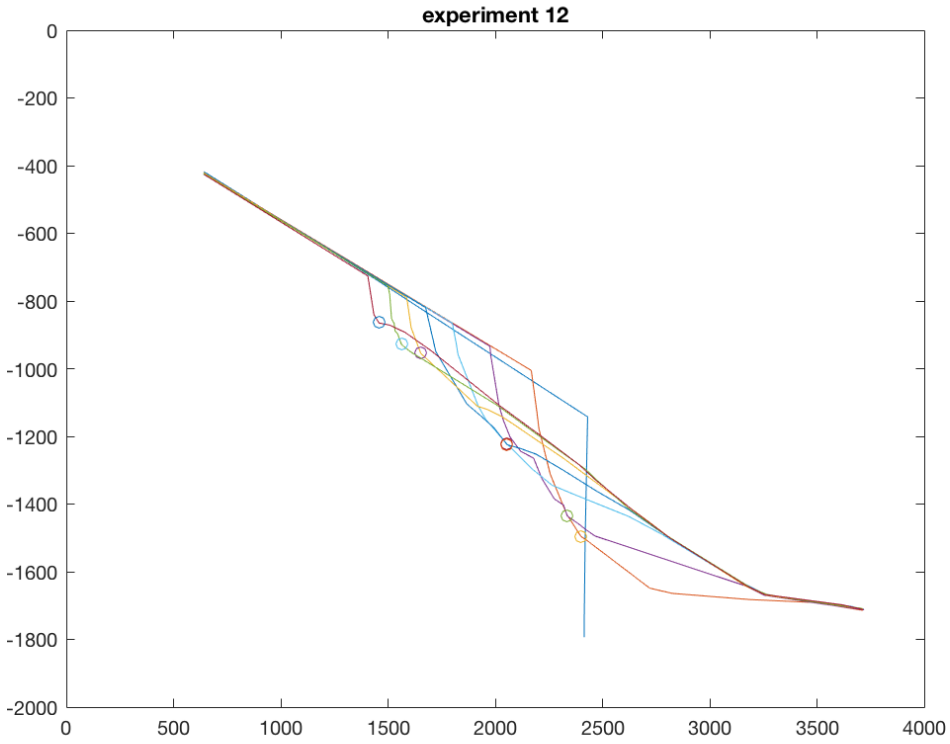
experiment 12
0
-200
-400
-600
-800
-1000
-1200
-1400
-1600
-1800
-2000
0
500
1000
1500
2000
2500
3000
3500
4000

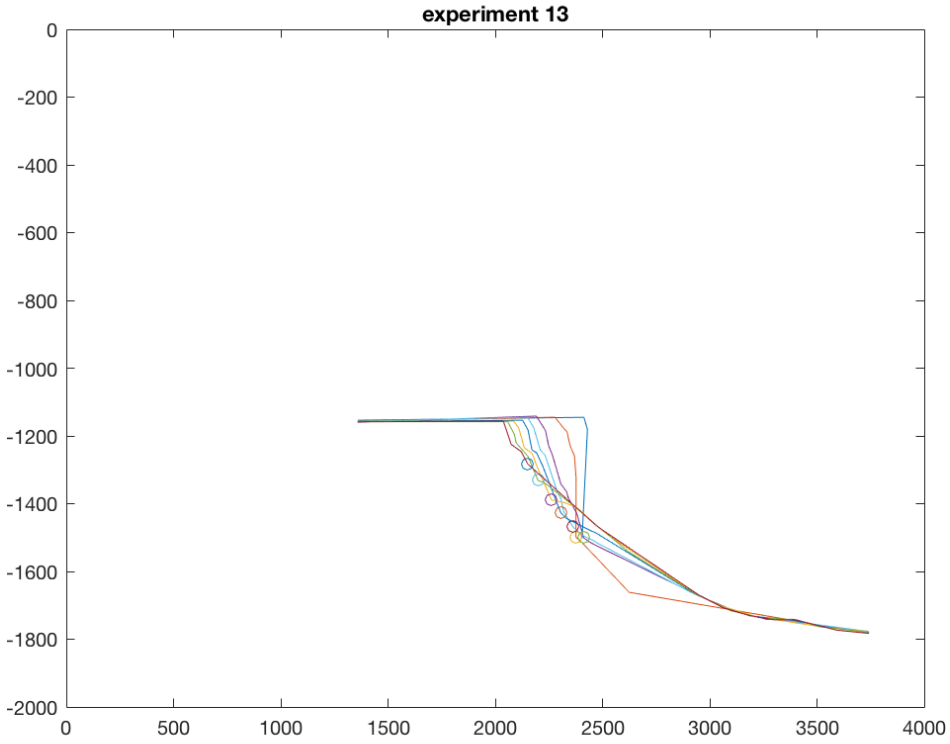
experiment 13
0
-200
-400
-600
-800
-1000
-1200
-1400
-1600
-1800
-2000
0
500
1000
1500
2000
2500
3000
3500
4000

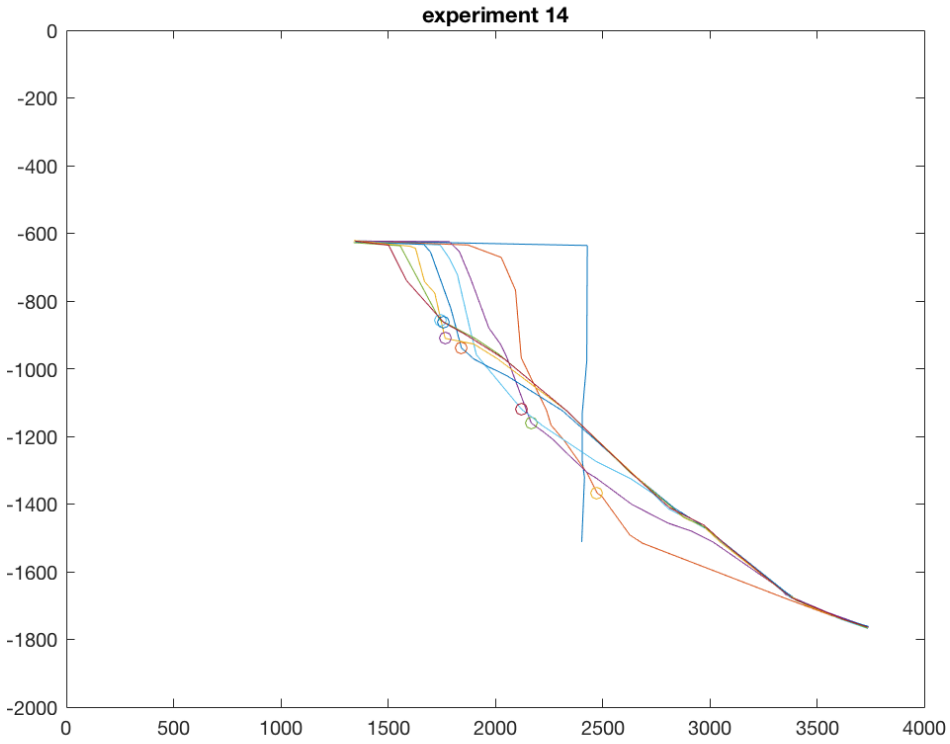
experiment 14
0
-200
-400
-600
-800
-1000
-1200
-1400
-1600
-1800
-2000
0
500
1000
1500
2000
2500
3000
3500
4000

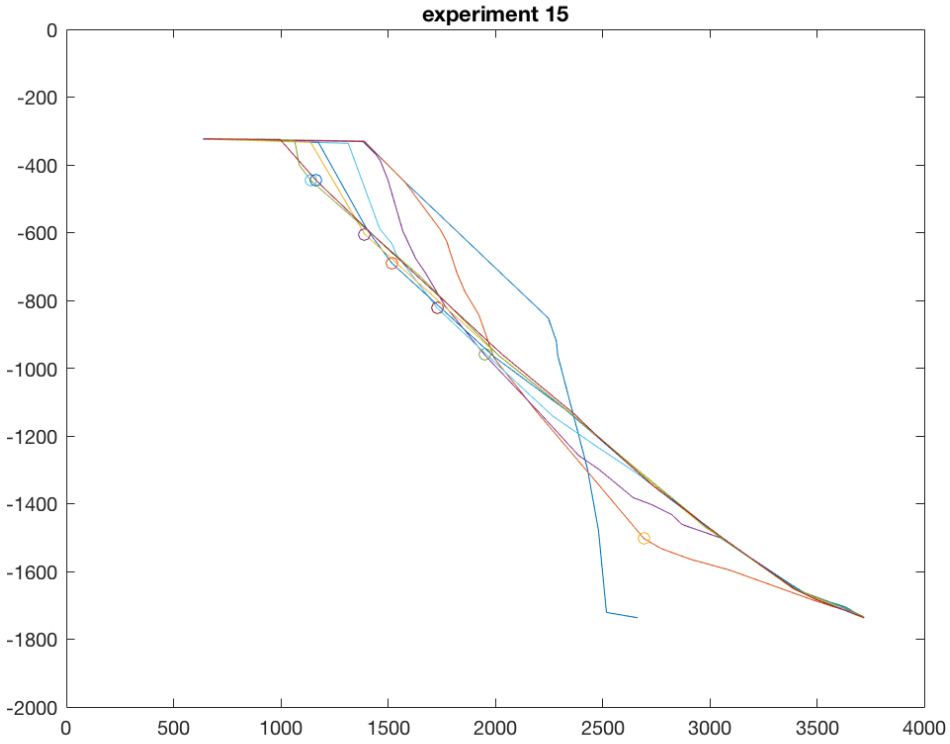
experiment 15
0
-200
-400
-600
-800
-1000
-1200
-1400
-1600
-1800
-2000
0
500
1000
1500
2000
2500
3000
3500
4000

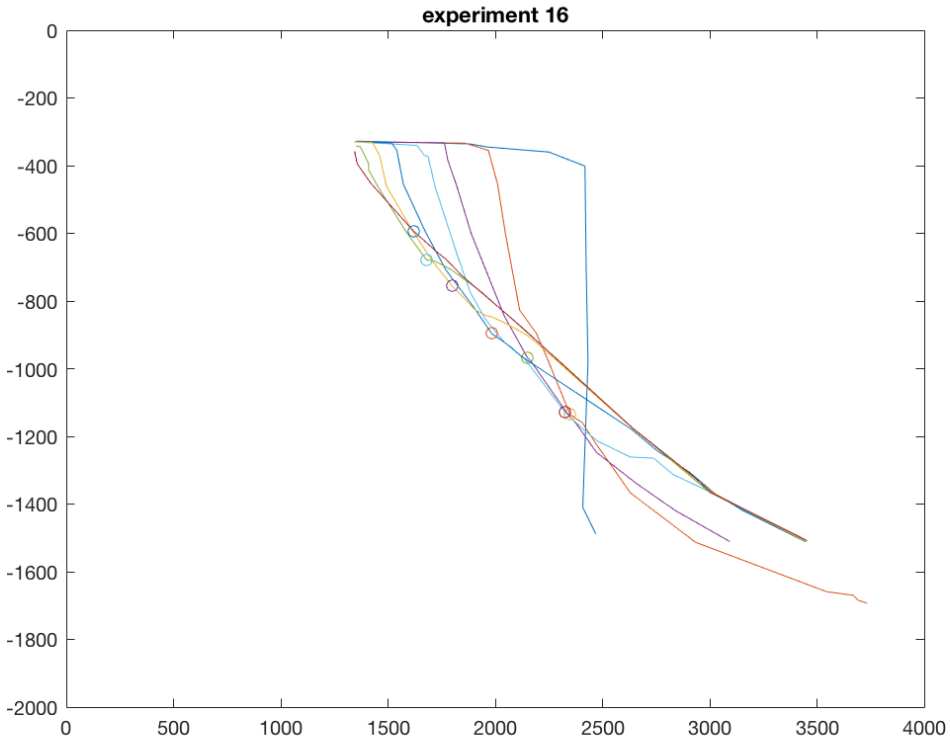
experiment 16
0
-200
-400
-600
-800
-1000
-1200
-1400
-1600
-1800
-2000
0
500
1000
1500
2000
2500
3000
3500
4000

Appendix F Pressure Experiments

The underpressures of all experiments can be seen. Also with a filtered underpressure. The underpressure of some of the experiments were discarded.

Experiment 3:

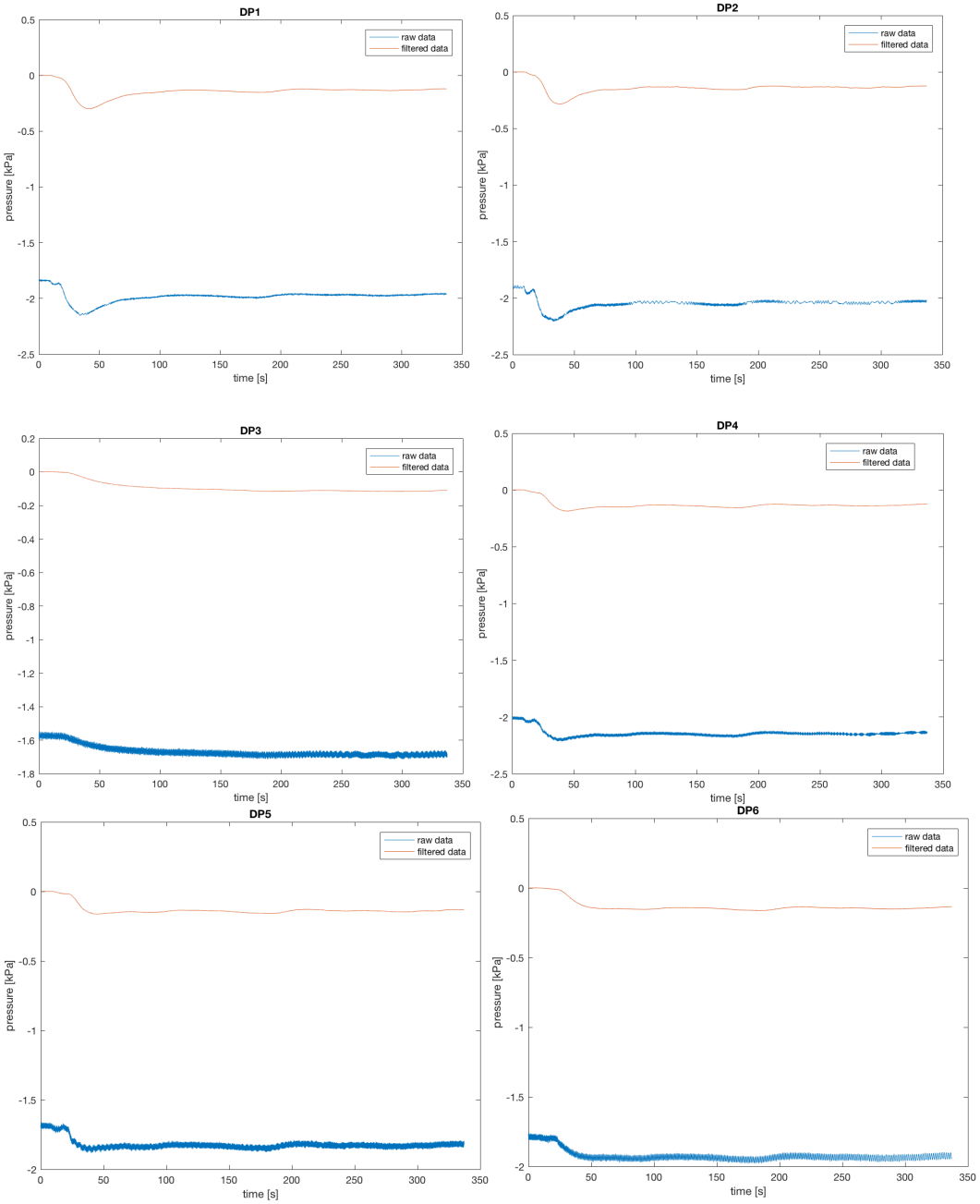

Experiment 4

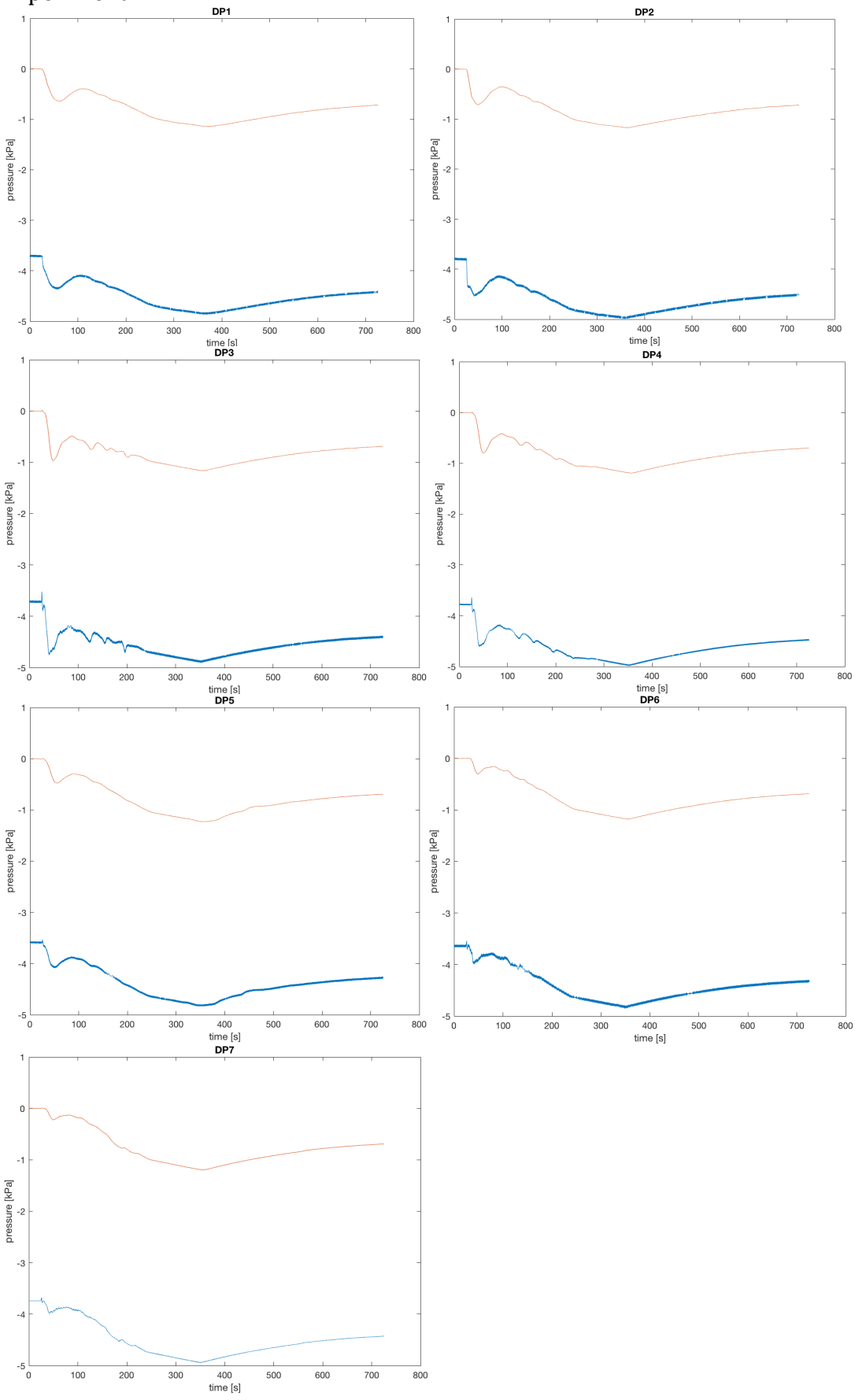

Experiment 5

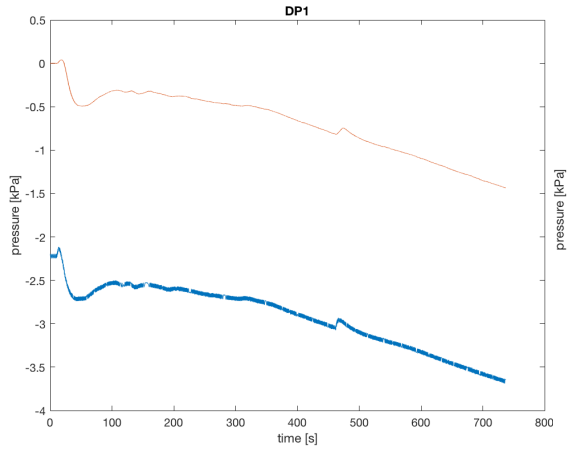

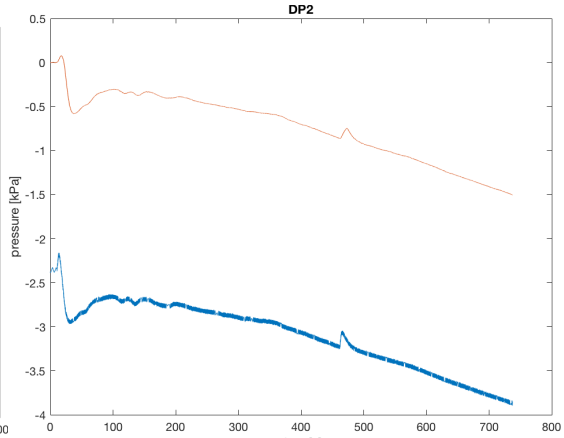

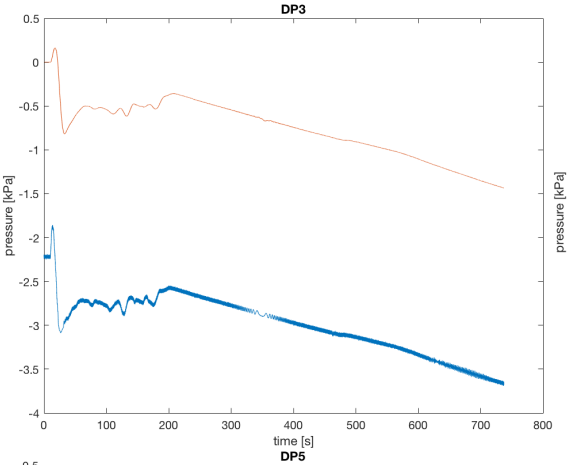

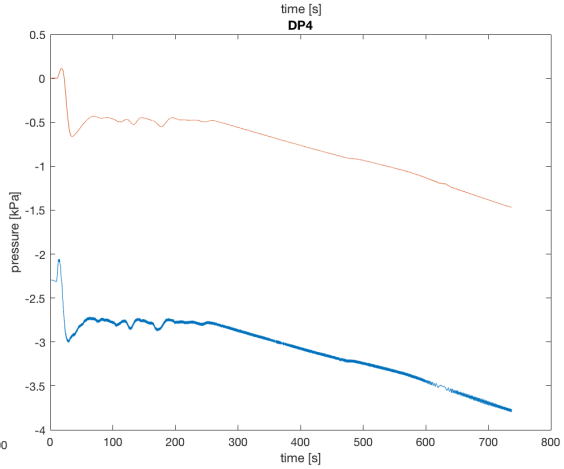

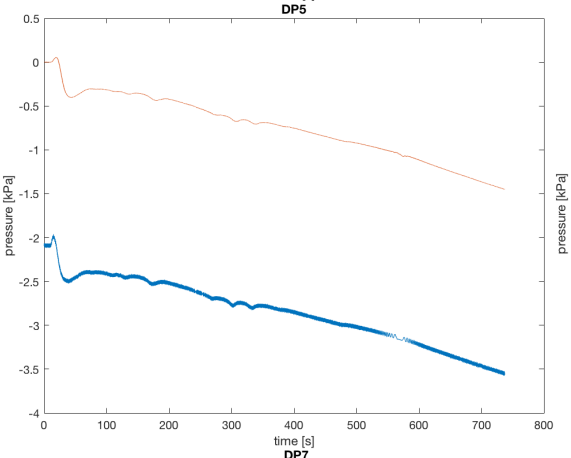

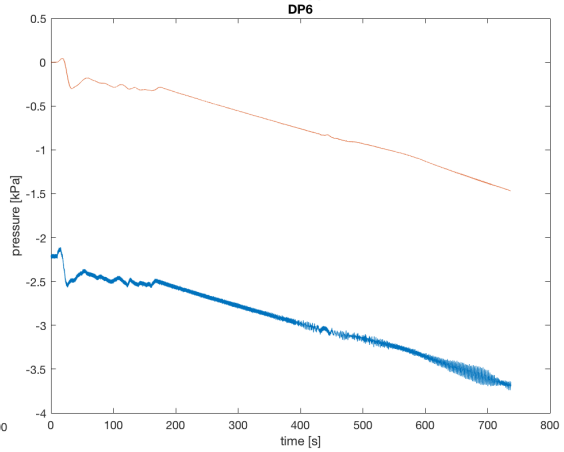

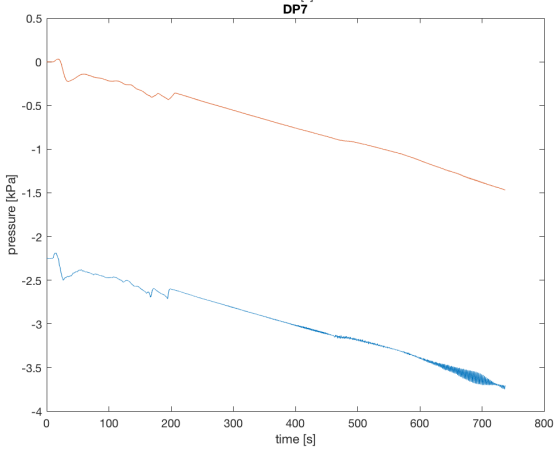

Experiment 6:

DP1

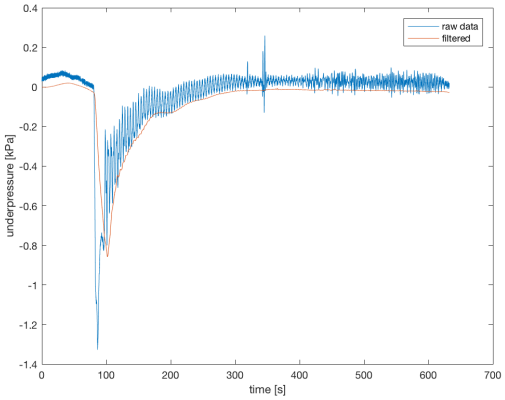

DP2

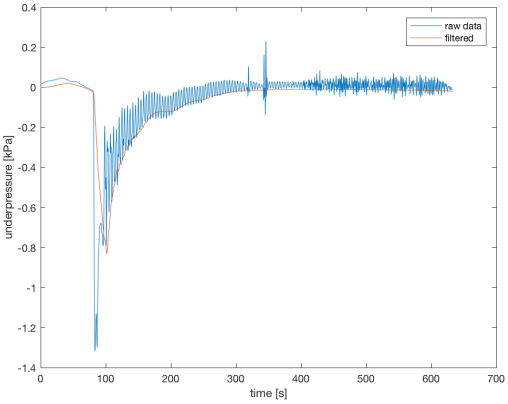

DP3

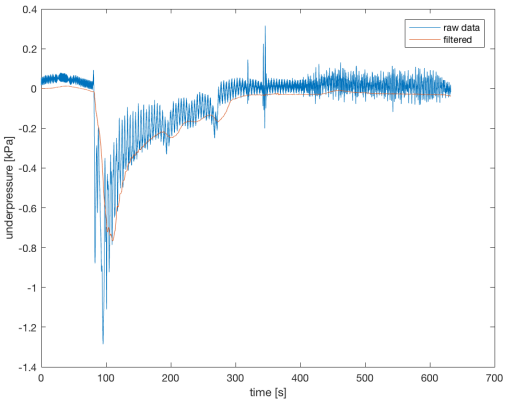

DP4

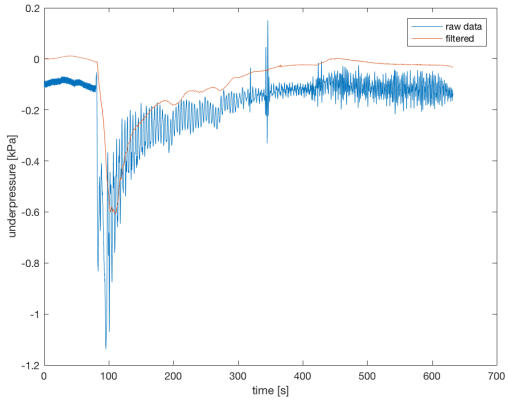

DP5

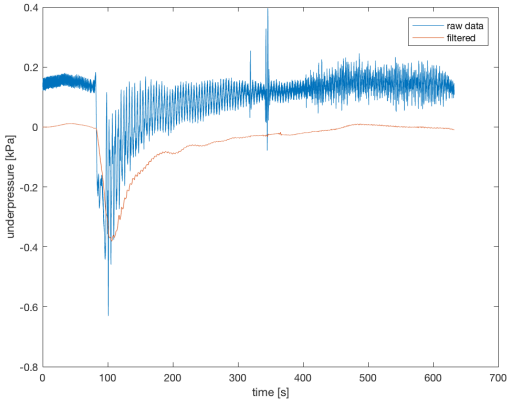

DP6

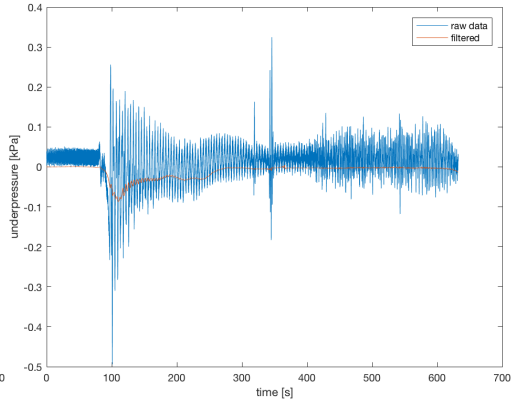

DP7

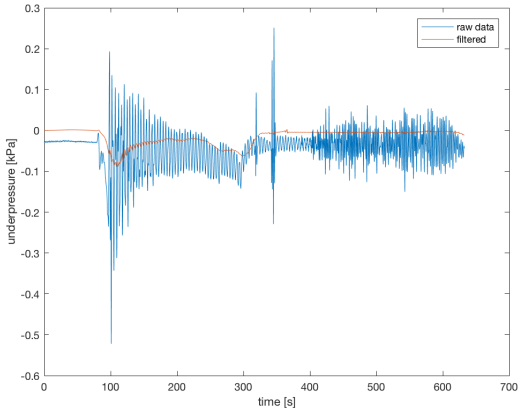

Experiment 7

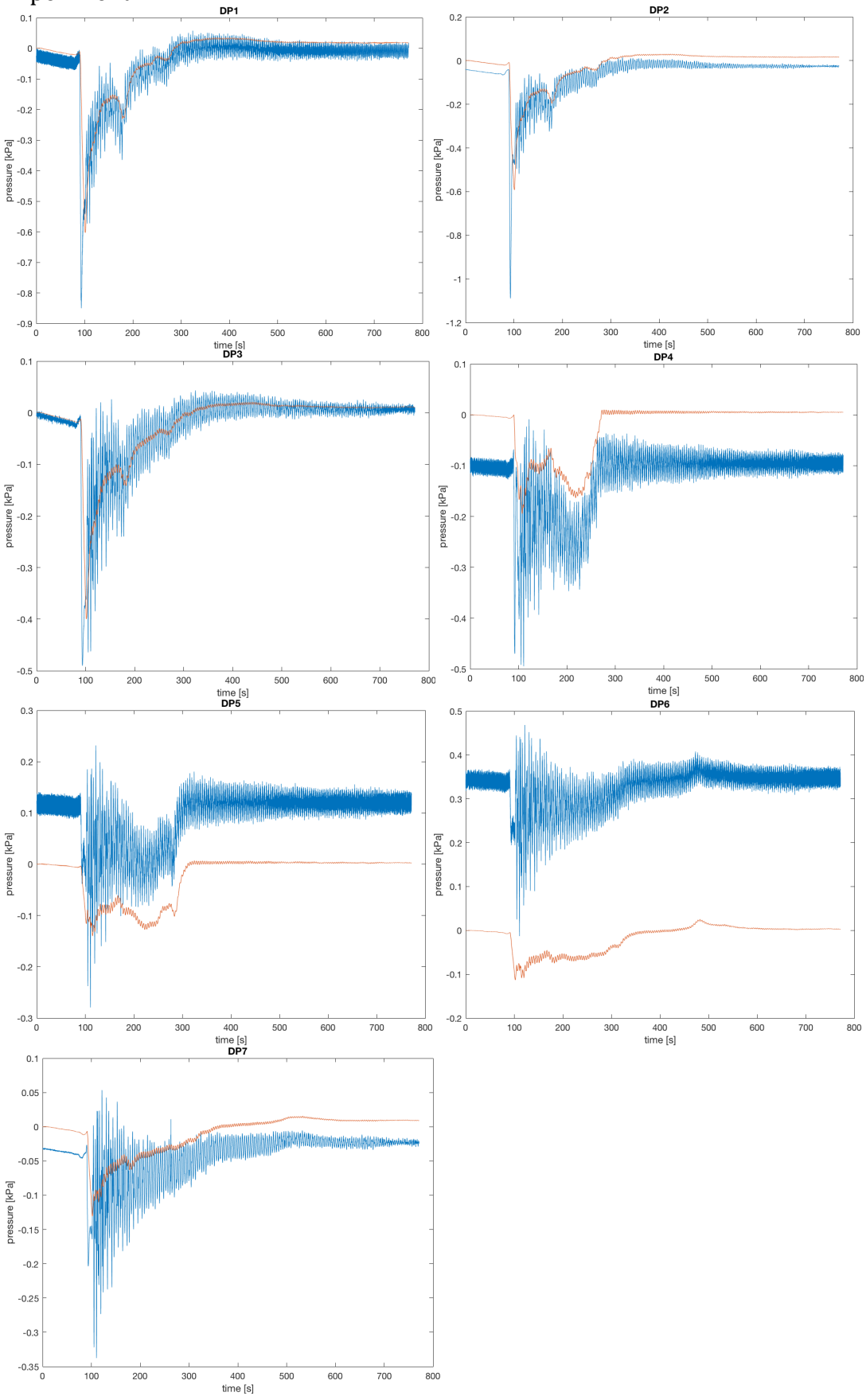

Experiment 8

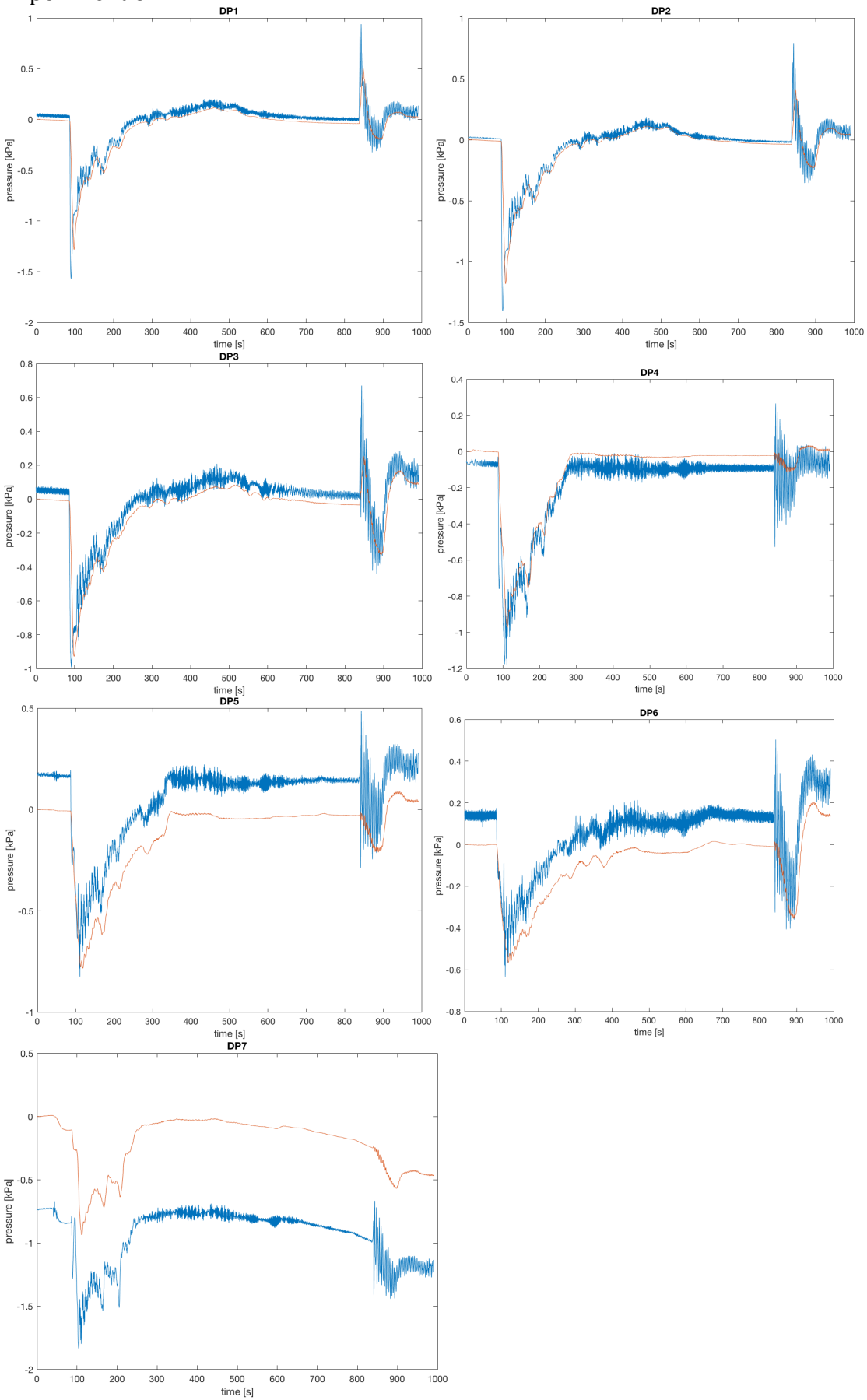

Experiment 9

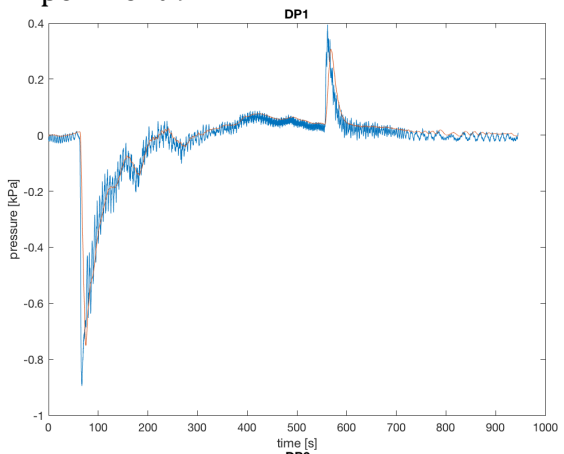

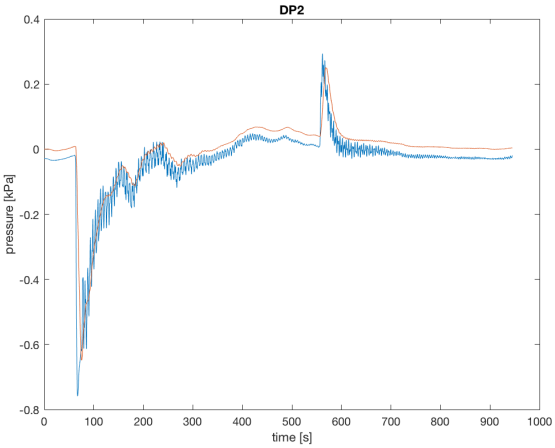

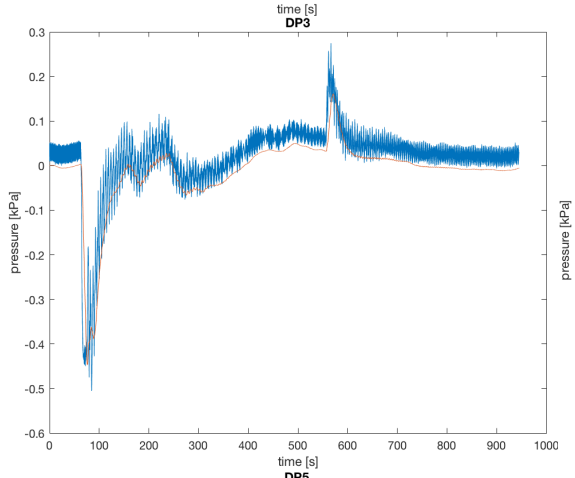

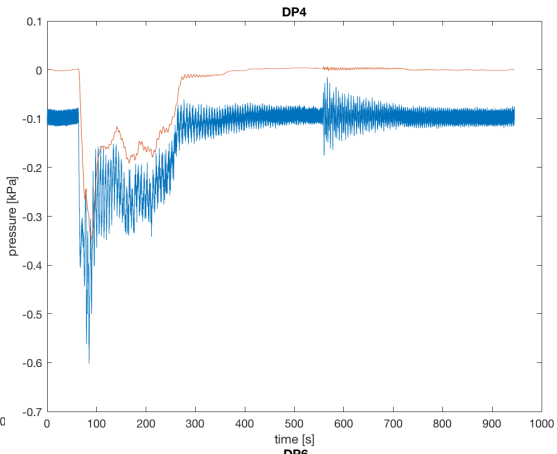

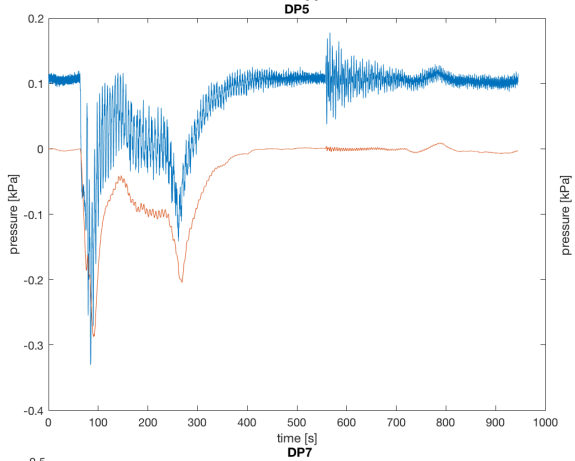

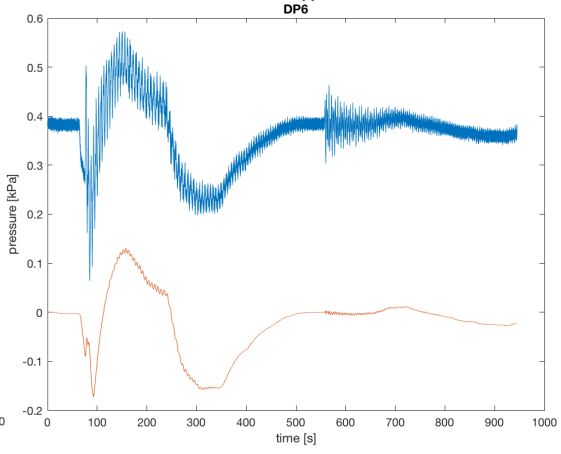

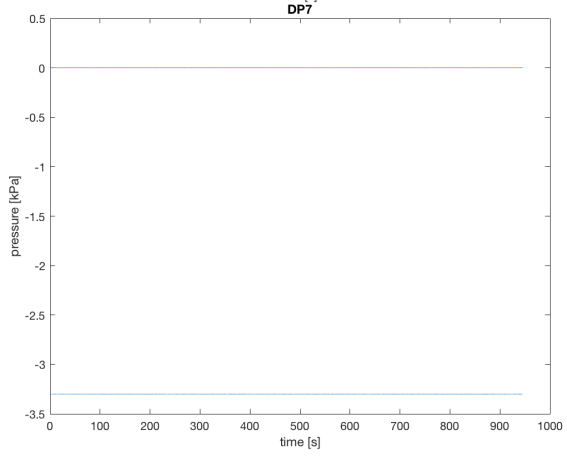

Experiment 10

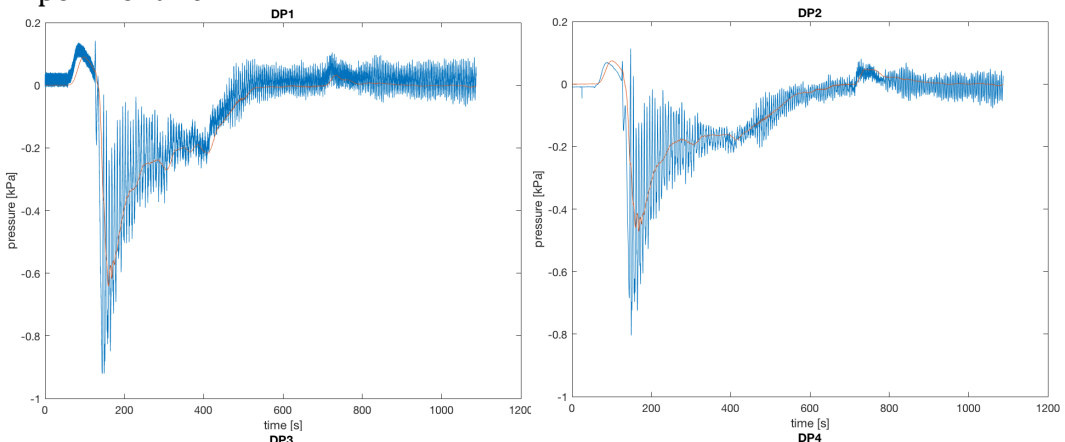

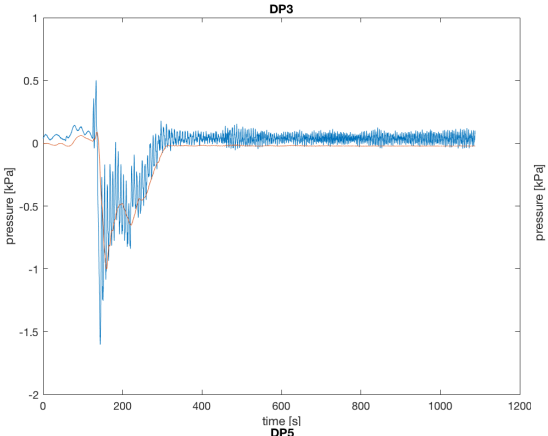

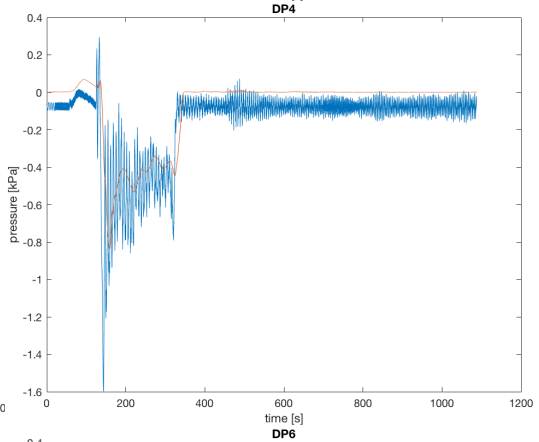

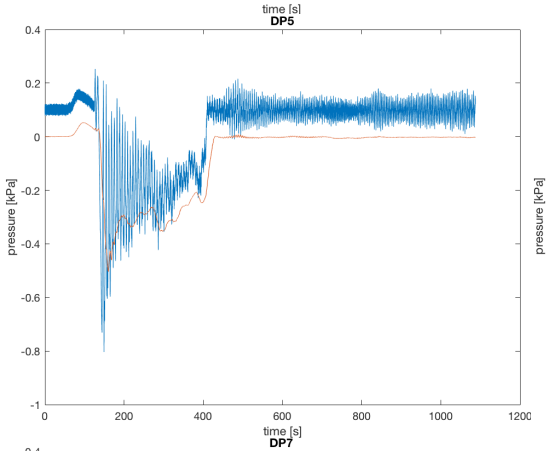

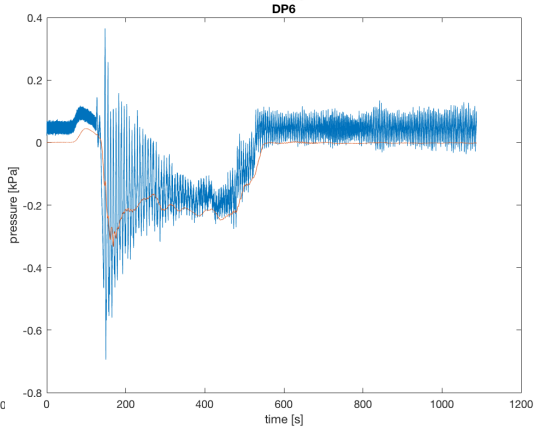

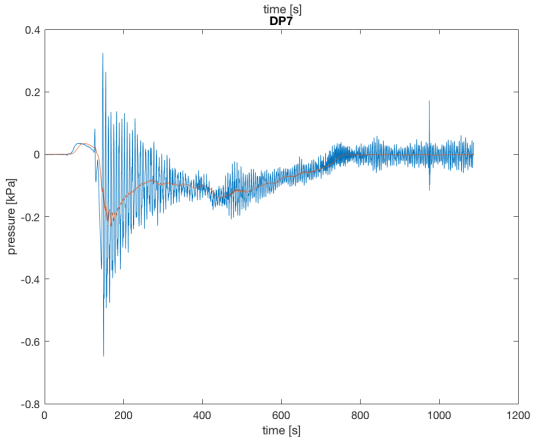

Experiment 11

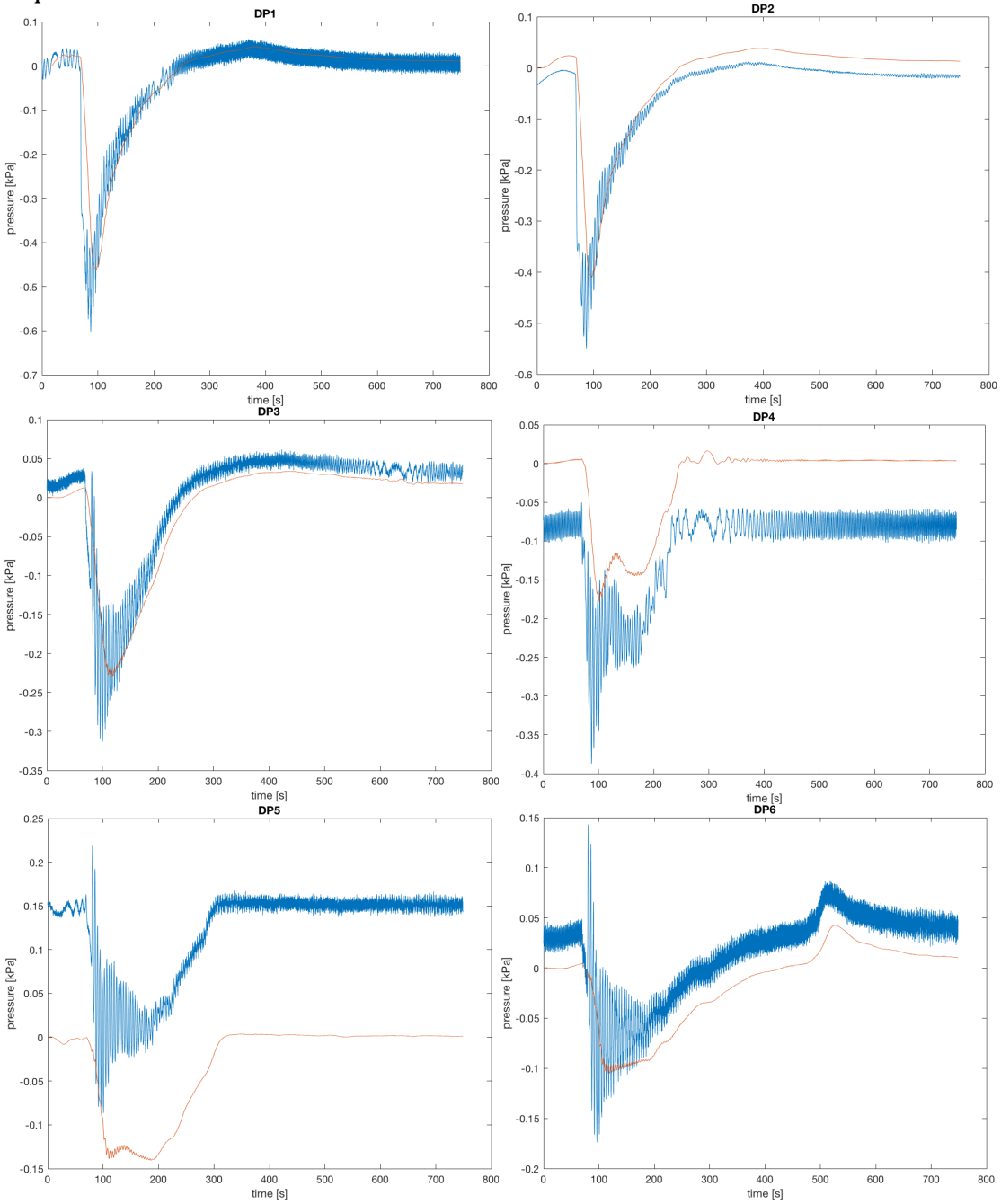

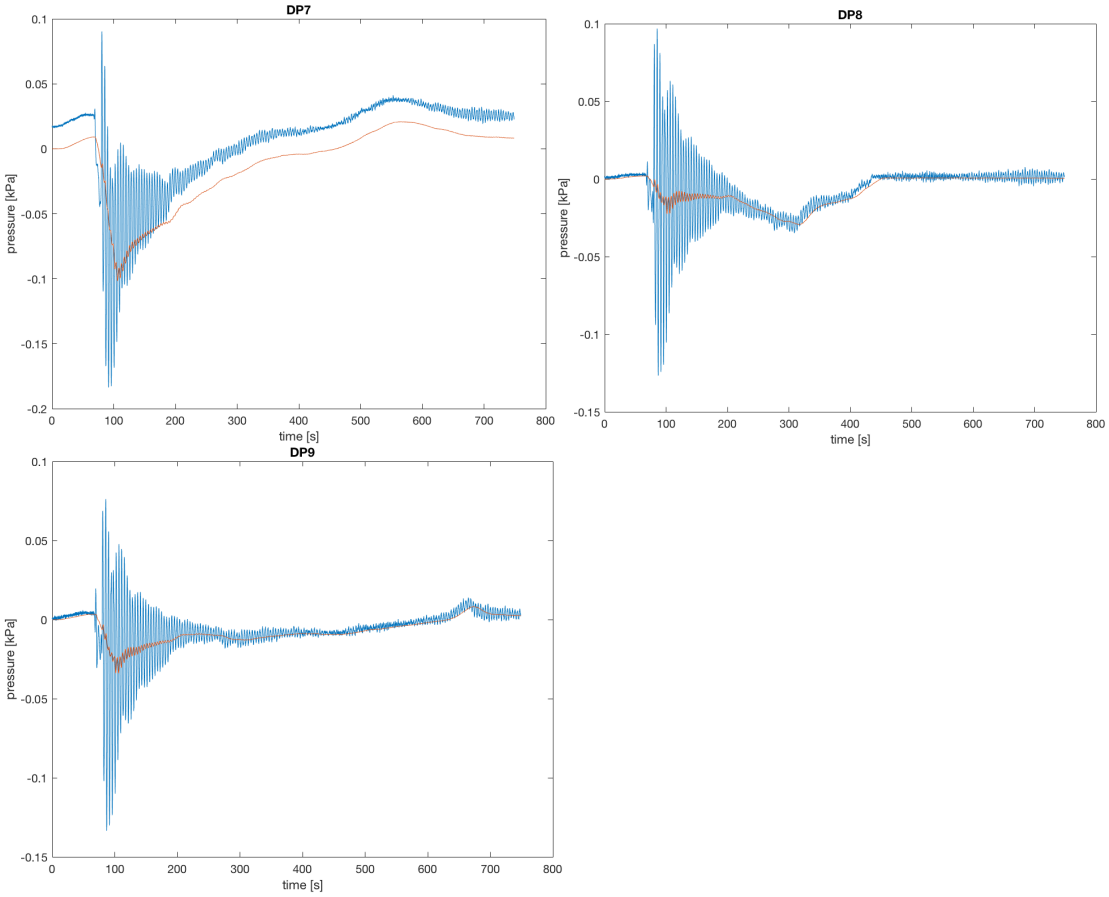
DP7
DP8
DP9
pressure [kPa]
time [s]
0.1
0.05
0
-0.05
-0.1
-0.15
-0.2
0
100
200
300
400
500
600
700
800

Experiment 12

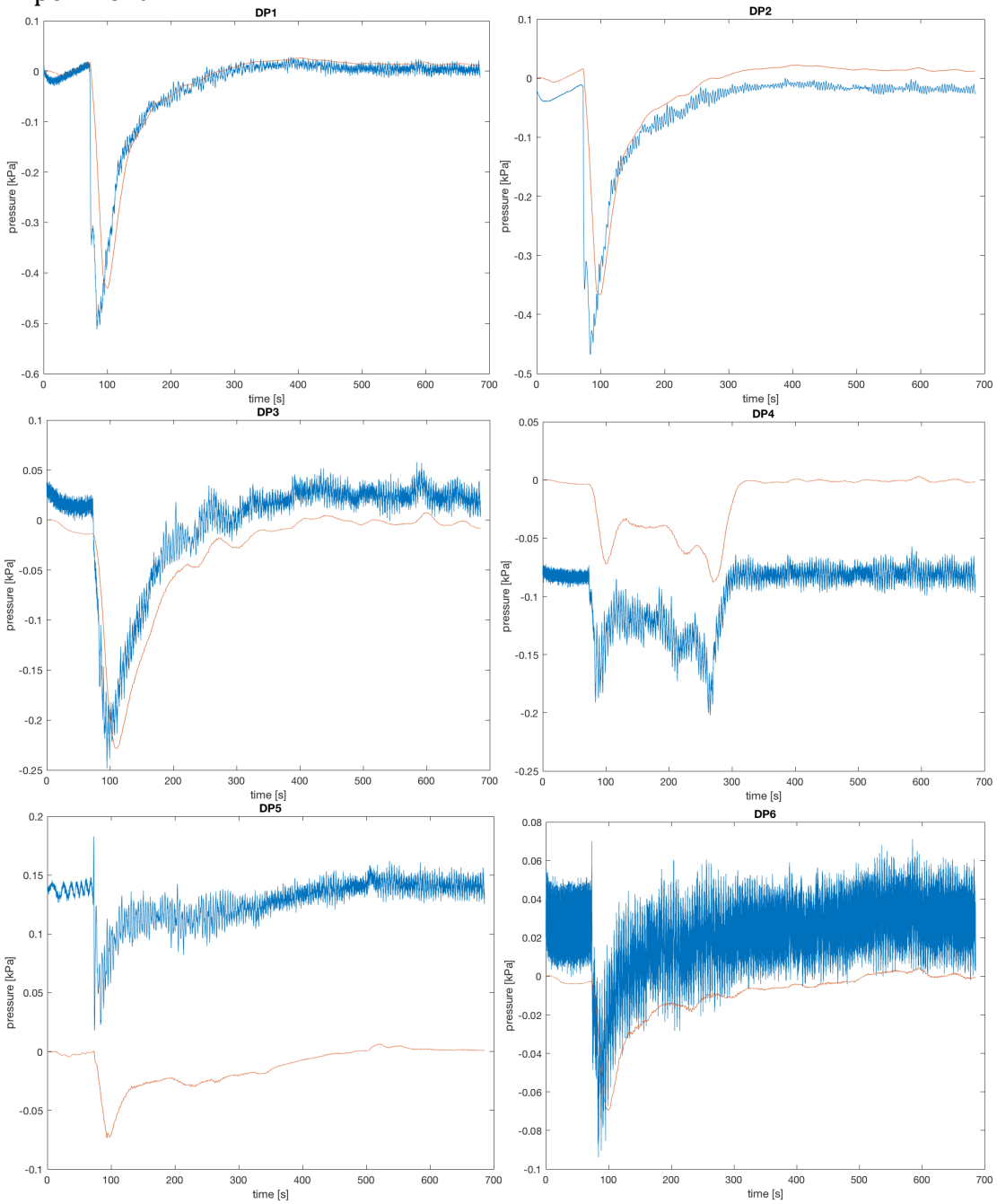

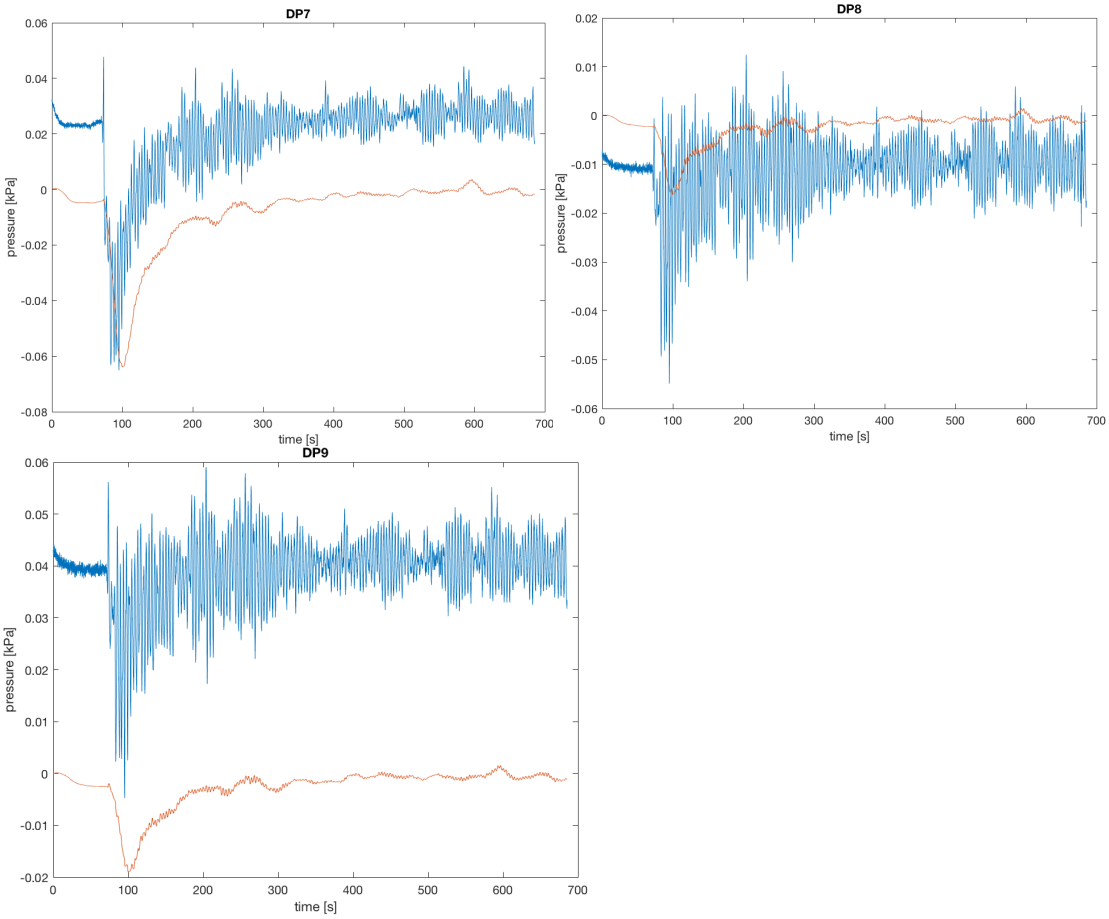
DP7
pressure [kPa]
time [s]
DP8
pressure [kPa]
time [s]
DP9
pressure [kPa]
time [s]

Experiment 13

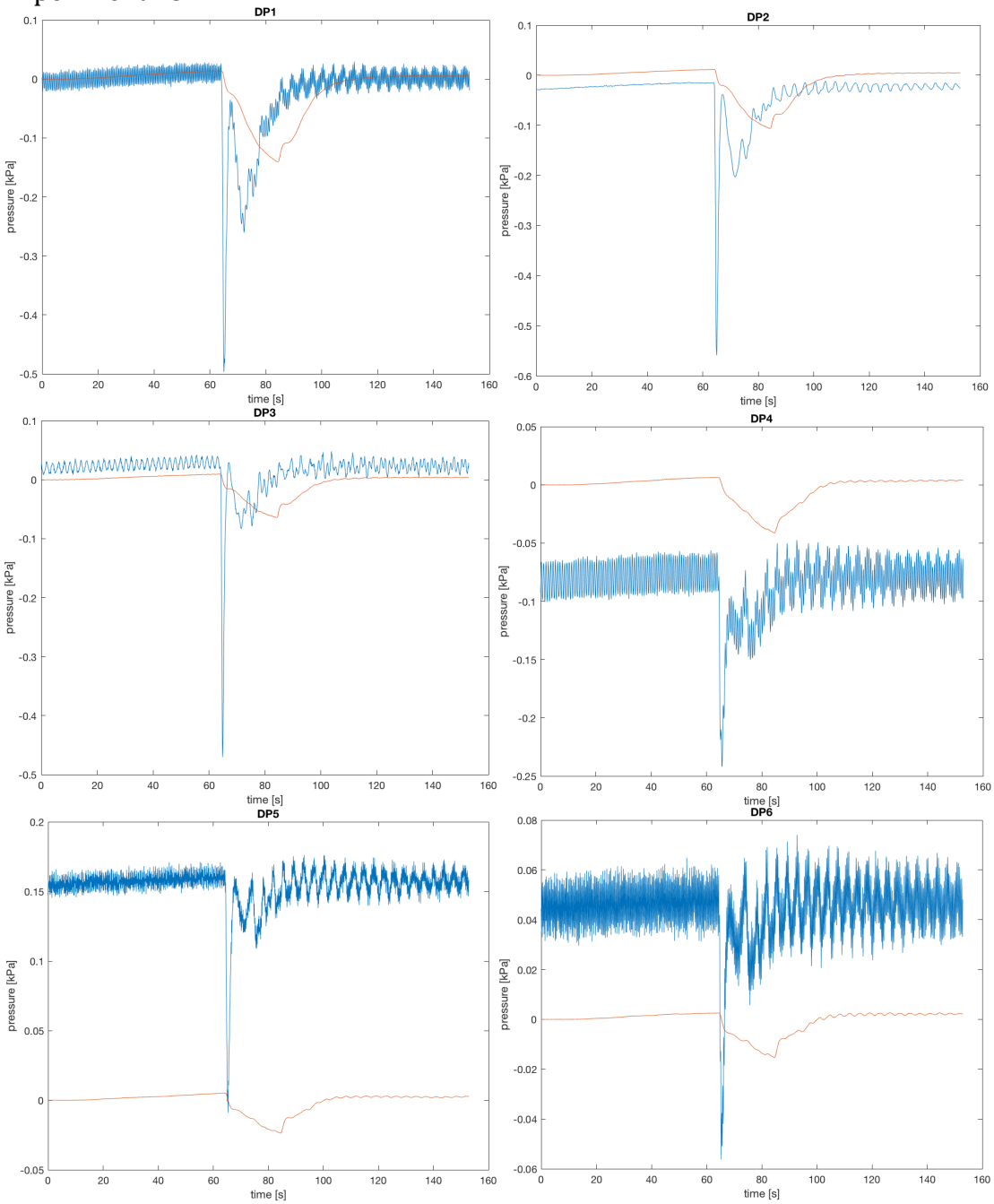

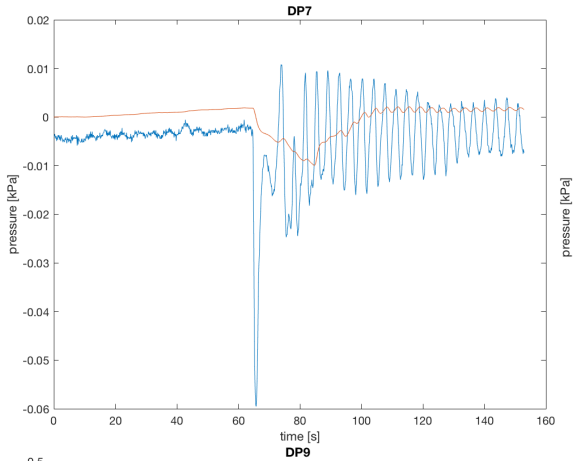
DP7
pressure [kPa]
time [s]

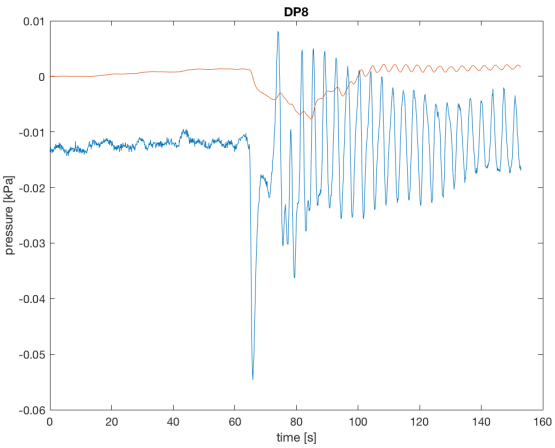
DP8
pressure [kPa]
time [s]

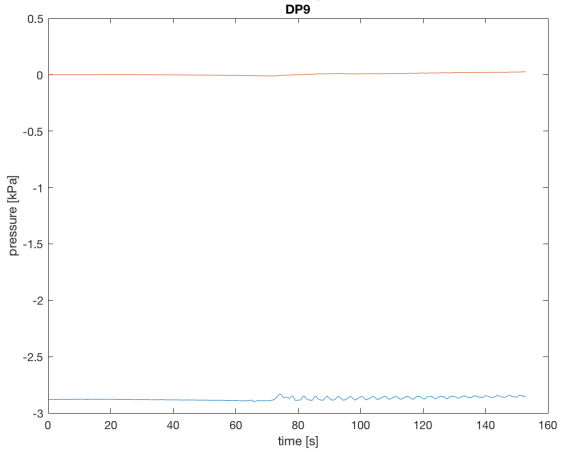
DP9
pressure [kPa]
time [s]

Experiment 14

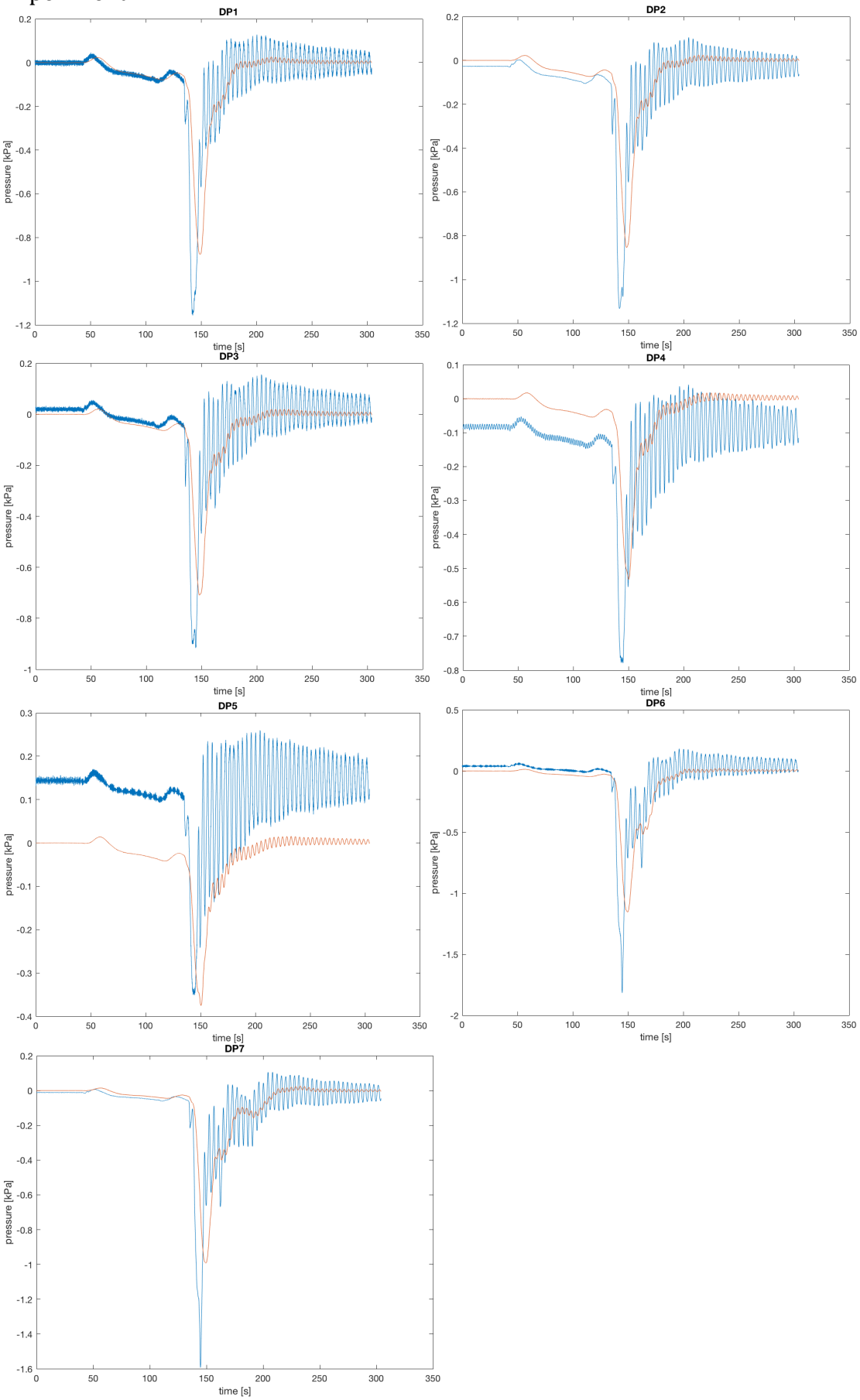

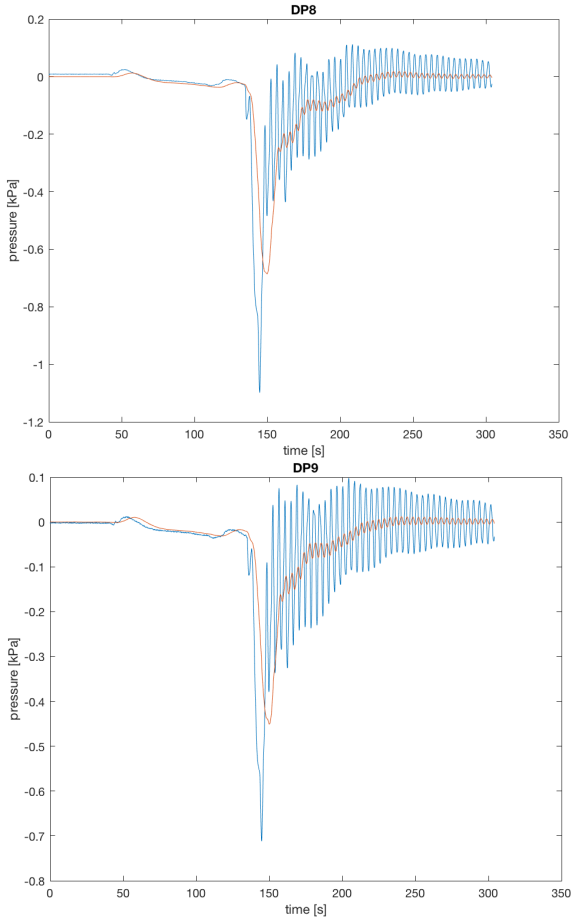
DP8
pressure [kPa]
time [s]
DP9
pressure [kPa]
time [s]

Experiment 15

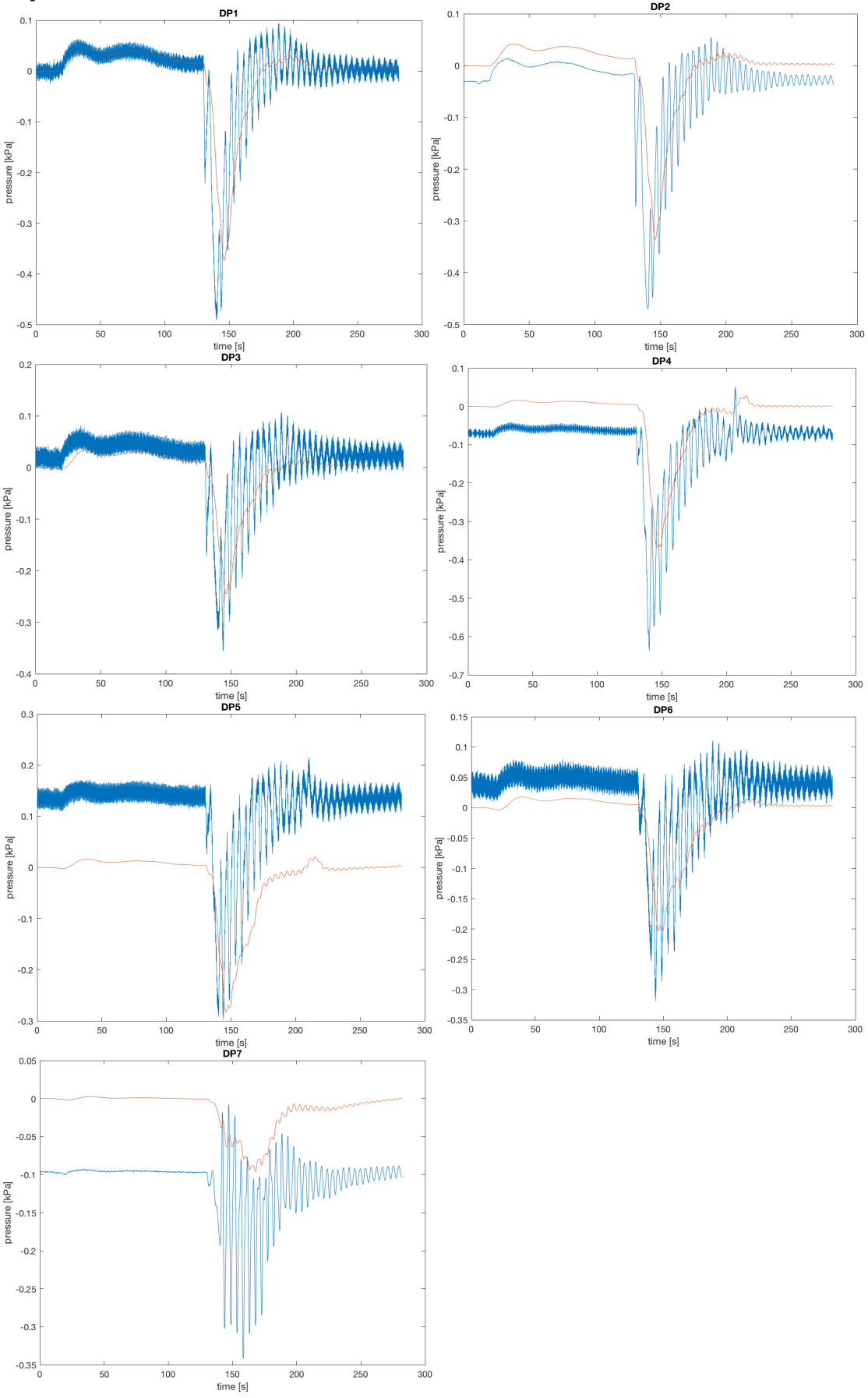

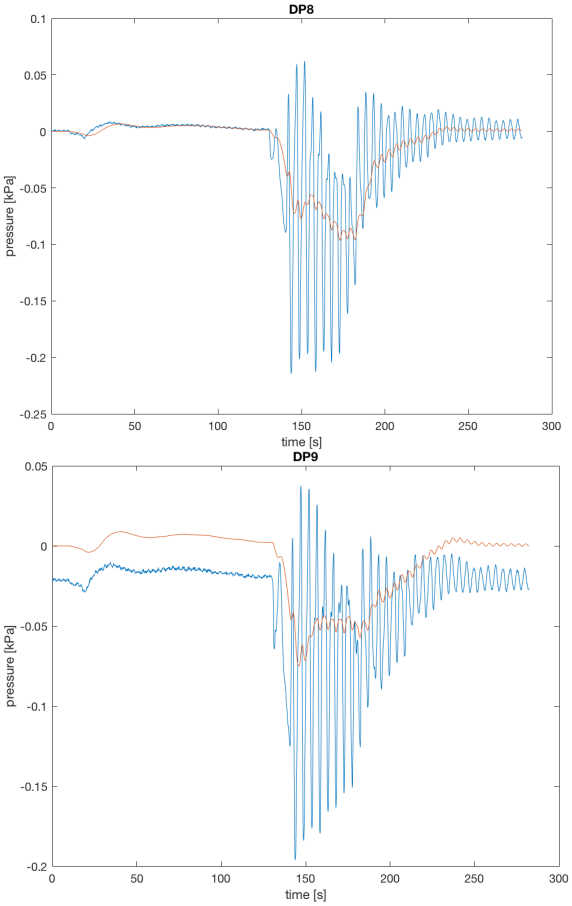
DP8
pressure [kPa]
time [s]
DP9
pressure [kPa]
time [s]

Appendix G Active Breaching Height

The active breaching height can be seen in the tables.

Experiment 1	Active breaching height [mm]
0 sec	655
25 sec	393
50 sec	383
75 sec	340
100 sec	287
125 sec	279
150 sec	106
175 sec	14

Experiment 2	Active breaching height [mm]
0 sec	655
30 sec	389
60 sec	392
90 sec	336
120 sec	232
150 sec	179
180 sec	118
210 sec	51

Experiment 3	Active breaching height [mm]
0 sec	655
30 sec	395
60 sec	378
90 sec	330
120 sec	269
150 sec	227
180 sec	161
210 sec	85

Experiment 4	Active breaching height [mm]
0 sec	1170
60 sec	836
120 sec	811
180 sec	695
240 sec	637
300 sec	377
360 sec	374
420 sec	118

Experiment 5	Active breaching height [mm]
0 sec	1170
60 sec	913
120 sec	779
180 sec	400
240 sec	713
300 sec	545
360 sec	362
420 sec	217

Experiment 6	Active breaching height [mm]
0 sec	1170
60 sec	715
120 sec	545
180 sec	493
240 sec	334
300 sec	269
360 sec	164
420 sec	74

Experiment 7	Active breaching height [mm]
0 sec	1170
60 sec	1150
120 sec	943
180 sec	795
240 sec	633
300 sec	556
360 sec	460
420 sec	388

Experiment 8	Active breaching height [mm]
0 sec	1470
90 sec	1150
180 sec	1120
270 sec	962
360 sec	644
450 sec	644
540 sec	520
630 sec	323

Experiment 9	Active breaching height [mm]
0 sec	1170
90 sec	1140
180 sec	988
270 sec	863
360 sec	661
450 sec	649
540 sec	366
630 sec	327

Experiment 10	Active breaching height [mm]
0 sec	1470
90 sec	1070
180 sec	1080
270 sec	933
360 sec	807
450 sec	589
540 sec	380
630 sec	324

Experiment 11	Active breaching height [mm]
0 sec	1170
60 sec	1130
120 sec	1020
180 sec	856
240 sec	803
300 sec	648
360 sec	539
420 sec	445

Experiment 12	Active breaching height [mm]
0 sec	1170
60 sec	1070
120 sec	1010
180 sec	796
240 sec	803
300 sec	535
360 sec	503
420 sec	439

Experiment 13	Active breaching height [mm]
0 sec	655
5 sec	370
10 sec	357
15 sec	313
20 sec	294
25 sec	240
30 sec	180
35 sec	125

Experiment 14	Active breaching height [mm]
0 sec	1170
15 sec	746
30 sec	538
45 sec	496
60 sec	314
75 sec	289
90 sec	229
105 sec	240

Experiment 15	Active breaching height [mm]
0 sec	1170
15 sec	1180
30 sec	637
45 sec	499
60 sec	367
75 sec	281
90 sec	124
105 sec	123

Experiment 16	Active breaching height [mm]
0 sec	1470
15 sec	805
30 sec	639
45 sec	798
60 sec	567
75 sec	426
90 sec	337
105 sec	236

Appendix H Headwall velocity Analysis Results

The wall velocities and headwall velocities are plotted against each other. The yellow line is the calculated wall velocity obtained from the headwall velocity and the percentage of sliding wedges.

Experiment 1

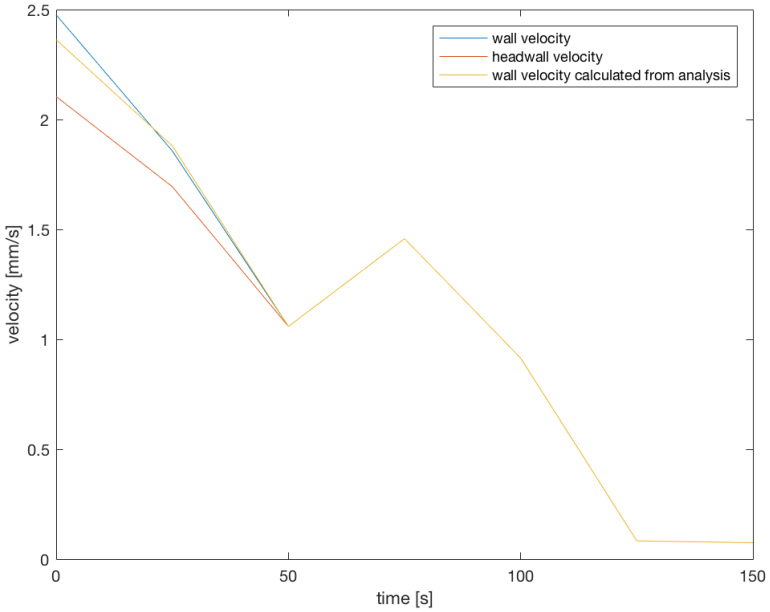

Experiment 2

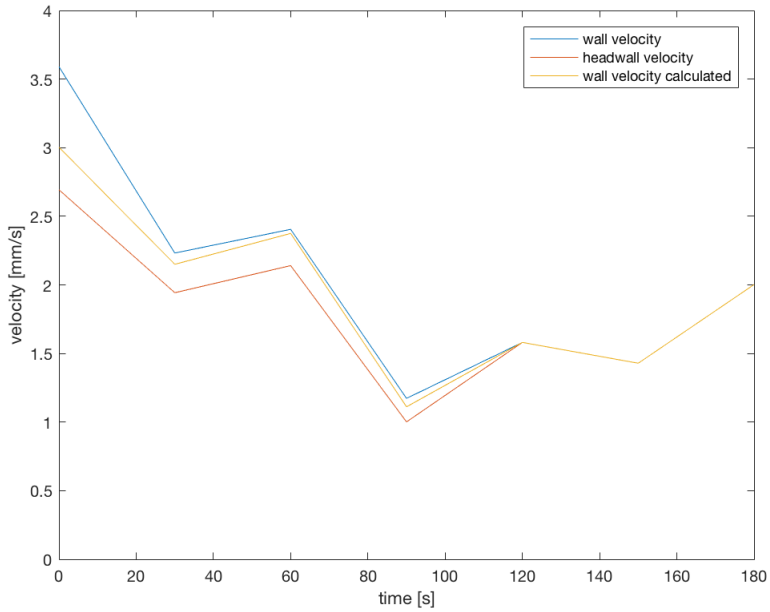

Experiment 3

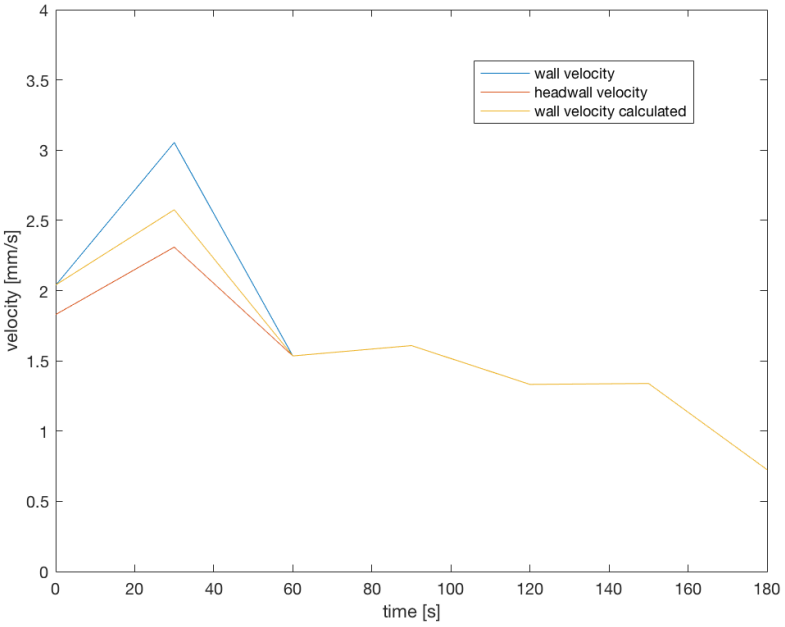

Experiment 4

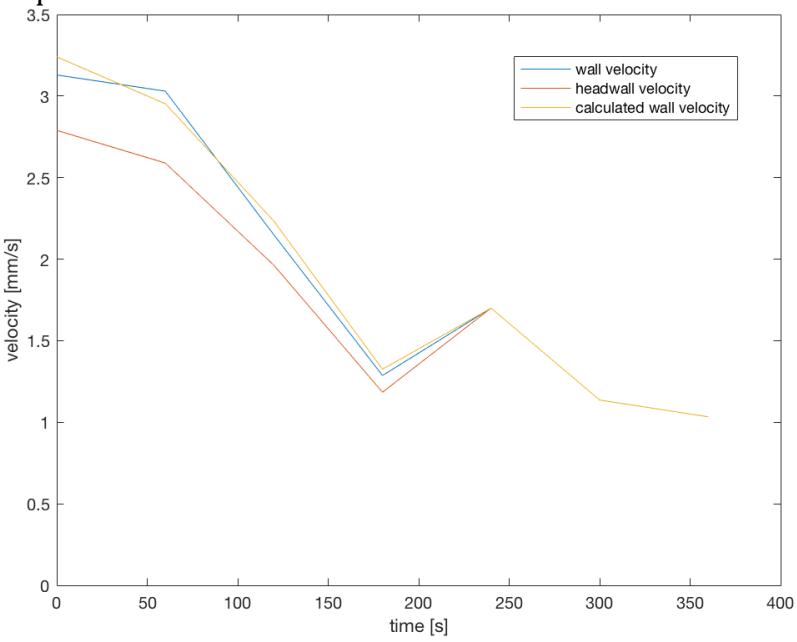

Experiment 5

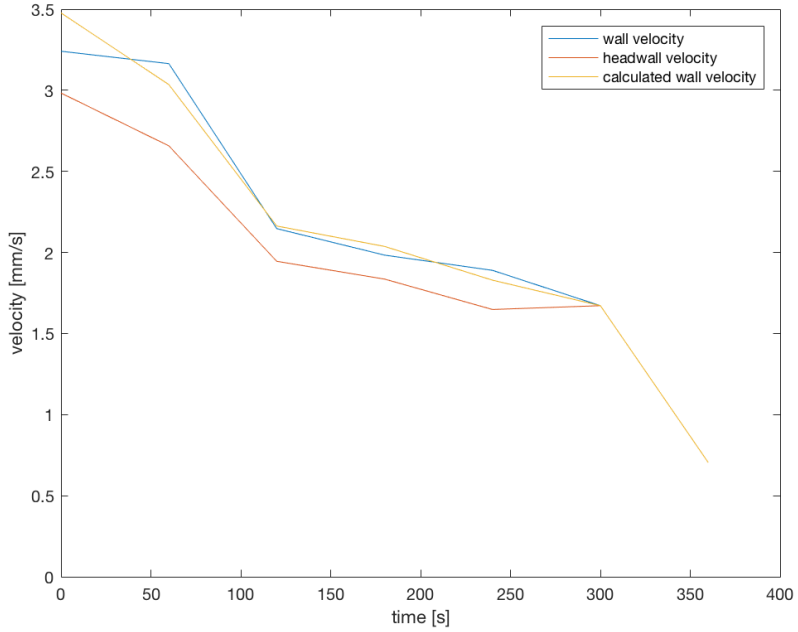

Experiment 6

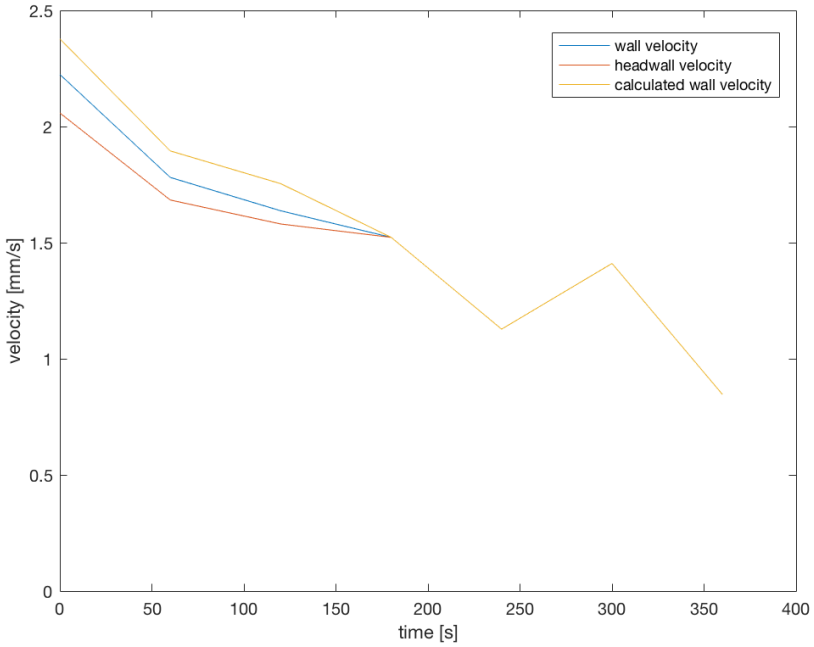

Experiment 7

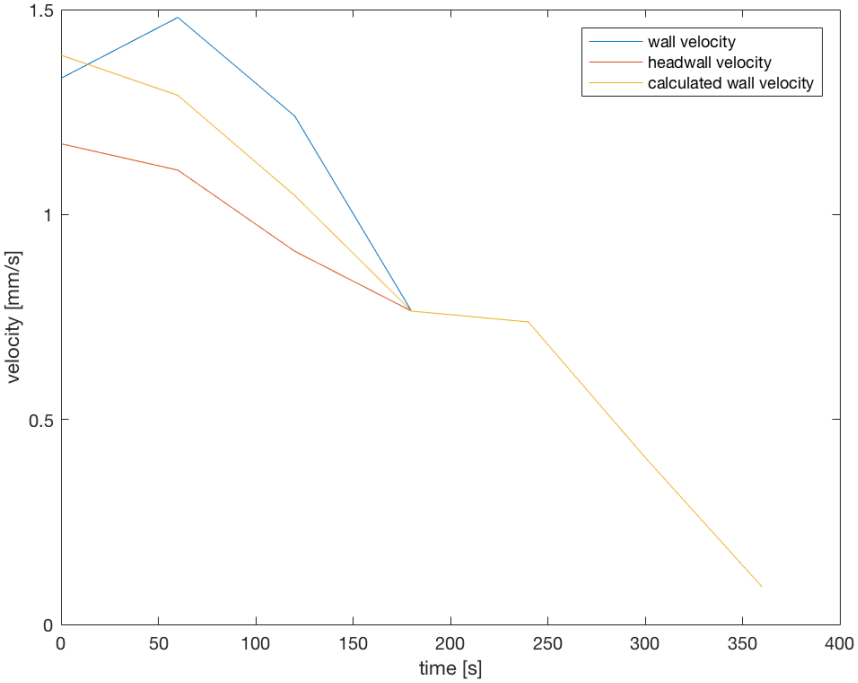

Experiment 8

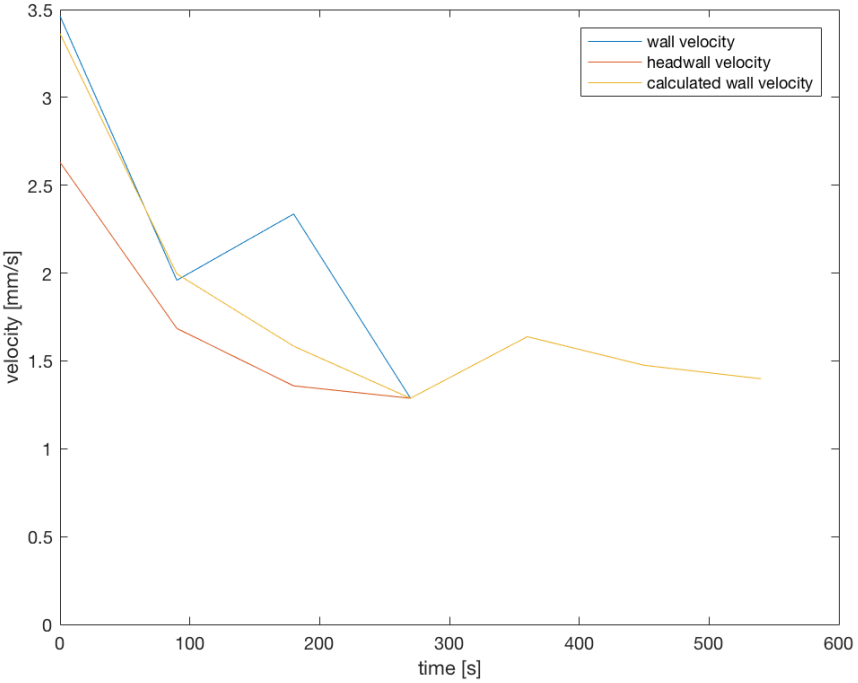

Experiment 9

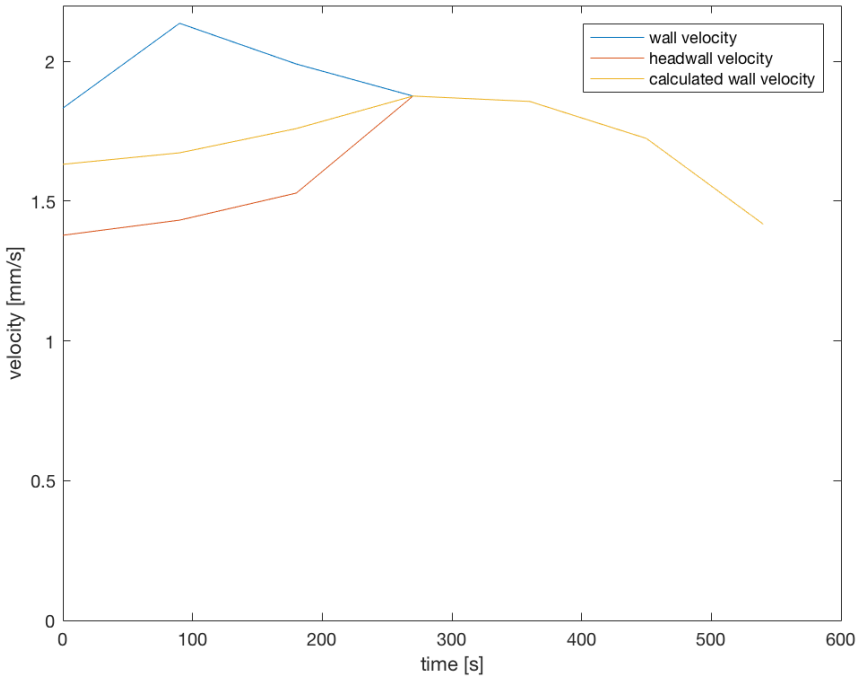

Experiment 10

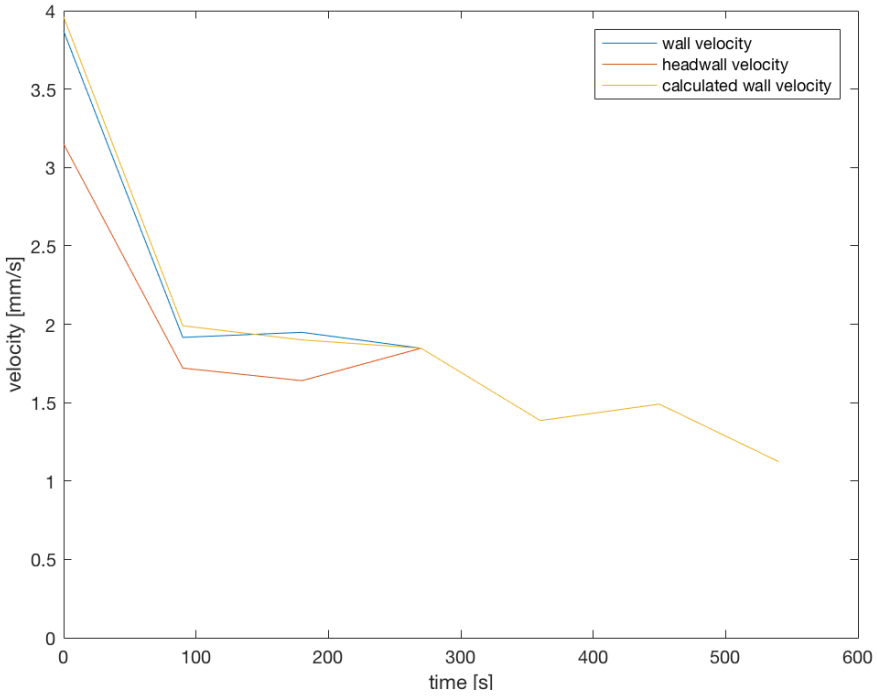

Experiment 11

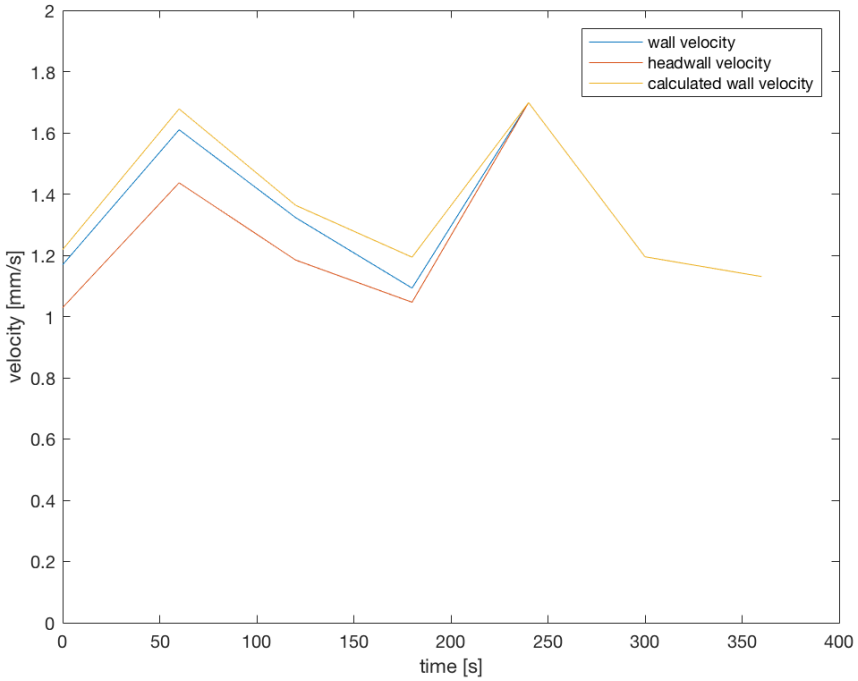

Experiment 12

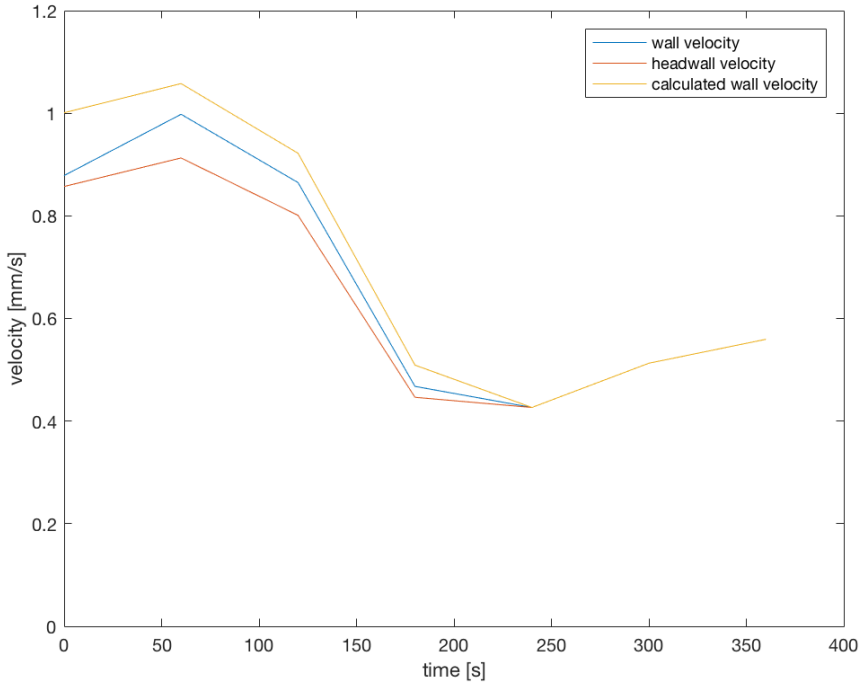

Experiment 13

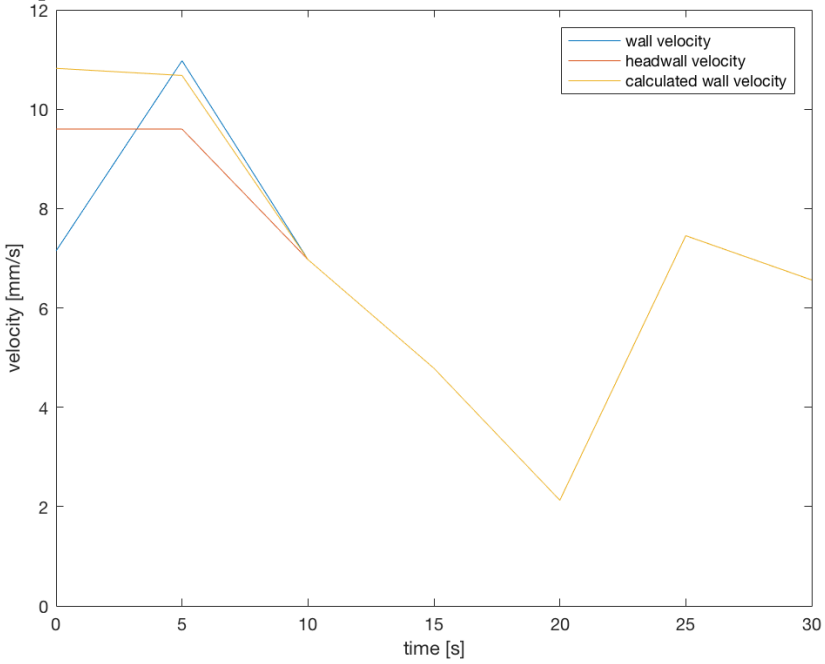

Experiment 14

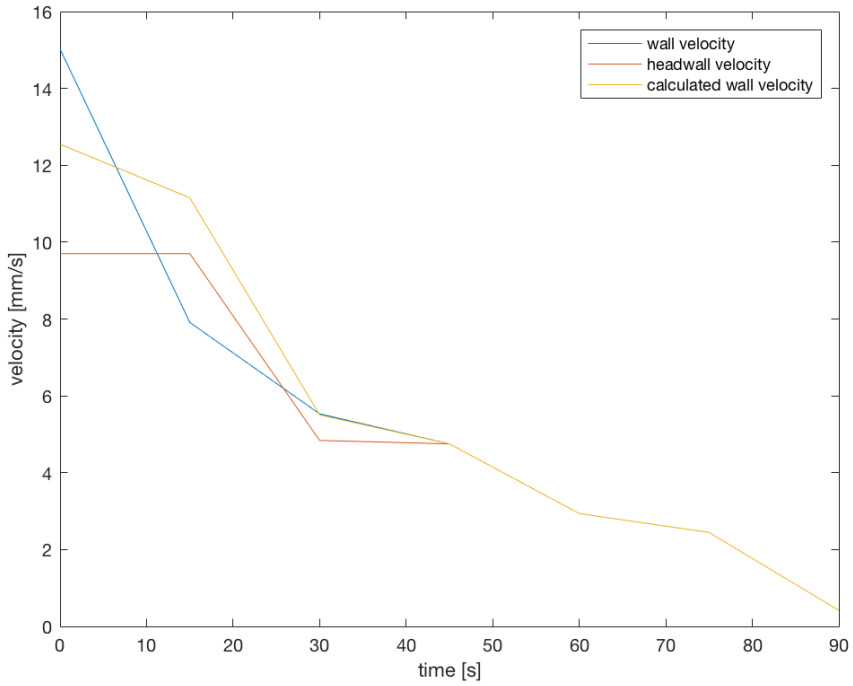

Experiment 15

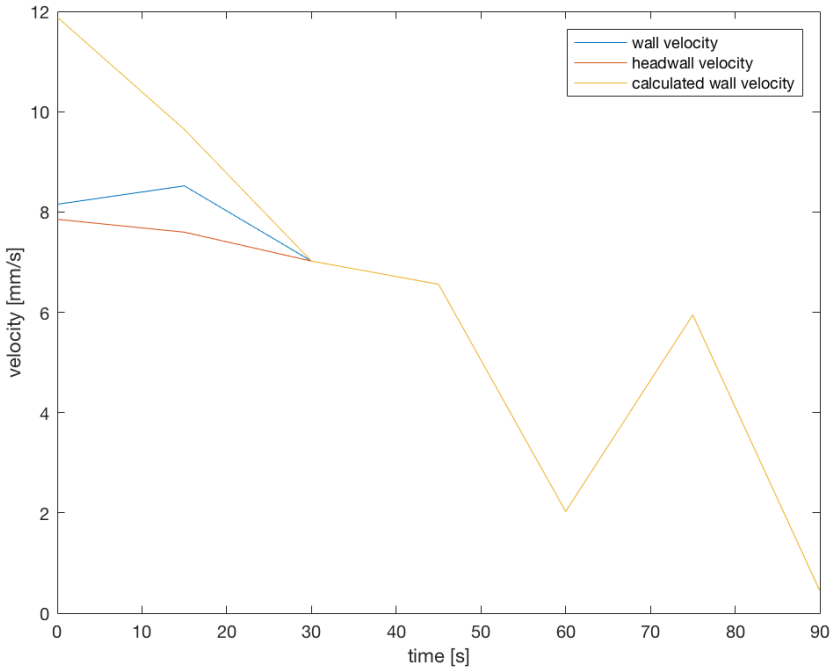

Experiment 16

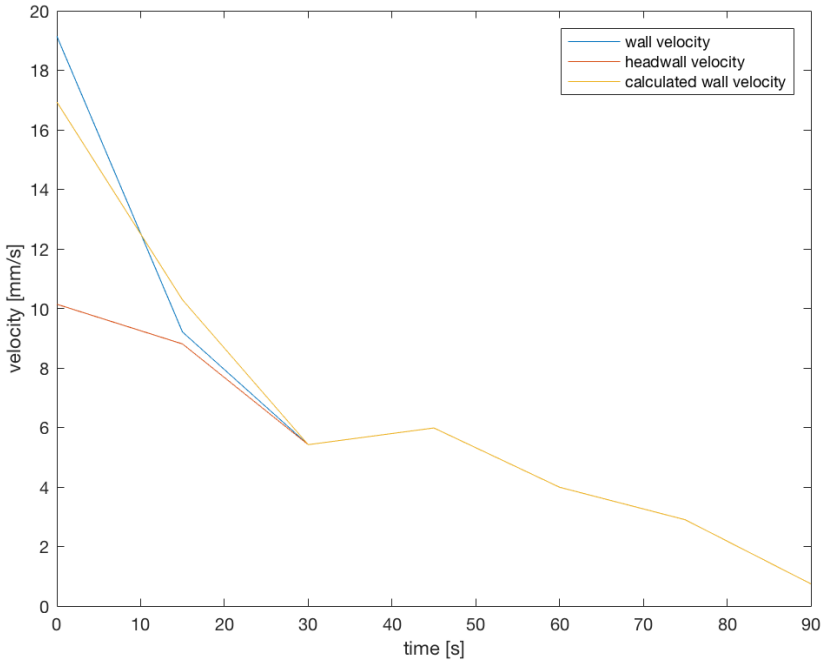

Appendix I DP Sensor data

It is important to know what sensors were used in the setup, also for further research.

Sensor	Manufacturer & Type	Serial Number
DP1	Rosemount DP3	7031874
DP2	Rosemount DP3	8297400
DP3	Rosemount DP4	8649805
DP4	Rosemount DP4	8649807
DP5	Rosemount DP3	8649808
DP6	Rosemount DP4	8649804
DP7	Rosemount DP4	8649806
DP8	Rosemount DP4	7389288
DP9	Rosemount DP4	8649809

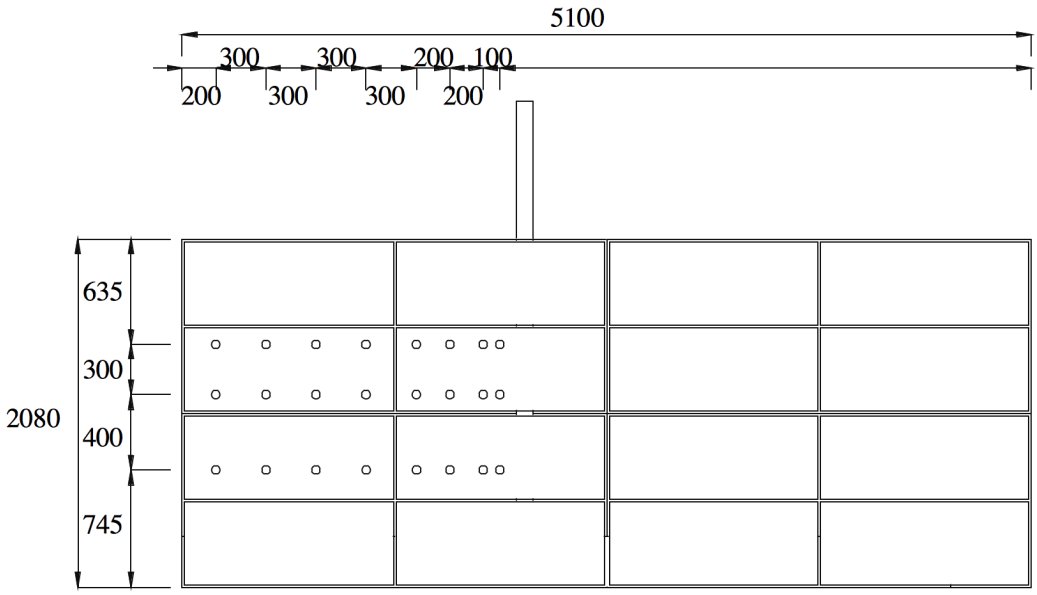
5100
300
300
200
100
200
300
300
200
2080
635
300
400
745

4x glass panel 2550x1040
4x steel panel 2550x1040

4x steel panel 500x1040
4x steel panel 200x1040

8x corner panel

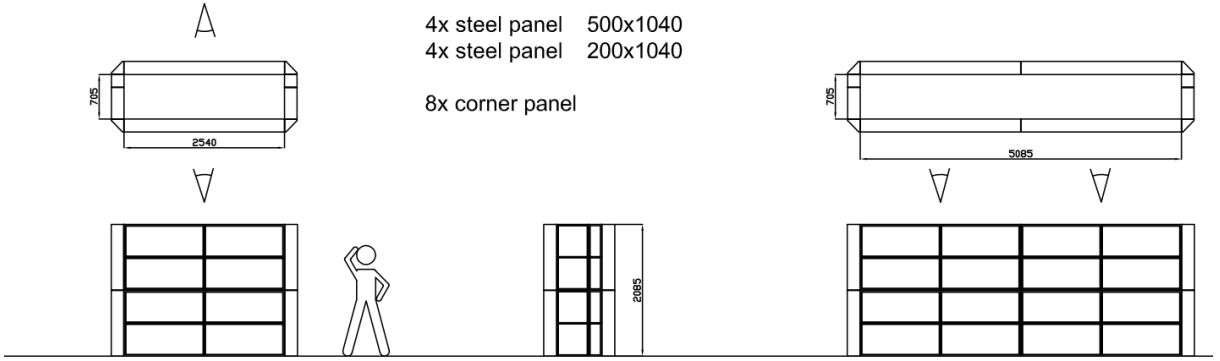

Appendix J Pump Data

No: PD546020-INT | Revision 1 2015.09 | 50 Hz 8146.020

Bravo 200

Electrical submersible slurry pump

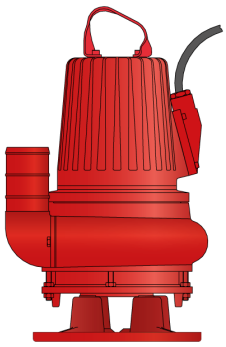

50 Hz	Bravo 200
Discharge connection	4"
Rated power P_2 [kW]	4,7
Max. power consumption P_1 [kW]	5.7
Shaft speed [rpm]	1445
Rated current at 230V	17 A
Rated current at 400V	9.6 A
Rated current at 500V	7.7 A
Solids passage [mm]	50
Height [mm]	760
Diameter [mm]	460
Weight [kg]	157

Other voltages on request

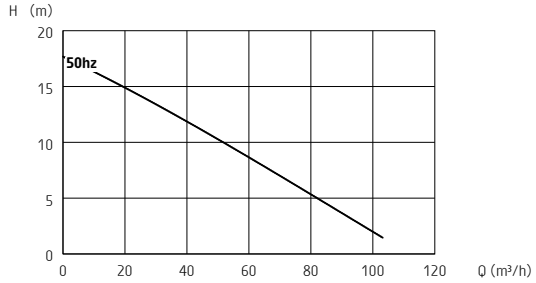

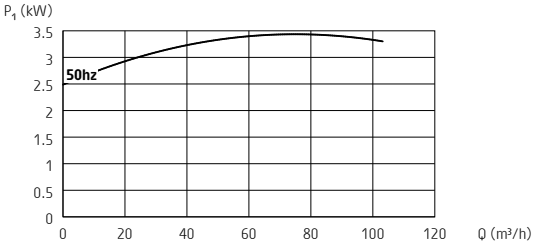

ISO 9906/A

General description
Submersible pump for pumping water containing abrasive particles, ground water, slurries

Classification
Electrical submersible slurry pump
Protection class: IP 68

Electrical motor
Squirrel cage induction motor
Insulation class: H (IEC 85), DOL or star/delta

Motor protection
Thermo switches in motor windings
This pump must be used with external motor protection in accordance with technical data

Cable - SubCab 20 m (66 ft)
DOL: 4x2.5mm² + 2x1.5mm²
Y/D: 7x2.5mm² + 2x1.5mm²

Shaft seals
Double mechanical seal running in an oil compartment
Material lower seal: tungsten carbide - tungsten carbide
Material upper seal: tungsten carbide - aluminium oxide

Materials
Drive unit: *Cast iron*
Pump housing: *Cast iron*
Impeller: Hard-IronTM
Discharge connection: *Cast iron*
Wear plate: *Nitrile rubber*
Lifting handle: *Galvanized steel*
Shaft: *Stainless steel*
Studs, screws and nuts: *Stainless steel*
O-rings: *Nitrile rubber*

Limitations
Max. submersion depth: 20 m (66 ft)
Max. liquid temperature: 40 °C (104 °F)
Allowed pH range: 5.5 - 14

Specifications can be changed without notice

Grindex AB •P.O. Box 7025 •174 07 Sundbyberg •Sweden •Ph: +46 8 606 6600 •Fax: +46 8 745 5328 •marketing@grindex.com •www.grindex.com

2640.180 50Hz

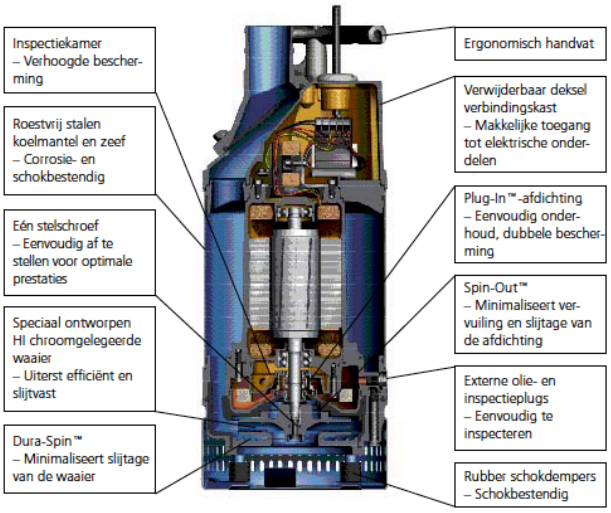

Prestaties

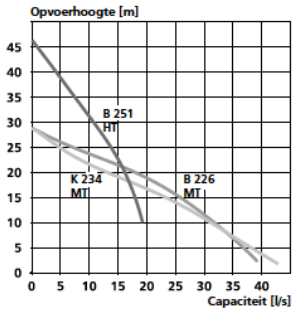

HT = Grote opvoerhoogte
MT = Middelgrote opvoerhoogte
B = slijtvast
K = slijtvast met grove delen

Afmetingen

Hoogte	758 mm
Diameter	286 mm

2640.180

Onderwaterpomp voor de drainage van bouwterreinen en mijnen, het afpompen van overstroomde gebieden en andere toepassingen waarbij de vloeistoffen slijtende delen kunnen bevatten.

Productnaam

Productcode	2640.180
Installatie	Transportabel
Waaierkenmerken	
slijtvast middelgrote opvoerhoogte (B 226, MT)	
grote opvoerhoogte (B 251, HT)	
slijtvast met grove delen (K 234, MT)	
Aansluitkoppeling	4", 3"

Procesgegevens

Vloeistoftemperatuur	max. +40°C
Dompeldiepte	max. 20 m
Vloeistofdichtheid	max. 1.100 kg/m³
Zeefgaten	8 mm x 18 mm
pH-waarde van de verpompte vloeistof	pH 5–8

Motorgegevens

Driefase kooianker-inductiemotor	
Frequentie	50 Hz
Isolatieklasse	H (+180 °C)
Motor voorzien van thermocontacten	
Aantal startbeurten/uur	max. 30

Kabels

SUBCAB®	onderwaterkabel

Stekkers

5 polige CEE 32A stekker met fase indicator en fasewisselaar

Controleapparatuur

Openingstemperatuur thermische contacten	+140 °C

Materialen

Buitenmantel	roestvrij staal
Waaier	HI chroomgelegeerd
Slijtstukken	nitriel rubber
Statorhuis	gietijzer
Zeef	roestvrij staal
As	roestvrij staal
O-ringen	nitriel rubber

Mechanische afdichtingen

Binnendichtingen	hard metaal
Buitendichtingen	hard metaal

Gewicht

Totaal (excl. kabel)	51 kg

Opties

Uitvoering warme vloeistoffen	max. +70 °C
Snelkoppelingen	4", 3"
Starters	
Zinkanodes	

Accessoires

Adapters, slangaansluitingen en andere mechanische toebehoren. Elektrische toebehoren zoals pompcontrollers, bedieningspanelen en monitorrelais.

Nominale waarden

3~

Nominaal vermogen	5,6 kW
Toerental	2895 omw/min

Spanning V	Nominale stroom A	Start-stroom* A
400 D	11,0	77,7

* bij directe inschakeling

2640.04.01.Holl.12.06 130 Trosa Tryckeri AB 58265

Appendix K Calibration Formulas DP Sensors

DP1: 1.5084x – 4.5013
DP2: 1.5103x – 4.5149
DP3: 1.5112x – 4.5164
DP4: 1.5009x – 4.5002
DP5: 1.5016x – 4.5036
DP6: 1.5108x – 4.5044
DP7: 1.5110x – 4.5131
DP8: 1.5148x – 4.5107
DP9: 1.5074x – 4.5188

Appendix L Soil Data

Some tests with sieves were conducted to know the particle size distribution.

Dorsilit 9 sieve curve

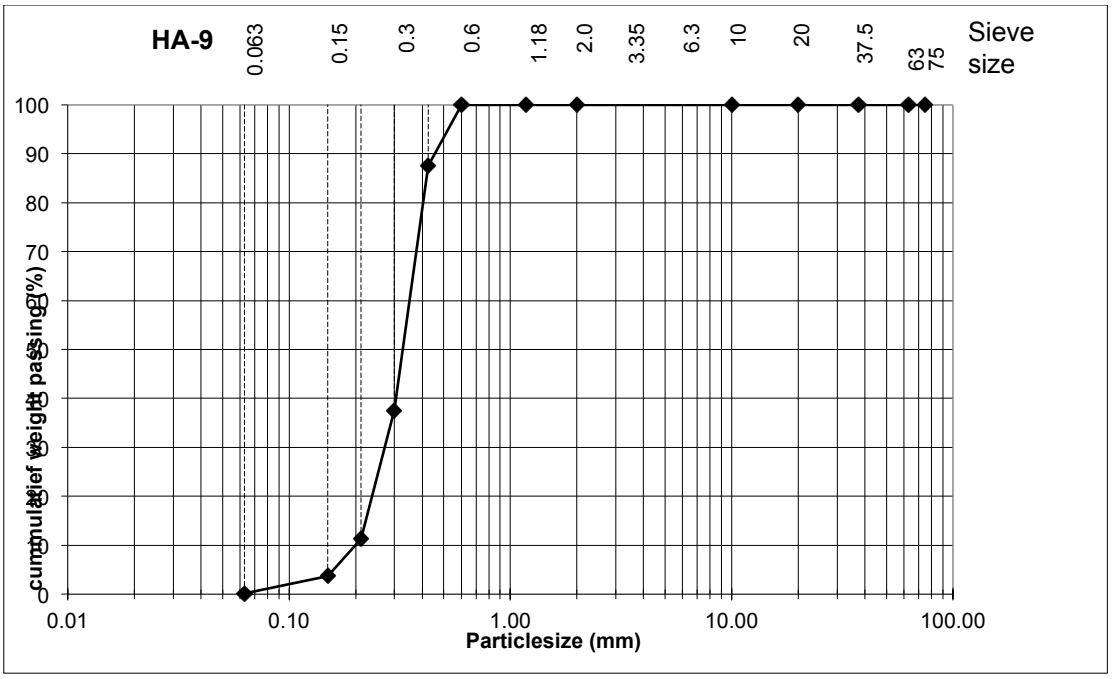

Geba Weiss

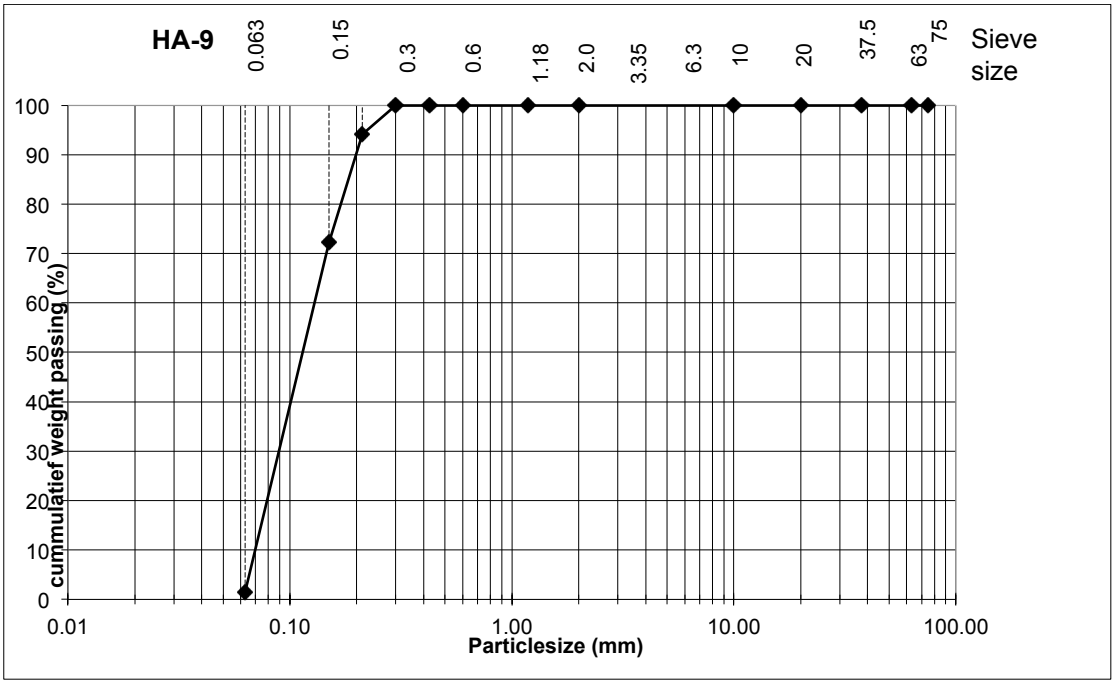

Permeability tests were conducted in the department of Civil Engineering. The permeability were obtained from a falling head test. The first table will be Geba Weiss sand and the second Dorsilit 9

KSAT
Software Version 1.2.0
Firmware Version 1.4
Last setting of the zero point 1-1-
0001
Serial Number 0034

PARAMETER
Mode FallingHead
Sample name Gebat1_001
cross-sectional area of the burette [cm2] 4,536
Cross-sectional area of the sample [cm2] 50,18
Sample length [cm] 5,0
Plate thickness [cm] 1,0
Crown type FilterPlateCrown
Saturated plate conductivity [cm/d] 20000,000
Start of measurement 17-11-2016 11:52:29
Test duration 00:01:00

RESULT
Use auto offset adjustment True
Fitting Parameter a [cm] 4,98
Fitting Parameter b [s-1] -1,59E-02
Fitting Parameter c [cm]
Fitting Parameter r2 [-] 0,9998
Ks Total [cm/d] 781
Ks Total [m/s] 9,08E-05
Ks Soil [cm/d] 625
Ks Soil [m/s] 7,27E-05

Ks Soil normalized at 25,0 Â°C [cm/d] [cm/d] 621
Ks Soil normalized at 25,0 Â°C [cm/d] [m/s] 7,22E-05

KSAT
Software Version 1.2.0
Firmware Version 1.4
Last setting of the zero point 1-1-
0001
Serial Number 0034

PARAMETER
Mode FallingHead
Sample name Dorsilit1_001
cross-sectional area of the burette [cm2] 4,536
Cross-sectional area of the sample [cm2] 50,18
Sample length [cm] 5,0
Plate thickness [cm] 1,0
Crown type FilterPlateCrown
Saturated plate conductivity [cm/d] 20000,000
Start of measurement 17-11-2016 15:16:27
Test duration 00:00:25

RESULT
Use auto offset adjustment True
Fitting Parameter a [cm] 5,01
Fitting Parameter b [s-1] -4,76E-02
Fitting Parameter c [cm] -,1
Fitting Parameter r2 [-] 0,9996
Ks Total [cm/d] 2340
Ks Total [m/s] 2,72E-04
Ks Soil [cm/d] 1910
Ks Soil [m/s] 2,22E-04

Ks Soil normalized at 25,0 Â°C [cm/d] [cm/d] 1880
Ks Soil normalized at 25,0 Â°C [cm/d] [m/s] 2,19E-04

The anaraki method was used in order to obtain the minimum and maximum porosities of the sand types. For both sand types it was tested three times, in order to get an average.

Geba Weiss:

Maximum packing:
Porosity:
0.390384992
0.391597955
0.399920229
Minimum packing:
Porosity:
0.479167148
0.467812466
0.467003824

Dorsilit 9

Maximum packing:
Porosity:
0.410634736
0.417171259
0.41097167
Minimum packing:
Porosity:
0.477280317
0.469665604
0.476404288

Appendix M Vibrating Needle

TECHNICAL DATA SHEET

LIEVERS HOLLAND

Partner for concrete solutions

P14E

Rev. 2/28-06-2010

ELEKTRISCHE HANDSTOKTRILNAALD

Speciaal ontworpen voor het verdichten van vloeren, balken, funderingen, lateien, wanden en kolommen.

Toepassing
Deze P14 trilnaald is een handzame, lichtgewicht machine (ca. 6 Kg), die gebruikt kan worden voor het verdichten van vrijwel alle betonsamenstellingen. De speciaal ontworpen 230/115V 1-fase motor drijft een flexibele as aan met maar 4.000 toeren. Door het klepel trilsysteem (pendulum) produceert de trilnaald 12.000 trillingen per minuut wat samen met de grote amplitude zorgt voor een perfecte betonverdichting.

Kenmerken
De belangrijkste kenmerken van de P14E zijn:

- Krachtig klepel trilsysteem.
- Flexibele as draait slechts 4.000 omw./min.
- Gehard stalen klepel en trilmantel.
- Geen onderhoud, niet smeren.
- De naald hoeft niet gekoeld te worden in het beton.
- Rubber slang met gevlochten staalgordel en verenstaal spiraal. Olie en chemicaliën bestendig.
- Unieke koppeling met snelspanner voor het snel wisselen van trilnaalden aan de elektromotor.
- Lichtgewicht (3 kg) aandrijfmotor, dubbel geïsoleerd, IP 54 afdichting.

Technische informatie

TRILNAALD DIA.	GEWICHT	TRILLINGEN	TRIL-KRACHT	AMPLITUDE	SLANGLENGTE**
mm	kg	per min	N	mm	m
Ø28	2.0	12.000	2.500	0.8	1.0-1.5-2.0-2.5-3.0-3.5-4.0
Ø38*	3.4	12.000	3.900	1.0	1.0-1.5-2.0-2.5-3.0-3.5-4.0
Ø45*	3.6	12.000	4.500	1.5	1.0-1.5-2.0-2.5-3.0-3.5-4.0

* Ook leverbaar met rubberkop
** Slanglengte inclusief trilfles

Het gewicht is weergegeven voor standaard lengte 1 meter.
De aandrijfmotor is ook leverbaar in 115 / 1-fase / 50-60 Hz.

Lievers Holland, Postbus 103, 3640 AC Mijdrecht (NL)
Tel.: +31(0) 297 231 900, Fax: +31(0) 297 231 909, E-mail: info@lieversholland.nl, Website: www.lieversholland.nl

Appendix N Breaching Height

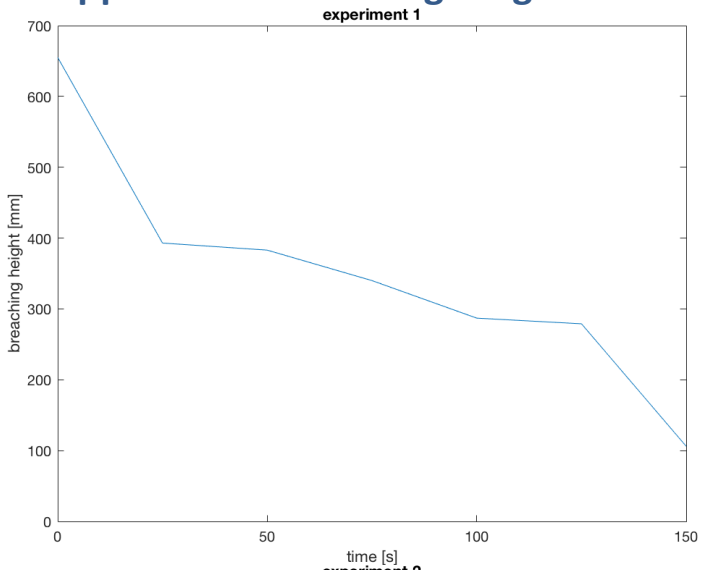

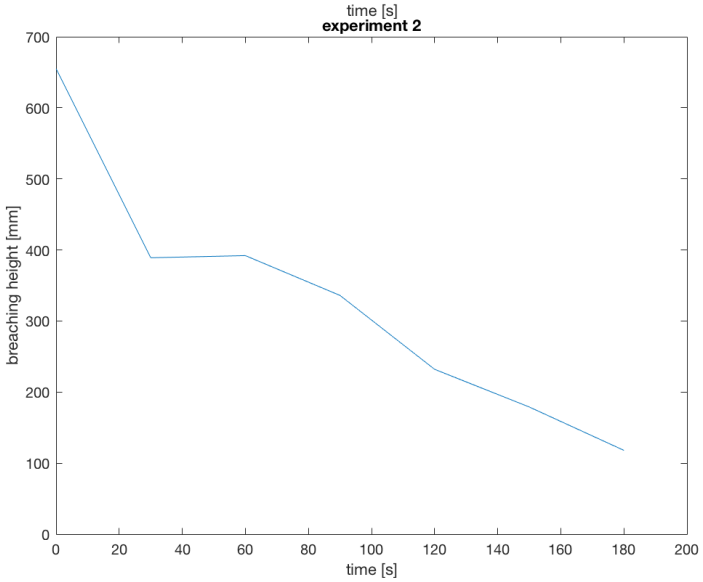

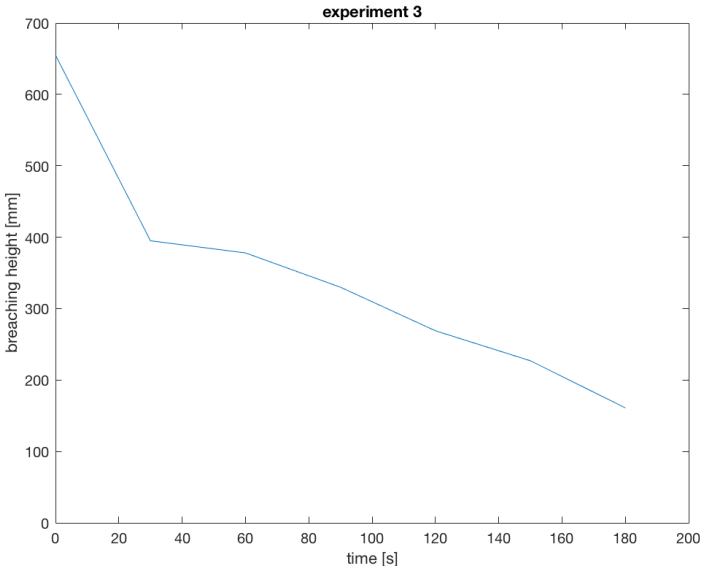

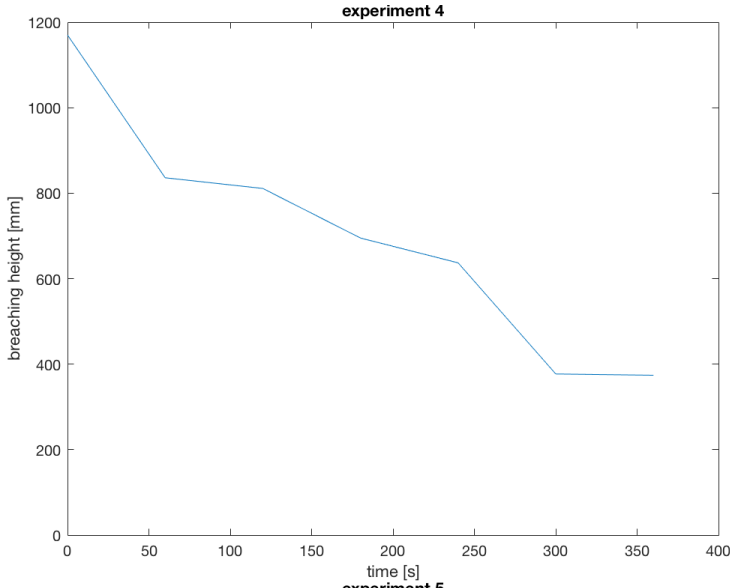
experiment 4
breaching height [mm]
time [s]
0
200
400
600
800
1000
1200
0
50
100
150
200
250
300
350
400

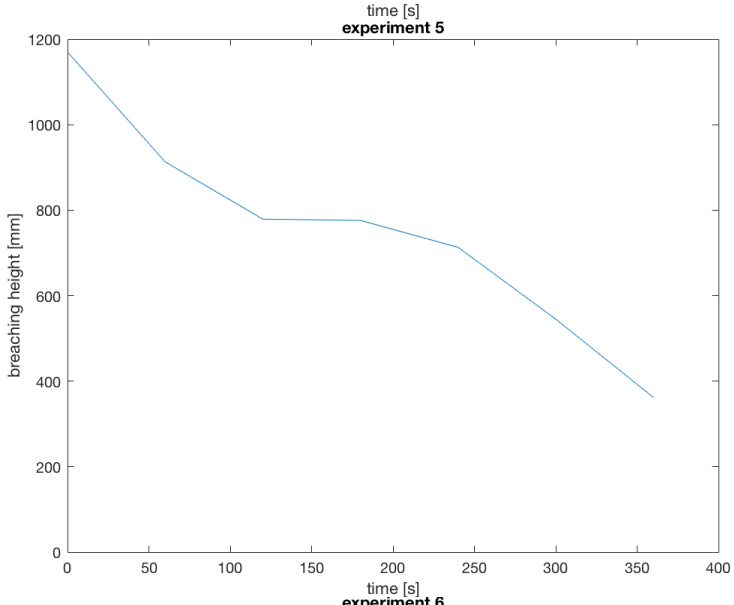
experiment 5
breaching height [mm]
time [s]
0
200
400
600
800
1000
1200
0
50
100
150
200
250
300
350
400

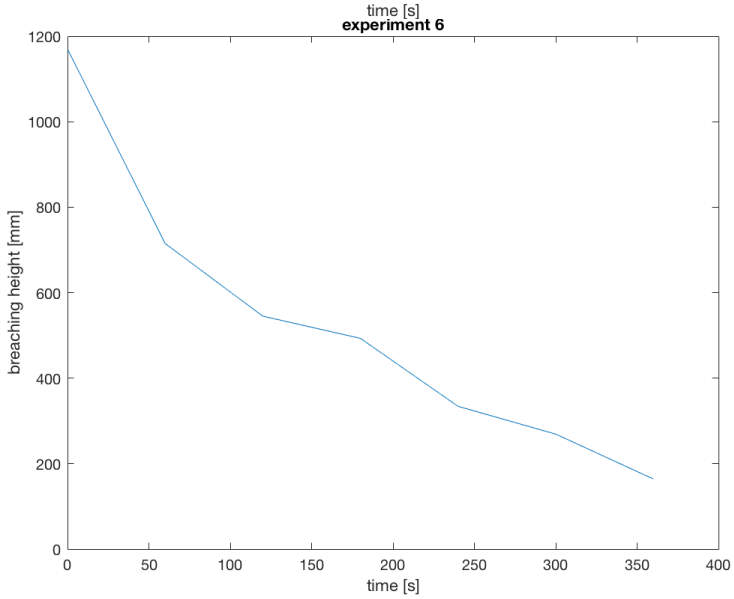
experiment 6
breaching height [mm]
time [s]
0
200
400
600
800
1000
1200
0
50
100
150
200
250
300
350
400

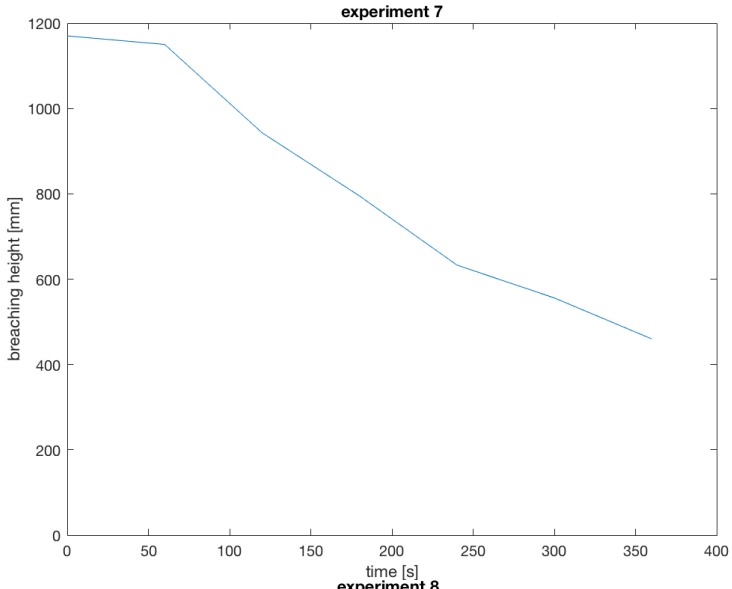
experiment 7
breaching height [mm]
time [s]
0
200
400
600
800
1000
1200
0
50
100
150
200
250
300
350
400

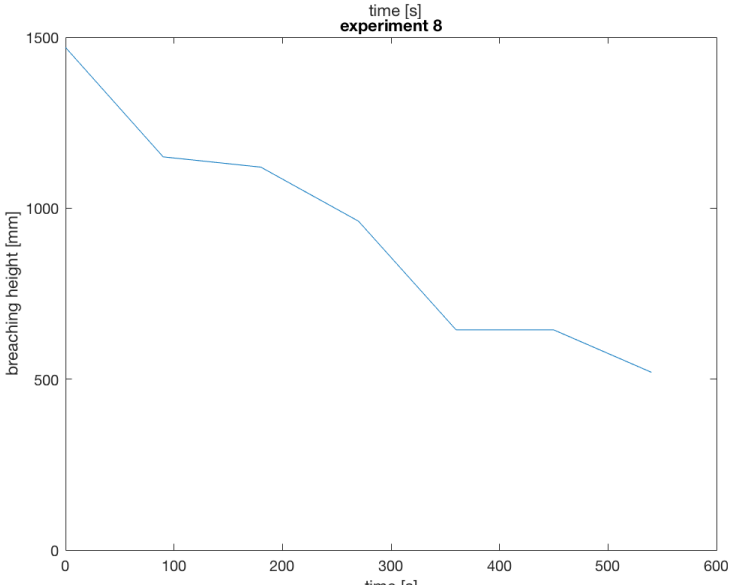
experiment 8
breaching height [mm]
time [s]
0
500
1000
1500
0
100
200
300
400
500
600

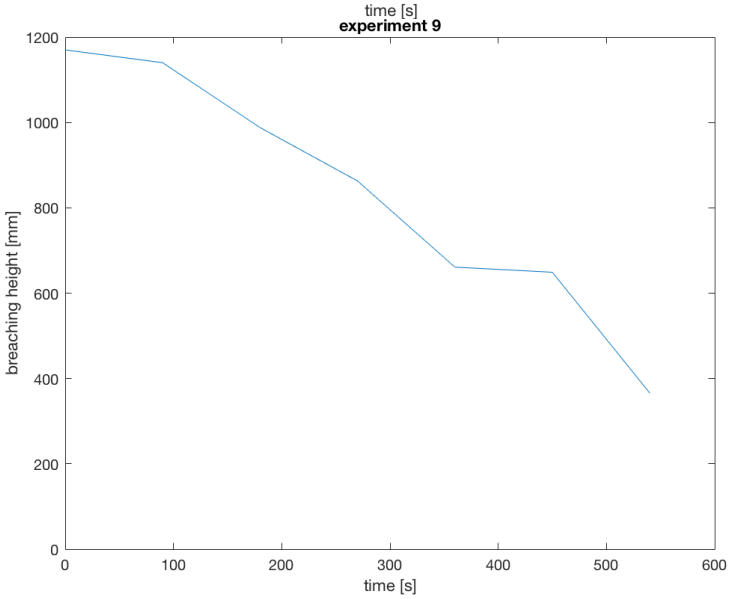
experiment 9
breaching height [mm]
time [s]
0
200
400
600
800
1000
1200
0
100
200
300
400
500
600

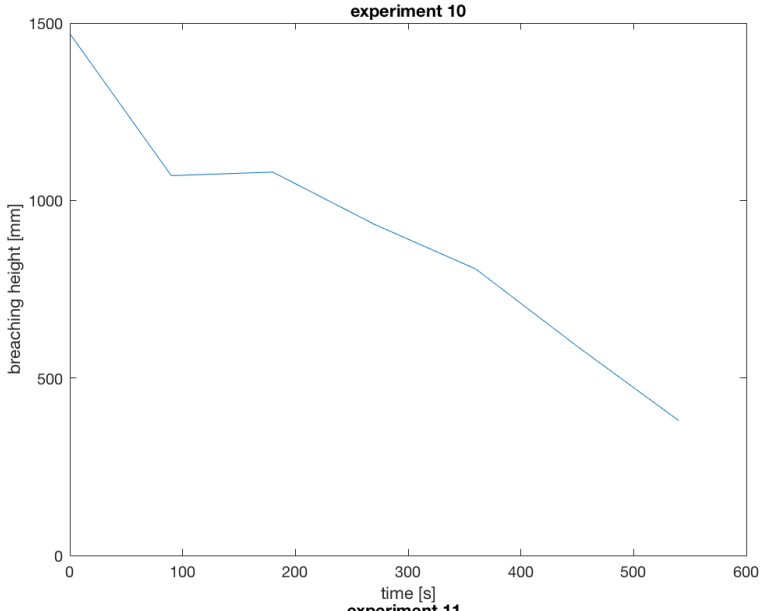
experiment 10
breaching height [mm]
time [s]
0
500
1000
1500
0
100
200
300
400
500
600

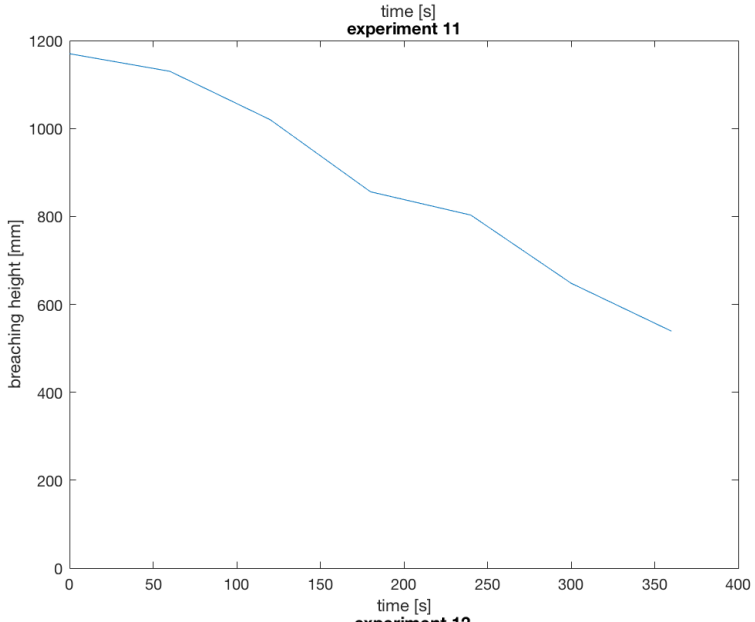
experiment 11
breaching height [mm]
time [s]
0
200
400
600
800
1000
1200
0
50
100
150
200
250
300
350
400

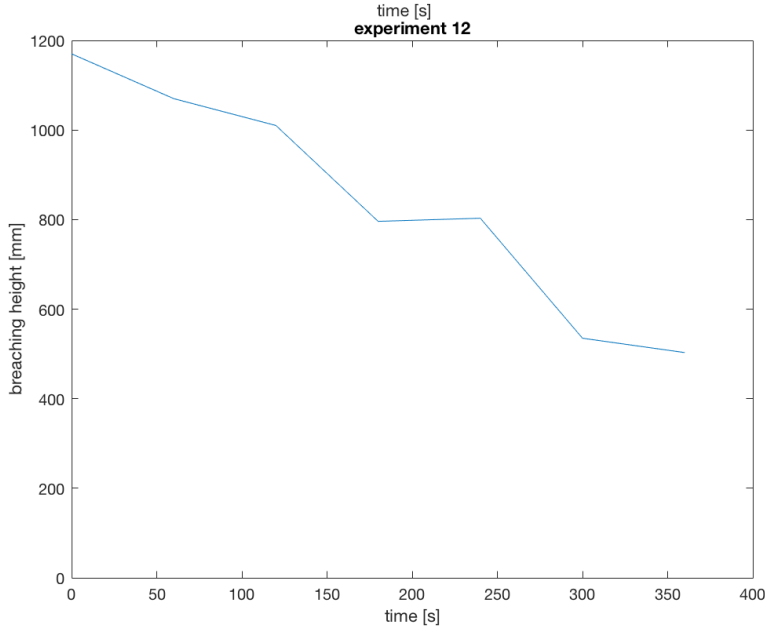
experiment 12
breaching height [mm]
time [s]
0
200
400
600
800
1000
1200
0
50
100
150
200
250
300
350
400

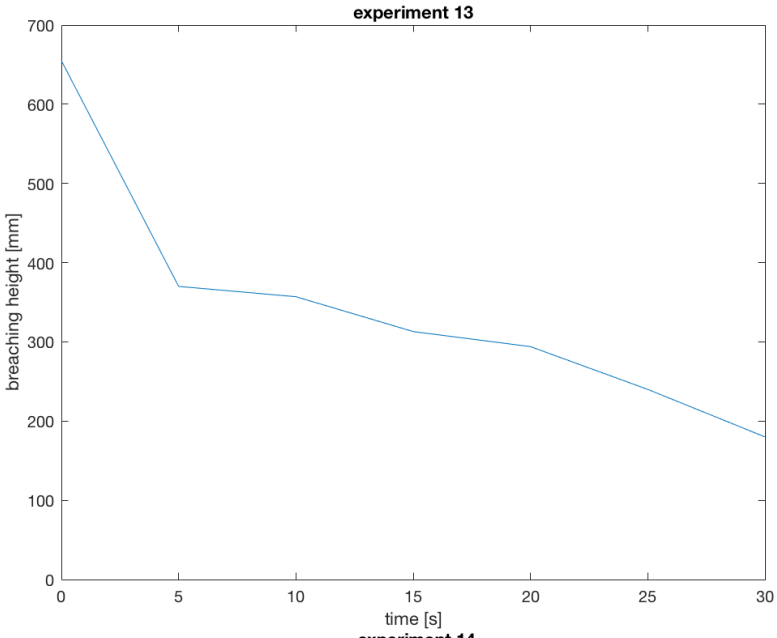
experiment 13
breaching height [mm]
time [s]
0
100
200
300
400
500
600
700
0
5
10
15
20
25
30

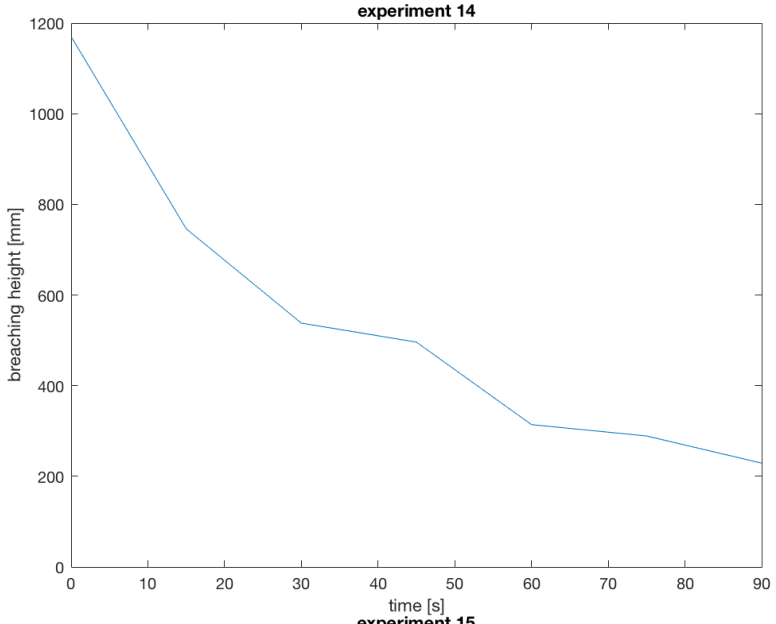
experiment 14
breaching height [mm]
time [s]
0
200
400
600
800
1000
1200
0
10
20
30
40
50
60
70
80
90

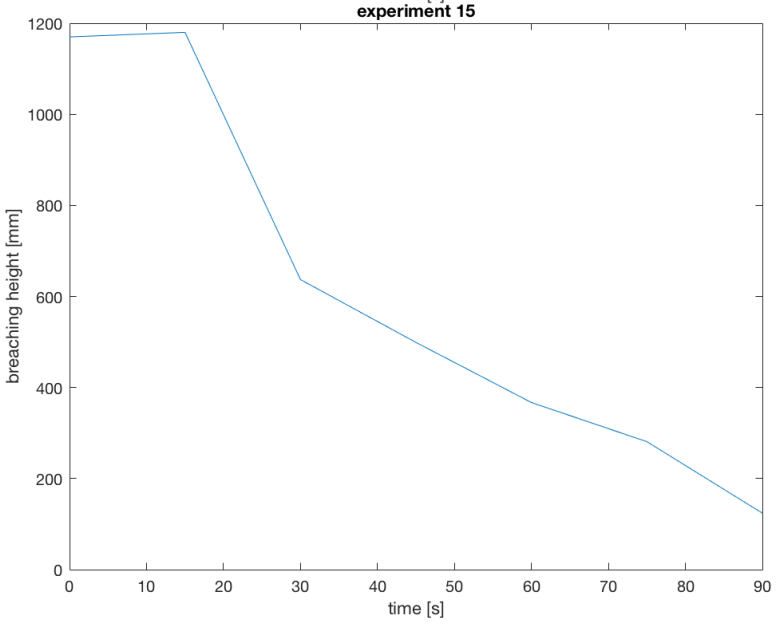
experiment 15
breaching height [mm]
time [s]
0
200
400
600
800
1000
1200
0
10
20
30
40
50
60
70
80
90

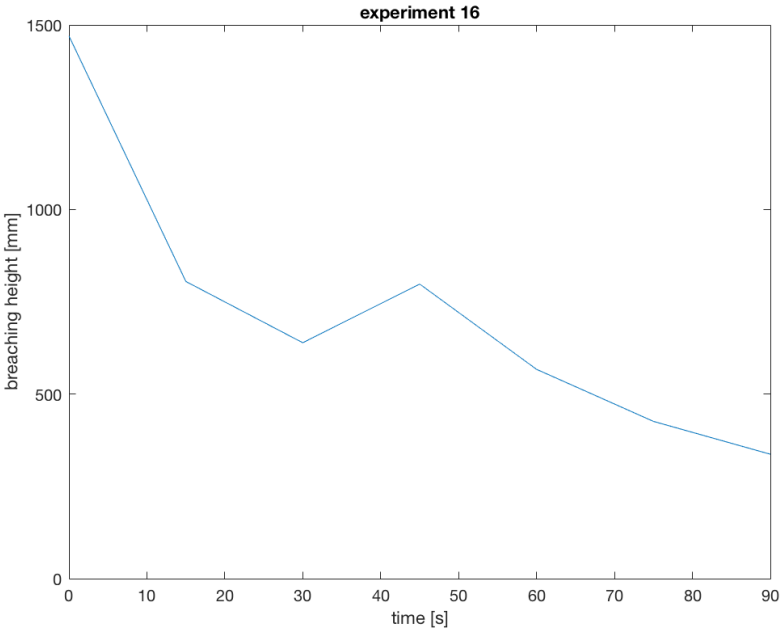
experiment 16
breaching height [mm]
time [s]
0
500
1000
1500
0
10
20
30
40
50
60
70
80
90